Are the excitons in colloidal InP quantum dots suitable for quantum photonics?

Vigneshwaran Chandrasekaran

A dissertation submitted in fulfillment of requirements for the degree of
Doctor in Science: Physics

Fall 2019

Promotors:
Prof. Dr. Ir. Zeger Hens
Prof. Dr. Wolfgang Langbein

Physics and Chemistry of Nanostructures,
Department of Chemistry, Ghent University,
Krijgslaan 281-S3, 9000 Ghent, Belgium

GHENT UNIVERSITY

FACULTY OF SCIENCES

PCN

This work was supported by the European Commission via the Marie-Skłodowska Curie action Phonsi
(H2020-MSCA-ITN-642656).

Examination Board

Chair

Prof. Christophe Detavernier
(Department of Solid state sciences - Ghent University, Belgium)

Reading Committee

Prof. Dirk Poelman
(Department of Solid state sciences - Ghent University, Belgium), Secretary

Prof. Iwan Moreels
(Department of Chemistry - Ghent University, Belgium)

Prof. Dries Van Thourhout
(Department of Information technology - Ghent University & IMEC, Belgium)

Prof. David Norris
(Department of Mechanical and Process Engineering - ETH Zürich, Switzerland)

Other members

Prof. Zeger Hens
(Department of Chemistry - Ghent University, Belgium), Supervisor

Prof. Wolfgang Langbein
(School of Physics and Astronomy, Cardiff University, United Kingdom), Supervisor

ஊழையும் உப்பக்கம் காண்பர் உலைவின்றித்
தாழாது உஞற்று பவர்

- திருவள்ளுவர்
(குறள்: 620)

Who strive with undismayed, unfaltering mind
At length shall leave opposing fate behind

- Thiruvalluvar
(Kural: 620)

Contents

Preface

With wave-particle duality and the quantization of light, the first quantum revolution enabled the advent of modern devices from transistors to lasers. Now we are on the verge of a second quantum revolution with devices that are able to generate, manipulate and measure the quantum states of light. Quantized electromagnetic field consists of discrete particles known as photons and a single photon is one such quantum state of light. Single photon sources are essential for realizing quantum technologies like quantum communication, quantum computation, quantum simulation and quantum sensing. They are ideally required to have pure single photon emission with higher on-demand emission rate and identical photon wave packets. A two-level system is the main building block of photonic quantum technologies that can create pure & indistinguishable single photons. Attenuated lasers or weak coherent pulses as single photon sources are probabilistic in nature and they are not ideal two-level quantum emitters. Heralded single photon sources using spontaneous parametric down-conversion set the benchmark for single-photon technology, but they are also probabilistic in nature, and are therefore not scalable and have lower brightness. The generation of single photons by two-level system like atoms are not reliable and less efficient with lower operation rates. On the other hand, solid-state emitters such as color centers or defects in crystalline hosts, carbon nanotubes, transition metal dichalcogenides, epitaxial or self-assembled quantum dots and colloidal nanocrystals (NCs) or colloidal quantum dots (QDs) are attractive as non-classical light sources because of the scalability of their host matrix system and their 'on-demand' emission. Among these, colloidal QDs stand out since they offer an extensive design freedom that can be prepared economically (both at the level of nanocrystal synthesis and device integration) as well as room temperature operation. This dissertation discusses how colloidal InP QDs fare in this aspect.

The nanoscale light-matter interaction for realizing quantum photonics comprises the central part of this dissertation. The matter being the NCs prepared from the bottom-up approach using wet-chemical synthesis. Colloidal NCs synthesized in solution phase are surrounded by capping agents to prevent uncontrolled growth and agglomeration of the nanoparticles. NCs are nothing but a collection of periodically arranged atoms (100-10000) with the dimension in the scale of few nanometers, making their optical properties somewhere between the bulk material and molecules. The overlap of fewer numbers of atomic orbitals in NCs results in discrete levels instead of energy bands, called quantized energy levels. NCs made of a semiconductor have an energy bandgap between highest occupied level (originating from the valence band of bulk) and lowest unoccupied level (originating from the conduction band of bulk). When a photon having certain energy equal or above this energy gap is absorbed by the NC, an electron transit from the 'ground' state to 'excited' state forming a quasi-particle electron-hole pair state, also known as exciton. The exciton relaxes back after over an average time called as fluorescent lifetime, releasing a photon. When the size of the NC is smaller than the bulk exciton Bohr radius, the confinement energy of both electron & hole is larger than their Coulomb interaction energy and this regime of operation is called as strong confinement. Due to quantum confinement effect, reducing the size of NCs increases their energy bandgap which makes it possible to tune the light emission wavelength to smaller values. NCs are also called artificial atoms due to their discrete

nature of energy levels and are also referred to as QDs because of the quantum confinement in all three dimensions.

The light emission in QDs can be observed in both spectral and time domain, from which it can be inferred that the relaxation pathway is not simple with the contribution of both radiative and non-radiative recombinations. Ensemble spectra are inhomogeneously broadened due to the size dispersion. Even when observing single QDs after spatial dilution, slow time-evolutions compared to the emission lifetime (usually in the order of nanoseconds) influence the emission spectra observed in typical experimental settings (in the order of seconds). These slow time-evolutions called as spectral diffusion, which are mostly due to charge trapping in the QDs and their surroundings, lead to an effective inhomogeneous broadening. Further the lowest exciton emission line, much similar to the atomic fine structure spectral lines, consists of several splitted states due to electron-hole exchange interaction with their different spin configurations and the anisotropical shape of the QD. At room temperature, the homogeneous lineshape is typically dominated by phonon-induced broadening in the order of 10-100 meV which is much larger than the lifetime limited natural broadening in the μeV range. Reducing the temperature, the lattice vibrations are frozen out and the above discussed details in the emission spectra can be observed on a single QD. Key inhibiting factors in using colloidal QDs for quantum photonics are described as *bleaching* (fluorescence emission stops after some time), *blinking* (fluorescence intermittency), and *jittering* (fluorescence energy shift with time). Photoluminescence quantum yield (PLQY), a measure of the number of photons emitted as a fraction of the number of photons absorbed, is lower in QDs because of the surface trap sites. Much progress has been made in improving the optical properties of QDs with hetero-structures approaching 100% PLQY. Here, the core material is encapsulated by a shell of a semiconductor with higher bandgap that prevents the ground-state exciton wavefunctions from reaching the surface.

Ever since the QDs were synthesized economically in colloidal solution form, the scientific interest in the fundamental understanding of their optical properties has been anything but stagnant. The synthesis protocols have been molded time and again aimed at several applications from bio-implants to television displays. Both the fundamental knowledge of optical properties in QDs and the improvement in their synthesis with a precise 'engineered' control of dimensions, shape and composition has been achieved with the detailed study on CdSe QDs belonging to II-VI group for visible wavelength range and PbS QDs belonging to IV-VI group for infrared wavelength range. The rising concern over using the heavy metal ions in the end user applications have necessitated the synthesis of QDs constituted of nontoxic and earth-abundant materials. One of the promising alternative semiconductor material in the visible-near infrared range is InP belonging to III-V group. Though indium belong to smaller earth abundant material, it does not have the toxicity of Cd. For convenience, CdSe QDs are taken as prototypical material in comparison to explain the optical properties of InP. The first difference is the cubic (zincblende) crystal structure in InP whereas it is hexagonal (wurtzite) structure for CdSe where there is an additional in-built crystal field splitting contributing to the fine structure. Note that the CdSe QDs can also be synthesized with a zincblende structure. In contrast to ionic bonds in II-VI group materials like CdSe, InP belonging to III-V group has a more covalent bond formation which is stronger and thus requires a high temperature, longer reaction times and more reactive precursors for their synthesis. InP is prone to oxidation, requiring stringent air-free conditions during synthesis and subsequent protection with an appropriate shell material. InP QDs have traditionally broader ensemble emission spectra and larger Stokes shifts than the counterpart CdSe QDs. The reason for this is still under discussion with reasons including polydispersity or fine structure or vibrational contribution or emission from trapped states. InP has a larger exciton Bohr radius of about 10 nm (1.35 eV bandgap) compared to about 5 nm (1.7 eV bandgap) in CdSe and thus they could experience a stronger quantum confinement effect for a similar sized QD. This could explain the broadened ensemble emis-

sion spectra in InP compared to CdSe since a mere change in the size distribution could result in a shift in the peak emission energies. Though it is difficult to predict the size-dependent energies owing to their oxidation and poor contrast in TEM images, some studies observed a steeper relation between the bandgap and size in InP compared to CdSe. Such discrepancies call for a more in-depth study on the exciton properties in InP QDs. Here in this dissertation, InP QDs synthesized using an economical aminophosphine-based precursor enabling to work under ambient condition are studied. Regarding the shell, a type I heterostructure is more suitable for single photon emission with both the charge carriers confined within the core giving a larger spatial overlap and thus stronger radiative coupling. In this respect, the InP/ZnSe core/shell combination is interesting for quantum photonics. It features a similar, type I band alignment as CdSe/ZnS, yet the InP/ZnSe lattice mismatch amounts to a mere 3%, in stark contrast to the 12% mismatch between CdSe and ZnS. InP/ZnS is also a type I structure with higher barriers but with a lattice mismatch of 7.7%. InP/ZnSe heterostructure QDs are studied in this dissertation.

The fundamental properties of the material to be used for any applications need to be well known and this dissertation is aimed at further proliferating the interest in using the 'economically' synthesized colloidal QDs for quantum photonics amid a strong competition from already established, yet expensive, epitaxial or self-assembled QDs and other solid state materials. As described before, an ideal quantum emitter interacts only with the electromagnetic environment producing indistinguishable photons having a lifetime-limited spectral distribution, while the additional interaction with vibrational degrees of freedom and the environment results in more complex spectral features in QDs. The fundamental properties of excitons in visible-wavelength emitting InP/Znse QDs under optical excitation are addressed in this dissertation. InP/ZnSe QDs are characterized at room & cryogenic temperatures from the ensemble down to the single QD level using various spectroscopy methods and theoretical models. This dissertation answers the following questions listed in the order of chapters: "*What role the QD has in nanotechnology?, How efficient is the single photon emission from InP/ZnSe QDs? How the electronic level structure looks like?, Which factors influence the decoherence in exciton emission ultimately limiting the homogeneous linewidth?, How do the charge fluctuations affect the optical properties in QDs?, and, Is it possible to have an integrated single photon source based on colloidal QD in silicon chip?.*" In the conclusion, selection criteria for colloidal QDs for use as single photon sources are devised from the experimental results here and also from the literature review of performances of other colloidal NCs. Further, possible future directions & suggestions in using colloidal NCs for quantum photonics, for instance single photon sources as random number generators at room temperature, are discussed. While the quantum territory is gargantuan to be covered in its entirety and the photophysical mechanism behind the exciton properties differ from one material to another, this dissertation limits itself in explaining the mechanisms behind the 'behavior' of InP/ZnSe QDs that could be used as a model system to emulate for other types of colloidal QDs as well to be ultimately used for quantum photonics.

Voorwoord

Met dualiteit van golfdeeltjes en de kwantisatie van licht, maakte de eerste kwantumrevolutie de komst van moderne apparaten mogelijk, van transistoren tot lasers. Nu staan we aan de vooravond van een tweede kwantumrevolutie met apparaten die in staat zijn de kwantumtoestanden van licht te genereren, manipuleren en meten. Een gekwantiseerd elektromagnetisch veld bestaat uit afzonderlijke deeltjes die bekend staan als fotonen en één enkel foton is een dergelijke kwantumtoestand van licht. Zogenaamde *single photon sources*, zijn in staat één enkel foton uit te sturen en zijn essentieel voor het realiseren van kwantumtechnologieën zoals kwantumcommunicatie, kwantumberekening, kwantumsimulatie en kwantumdetectie. *Single photon sources* worden gekenmerkt door zuivere enkelvoudige fotonenemissie met een hoge emissiesnelheid en identieke fotonengolfpakketten. Een systeem met twee niveaus is de belangrijkste bouwsteen van fotonische kwantumtechnologieën die zuivere en niet te onderscheiden afzonderlijke fotonen kunnen creëren. Geattenueerde lasers of zwakke coherente pulsen als afzonderlijke fotonenbronnen zijn probabilistisch van aard en zijn geen ideale kwantumemitters met twee niveaus. Gekende *single photon sources* die gebruik maken van spontane parametrische fluorescentie zetten de maatstaf voor de *single photon* technologie, maar ze zijn ook probabilistisch van aard en zijn daarom niet schaalbaar en hebben een lagere helderheid. Het genereren van afzonderlijke fotonen door een systeem met twee energieniveaus zoals bevoorbeeld atomen is ook niet betrouwbaar en minder efficiënt met lagere snelheden. Anderzijds zijn vaste-stofstralers zoals kleurcentra of defecten in kristallijne gastheren, koolstofnanobuizen, transitiemetaaldichalcogeniden, epitaxiale of zelf-geassembleerde kwantumstippen en colloïdale nanokristallen (NK'en) of colloïdale kwantumstippen (QD's) aantrekkelijk als niet -klassieke lichtbronnen vanwege de schaalbaarheid van hun hostmatrixsysteem en hun *'on-demand'*-emissie. Tot deze categorie horen colloïdale QD's. Deze QD's zijn opvallend door een uitgebreide ontwerpvrijheid en economische toegankelijkheid zowel op het niveau van nanokristalsynthese en apparaatintegratie. Dit proefschrift bespreekt colloïdale InP QDs met betrekking tot hun prestatie als *single photon sources*.

De licht-materie-interactie op nanoschaal voor het realiseren van kwantumfotonica vormt het centrale deel van dit proefschrift. Het gaat hier om de NK'en die zijn voorbereid met behulp van nat-chemische synthese. Colloïdale NK'en gesynthetiseerd in oplossingsfase worden omgeven door moleculaire liganden om ongecontroleerde groei en agglomeratie van de nanodeeltjes te voorkomen. NK'en zijn niets anders dan een verzameling periodiek gerangschikte atomen (100-10000) met de afmeting in de schaal van enkele nanometer, waardoor hun optische eigenschappen ergens tussen degene van een bulkmateriaal en moleculen liggen. De overlap van een gelimiteerd aantal atomaire orbitalen in NK'en resulteert in discrete, gekwantiseerde energieniveaus in plaats van energiebanden. NK'en gemaakt van een halfgeleider hebben een energiebandafstand tussen het hoogste bezette niveau (afkomstig van de valentieband van bulk) en het laagste onbezette niveau (afkomstig van de geleidingsband van bulk). Wanneer een foton met een bepaalde energie gelijk aan of groter dan deze energiekloof wordt geabsorbeerd door het NK, gaat een elektron over van de 'grond'-toestand naar de 'geëxciteerde'-toestand en

Translation by Mr. Jari Leemans, Ghent University, Belgium

vormt een elektron-gat quasideeltje, ook bekend als exciton. Dit exciton relaxeert na een gemiddelde fluorescentielevensduur, waarbij een foton wordt uitgestraald. Wanneer de grootte van het NK kleiner is dan de exciton Bohr-straal van het bulkmateriaal, is de opsluitingsenergie van zowel elektron en gat groter dan hun Coulomb interactie-energie en dit regime van werking wordt *strong confinement* genoemd. Vanwege het *quantum confinement effect* vergroot het verkleinen van een NK zijn energiebandafstand waardoor de lichtemissiegolflengte kleinere waarden aanneemt. NK'en worden ook kunstmatige atomen genoemd vanwege hun discrete aard van energieniveaus en worden ook QD's genoemd vanwege het *quantum confinement effect* in alle drie dimensies.

De lichtemissie in QDs kan worden waargenomen in zowel spectraal als tijdsdomein, waaruit kan worden afgeleid dat de relaxatieroute niet eenvoudig is met de bijdrage van zowel stralende als niet-stralende recombinaties. Ensemblespectra worden inhomogeen verbreed vanwege de spreiding aan groottes van de NK'en. Zelfs bij het waarnemen van afzonderlijke QD's na ruimtelijke verdunning, hebben langzame tijdevoluties in vergelijking met de emissielevensduur (meestal in de orde van nanoseconden) invloed op de emissiespectra waargenomen in typische experimentele condities(in de grootteorde van seconden). Deze langzame tijdsevoluties die worden aangeduid als spectrale diffusie, die meestal het gevolg zijn van niet gedelokaliseerde elektronische toestanden in de QD's en hun omgeving, leiden tot een effectieve inhomogene verbreding. Verder bestaat de laagste exciton-emissielijn, die veel lijkt op de fijnstructuur van atomaire spectrale lijnen, uit verschillende gesplitste toestanden vanwege elektron-gatuitwisselingsinteractie met hun verschillende spinconfiguraties en de anisotrope vorm van de QD. Bij kamertemperatuur wordt de homogene lijnvorm meestal gedomineerd door fonon-geïnduceerde verbreding in de orde van 10-100 meV die veel groter is dan de natuurlijke verbreding omwille van de levensduur van de toestand. Door de temperatuur te verlagen, worden de roostertrillingen bevroren en kunnen de hierboven besproken details in de emissiespectra worden waargenomen op een enkele QD. Belangrijke remmende factoren bij het gebruik van colloïdale QD's voor kwantumfotonica worden beschreven als *bleken* (fluorescentie-emissie stopt na enige tijd), *knipperen* (fluorescentie-intermittency) en *spectrale verschuiving* (fluorescentie-energieverschuiving met de tijd). De fotoluminescente kwantumopbrengst (PLQY) is een maat voor het aantal uitgezonden fotonen als een fractie van het aantal geabsorbeerde fotonen en is lager in QD's omwille van gelokaliseerde elektronische toestanden aan het oppervlak van de QD's. Er is veel vooruitgang geboekt bij het verbeteren van de optische eigenschappen van QD's met heterostructuren die 100% PLQY benaderen. Hier wordt het fluorescente materiaal ingekapseld door een schil van een halfgeleider met een hogere energy gap die voorkomt dat de excitongolffuncties in de grondtoestand het oppervlak bereiken.

Omdat de QD's economisch in de vorm van een colloïdale oplossing zijn gesynthetiseerd, is de wetenschappelijke belangstelling voor het fundamentele begrip van hun optische eigenschappen allesbehalve stilstaand. De synthese-protocollen zijn keer op keer gevormd voor verschillende toepassingen, van bio-implantaten tot televisieschermen. Zowel de fundamentele kennis van optische eigenschappen in QD's als de verbetering in hun synthese met een precieze controle van afmetingen, vorm en samenstelling is bereikt met de gedetailleerde studie van CdSe QD's voor zichtbaar golflengtes en PbS QD's voor infrarood golflengtes. De toenemende bezorgdheid over het gebruik van de zware metaalionen in de eindgebruikerstoepassingen heeft de beschikbaarheid van QD's nodig gemaakt die uit niet-toxische en abundante materialen bestaan. Een van de veelbelovende alternatieve halfgeleidermaterialen in het zichtbare tot nabij-infraroodbereik is InP behorende tot de III-V-groep. Hoewel indium weinig abundant is, is het veel minder toxisch dan Cd. Omwille van de kennis omtrent CdSe QD's, worden deze hier als benchmark systeem genomen om de optische eigenschappen van InP in kaart te brengen. Opmerkelijke verschillen zijn de kubieke (zinkblende) kristalstructuur in InP, terwijl CdSe vaak een hexagonale (wurtziet) structuur vertoond, waarbij er een extra ingebouwde kristalveldsplitsing is die bijdraagt aan de fijnstructuur van emissielijnen. In tegenstelling tot chemische bindingen in

CdSe die een grootte ionaire bijdrage hebben, heeft InP behorende tot III-V-groep een meer covalent kristalrooster waardoor hun synthese een hoge temperatuur, lange reactietijden en reactievere precursoren vereist. Verder is InP gevoelig voor oxidatie en vereist luchtvrije omstandigheden tijdens de synthese en daaropvolgende bescherming met een geschikt schilmateriaal. InP QDs hebben ook traditioneel bredere ensemble-emissiespectra en grotere Stokes-verschuivingen dan de tegenhanger CdSe. De reden hiervoor zijn polydispersiteit, fijnstructuur, trillingsbijdragen of emissie uit gelokaliseerde energieniveaus. InP heeft een grotere exciton Bohr-straal van ongeveer 10 nm (1,35 eV-bandafstand) vergeleken met ongeveer 5 nm (1,7 eV-bandafstand) in CdSe en dus kunnen ze een sterker quantum confinement effect ervaren voor een QD van vergelijkbare grootte. Dit zou de verbrede ensemble-emissiespectra in InP ten opzichte van CdSe kunnen verklaren, omdat alleen een wijziging in de grootteverdeling kan leiden tot een verschuiving in de piekemissie-energieën. Hoewel het moeilijk is om de grootte-afhankelijke energieën te voorspellen vanwege hun oxidatie en slecht contrast in TEM-afbeeldingen, hebben sommige onderzoeken een steilere relatie waargenomen tussen de bandafstand en de grootte in InP. Zulke verschillen vragen om een diepgaander onderzoek naar de exciton-eigenschappen in InP QDs. Hier in dit proefschrift worden InP QDs bestudeerd die zijn gesynthetiseerd met behulp van een economische op aminofosfine gebaseerde precursor die het mogelijk maakt om onder omgevingscondities te werken. Wat de schil betreft, is een type I heterostructuur meer geschikt voor enkele fotonenemissie waarbij beide ladingsdragers in de kern zijn ingesloten en er dus een grotere ruimtelijke overlap is van elektron en gat golffuncties. In dit opzicht is de InP/ZnSe kern/schil-combinatie interessant voor kwantumfotonica. Het heeft een vergelijkbare, type I bandenstructuur als CdSe/ZnS, maar het verschil tussen het kristalrooster van InP en ZnSe bedraagt slechts 3%, in schril contrast met de 12% tussen CdSe en ZnS. InP/ZnS is ook een type I-structuur met hogere barrières maar met een rooster-mismatch van 7,7%. In dit proefschrift worden InP/ZnSe QD's bestudeerd.

De fundamentele eigenschappen van enig materiaal dat voor een technologie gebruikt zou worden moeten goed omschreven zijn en dit proefschrift dient erin om de economisch gesynthetiseerde colloïdale InP QD's te kwalificeren als nuttig materiaal in een veld waar performante, maar dure materialen reeds beschreven zijn. Zoals eerder beschreven, werkt een ideale kwantum straler alleen samen met de elektromagnetische omgeving die niet te onderscheiden fotonen produceert met een door levensduur beperkte spectrale verdeling, terwijl de extra interactie met trillingsvrijheidsgraden en de omgeving resulteert in complexere spectrale kenmerken in QDs. De fundamentele eigenschappen van excitonen in InP/ZnSe QD's onder optische excitatie worden in dit proefschrift behandeld. InP/ZnSe QD's worden gekenmerkt bij kamer- en cryogene temperaturen van het ensemble tot het "single QD"-niveau met behulp van verschillende spectroscopiemethoden en theoretische modellen. Dit proefschrift beantwoordt de volgende vragen in de volgorde van hoofdstukken: *"Welke rol heeft de QD in nanotechnologie? Hoe efficiënt is de* single photon *emissie van InP/ZnSe QD's? Hoe ziet de elektronische energieniveaustructuur eruit? Welke factoren beïnvloeden de decoherentie in excitonemissie die uiteindelijk de homogene lijnbreedte beperken? Hoe beïnvloeden de ladingsfluctuaties de optische eigenschappen in QDs? En, is het mogelijk om een geïntegreerde* "single photon source" *te hebben op basis van colloïdale QD's in een siliciumchip?"* In de conclusie zijn selectiecriteria voor colloïdale QD's voor gebruik als *single photon sources* ontwikkeld op basis van de experimentele resultaten hier en ook uit de literatuurstudie van de prestaties van andere colloïdale NK'en. Verder worden mogelijke toekomstige aanwijzingen en suggesties voor het gebruik van colloïdale NK'en voor kwantumfotonica, bijvoorbeeld *single photon sources* als *random number generators* bij kamertemperatuur, besproken. Omdat het kwantumgebied te groot is om volledig te omschrijven en het fotofysische mechanisme achter de exciton-eigenschappen van materiaal tot materiaal verschilt, beperkt dit proefschrift zich tot het verklaren van de mechanismen achter het gedrag van InP/ZnSe QDs, deze kunnen gebruikt worden als modelsysteem voor andere soorten colloïdale QD's en uiteindelijk een bijdrage leveren in

de kwantumfotonica.

Chapter 1.

Introduction

Contents

Synopsis

This chapter provides the basic understanding of excitons in colloidal quantum dots (QDs) which are required to understand the following chapters. This chapter also discusses the specific material (InP/ZnSe QDs) to be investigated in this dissertation. The motivation of this dissertation is also addressed including the key inhibiting factors in using colloidal QDs for quantum photonics. The dissertation structure is listed at the end of the chapter.

1.1. Nanotechnology

Nanotechnology is a booming field of research that conglomerates science and engineering and involves materials that are minuscule in size ranging from one to hundred nanometers. A nanometer is 1 billionth of a meter or 1 millionth size of a dot at the end of this sentence. Richard P. Feynman, a Nobel prize winning theoretical physicist on quantum electrodynamics, is widely considered as the visionary father of nanotechnology from the renowned lecture *"There's plenty of room at the bottom"* he delivered in 1959[1, 2] even before the term nanotechnology was coined later in 1974 by Norio Taniguchi.[3] Building on Feynman's ideas of making use the incredibly small scale of atoms, a whole field has emerged driven by the aim of fabricating, analyzing and imaging materials with atomic precision and making best use of the properties of these materials.[4]

Much before the modern scientific methods of preparing nanomaterials using state of the art fabrication equipments and analytical instruments, nanoparticles have been unintentionally prepared and used throughout history. More than 4000 years ago, ancient Egyptians prepared black colored hair dye by mixing lead oxide nanoparticles and slaked lime[8] The Lycurgus cup, a decorative artefact vessel made around 400 AD during the Roman era, is an another example. This cup is made of glass that contains gold and silver alloyed nanoparticles which give the cup a pale-green color in reflected light and

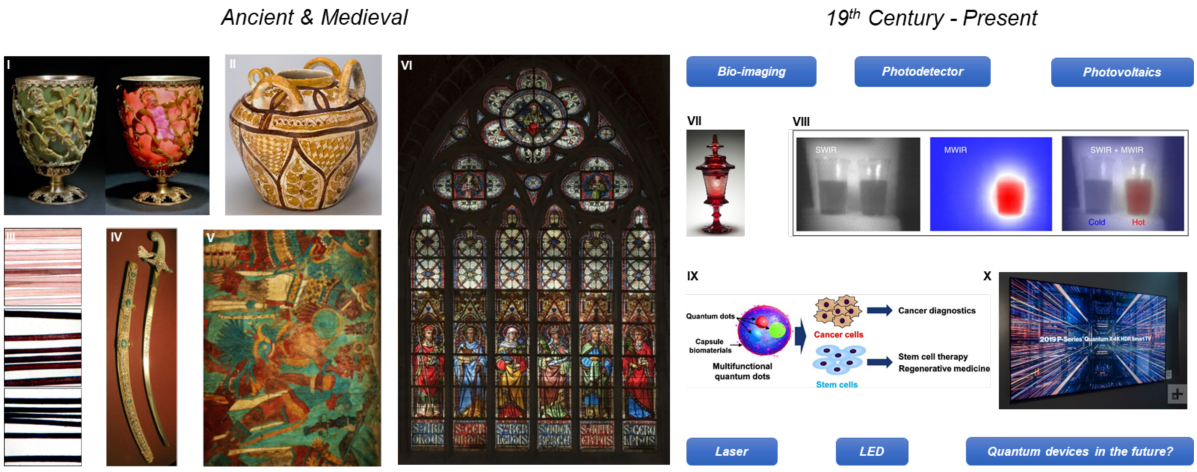

Figure 1.1. | Nanoparticles in use. (I) A fourth century Roman Lycurgus cup made of dichroic glass containing gold and silver alloyed nanoparticles changes its color from pale-green in reflected light to bright-red when light passes through it.[5] [image: ©British Museum]. (II) A ninth century glazed ceramics with metallic lustre decoration is made of silver and copper nanoparticles which can produce a golden shine under specular reflection.[6] [image: ©Art Institute of Chicago[7]]. (III) Thousands of years ago, ancient Egyptians used a mixture of lead oxide and slaked lime as hair dye which contained PbS nanoparticles. Image shows the blackening of hair over the time.[8] (IV) Seventeenth century Damascus blades contained carbon nanotubes and nanowires that could have made them durable and sharp.[9] [image: ©The New York Times[10]]. (V) During the eighth century Pre-Columbian era, a permanent organic pigment called as Maya Blue is made of a mixture of indigo dye from a plant and nanofibres of palygorskite clay.[11] [image is a mural in Cacaxtla[12]]. (VI) Stained glass windows in European cathedrals from sixth to fifteenth century contain nanoparticles that give them the beautiful range of colors [image: Saint-Bavo's cathedral in Ghent, Belgium[13]]. (VII) A 19th century Bohemian ruby glass made of gold nanoparticles [image: ©Cleveland Museum of Art[14]]. (VIII) Infrared images of hot and cold water using photodiode made of HgTe colloidal nanocrystals.[15] (IX) Quantum dots-based cancer diagnostics and stem cell therapeutics for regenerative medicine.[16] (X) Modern television displays contain nanoparticles where quantum dots or nanocrystals act as phosphors [image: ©Digital Trends[17]].

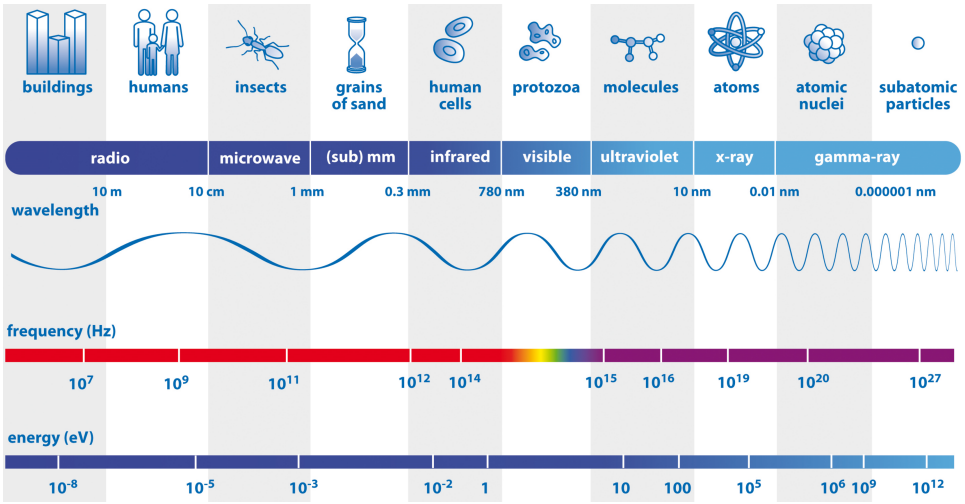

Figure 1.2. | Light as an electromagnetic wave. Size equivalent to wavelength, frequency and energy of light.[20]

bright-red for transmitted light.[5] During the medieval period of 600-1500 AD, the stained glass windows prevalent in European cathedrals were made of gold and silver nanoparticles. Around 800 AD in the Pre-Columbian era, a corrosion resistant and environmentally benign organic pigment called Maya Blue was used in mural paintings, ceramics and codices. This pigment is made of a mixture of indigo dye from a plant and nanofibres of palygorskite clay.[11] During the Abbasid caliphate period around 900 AD, an 'alchemy' was made possible by taking ordinary earthly materials and turning them into an extraordinary piece of art. Glazed ceramics with metallic lustre decoration is made of silver and copper nanoparticles which can produce a golden shine under specular reflection.[6] While today carbon nanotube finds its application from tennis rackets to space vehicles because of their stronger and lightweight nature,[18] the Damascus blades made of steels imported from India were used by the Crusaders during 1096 to 1294 AD which was later found to have traces of carbon nanotube and nanowires that could have made them durable and sharp.[9] Purple of Cassius or Ruby glass surfaced in 1700 AD used the red coloring properties of gold nanoparticles.[19]

1.2. Colloidal quantum dots

1.2.1. Semiconductor nanocrystals

While Feynman made a pun at the chemists in his lecture[1] by saying "The chemist does a mysterious thing when he wants to make a molecule. He sees that it has got that ring, so he mixes this and that, and he shakes it, and he fiddles around", the ability to build and assemble nanostructures today is possible by both physical and chemical methods. Semiconductor nanostructures can be precisely prepared with such small dimensions that they exhibit opto-electronic properties quite distinct from the bulk material made of same semiconductor (see section 1.2.2). The so-called quantum dots (QDs), coined by Reed *et al.* in 1980s,[21, 22] can be classified into two groups based on their method of preparation: self-assembled QDs or epitaxial QDs are fabricated by means of top-down lithography on pre-patterned surfaces and colloidal QDs or semiconductor nanocrystals (NCs) by means of wet-chemical synthesis. The latter method is more economical and colloidal QDs offer an extensive design freedom (both at the level

of NC synthesis and device integration) as well as room temperature operation. In this dissertation, colloidal QDs synthesized in solution phase using chemical methods are studied.

The term colloid was coined by Graham in 1861.[23] Michael Faraday and Nobel prize winning chemist Richard Zsigmondy could be considered the pioneers of modern colloidal nanoparticles from their respective experiments on colloidal 'ruby' gold sols in 1857 and 1898. They observed gold nanoparticles under certain lighting conditions producing different colored solutions.[24, 25] Faraday also explained this phenomenon in a lecture *Experimental Relations of Gold (and other Metals) to Light* in 1857 where he termed the currently known nanoparticles as "very minute in their dimensions", further adding, "the gold is reduced in exceedingly fine particles, which becoming diffused, produce a beautiful ruby fluid…the various preparations of gold, whether ruby, green, violet or blue in color,… consist of that substance in a metallic divided state".[26] In 1932, Ruby colored glasses had traces of CdSe and CdS nanoparticles.[27] In 1981, Ekimov and Onushchenko observed a blueshift in the absorption spectrum of CuCl nanocrystals in silicate glass matrix which forms the first recent modern experimental observation of the quantum confinement effect.[28] Subsequently in 1982, Efros and Efros developed a theoretical model to explain the size-dependent optical properties of spherical shaped nanocrystals.[29] In 1983, CdS nanocrystals dissolved in colloidal aqueous solution were reported for the first time by Rossetti et al,[30] followed by a size dependent synthesis.[31] The effect of Coulomb and exchange interaction on the lowest excited electronic state energy for CdS nanocrystals was discussed by Brus in 1984.[32] Modern synthesis of colloidal QDs typically involves controlled nucleation and rapid growth of particles in a solution of chemical precursors containing a coordinating solvent.[33, 34] NCs with nearly atomic precision can be synthesized with diameters ranging from few nanometers to tens of nanometers. In the last 3 decades, several economical and versatile colloidal synthesis methods were developed that offered extensive control over the QD size and shape to tune the emission wavelength, and enabled complex heterostructures to be formed from several semiconductors including II-VI and III-V groups.[35–51]

The role of the surface in nanocrystals

NCs are composed of a semiconductor core surrounded by capping agents, predominantly organic molecules or ligands (see Figure 1.3d). NCs have a surface to volume ratio which scales inversely with linear dimensions and thus the surface plays an important role in the physical & chemical processes of NCs.[52] First, the ligand capping keeps the NCs stable in the colloidal dispersion, preventing uncontrolled growth and agglomeration of the nanoparticles. The choice of the appropriate capping agent also determines the solubility and chemical reactivity of the NCs enabling to synthesize NCs of different sizes & shapes ultimately controlling their emission and absorption wavelengths[40, 45, 53–56] and also superstructures like 1D, 2D and 3D NC arrays.[57] However, electrically insulating longer ligands typically form a wide tunneling potential barrier to charge transport and thus require further treatments for charge transport applications.[58–61] The surface ligands also play a role in the preparation of homogeneous thin films or mono-layers of NCs. Further, ligands can also passivate the NC surface, which means that ligands terminate the dangling bonds that remain on the surface. One of the applications of NCs is related to light emission and its efficiency can be quantified in terms of the photoluminescence quantum yield (PLQY), a measure of the number of photons emitted as a fraction of the number of photons absorbed. Compared to a core-only NC, hetero-structures where the 'core' material is encapsulated by a shell of a semiconductor with higher bandgap prevents the ground-state exciton wavefunctions from reaching the surface.[36, 38] This can result in QDs having PLQY approaching 100%[62] (see section 1.2.5). The light emission in QDs can be observed in both spectral and time

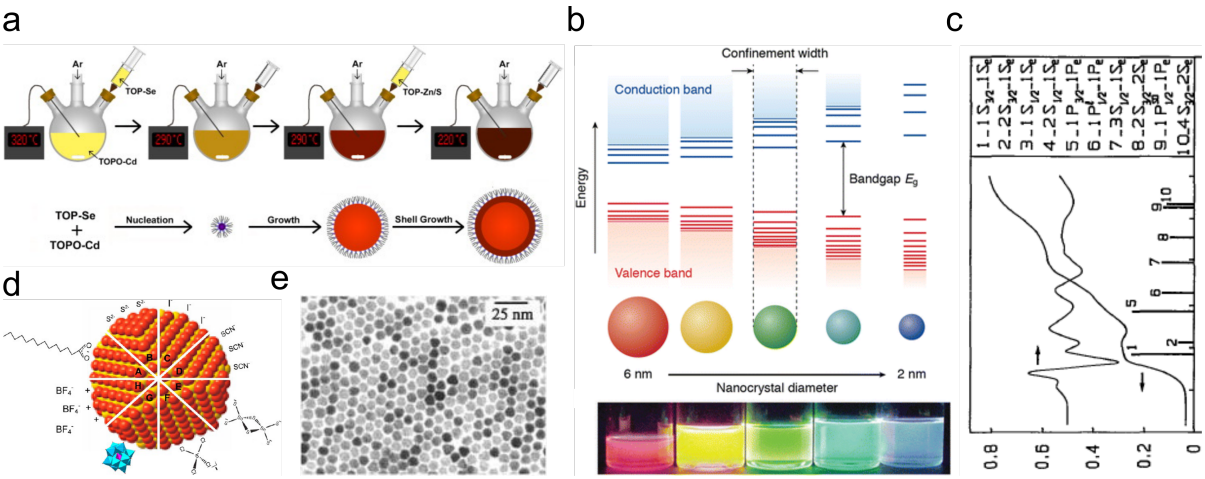

Figure 1.3. | Nanocrystals & quantum confinement effect. (a) Synthesis of CdSe NCs.[104] (b) The discrete energy levels in smaller sized nanocrystals are well separated near the band edges. The bandgap of nanocrystals increases when their size is reduced due to quantum confinement and correspondingly the fluorescence emission changes its color from red to blue.[105] (c) Absorption spectra of CdSe QDs showing optically allowed band edge transitions[106] (d) Structure of a nanocrystal with possible capping agents[51] (e) TEM images of CdSe quantum dots[39]

domain, from which it can be inferred that the relaxation pathway is not simple with the contribution of both radiative and non-radiative recombinations (see section 1.2.4).

The ability to tune the NC size and shape by different means[40, 45, 53–56] enables to control NC properties such as emission and absorption wavelengths because of the quantum size effect (see section 1.2.2) and thus can be chosen for suitable applications. NCs are used for several applications like bio-imaging or labeling,[63–67] bio-sensing[68–70] & bio-probes,[71, 72] absorption filters,[73] digital imagers,[74] photodetectors,[75] photovoltaics,[76–79] photocatalysis,[80–82] thermoelectrics,[83–85] lasers,[86–88] transistors,[89] spectrometers,[90] saturable absorbers,[91–94] LEDs,[95–100] and displays.[101–103]

1.2.2. Free particle model

A basic understanding of QDs can be obtained by a free particle model.[108] A free moving particle like electron (or hole) has a momentum $p = \hbar k$ where $\hbar = h/2\pi$ is the reduced Planck constant and $k = 2\pi/\lambda$ is the wavevector. Here λ is the de Broglie wavelength of the free electron. A free moving electron with mass m can be described by the time-independent Schrödinger equation:

$$-\frac{\hbar^2}{2m}\frac{d^2\Psi(x)}{dx^2} = E\Psi(x) \tag{1.1}$$

with $\Psi(x)$ representing the wavefunction of the electron, and E the energy of the electron.

The solutions to the above differential equation 1.1 are plane waves of the form:

$$\Psi(x) = \exp(ikx) \tag{1.2}$$

A free electron has a continuum of energy levels given by the dispersion relation:

$$E(k) = \frac{\hbar^2 k^2}{2m} \tag{1.3}$$

This solution shows that the energy of the electron is continuous having a parabolic form as a function of wavevector.

Particle in a 1-D box

Electrons in a bulk semiconductor experience a periodic potential caused by the atoms in the crystal lattice. For a simplification, the time-independent Schrödinger equation for an electron subjected to a potential in 1-dimension can be written as:

$$-\frac{\hbar^2}{2m^*}\frac{d^2\Psi(x)}{dx^2} + V(x)\Psi(x) = E\Psi(x) \tag{1.4}$$

where $V(x)$ describes the periodic potential set by the crystal lattice. Note that the free particle mass (m) is replaced by the effective mass (m^*) in bulk crystal to account for the interaction of the particle with the periodic crystal lattice. Since the potential is periodic over the lattice constant a, $V(x) = V(x+a)$. The wavefunction that still has the same Eigenvalue after translation over distance a can be written as:

$$\Psi_{bloch,k}(x) = u_k(x)\exp(ikx) \tag{1.5}$$

This wavefunction is called as Bloch function and is a plane wave ($\exp(ikx)$) modulated by a periodic function ($u_k(x)$). When the wavelength of electron is twice the lattice spacing i.e. $k = \pi/a$, electron is reflected by the periodic potential of the crystal lattice. The periodicity of the lattice causes the

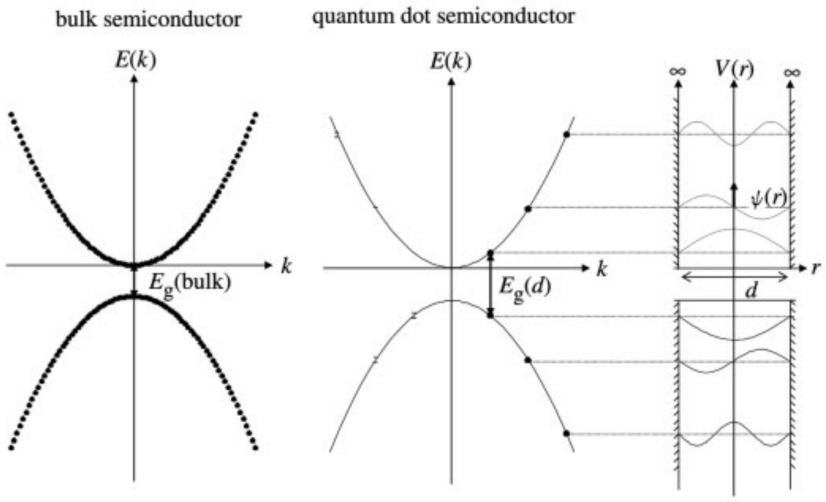

Figure 1.4. | Energy bands in semiconductors. Energy dispersion curve ($E \propto k^2$) for bulk crystal having quasi-continuous energy bands and QD having discrete energy levels. [image from reference[107]]

reflections to occur at every $k = n\pi/a$, where n is an integer. At other values, the energy of the electron can be approximated to that of the free electron. This leads to a dispersion relation containing multiple energy gaps, which are referred to as band gaps. This representation is called the extended Brillouin zone. Due to the periodicity in k, the wavefunctions with values of k that differ by $n2\pi/a$ are equivalent. This means that the energy dispersion relation may be restricted to values of k between $-\pi/a < k < \pi/a$ with the other interval values folded/reflected back into the first interval. This representation is called the first Brillouin zone or reduced Brillouin zone.[108]

Particle in a 3-D spherical box

Looking at the NC from a 'top-down' perspective, NCs are an intermediate between molecules (few atoms) and bulk crystals (millions of atoms in each spatial dimensions). The overlap of fewer numbers of atomic orbitals in NCs result in discrete levels instead of energy bands, called quantized energy levels. NCs made of a semiconductor have an energy bandgap between highest occupied level (originating from the valence band VB of bulk) and lowest unoccupied level (originating from the conduction band CB of bulk). When a photon having certain energy equal or above this energy gap is absorbed by the NC, an electron transit from the 'ground' state to 'excited' state forming a quasi-particle electron-hole pair state, also known as *exciton*.

The total wave function for a NC can be represented by the product of the Bloch function describing the bulk properties of the semiconductor, and the envelope function that describes the confinement effects of the charge carriers or exciton in the NC.

$$\Psi_{total}(x) = \Psi_{bloch}(x).\varphi_{env}(x) \tag{1.6}$$

Since the confinement is same in all directions in a NC, they can be better represented in the form of a spherical potential box. Here, the eigenfunctions are described as the product of a radial Bessel function $R_{nl}(r)$ and spherical harmonics $Y_{lm}(\theta, \phi)$:

$$\varphi_{env}(\theta, \phi, r) = R_{nl}(r).Y_{lm}(\theta, \phi) \tag{1.7}$$

As the electrons experience a spherical potential well of radius a, the potential is finite for $r < a$ and zero elsewhere. The solutions for the discrete energy levels of a confined electron in a spherical well after solving the Schrödinger equation is:

$$E_{nl} = \frac{\hbar^2 \chi_{nl}^2}{2m^* a^2} \tag{1.8}$$

where m^* is the effective mass of electrons (or holes) and χ_{nl} are the roots of the Bessel function. The values of χ_{nl} depend on principal quantum numbers n (1, 2, 3,...) and azimuthal quantum number l (0,1,2,..., corresponding to s, p, d,..., orbitals).[108] Since the envelope wave functions of the lowest lying energy levels resemble atomic discrete energy levels, NCs or QDs are also called as "artificial atoms". See Chapter 3 for more details on the quantum size level (lowest bandedge exciton energy level) in a QD.

1.2.3. Quantum confinement effect

The band gap of a QD is the sum of the fundamental bulk bandgap (E_g) and the confinement energy of both the electrons and holes. Including the Coulomb interaction energy, the energy of the ground to lowest excited state electron-hole pair or exciton in a QD of radius a is given by:[32]

$$E = E_g + \frac{\hbar^2\pi^2}{2a^2}\left(\frac{1}{m_e^*} + \frac{1}{m_h^*}\right) - \frac{1.8e^2}{\epsilon a} \tag{1.9}$$

where m_e^* & m_h^* are effective masses of electron & hole respectively and ϵ is the dielectric constant of the core material.

Equation 1.9 implies that the band gap of a NC becomes smaller with increasing size (inverse scaling with a^2 in an infinite barrier regime) if the Coulomb interaction is negligible (inverse scaling with a). Equations 1.8 and 1.9 show that discrete energy levels arise at the band-edges of both the CB and VB with different quantum numbers. The discrete energy levels in smaller sized QDs are well separated near the band edges. The bandgap of QDs increases when their size is reduced and correspondingly the fluorescence emission changes its color from red to blue (see Figure 1.3b). This phenomenon is called as *quantum confinement effect*. The relative magnitude of the confinement energy and the Coulomb interaction energy gives the QD its confinement regime. For a QD with size $a \ll a_B$ (bulk exciton Bohr radius), the confinement energy is greater than the Coulomb interaction energy and this is called as stronger confinement regime.

1.2.4. Relaxation pathways

Relaxation of the excited charge carriers back to the ground state involves several recombination pathways. The hot charge carriers in a state above the single particle ground states in CB and VB (neglecting coulomb interaction) initially thermalize to the bandgap level via electron-phonon and electron-hole interactions typically over a timescale of sub-picosecond to few picoseconds. After they reach the lowest single particle energy level (lowest level of CB & highest level of VB), the charge carriers can recombine either through radiative or non-radiative channels. While the radiative recombination results in the emission of photon, the non-radiative recombination can occur through either Auger scattering or trapping. There are also reports that surface ligands too influence the intraband-relaxation process in QDs.[109–112]

Auger channel: Since the electronic level differences can be much larger than the phonon spacings, also known as *phonon bottleneck* effect, the relaxation of hot charge carriers is expected to be slower in QDs.[113–115] But the electron relaxation happens in a much faster time scale (sub-picosecond to few picosecond) attributed to non-radiative Auger relaxation where the electron transfers the energy to the hole via their Coulomb interaction.[116–119] The biexciton (XX) state has two electron-hole pairs and trion (T) is a charged state with the presence of an electron-hole pair & an additional charge carrier being either electron (negative trion) or hole (positive trion). The recombination of one electron-hole pair in case of both XX & T can be radiative, releasing the energy as a photon. But it can also be non-radiative, transferring the energy to another charge carrier using which it moves to an another quantized energy level and this process of non-radiative channel is called Auger recombination. The Auger effect is also shown to be size-dependent because of the quantum confinement effect in QDs.[120] Considerable efforts have been made to design the nanocrystals, especially the heterostructures, to

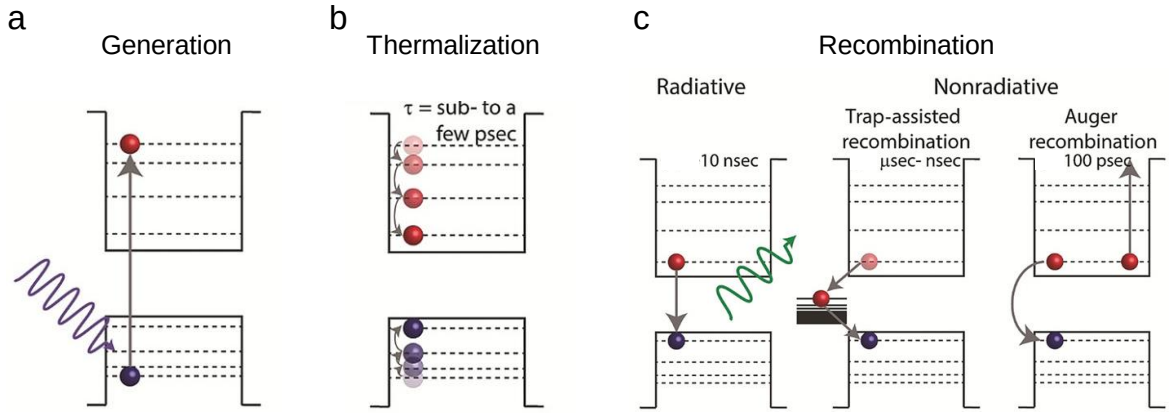

Figure 1.5. | Relaxation pathways. (a) Upon optical excitation, an electron-hole pair (aka exciton) is created. (b) Thermalization process relaxes the single carrier to the bandgap level. (c) Exciton recombination can be either radiative or non-radiative, with the latter assisted through trap states or Auger channel. [image from reference[124]]

slow down this Auger rate which involves thick shell, alloyed gradient shell[121, 122] and dimensional alteration.[123] Note that charging and the trion formation is ubiquitous in NCs.

> *The role of Auger process in quenching the radiative recombination of mulitple excitons is described in Chapter 2. Although the presence of Auger process in QDs might limit their use for light amplification applications like lasing, it leads to single photon emitters as multi-photon emission is quenched (see Chapter 2).*

Trap-assisted channel: In QDs, the presence of trap states resulting from several factors like structural defects, atomic vacancies, dangling bonds, and adsorbates at the interface can also influence their optical properties. One of the charge carriers in the electron-hole pair could get trapped in these sites via phonon emission and thus hamper their radiative recombination. Radiative recombination of the 'trapped charge carriers' can then happen with the photoluminescence substantially red-shifted from the ground state excitonic transition of a trap-free QD.

Stokes shift: The emission spectral line after the relaxation process is separated by certain energy from the band edge absorption peak which is called as Stokes shift. This is caused by several factors such as a size-dependent exchange interaction inducing fine structure split bandedge states,[125, 126] polydispersity,[127] vibrational (Franck–Condon) contribution via excited states[128] & surface ligands,[129] defects and trap states.[130–132] While this is undesired for light emitting diodes that require higher transition oscillator strength, the larger Stokes shifts in NCs find its application in solar concentrators.[133]

1.2.5. Heterostructures

Colloidal QDs synthesized in solution phase are surrounded by capping agents that play a significant role in their chemical reactivity (see section 1.2.1). Much progress has been made in improving the optical properties of QDs with hetero-structures approaching 100% PLQY.[62] Here, the core material is encapsulated by a shell of a semiconductor with higher bandgap that prevents the ground-state exciton wavefunctions from reaching the surface.[36, 38] Further, core materials surrounded by gradient

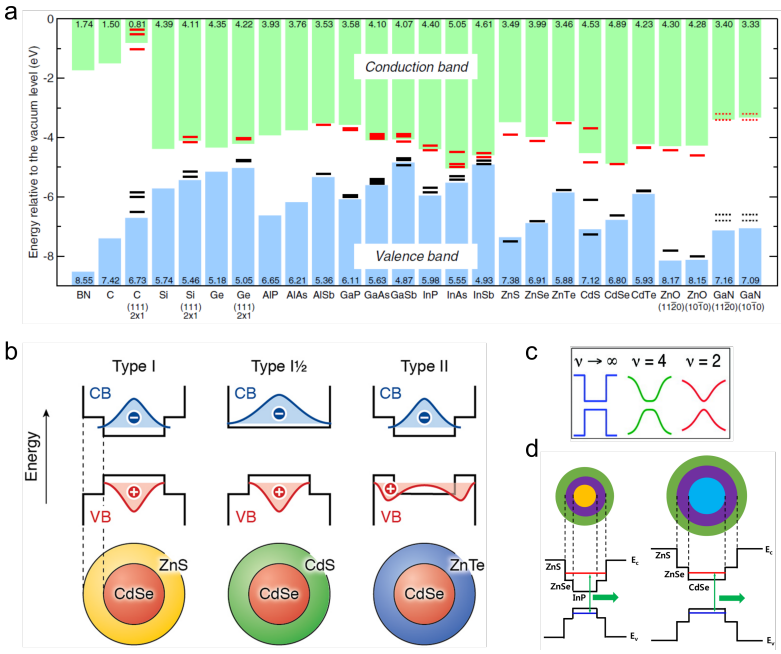

Figure 1.6. | Heterostructures. (a) Band alignment for different types of semiconductors.[135] (b) Three types of core/shell heterostructures in NCs.[105] (c) Smoothening of the confinement potential in graded-alloyed shell QDs. Here, ν controls the smoothness, and therefore the confining boundary becomes sharper with increasing ν value.[121] (d) Energy diagram and layer structure of multiple-shell QDs.[136]

shelled or multiple shelled QDs have been introduced for applications like lasing and solar cells where the 'smooth' interface rather than an 'abrupt' interface between core and shell reduces the Auger non-radiative recombination. This subsequently improves the optical gain by reducing the excitation intensity threshold for amplified spontaneous emission.[121, 122, 134] See section 1.3.2 for a description about spontaneous and stimulated emission processes. The optical properties of QDs depend on the spatial distribution of ground state electron and hole wave functions in such heterostructures having different band offsets (see Figure 1.6). In a type I structure, both the charge carriers in CB and VB are confined because of the difference in band offsets acting as an energy barrier that prevents escaping of charge carriers from core to shell. In type I 1/2 or quasi type II structure, one charge carrier is delocalized and the other is localized in either the core or the shell. In a type II structure, one charge carrier is localized in the core and the other in the shell. In multiple-shell structure, band offsets typically increase towards the surface with smaller lattice mismatches between adjacent shells reducing the interface strain while preventing the charge carrier leakage in such a cumulative thick shell. In type-I graded-alloyed shell structure, the composition varies continuously from the core to the shell, smoothening the confinement potential. There are also inverted type-I structure where both charge carriers are localized in the shell.

1.3. Single photon emitters

1.3.1. Non-classical light

With wave-particle duality and the quantization of light, the first quantum revolution enabled the advent of modern devices from transistors to lasers. Now we are on the verge of a second quantum re-

volution with devices that are able to generate, manipulate and measure the quantum states of light.[139] Quantized electromagnetic field consists of discrete particles known as photons and a single photon is one such quantum state of light. Single photon sources form an integral part in realizing quantum technological applications such as quantum computing,[140] quantum cryptography,[141–143] quantum simulation[144–146] and quantum metrology.[147, 148]

Quantum light or non-classical light, is the light that cannot be described using classical electromagnetism.[149, 150] Light emitting sources can be distinguished by measuring the temporal sequence of the emitted photons and defining the photon statistics for each cases (see Figure 1.7). The photons from classical light sources like a thermal light source arrive in bunches described as photon bunching. This is well represented by super-Poissonian statistics considering that the intensity fluctuations are higher with a standard deviation greater than $\sqrt{\text{mean}}$. Coherent light emitted from a laser has no preferred time interval between photons and thus they are completely uncorrelated described as random process. This can be represented by Poissonian statistics. A single quantum system like an atom emits only a single photon at a particular time and the next emission event can be well separated from the first emission which depends on the re-excitation and recombination rates. This is described as anti-bunching which has a sub-Poissonian photon statistics. A convenient method to identify if the source material can emit single photons is by measuring the second-order correlation function. A classical representation of this function is given by:[137]

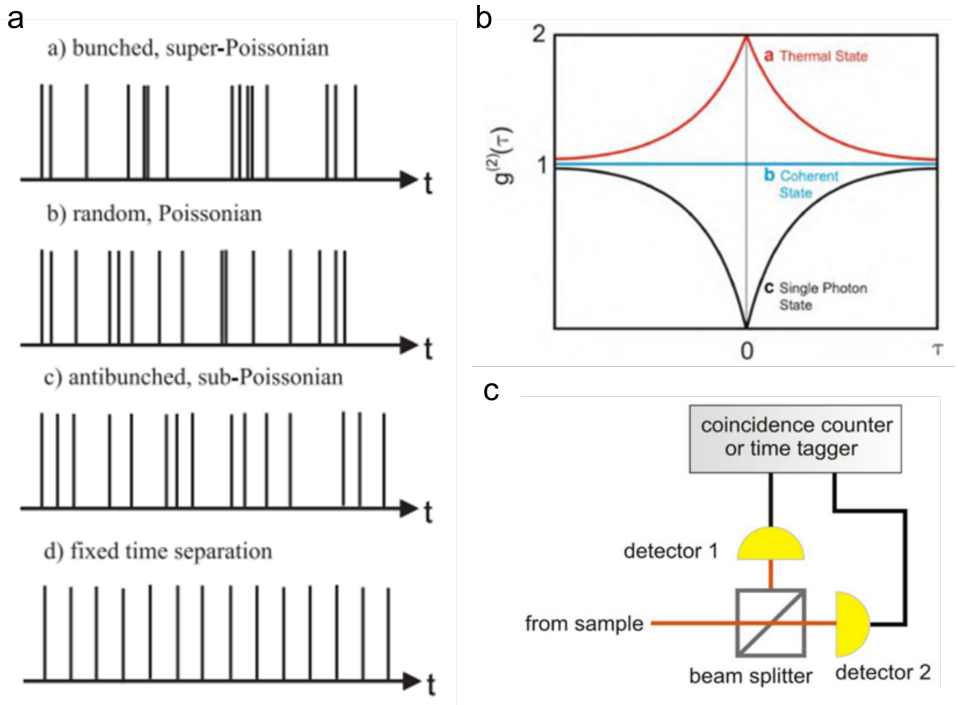

Figure 1.7. | Photon states. (a) Photon detection event in the case of thermal sources (bunch), laser (random), single photon source (antibunched). The bottom panel shows an 'on-demand' emitting ideal single photon source that has a fixed time separated event.[137] (b) Second order correlation function $g^2(t)$ for the three states of light mentioned above.[138] (c) Hanbury Brown Twiss setup to measure the $g^2(\tau)$ where the light emitted by the source is passed through a 50:50 beamsplitter and detected in two detectors. The event of arrival of time in the two detectors in coincidence is recorded in the time tag correlator to calculate correlation functions.[image from https://www.picoquant.com/quantum]

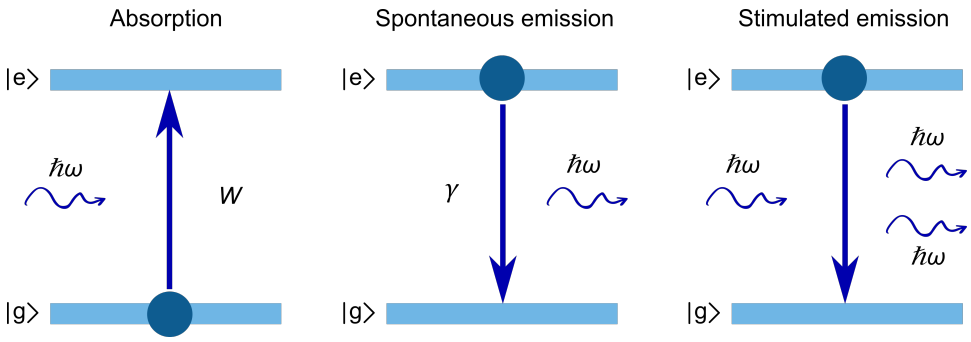

Figure 1.8. | Optical transitions in a two level system. Left: Absorption of a photon from ground state to excited state with a rate W. Middle: Spontaneous emission from the excited state to the ground state with a rate γ. Right: Stimulated emission by an another photon at the input by population inversion.

$$g^2(\tau) = \frac{\langle I(t)I(t+\tau)\rangle}{\langle I(t)\rangle^2} \tag{1.10}$$

where $I(t)$ and $I(t+\tau)$ are the measured intensities at time t and $t+\tau$. $g^2(\tau)$ describes the probability to measure a photon at time τ on condition that a first photon has been detected at time τ = 0. $g^2(\tau)$ is usually measured by a Hanbury-Brown and Twiss setup[151] where the light emitted by the source is passed through a 50:50 beam-splitter and detected in two detectors (see Figure 1.7c). The event of arrival of time in the two detectors in coincidence is recorded in the time tag correlator to calculate correlation functions.

1.3.2. Ideal quantum emitter

An ideal quantum emitter interacts only with the electromagnetic environment producing indistinguishable single photons with high purity ($g^2(0) = 0$), high brightness (probability that each emitted light pulse contains a single photon; this parameter includes source repetition rate, high transmission and detector efficiencies) and identical photon wavepackets.[152] A two-photon interference effect is commonly used to determine the indistinguishability since two identical single photons entering a 50:50 beam-splitter would leave from the same end because of the 'coalescing' behavior of photons. The degree of indistinguishability is measured using a Hong-Ou-Mandel setup where a delay is applied to the arrival times of the two single photons and the coincidence counts are monitored on the two output detectors.[153] Indistinguishable single photons can be expected if both the spatial and temporal overlaps of their wavepackets are identical in terms of emission frequency, pulse-width, spectral bandwidth, polarization, transverse mode profile and arrival time at the beam splitter.[138] In case of indistinguishable single photons from sources having Fourier-transform-limited spectral bandwidths, the coincidence counts would fall to zero at exactly the zero delay which is commonly known as Hong-Ou-Mandel (HOM) dip.

The photophysical mechanisms by which the single photons are generated varies for different kinds of emitters. An ideal single photon source like an atom should be a two-level system with a ground state $|g\rangle$ and an excited state $|e\rangle$. Einstein defined three processes for optical transitions in such a system such as: absorption, spontaneous emission and stimulated emission (see Figure 1.8). Upon absorption of a photon given by a rate W, an electron transitions from the ground to the excited state. Spontaneous emission is the process by which the electron transitions from the excited to the ground state by

releasing the energy as photon into the photon vacuum state with a rate γ. Stimulated emission is the process in which an electron transitions from the excited state to the ground state emitting a photon into a light mode due to the presence of one or more photons in this mode. A good single photon emitter has an enhanced spontaneous emission rate with a release of pure & indistinguishable single photon.

1.3.3. Implementations & technology

The first single photons were demonstrated in an attenuated sodium beam,[154, 155] and the cascaded atomic sources were also used for experiments on Bell's inequalities.[156–158] This was followed by single photon demonstration by means of ion traps.[159] The generation of single photons by two-level system like atoms are not reliable and less efficient with lower operation rates.[160] While single photons generated by attenuated laser or weak coherent pulse are suitable for quantum technologies,[161, 162] they are probabilistic in nature and are not ideal two-level quantum emitters. Heralded single photon sources using spontaneous parametric down-conversion[163, 164] set the benchmark for single-photon technology, but they are also probabilistic in nature, not scalable and have lower brightness.[165] On the other hand, solid-state emitters such as color centers or defects in crystalline hosts,[166–168] carbon nanotubes,[169] transition metal dichalcogenides,[170] epitaxial QDs[171–173] and colloidal QDs[174–177] are attractive as non-classical light sources because of the scalability of their host matrix system and their on-demand emission.

State-of-the-art single-photon sources based on solid-state materials are described in recent review articles.[152, 178] Among them, epitaxial QDs have progressed well since their first demonstration of single photon emission from an isolated single QD in the year 2000.[179] Key progresses are: deterministic fabrication of single photon sources (for scalability),[180] electrical excitation (for practical application),[181] resonant excitation (direct excitation into an excited state of the QD for pure single photon emission & indistinguishability by reducing the time jitter induced by non-resonant excitation),[182] coupling to nano-photonic structures (for enhancing the spontaneous emission and efficient photon extraction known under the term 'brightness'),[173, 183–186] infrared single photon sources (for telecom wavelength operation)[187] and frequency conversion (for converting the optimal single photon source from one wavelength to desired wavelength[188] and aligning the central emission energy of multiple QDs for indistinguishability[189]). The majority of the epitaxial QDs as single photon sources only operate at cryogenic temperatures with few exceptions depending on the type of material. For instance, III-nitride site-controlled nanowire QD was shown to be emitting single photons at room temperature.[190]

1.4. Colloidal quantum dots as single photon emitters

1.4.1. State-of-the-art technology

Colloidal QDs offer an extensive design freedom (both at the level of nanocrystal synthesis and device integration) as well as room temperature operation.[171] The economical and versatile synthesis routes of colloidal QDs allow the tuning of emission wavelength by changing their diameter, and they can be formed from several semiconductors. Moreover, colloidal synthesis methods offer a great control over the QD size and shape, and enable complex heterostructures to be formed. In addition, the resulting QD dispersion or inks can be readily combined with a multitude of technology platforms for further

processing. The solution-processed QDs can be efficiently integrated into silicon or silicon nitride photonic integrated circuits.[191]

For artificial atoms like QD to be a good single photon source, it needs to be operating as a two-level system for a spontaneous emission of single photon from a single exciton state. A type I structure in QDs (see section 1.2.5) has a stronger confinement and thus produces discrete exciton levels similar to atomic or molecular levels. Even under non-resonant excitation, the charge carriers relax back to the first excited state rapidly such that no emission from these higher excited states can be detected. Also, Auger process in QDs quenches the radiative recombination of the multiple excitons (see section 1.2.4). So the emission in QDs can be considered happening between the lowest two levels at room temperature which can make QDs behaving as a quasi two-level emitter.[192]

Room temperature photon antibunching in the luminescence of single colloidal QDs was first reported for CdSe/ZnS core/shell QDs and attributed to the highly efficient, non-radiative Auger recombination of multi-excitons.[193, 194] This enabled the emission of a single photon to be triggered by a high-intensity excitation pulse, with a near-unity probability of photo-excitation and a high-purity single photon emission.[174, 175] On the other hand, the further development of CdSe/ZnS QDs as single photon emitters stalled because of their intermittent fluorescence or blinking, which leads to an unpredictable succession of bright and dark periods.[174, 194, 195] In the case of CdSe/CdS core/shell QDs, it was shown that blinking can be suppressed by implementing sufficiently thick CdS shells.[196, 197] However, this approach leads to a significant reduction of the Auger recombination rate, possibly linked to the formation of alloyed interfaces (for instance, extension of the electron wavefunction in creating negatively charged trions). While the alloyed interfaces may reduce the lattice mismatch between core and shell, yet the shallow conduction band offset and smoothening of the potential barrier enhances the radiative recombination of multi-excitons. The concomitant promotion of the radiative recombination of multi-excitons reduces photon anti-bunching, an effect that is the more pronounced the higher the biexciton photoluminescence quantum yield.[198, 199] The same issue is faced by attempts to suppress blinking by speeding up radiative recombination through, for example, plasmonic effects.[200] Since accelerating radiative recombination shifts the balance between radiative and non-radiative Auger recombination of multi-excitons, blinking suppression by enhancing radiative recombination also results in a loss of purity of single photon emission.[201]

Currently, the focus of QD synthesis research is shifting to materials made from semiconductors that offer even better optical properties, such as caesium lead halide perovskites ($CsPbX_3$, X=Cl,Br,I), or have a composition non restricted by the toxicity regulations on heavy-metal ions in electronic and electro-optical devices, of which InP QDs are the most notable example. Rapidly after the first reports on their synthesis,[202] single $CsPbBr_3$ NCs were shown to exhibit photon anti-bunching and, in one study, reduced blinking.[203, 204] However, as these nanocrystals showed significant photodegradation, it remains unclear whether $CsPbBr_3$ nanocrytals can provide single photons on demand. Opposite from $CsPbBr_3$ nanocrystals, InP QDs received little attention, if any, as possible single-photon emitters even if first syntheses were developed shortly after the first hot injection synthesis of CdSe QDs.[205] Note that the electrically driven single photon sources based on colloidal CdSe/CdS QDs have only been recently reported.[206]

1.4.2. Key inhibiting factors

An ideal quantum emitter interacts only with the electromagnetic environment producing indistinguishable photons having a lifetime-limited spectral distribution, but the additional interaction with vibrational degrees of freedom and the environment results in more complex spectral features in QDs. Key inhibiting factors in using colloidal QDs for quantum photonics are described as:

- *Stability*: fluorescence emission of a QD stops over the time which is known as *bleaching* and fluorescence intermittency with the emission going to random on & off times known as *blinking*. See Chapter 2.
- *Fine structure*: electronic structure of a QD contains exciton-manifolds in the band-edge arising from the contribution of electron-hole exchange interaction and shape anisotropy. See Chapter 3.
- *Dephasing*: loss of coherence of the emitter affecting the phase stability of the light and ultimately broadening the spectral linewidth, which reduces the indistiguishability. See Chapter 4.
- *Spectral diffusion or jitter or wandering*: fluorescence energy shift with time attributed to the charge fluctuations in and around the QD environment. See Chapter 5.

  Note: Spectral linewidth of a QD is naturally broadened by the radiative lifetime (average time the excited charge carriers take to relax back to the ground state). However, the dephasing time in QD is typically much faster than the radiative lifetime. Overall, a single QD is broadened by the cumulative effect of lifetime, fine structure, dephasing by phonon-assisted transitions between the fine structure states, and phonon-assisted emission and spectral diffusion. Moreover, there are size & shape dependent variations in the aforementioned properties for QDs.
- *Non-deterministic integrated source*: Demonstration of pure single photon emission from a deterministically positioned single QD on a silicon chip is the stepping stone for scalability. This will be required for ultimately describing factors (unreported for colloidal QDs) such as indistinguishability and brightness. This is a also prerequisite for coupling the QDs to nanophotonic devices to further improve their optical properties. For instance, the typical lifetime of colloidal QD ranges in few tens of nanoseconds and therefore a mechanism to enhance the spontaneous emission rate is critical for higher rate operation. See Chapter 6.

1.5. Materials & methods

1.5.1. Colloidal InP quantum dots

Both the fundamental knowledge of optical properties in QDs and the improvement in their synthesis with a precise 'engineered' control of dimensions, shape and composition has been achieved with the detailed study on CdSe QDs belonging to II-VI group for visible wavelength range and PbS QDs

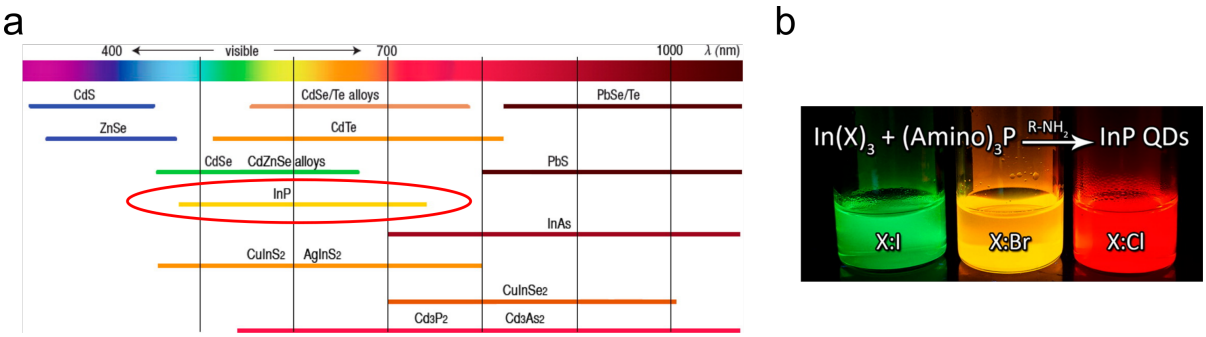

Figure 1.9. | Colloidal InP QDs. (a) Spectral range of emission for the most widely studied types of semiconductor NCs.[207] (b) In this dissertaion, InP QDs synthesized using indium halide and aminophosphine precusors are studied. Replacing $In(Cl)_3$ by $In(Br)_3$ or $In(I)_3$ leads to InP QDs with smaller diameters at the end of the reaction and therefore variations in their emission wavelength.[208]

belonging to IV-VI group for infrared wavelength range. The rising concern over using the heavy metal ions in the end user applications have necessitated the synthesis of QDs constituted of nontoxic and earth-abundant materials.[207] One of the promising alternative semiconductor material in the visible-near infrared range is InP belonging to III-V group. Though indium belong to smaller earth abundant material, it does not have the toxicity of Cd.[207, 209–211]

For convenience, CdSe QDs are taken as prototypical material in comparison to explain the optical properties of InP. The first difference is the cubic (zincblende) crystal structure in InP whereas it is hexagonal (wurtzite) structure for CdSe where there is an additional in-built crystal field splitting contributing to the fine structure. Note that the CdSe QDs can also be synthesized with a zincblende structure. Zincblende structure usually has a T_d point-group symmetry. In contrast to ionic bonds in II-VI group materials like CdSe, InP belonging to III-V group has a more covalent bond formation which is stronger and thus requires a high temperature, longer reaction times and more reactive precursors for their synthesis. InP is prone to oxidation, requiring stringent air-free conditions during synthesis and subsequent protection with an appropriate shell material.[211] InP QDs have traditionally broader ensemble emission spectra and larger Stokes shifts than the counterpart CdSe QDs.[132] The reason for this is still under discussion with reasons including polydispersity or fine structure or vibrational contribution or emission from trapped states. InP has a larger exciton Bohr radius of about 10 nm (1.35 eV bandgap) compared to about 5 nm (1.7 eV bandgap) in CdSe and thus they could experience a stronger quantum confinement effect for a similar sized QD. This could explain the broadened ensemble emission spectra in InP compared to CdSe since a mere change in the size distribution could result in a shift in the peak emission energies. Though it is difficult to predict the size-dependent energies owing to their oxidation and poor contrast in TEM images, some studies observed a steeper relation between the bandgap and size in InP compared to CdSe.[132, 212–214] Such discrepancies call for a more in-depth study on the exciton properties in InP QDs.

1.5.2. Synthesis of InP/ZnSe quantum dots

Initially, the dehalosilylation reaction[215, 216] using tris(trimethylsilyl)phosphine as phosphorous precursor was modified by Micic *et al.*[205] to synthesize colloidal InP QDs. Following the procedure of CdSe QDs that allowed better control of the particle growth,[35] Micic *et al.* synthesized InP QDs in the presence of coordinating trioctylphosphine (TOP) and trioctylphosphine oxide (TOPO) solvent. This was followed by several methods of synthesis of InP QDs: using a size-selective precipitation

to control the size of particles,[217] using a non-coordinating solvent and fatty acid as ligands,[218] low temperature (<190 °C) synthesis by the activation of In carboxylate precursors with fatty amines,[219] and using air-stable & low-cost calcium phosphide as phosphorous precursor.[220]

More recently, a further approach to form InP-based QDs has been introduced, based on aminophosphines as the phosphorous precursor.[208, 221, 222] This method enabled a variety of InP-based core/shell QDs to be formed with widely tunable optical properties. The type I heterostructures formed are suitable for single photon emission (see section 2.1.1). In this respect, the InP/ZnSe core/shell combination is interesting for quantum photonics. It features a similar band alignment as CdSe/ZnS, yet the InP/ZnSe lattice mismatch amounts to a mere 3%, in contrast to the 12% mismatch between CdSe and ZnS. Although the atomistic origin of blinking in QDs is still debated,[223] the low-strain, type I combination offered by the InP/ZnSe core/shell system could offer a pathway to reconcile non-blinking characteristics with single-photon emission by colloidal QDs. Note that InP/ZnS is also a type I structure with higher barriers but with a lattice mismatch of 7.7%.

Here in this dissertation, thiol-capped InP/ZnSe QDs were synthesized by *Dr. Dorian Dupont (Ghent University, Belgium)* using an economical aminophosphine-based precursor enabling to work under ambient condition.[208, 224] To obtain 10-nm core/shell structures with a 3.2-nm core diameter, the following procedure was applied. 50 mg (0.23 mmol) of indium(III) chloride and 150 mg (1.1 mmol) of zinc(II) chloride are first mixed in 2.5 ml (7.5 mmol) of technical oleylamine (OLA). The reaction mixture is stirred and degassed at 120 °C for an hour and then heated to 180 °C under inert atmosphere. Upon reaching 180 °C, the synthesis of InP nanocrystals is initiated by quickly injecting a volume of 0.23 ml (0.8 mmol) of tris(diethylamino)phosphine in the above mixture. After a reaction time of 20 min, 3.2-nm InP QD cores are formed. The formation of the ZnSe shell is initiated by injecting 0.45 ml of stoichiometric TOP-Se (2.24 M). At 140 min, a mixture of 2 g (3 mmol) of Zn(stearate)$_2$, 8 ml of octadecene (ODE) and 2 ml of OLA is injected. The temperature is increased from 180 °C to 320 °C and 1.4 ml of TOP-Se is injected drop by drop during the rise of temperature. At 240 min, the reaction is stopped. InP/ZnSe QDs are then precipitated once in ethanol and suspended in toluene.

1.6. Dissertation structure

In addition to a brief history of nanotechnology, the current **Chapter 1** gives a basic understanding of QDs required to understand the following chapters. This chapter also addresses the colloidal InP/ZnSe QDs to be investigated in this dissertation. *Highlight:* Key inhibiting factors in using colloidal QDs for quantum photonics are also described.

Which non-classical photonic property is discussed? **Chapter 2** discusses the characterization results on both ensemble and single InP/ZnSe QDs at room temperature under optical excitation. *Highlight:* Single InP/ZnSe core/shell QDs exhibiting type I structure is an efficient single photon emitter demonstrated by a strong antibunching at room temperature even at saturation intensities. This is attributed to the fast Auger recombination of multiple excitons. Single QDs display very little blinking which places these QDs in the class of nearly blinking-free QDs, with emission stability comparable to state-of-the-art thick-shell and alloyed-interface CdSe/CdS.

How does the electronic structure looks like? **Chapter 3** describes the band edge exciton energy level structure of InP/ZnSe QDs by combining micro-PL spectroscopy on single QDs and fluorescence line narrowing (FLN) spectroscopy on ensemble of QDs at cryogenic temperature. The exchange interaction splits the eight-fold degenerate band edge exciton levels into an optically dark low energy quintuplet and a high energy bright triplet states. Depending on the excitation power, single QDs

show emissions from bright exciton as a doublet, a trion singlet and a biexciton doublet that all show a pronounced polarization. FLN spectra of an ensemble of QDs in magnetic fields demonstrate that the bright exciton effectively consists of three states. *Highlight:* The Zeeman splitting of these states is well described by an isotropic exciton model, where the fine structure is dominated by electron-hole exchange and shape anisotropy only leads to a minor splitting of the bright triplet, all because of the particular ratio of light and heavy hole masses naturally occurring in InP material.

What factors influence the decoherence in exciton emission ultimately limiting the homogeneous linewidth? **Chapter 4** discusses the exciton dephasing and population dynamics using transient resonant four wave mixing (FWM) spectroscopy on ensemble of InP/ZnSe QDs. In photon echo experiment (5 K - 31 K), the FWM signal decays with an initial sub-picosecond component followed by a mono-exponential component at longer delay times which is a representation of acoustic phonon sidebands & exciton ZPL respectively. ZPL linewidth and ZPL weight with respect to the phonon sidebands are reported at cryogenic temperatures. The recombination rate of exciton is deduced from the transient grating experiment from 5 K - 107 K and the radiative lifetime values of bright & dark exciton and the energy splitting between them are reported. *Highlight:* Contrary to a rapid spin-flip mediated dephasing from bright-to-dark exciton in CdSe QDs, the exciton ZPL dephasing in InP QDs is explained by the domination of phonon-scattering within the closely spaced bright exciton triplets. Further, the correspondence between ZPL of the narrowest single QD (50 ± 1 μeV at 5 K) and the homogeneous linewidth obtained using FWM (56.8 ± 2.1 μeV at 5 K) indicates the presence of band edge exciton rather than a trap assisted recombination hitherto believed to be prevalent in InP core/shell QDs. Note that this linewidth is not lifetime-limited.

How does the charge fluctuations affect the optical properties in QDs which usually have a larger surface to volume ratio? Using micro-PL spectroscopy at cryogenic temperature on single InP/ZnSe QDs, **Chapter 5** discusses the polarizability of exciton, biexciton and trion by correlating their level of spectral shifts due to quantum confined stark effect (QCSE). *Highlight:* QCSE is reduced in multiple-exciton species than neutral exciton, because the presence of an external charge on the QD surface splits electron & hole and thus weakening their mutual interaction (V_{eh}) which has a stronger effect than electron-electron (V_{ee}) or hole-hole (V_{hh}) interaction. Using InP/ZnSe QDs as an optimized system to minimize spectral diffusion (SD), a theoretical understanding of the structural conditions that determine the magnitude of QCSE in core-shell QDs is provided. As such, minimal SD can be expected for strongly confined cores (large band-offset, moderately small core) and multi-excitonic species.

Is it possible to have an integrated single photon sources based on colloidal QDs in silicon chip? **Chapter 6** describes how silicon nitride photonics platform is favorable for integration of colloidal QDs. Accordingly, a deterministic positioning of single InP/ZnSe QDs from solution phase to silicon chip is attempted using electron-beam lithography, but with a result of 'probabilistic' 30% accuracy. *Highlight:* On-chip emission from single QD embedded in silicon nitride waveguide is demonstrated. While the collection efficiency currently limits the demonstration of single photon emission with high purity, there are greater prospects to further improve the design which are also discussed in this chapter.

Chapter 7 recaps the main results while addressing the title question of this dissertation. Further, possible future directions in using colloidal QDs for quantum photonics are also discussed. *Highlight:* While indistinguishable photons are obligatory for a quantum information processing applications such as qubits, it is not necessary for quantum cryptography like random number generator which only requires a high pure single photon emission at room temperature. Colloidal QDs could be suitable for this application except that the emission needs to be stable and free from blinking.

Appendix A lists the journal articles and conference papers & presentations. **Appendix B** lists the acronyms. **Appendix C** lists the spectroscopy methods employed and the layout of the optical set-ups. **Appendix D** lists the acknowledgements.

Bibliography

[1] Richard P. Feynman. There's plenty of room at the bottom. *Engineering and Science*, 23(5):22–36, feb 1960.

[2] Richard P. Feynman, Robert B. Leighton, Matthew Sands, and E. M. Hafner. The feynman lectures on physics; vol. i. *American Journal of Physics*, 33(9):750–752, sep 1965.

[3] N. Taniguchi. On the basic concept of nano-technology. *Proceedings of the International Conference on Production Engineering (Tokyo)*, Part II, 1974.

[4] Noriaki Oyabu, Óscar Custance, Insook Yi, Yasuhiro Sugawara, and Seizo Morita. Mechanical vertical manipulation of selected single atoms by soft nanoindentation using near contact atomic force microscopy. *Physical Review Letters*, 90:176102, may 2003.

[5] Ian Freestone, Nigel Meeks, Margaret Sax, and Catherine Higgitt. The lycurgus cup — a roman nanotechnology. *Gold Bulletin*, 40(4):270–277, dec 2007.

[6] Philippe Sciau, Claude Mirguet, Christian Roucau, Delhia Chabanne, and Max Schvoerer. Double nanoparticle layer in a 12th century lustreware decoration: Accident or technological mastery? *Journal of Nano Research*, 8:133–139, sep 2009.

[7] Jar - abbasid caliphate (750–1258), 9th century.

[8] Philippe Walter, Eléonore Welcomme, Philippe Hallégot, Nestor J. Zaluzec, Christopher Deeb, Jacques Castaing, Patrick Veyssière, René Bréniaux, Jean-Luc Lévêque, and Georges Tsoucaris. Early use of PbS nanotechnology for an ancient hair dyeing formula. *Nano Letters*, 6(10):2215–2219, oct 2006.

[9] M. Reibold, P. Paufler, A. A. Levin, W. Kochmann, N. Pätzke, and D. C. Meyer. Carbon nanotubes in an ancient damascus sabre. *Nature*, 444(7117):286–286, nov 2006.

[10] Henry Fountain. Nanotechnology in Sabres From Damascus, a New Look at the Seafloor and Predicting Reef Damage. *The New York Times*, November 2006.

[11] G. Chiari, R. Giustetto, J. Druzik, E. Doehne, and G. Ricchiardi. Pre-columbian nanotechnology: reconciling the mysteries of the maya blue pigment. *Applied Physics A*, 90(1):3–7, oct 2007.

[12] Manuel Sánchez del Río, Antonio Doménech, María Teresa Doménech-Carbó, María Luisa Vázquez de Agredos Pascual, Mercedes Suárez, and Emilia García-Romero. The maya blue pigment. In *Developments in Clay Science*, pages 453–481. Elsevier, 2011.

[13] photo (JanBaptiste de Bethune) Source: (Saint-Bavo's cathedral Ghent), www.lukasweb.be Art in Flanders.

[14] Covered cup accessed from `https://clevelandart.org/art/1947.274`.

[15] Xin Tang, Matthew M. Ackerman, Menglu Chen, and Philippe Guyot-Sionnest. Dual-band infrared imaging using stacked colloidal quantum dot photodiodes. *Nature Photonics*, 13(4):277–282, feb 2019.

[16] Daisuke Onoshima, Hiroshi Yukawa, and Yoshinobu Baba. Multifunctional quantum dots-based cancer diagnostics and stem cell therapeutics for regenerative medicine. *Advanced Drug Delivery Reviews*, 95:2–14, dec 2015.

[17] CES 2019 | Vizio's New TV Lineup Includes P-Series Quantum X, January 2019.

[18] Nicole Grobert. Carbon nanotubes – becoming clean. *Materials Today*, 10(1-2):28–35, jan 2007.

[19] L. B. Hunt. The true story of purple of cassius. *Gold Bulletin*, 9(4):134–139, dec 1976.

[20] UV Light accessed from http://solar-center.stanford.edu/about/uvlight.html.

[21] M. A. Reed. Spatial quantization in GaAs–AlGaAs multiple quantum dots. *Journal of Vacuum Science & Technology B: Microelectronics and Nanometer Structures*, 4(1):358, jan 1986.

[22] M. A. Reed, J. N. Randall, R. J. Aggarwal, R. J. Matyi, T. M. Moore, and A. E. Wetsel. Observation of discrete electronic states in a zero-dimensional semiconductor nanostructure. *Physical Review Letters*, 60:535–537, feb 1988.

[23] Thomas Graham. X. liquid diffusion applied to analysis. *Philosophical Transactions of the Royal Society of London*, 151:183–224, jan 1861.

[24] David Thompson. Michael faraday's recognition of ruby gold: the birth of modern nanotechnology. *Gold Bulletin*, 40(4):267–269, dec 2007.

[25] Richard Zsigmondy. Die chemische natur des cassiusschen goldpurpurs;. *Justus Liebig's Annalen der Chemie*, 301(2-3):361–387, 1898.

[26] Peter P. Edwards and John Meurig Thomas. Gold in a metallic divided state—from faraday to present-day nanoscience. *Angewandte Chemie International Edition*, 46(29):5480–5486, jul 2007.

[27] H.P. Rooksby. The colour of selenium ruby glasses. *Journal of the Society of Glass Technology*, 16(171–181), 1932.

[28] AA Onushchenko AI Ekimov. Quantum size effect in three-dimensional microscopic semiconductor crystals. *Journal of Experimental and Theoretical Physics Letters*, 34(6):345–349, sep 1981.

[29] Efros A.L Efros A.L. Interband absorption of light in a semiconductor sphere. *Soviet Physics Semiconductors*, 16(7):772–775, 1982.

[30] R. Rossetti, S. Nakahara, and L. E. Brus. Quantum size effects in the redox potentials, resonance raman spectra, and electronic spectra of CdS crystallites in aqueous solution. *The Journal of Chemical Physics*, 79(2):1086–1088, jul 1983.

[31] R. Rossetti, J. L. Ellison, J. M. Gibson, and L. E. Brus. Size effects in the excited electronic states of small colloidal CdS crystallites. *The Journal of Chemical Physics*, 80(9):4464–4469, may 1984.

[32] L. E. Brus. Electron–electron and electron-hole interactions in small semiconductor crystallites: The size dependence of the lowest excited electronic state. *The Journal of Chemical Physics*, 80(9):4403–4409, 1984.

[33] Victor K. LaMer and Robert H. Dinegar. Theory, production and mechanism of formation of monodispersed hydrosols. *Journal of the American Chemical Society*, 72(11):4847–4854, nov 1950.

[34] J.Th.G. Overbeek. Monodisperse colloidal systems, fascinating and useful. *Advances in Colloid and Interface Science*, 15(3-4):251–277, mar 1982.

[35] C. B. Murray, D. J. Norris, and M. G. Bawendi. Synthesis and characterization of nearly monodisperse CdE (e = sulfur, selenium, tellurium) semiconductor nanocrystallites. *Journal of the American Chemical Society*, 115(19):8706–8715, sep 1993.

[36] Margaret A. Hines and Philippe Guyot-Sionnest. Synthesis and characterization of strongly luminescing ZnS-capped CdSe nanocrystals. *The Journal of Physical Chemistry*, 100(2):468–471, jan 1996.

[37] Xiaogang Peng, Michael C. Schlamp, Andreas V. Kadavanich, and A. P. Alivisatos. Epitaxial growth of highly luminescent CdSe/CdS core/shell nanocrystals with photostability and electronic accessibility. *Journal of the American Chemical Society*, 119(30):7019–7029, jul 1997.

[38] B. O. Dabbousi, J. Rodriguez-Viejo, F. V. Mikulec, J. R. Heine, H. Mattoussi, R. Ober, K. F. Jensen, and M. G. Bawendi. (CdSe)ZnS core-shell quantum dots: synthesis and characterization of a size series of highly luminescent nanocrystallites. *The Journal of Physical Chemistry B*, 101(46):9463–9475, nov 1997.

[39] Xiaogang Peng, J. Wickham, and A. P. Alivisatos. Kinetics of II-VI and III-v colloidal semiconductor nanocrystal growth: "focusing" of size distributions. *Journal of the American Chemical Society*, 120(21):5343–5344, jun 1998.

[40] Xiaogang Peng, Liberato Manna, Weidong Yang, Juanita Wickham, Erik Scher, Andreas Kadavanich, and A. P. Alivisatos. Shape control of CdSe nanocrystals. *Nature*, 404(6773):59–61, mar 2000.

[41] C. B. Murray, C. R. Kagan, and M. G. Bawendi. Synthesis and characterization of monodisperse nanocrystals and close-packed nanocrystal assemblies. *Annual Review of Materials Science*, 30(1):545–610, aug 2000.

[42] Tito Trindade, Paul O'Brien, and Nigel L. Pickett. Nanocrystalline semiconductors: synthesis, properties, and perspectives. *Chemistry of Materials*, 13(11):3843–3858, nov 2001.

[43] Yadong Yin and A. Paul Alivisatos. Colloidal nanocrystal synthesis and the organic–inorganic interface. *Nature*, 437(7059):664–670, sep 2004.

[44] Jongnam Park, Kwangjin An, Yosun Hwang, Je-Geun Park, Han-Jin Noh, Jae-Young Kim, Jae-Hoon Park, Nong-Moon Hwang, and Taeghwan Hyeon. Ultra-large-scale syntheses of monodisperse nanocrystals. *Nature Materials*, 3(12):891–895, nov 2004.

[45] Clemens Burda, Xiaobo Chen, Radha Narayanan, and Mostafa A. El-Sayed. Chemistry and properties of nanocrystals of different shapes. *Chemical Reviews*, 105(4):1025–1102, apr 2005.

[46] Xun Wang, Jing Zhuang, Qing Peng, and Yadong Li. A general strategy for nanocrystal synthesis. *Nature*, 437(7055):121–124, sep 2005.

[47] Jongnam Park, Jin Joo, Soon Gu Kwon, Youngjin Jang, and Taeghwan Hyeon. Synthesis of monodisperse spherical nanocrystals. *Angewandte Chemie International Edition*, 46(25):4630–4660, jun 2007.

[48] D. J. Norris, A. L. Efros, and S. C. Erwin. Doped nanocrystals. *Science*, 319(5871):1776–1779, mar 2008.

[49] Nikolai Gaponik, Stephen G. Hickey, Dirk Dorfs, Andrey L. Rogach, and Alexander Eychmüller. Progress in the light emission of colloidal semiconductor nanocrystals. *Small*, 6(13):1364–1378, jun 2010.

[50] Jin Young Kim, Oleksandr Voznyy, David Zhitomirsky, and Edward H. Sargent. 25th anniversary article: Colloidal quantum dot materials and devices: A quarter-century of advances. *Advanced Materials*, 25(36):4986–5010, sep 2013.

[51] Maksym V. Kovalenko, Liberato Manna, Andreu Cabot, Zeger Hens, Dmitri V. Talapin, Cherie R. Kagan, Victor I. Klimov, Andrey L. Rogach, Peter Reiss, Delia J. Milliron, Philippe Guyot-Sionnnest, Gerasimos Konstantatos, Wolfgang J. Parak, Taeghwan Hyeon, Brian A. Korgel, Christopher B. Murray, and Wolfgang Heiss. Prospects of nanoscience with nanocrystals. *ACS Nano*, 9(2):1012–1057, jan 2015.

[52] Michael A. Boles, Daishun Ling, Taeghwan Hyeon, and Dmitri V. Talapin. The surface science of nanocrystals. *Nature Materials*, 15(2):141–153, jan 2016.

[53] Liberato Manna, Erik C. Scher, and A. Paul Alivisatos. Synthesis of Soluble and Processable Rod-, Arrow-, Teardrop-, and Tetrapod-Shaped CdSe Nanocrystals. *Journal of the American Chemical Society*, 122(51):12700–12706, dec 2000.

[54] Liang shi Li, Jiangtao Hu, Weidong Yang, and A. Paul Alivisatos. Band gap variation of size- and shape-controlled colloidal CdSe quantum rods. *Nano Letters*, 1(7):349–351, jul 2001.

[55] Feng Wang, Yu Han, Chin Seong Lim, Yunhao Lu, Juan Wang, Jun Xu, Hongyu Chen, Chun Zhang, Minghui Hong, and Xiaogang Liu. Simultaneous phase and size control of upconversion nanocrystals through lanthanide doping. *Nature*, 463(7284):1061–1065, feb 2010.

[56] S. Ithurria, M. D. Tessier, B. Mahler, R. P. S. M. Lobo, B. Dubertret, and Al. L. Efros. Colloidal nanoplatelets with two-dimensional electronic structure. *Nature Materials*, 10(12):936–941, oct 2011.

[57] C. B. Murray, C. R. Kagan, and M. G. Bawendi. Self-organization of CdSe nanocrystallites into three-dimensional quantum dot superlattices. *Science*, 270(5240):1335–1338, nov 1995.

[58] Yao Liu, Markelle Gibbs, James Puthussery, Steven Gaik, Rachelle Ihly, Hugh W. Hillhouse, and Matt Law. Dependence of carrier mobility on nanocrystal size and ligand length in PbSe nanocrystal solids. *Nano Letters*, 10(5):1960–1969, may 2010.

[59] Andrew W. Wills, Moon Sung Kang, Ankur Khare, Wayne L. Gladfelter, and David J. Norris. Thermally degradable ligands for nanocrystals. *ACS Nano*, 4(8):4523–4530, jul 2010.

[60] A. J. Nozik, M. C. Beard, J. M. Luther, M. Law, R. J. Ellingson, and J. C. Johnson. Semiconductor quantum dots and quantum dot arrays and applications of multiple exciton generation to third-generation photovoltaic solar cells. *Chemical Reviews*, 110(11):6873–6890, nov 2010.

[61] Fan Xu, Xin Ma, Chelsea R. Haughn, Jamie Benavides, Matthew F. Doty, and Sylvain G. Cloutier. Efficient exciton funneling in cascaded PbS quantum dot superstructures. *ACS Nano*, 5(12):9950–9957, nov 2011.

[62] Michel Nasilowski, Piernicola Spinicelli, Gilles Patriarche, and Benoît Dubertret. Gradient CdSe/CdS quantum dots with room temperature biexciton unity quantum yield. *Nano Letters*, 15(6):3953–3958, may 2015.

[63] Marcel Bruchez, Mario Moronne, Peter Gin, Shimon Weiss, and A. Paul Alivisatos. Semiconductor nanocrystals as fluorescent biological labels. *Science*, 281(5385):2013–2016, sep 1998.

[64] Warren C. W. Chan and Shuming Nie. Quantum dot bioconjugates for ultrasensitive nonisotopic detection. *Science*, 281(5385):2016–2018, sep 1998.

[65] X. Michalet, F. F. Pinaud, L. A. Bentolila, J. M. Tsay, S. Doose, J. J. Li, G. Sundaresan, A. M. Wu, S. S. Gambhir, and S. Weiss. Quantum dots for live cells, in vivo imaging, and diagnostics. *Science*, 307(5709):538–544, jan 2005.

[66] Igor L. Medintz, H. Tetsuo Uyeda, Ellen R. Goldman, and Hedi Mattoussi. Quantum dot bioconjugates for imaging, labelling and sensing. *Nature Materials*, 4(6):435–446, jun 2005.

[67] Min Fang, Ming Chen, Lulu Liu, and Yan Li. Applications of quantum dots in cancer detection and diagnosis: A review. *Journal of Biomedical Nanotechnology*, 13(1):1–16, jan 2017.

[68] Igor L. Medintz, Aaron R. Clapp, Hedi Mattoussi, Ellen R. Goldman, Brent Fisher, and J. Matthew Mauro. Self-assembled nanoscale biosensors based on quantum dot FRET donors. *Nature Materials*, 2(9):630–638, aug 2003.

[69] Christof M. Niemeyer. Functional hybrid devices of proteins and inorganic nanoparticles. *Angewandte Chemie International Edition*, 42(47):5796–5800, dec 2003.

[70] Rebecca C. Somers, Moungi G. Bawendi, and Daniel G. Nocera. CdSe nanocrystal based chem-/biosensors. *Chemical Society Reviews*, 36(4):579, 2007.

[71] Yongfen Chen and Zeev Rosenzweig. Luminescent CdS quantum dots as selective ion probes. *Analytical Chemistry*, 74(19):5132–5138, oct 2002.

[72] Wei Jun Jin, María T. Fernández-Argüelles, José M. Costa-Fernández, Rosario Pereiro, and Alfredo Sanz-Medel. Photoactivated luminescent CdSe quantum dots as sensitive cyanide probes in aqueous solutions. *Chemical Communications*, pages 883–885, 2005.

[73] N. F. Borrelli, D. W. Hall, H. J. Holland, and D. W. Smith. Quantum confinement effects of semiconducting microcrystallites in glass. *Journal of Applied Physics*, 61(12):5399–5409, jun 1987.

[74] Stijn Goossens, Gabriele Navickaite, Carles Monasterio, Shuchi Gupta, Juan José Piqueras, Raúl Pérez, Gregory Burwell, Ivan Nikitskiy, Tania Lasanta, Teresa Galán, Eric Puma, Alba Centeno, Amaia Pesquera, Amaia Zurutuza, Gerasimos Konstantatos, and Frank Koppens. Broadband image sensor array based on graphene–CMOS integration. *Nature Photonics*, 11(6):366–371, may 2017.

[75] Gerasimos Konstantatos, Ian Howard, Armin Fischer, Sjoerd Hoogland, Jason Clifford, Ethan Klem, Larissa Levina, and Edward H. Sargent. Ultrasensitive solution-cast quantum dot photodetectors. *Nature*, 442(7099):180–183, jul 2006.

[76] N. C. Greenham, Xiaogang Peng, and A. P. Alivisatos. Charge separation and transport in conjugated-polymer/semiconductor-nanocrystal composites studied by photoluminescence quenching and photoconductivity. *Physical Review B*, 54:17628–17637, dec 1996.

[77] Wendy U. Huynh, Janke J. Dittmer, and A. Paul Alivisatos. Hybrid nanorod-polymer solar cells. *Science*, 295(5564):2425–2427, mar 2002.

[78] Ilan Gur, Neil A. Fromer, Michael L. Geier, and A. Paul Alivisatos. Air-stable all-inorganic nanocrystal solar cells processed from solution. *Science*, 310(5747):462–465, oct 2005.

[79] Maksym V. Kovalenko. Opportunities and challenges for quantum dot photovoltaics. *Nature Nanotechnology*, 10(12):994–997, dec 2015.

[80] Michael A. Holmes, Troy K. Townsend, and Frank E. Osterloh. Quantum confinement controlled photocatalytic water splitting by suspended CdSe nanocrystals. *Chemical Communications*, 48(3):371–373, 2012.

[81] Zhiji Han, Fen Qiu, Richard Eisenberg, Patrick L. Holland, and Todd D. Krauss. Robust photogeneration of h2 in water using semiconductor nanocrystals and a nickel catalyst. *Science*, 338(6112):1321–1324, nov 2012.

[82] Michelle D. Regulacio and Ming-Yong Han. Multinary i-III-VI2 and i2-II-IV-VI4 semiconductor nanostructures for photocatalytic applications. *Accounts of Chemical Research*, 49(3):511–519, feb 2016.

[83] Dmitri V. Talapin, Jong-Soo Lee, Maksym V. Kovalenko, and Elena V. Shevchenko. Prospects of colloidal nanocrystals for electronic and optoelectronic applications. *Chemical Reviews*, 110(1):389–458, jan 2010.

[84] Defang Ding, Dawei Wang, Man Zhao, Jiawei Lv, Hong Jiang, Chenguang Lu, and Zhiyong Tang. Interface engineering in solution-processed nanocrystal thin films for improved thermoelectric performance. *Advanced Materials*, 29(1):1603444, oct 2016.

[85] Mohamad I. Nugraha, Hyunho Kim, Bin Sun, Md Azimul Haque, Francisco Pelayo Garcia Arquer, Diego Rosas Villalva, Abdulrahman El-Labban, Edward H. Sargent, Husam N. Alshareef, and Derya Baran. Low-temperature-processed colloidal quantum dots as building blocks for thermoelectrics. *Advanced Energy Materials*, 9(13):1803049, feb 2019.

[86] Hans-Jürgen Eisler, Vikram C. Sundar, Moungi G. Bawendi, Michael Walsh, Henry I. Smith, and Victor Klimov. Color-selective semiconductor nanocrystal laser. *Applied Physics Letters*, 80(24):4614–4616, jun 2002.

[87] S. Hoogland, V. Sukhovatkin, I. Howard, S. Cauchi, L. Levina, and E. H. Sargent. A solution-processed 1.53 μm quantum dot laser with temperature-invariant emission wavelength. *Optics Express*, 14(8):3273, 2006.

[88] Kaifeng Wu, Young-Shin Park, Jaehoon Lim, and Victor I. Klimov. Towards zero-threshold optical gain using charged semiconductor quantum dots. *Nature Nanotechnology*, 12(12):1140–1147, oct 2017.

[89] D. V. Talapin. PbSe nanocrystal solids for n- and p-channel thin film field-effect transistors. *Science*, 310(5745):86–89, oct 2005.

[90] Jie Bao and Moungi G. Bawendi. A colloidal quantum dot spectrometer. *Nature*, 523(7558):67–70, jul 2015.

[91] P. T. Guerreiro, S. Ten, N. F. Borrelli, J. Butty, G. E. Jabbour, and N. Peyghambarian. PbS quantum-dot doped glasses as saturable absorbers for mode locking of a cr:forsterite laser. *Applied Physics Letters*, 71(12):1595–1597, sep 1997.

[92] Jingzhou Li, Saifeng Zhang, Hongxing Dong, Yunfei Ma, Bin Xu, Jun Wang, Zhiping Cai, Zhanghai Chen, and Long Zhang. Ultrafast saturable absorption of core/shell colloidal quantum dots. *Particle & Particle Systems Characterization*, 34(1):1600193, oct 2016.

[93] Jingzhou Li, Hongxing Dong, Bin Xu, Saifeng Zhang, Zhiping Cai, Jun Wang, and Long Zhang. CsPbBr_3 perovskite quantum dots: saturable absorption properties and passively q-switched visible lasers. *Photonics Research*, 5(5):457, sep 2017.

[94] Ling Yun, Yang Qiu, Conghao Yang, Jie Xing, Kehan Yu, Xiangxing Xu, and Wei Wei. PbS quantum dots as a saturable absorber for ultrafast laser. *Photonics Research*, 6(11):1028, oct 2018.

[95] V. L. Colvin, M. C. Schlamp, and A. P. Alivisatos. Light-emitting diodes made from cadmium selenide nanocrystals and a semiconducting polymer. *Nature*, 370(6488):354–357, aug 1994.

[96] M. C. Schlamp, Xiaogang Peng, and A. P. Alivisatos. Improved efficiencies in light emitting diodes made with CdSe(CdS) core/shell type nanocrystals and a semiconducting polymer. *Journal of Applied Physics*, 82(11):5837–5842, dec 1997.

[97] Hedi Mattoussi, Leonard H. Radzilowski, Bashir O. Dabbousi, Edwin L. Thomas, Moungi G. Bawendi, and Michael F. Rubner. Electroluminescence from heterostructures of poly(phenylene vinylene) and inorganic CdSe nanocrystals. *Journal of Applied Physics*, 83(12):7965–7974, jun 1998.

[98] Seth Coe, Wing-Keung Woo, Moungi Bawendi, and Vladimir Bulović. Electroluminescence from single monolayers of nanocrystals in molecular organic devices. *Nature*, 420(6917):800–803, dec 2002.

[99] J. Lim, S. Jun, E. Jang, H. Baik, H. Kim, and J. Cho. Preparation of highly luminescent nanocrystals and their application to light-emitting diodes. *Advanced Materials*, 19(15):1927–1932, aug 2007.

[100] Fanglong Yuan, Ting Yuan, Laizhi Sui, Zhibin Wang, Zifan Xi, Yunchao Li, Xiaohong Li, Louzhen Fan, Zhan'ao Tan, Anmin Chen, Mingxing Jin, and Shihe Yang. Engineering triangular carbon quantum dots with unprecedented narrow bandwidth emission for multicolored LEDs. *Nature Communications*, 9(1), jun 2018.

[101] Tae-Ho Kim, Kyung-Sang Cho, Eun Kyung Lee, Sang Jin Lee, Jungseok Chae, Jung Woo Kim, Do Hwan Kim, Jang-Yeon Kwon, Gehan Amaratunga, Sang Yoon Lee, Byoung Lyong Choi, Young Kuk, Jong Min Kim, and Kinam Kim. Full-colour quantum dot displays fabricated by transfer printing. *Nature Photonics*, 5(3):176–182, feb 2011.

[102] Katherine Bourzac. Quantum dots go on display. *Nature*, 493(7432):283–283, jan 2013.

[103] Xingliang Dai, Yunzhou Deng, Xiaogang Peng, and Yizheng Jin. Quantum-dot light-emitting diodes for large-area displays: Towards the dawn of commercialization. *Advanced Materials*, 29(14):1607022, mar 2017.

[104] Robert E. Bailey, Andrew M. Smith, and Shuming Nie. Quantum dots in biology and medicine. *Physica E: Low-dimensional Systems and Nanostructures*, 25(1):1–12, oct 2004.

[105] Freddy T. Rabouw and Celso de Mello Donega. Excited-state dynamics in colloidal semiconductor nanocrystals. *Topics in Current Chemistry*, 374(5), aug 2016.

[106] A. I. Ekimov, I. A. Kudryavtsev, Al. L. Efros, T. V. Yazeva, F. Hache, M. C. Schanne-Klein, A. V. Rodina, D. Ricard, and C. Flytzanis. Absorption and intensity-dependent photoluminescence measurements on CdSe quantum dots: assignment of the first electronic transitions. *Journal of the Optical Society of America B*, 10(1):100, jan 1993.

[107] Wolfgang J. Parak, Liberato Manna, and Thomas Nann. *Fundamental Principles of Quantum Dots*, chapter 4, pages 73–96. American Cancer Society, 2010.

[108] Celso de Mello Donegá, editor. *Nanoparticles*. Springer Berlin Heidelberg, 2014.

[109] Philippe Guyot-Sionnest, Moonsub Shim, Chris Matranga, and Margaret Hines. Intraband relaxation in cdse quantum dots. *Physical Review B*, 60:R2181–R2184, jul 1999.

[110] V. I. Klimov, A. A. Mikhailovsky, D. W. McBranch, C. A. Leatherdale, and M. G. Bawendi. Mechanisms for intraband energy relaxation in semiconductor quantum dots: The role of electron-hole interactions. *Physical Review B*, 61:R13349–R13352, may 2000.

[111] Philippe Guyot-Sionnest, Brian Wehrenberg, and Dong Yu. Intraband relaxation in CdSe nanocrystals and the strong influence of the surface ligands. *The Journal of Chemical Physics*, 123(7):074709, aug 2005.

[112] Anshu Pandey and Philippe Guyot-Sionnest. Slow electron cooling in colloidal quantum dots. *Science*, 322(5903):929–932, nov 2008.

[113] U. Bockelmann and G. Bastard. Phonon scattering and energy relaxation in two-, one-, and zero-dimensional electron gases. *Physical Review B*, 42:8947–8951, nov 1990.

[114] H. Benisty, C. M. Sotomayor-Torrès, and C. Weisbuch. Intrinsic mechanism for the poor luminescence properties of quantum-box systems. *Physical Review B*, 44:10945–10948, nov 1991.

[115] T. Inoshita and H. Sakaki. Electron relaxation in a quantum dot: Significance of multiphonon processes. *Physical Review B*, 46:7260–7263, sep 1992.

[116] U. Bockelmann and T. Egeler. Electron relaxation in quantum dots by means of auger processes. *Physical Review B*, 46:15574–15577, dec 1992.

[117] Al. L. Efros, V.A. Kharchenko, and M. Rosen. Breaking the phonon bottleneck in nanometer quantum dots: Role of auger-like processes. *Solid State Communications*, 93(4):281–284, jan 1995.

[118] Victor I. Klimov and Duncan W. McBranch. Femtosecond $1P$-to- $1S$ electron relaxation in strongly confined semiconductor nanocrystals. *Physical Review Letters*, 80:4028–4031, may 1998.

[119] E. Hendry, M. Koeberg, F. Wang, H. Zhang, C. de Mello Donegá, D. Vanmaekelbergh, and M. Bonn. Direct observation of electron-to-hole energy transfer in cdse quantum dots. *Physical Review Letters*, 96:057408, feb 2006.

[120] V. I. Klimov, A. A. Mikhailovsky, D. W. McBranch, C. A. Leatherdale, and M. G. Bawendi. Quantization of multiparticle auger rates in semiconductor quantum dots. *Science*, 287(5455):1011–1013, feb 2000.

[121] George E. Cragg and Alexander L. Efros. Suppression of auger processes in confined structures. *Nano Letters*, 10(1):313–317, jan 2010.

[122] Wan Ki Bae, Lazaro A. Padilha, Young-Shin Park, Hunter McDaniel, Istvan Robel, Jeffrey M. Pietryga, and Victor I. Klimov. Controlled alloying of the core–shell interface in CdSe/CdS quantum dots for suppression of auger recombination. *ACS Nano*, 7(4):3411–3419, apr 2013.

[123] Freddy T. Rabouw, Per Lunnemann, Relinde J. A. van Dijk-Moes, Martin Frimmer, Francesca Pietra, A. Femius Koenderink, and Daniël Vanmaekelbergh. Reduced auger recombination in single CdSe/CdS nanorods by one-dimensional electron delocalization. *Nano Letters*, 13(10):4884–4892, sep 2013.

[124] Yossef E. Panfil, Meirav Oded, and Uri Banin. Colloidal quantum nanostructures: Emerging materials for display applications. *Angewandte Chemie International Edition*, 57(16):4274–4295, feb 2018.

[125] D. J. Norris, Al. L. Efros, M. Rosen, and M. G. Bawendi. Size dependence of exciton fine structure in CdSe quantum dots. *Physical Review B*, 53:16347–16354, jun 1996.

[126] Anjana Bagga, P. K. Chattopadhyay, and Subhasis Ghosh. Origin of stokes shift in inas and cdse quantum dots: Exchange splitting of excitonic states. *Physical Review B*, 74:035341, jul 2006.

[127] Oleksandr Voznyy, Larissa Levina, Fengjia Fan, Grant Walters, James Z. Fan, Amirreza Kiani, Alexander H. Ip, Susanna M. Thon, Andrew H. Proppe, Mengxia Liu, and Edward H. Sargent. Origins of stokes shift in PbS nanocrystals. *Nano Letters*, 17(12):7191–7195, nov 2017.

[128] A. Franceschetti and S. T. Pantelides. Excited-state relaxations and franck-condon shift in si quantum dots. *Physical Review B*, 68:033313, jul 2003.

[129] Timothy G. Mack, Lakshay Jethi, and Patanjali Kambhampati. Temperature dependence of emission line widths from semiconductor nanocrystals reveals vibronic contributions to line broadening processes. *The Journal of Physical Chemistry C*, 121(51):28537–28545, dec 2017.

[130] Justin R. Caram, Sophie N. Bertram, Hendrik Utzat, Whitney R. Hess, Jessica A. Carr, Thomas S. Bischof, Andrew P. Beyler, Mark W. B. Wilson, and Moungi G. Bawendi. PbS nanocrystal emission is governed by multiple emissive states. *Nano Letters*, 16(10):6070–6077, sep 2016.

[131] Yun Liu, Donghun Kim, Owen P. Morris, David Zhitomirsky, and Jeffrey C. Grossman. Origins of the stokes shift in PbS quantum dots: Impact of polydispersity, ligands, and defects. *ACS Nano*, 12(3):2838–2845, mar 2018.

[132] Eric M. Janke, Nicholas E. Williams, Chunxing She, Danylo Zherebetskyy, Margaret H. Hudson, Lili Wang, David J. Gosztola, Richard D. Schaller, Byeongdu Lee, Chengjun Sun, Gregory S. Engel, and Dmitri V. Talapin. Origin of broad emission spectra in InP quantum dots: Contributions from structural and electronic disorder. *Journal of the American Chemical Society*, 140(46):15791–15803, oct 2018.

[133] Francesco Meinardi, Hunter McDaniel, Francesco Carulli, Annalisa Colombo, Kirill A. Velizhanin, Nikolay S. Makarov, Roberto Simonutti, Victor I. Klimov, and Sergio Brovelli. Highly efficient large-area colourless luminescent solar concentrators using heavy-metal-free colloidal quantum dots. *Nature Nanotechnology*, 10(10):878–885, aug 2015.

[134] Young-Shin Park, Wan Ki Bae, Thomas Baker, Jaehoon Lim, and Victor I. Klimov. Effect of auger recombination on lasing in heterostructured quantum dots with engineered core/shell interfaces. *Nano Letters*, 15(11):7319–7328, oct 2015.

[135] Yoyo Hinuma, Andreas Grüneis, Georg Kresse, and Fumiyasu Oba. Band alignment of semiconductors from density-functional theory and many-body perturbation theory. *Physical Review B*, 90:155405, oct 2014.

[136] Deokho Jang, Younho Han, Seungin Baek, and Jungho Kim. Theoretical comparison of the energies and wave functions of the electron and hole states between CdSe- and InP-based core/shell/shell quantum dots: effect of the bandgap energy of the core material on the emission spectrum. *Optical Materials Express*, 9(3):1257, feb 2019.

[137] Peter Michler. *Nonclassical Light from Single Semiconductor Quantum Dots*, chapter 8, pages 315–347. Springer Berlin Heidelberg, Berlin, Heidelberg, nov 2003.

[138] Peter Michler. Quantum dot single-photon sources. In *Single Semiconductor Quantum Dots*, pages 185–225. Springer Berlin Heidelberg, 2009.

[139] Jonathan P. Dowling and Gerard J. Milburn. Quantum technology: the second quantum revolution. *Philosophical Transactions of the Royal Society of London. Series A: Mathematical, Physical and Engineering Sciences*, 361(1809):1655–1674, jun 2003.

[140] E. Knill, R. Laflamme, and G. J. Milburn. A scheme for efficient quantum computation with linear optics. *Nature*, 409(6816):46–52, jan 2001.

[141] Nicolas Gisin, Grégoire Ribordy, Wolfgang Tittel, and Hugo Zbinden. Quantum cryptography. *Reviews of Modern Physics*, 74(1):145–195, mar 2002.

[142] Alexios Beveratos, Rosa Brouri, Thierry Gacoin, André Villing, Jean-Philippe Poizat, and Philippe Grangier. Single photon quantum cryptography. *Physical Review Letters*, 89:187901, oct 2002.

[143] Tobias Heindel, Christian A Kessler, Markus Rau, Christian Schneider, Martin Fürst, Fabian Hargart, Wolfgang-Michael Schulz, Marcus Eichfelder, Robert Roßbach, Sebastian Nauerth, Matthias Lermer, Henning Weier, Michael Jetter, Martin Kamp, Stephan Reitzenstein, Sven Höfling, Peter Michler, Harald Weinfurter, and Alfred Forchel. Quantum key distribution using quantum dot single-photon emitting diodes in the red and near infrared spectral range. *New Journal of Physics*, 14(8):083001, aug 2012.

[144] S. Lloyd. Universal quantum simulators. *Science*, 273(5278):1073–1078, aug 1996.

[145] M. A. Broome, A. Fedrizzi, B. P. Lanyon, I. Kassal, A. Aspuru-Guzik, and A. G. White. Discrete single-photon quantum walks with tunable decoherence. *Physical Review Letters*, 104:153602, apr 2010.

[146] Max Tillmann, Borivoje Dakić, René Heilmann, Stefan Nolte, Alexander Szameit, and Philip Walther. Experimental boson sampling. *Nature Photonics*, 7(7):540–544, may 2013.

[147] Vittorio Giovannetti, Seth Lloyd, and Lorenzo Maccone. Quantum metrology. *Physical Review Letters*, 96:010401, jan 2006.

[148] Keith R. Motes, Jonathan P. Olson, Evan J. Rabeaux, Jonathan P. Dowling, S. Jay Olson, and Peter P. Rohde. Linear optical quantum metrology with single photons: Exploiting spontaneously generated entanglement to beat the shot-noise limit. *Physical Review Letters*, 114:170802, apr 2015.

[149] R. J. Glauber. Optical coherence and photon statistics. In C. Dewitt, A. Blandin, and C. Cohen-Tannoudji, editors, *Quantum Optics and Electronics*, page 63, 1965.

[150] Leonard Mandel and Emil Wolf. *Optical coherence and quantum optics*. Cambridge University Press, 1995.

[151] R. Hanbury Brown and R. Q. Twiss. Correlation between photons in two coherent beams of light. *Nature*, 177(4497):27–29, jan 1956.

[152] Pascale Senellart, Glenn Solomon, and Andrew White. High-performance semiconductor quantum-dot single-photon sources. *Nature Nanotechnology*, 12(11):1026–1039, nov 2017.

[153] C. K. Hong, Z. Y. Ou, and L. Mandel. Measurement of subpicosecond time intervals between two photons by interference. *Physical Review Letters*, 59:2044–2046, nov 1987.

[154] H. J. Kimble, M. Dagenais, and L. Mandel. Photon antibunching in resonance fluorescence. *Physical Review Letters*, 39:691–695, sep 1977.

[155] D. F. Walls. Evidence for the quantum nature of light. *Nature*, 280(5722):451–454, aug 1979.

[156] J F Clauser and A Shimony. Bell's theorem. experimental tests and implications. *Reports on Progress in Physics*, 41(12):1881–1927, dec 1978.

[157] Alain Aspect, Philippe Grangier, and Gérard Roger. Experimental tests of realistic local theories via bell's theorem. *Physical Review Letters*, 47:460–463, aug 1981.

[158] P Grangier, G Roger, and A Aspect. Experimental evidence for a photon anticorrelation effect on a beam splitter: A new light on single-photon interferences. *Europhysics Letters (EPL)*, 1(4):173–179, feb 1986.

[159] Frank Diedrich and Herbert Walther. Nonclassical radiation of a single stored ion. *Physical Review Letters*, 58:203–206, jan 1987.

[160] Axel Kuhn, Markus Hennrich, and Gerhard Rempe. Deterministic single-photon source for distributed quantum networking. *Physical Review Letters*, 89:067901, jul 2002.

[161] Charles H. Bennett, François Bessette, Gilles Brassard, Louis Salvail, and John Smolin. Experimental quantum cryptography. *Journal of Cryptology*, 5(1), sep 1992.

[162] Luigi Giannelli, Tom Schmit, and Giovanna Morigi. Weak coherent pulses for single-photon quantum memories. *Physica Scripta*, 94(1):014012, dec 2018.

[163] David C. Burnham and Donald L. Weinberg. Observation of simultaneity in parametric production of optical photon pairs. *Physical Review Letters*, 25:84–87, jul 1970.

[164] C. K. Hong and L. Mandel. Experimental realization of a localized one-photon state. *Physical Review Letters*, 56:58–60, jan 1986.

[165] N. Somaschi, V. Giesz, L. De Santis, J. C. Loredo, M. P. Almeida, G. Hornecker, S. L. Portalupi, T. Grange, C. Antón, J. Demory, C. Gómez, I. Sagnes, N. D. Lanzillotti-Kimura, A. Lemaítre, A. Auffeves, A. G. White, L. Lanco, and P. Senellart. Near-optimal single-photon sources in the solid state. *Nature Photonics*, 10(5):340–345, mar 2016.

[166] Igor Aharonovich and Elke Neu. Diamond nanophotonics. *Advanced Optical Materials*, 2(10):911–928, jul 2014.

[167] Anthony J. Morfa, Brant C. Gibson, Matthias Karg, Timothy J. Karle, Andrew D. Greentree, Paul Mulvaney, and Snjezana Tomljenovic-Hanic. Single-photon emission and quantum characterization of zinc oxide defects. *Nano Letters*, 12(2):949–954, jan 2012.

[168] T. Utikal, E. Eichhammer, L. Petersen, A. Renn, S. Götzinger, and V. Sandoghdar. Spectroscopic detection and state preparation of a single praseodymium ion in a crystal. *Nature Communications*, 5(1), apr 2014.

[169] Xuedan Ma, Nicolai F. Hartmann, Jon K. S. Baldwin, Stephen K. Doorn, and Han Htoon. Room-temperature single-photon generation from solitary dopants of carbon nanotubes. *Nature Nanotechnology*, 10(8):671–675, jul 2015.

[170] Yu-Ming He, Genevieve Clark, John R. Schaibley, Yu He, Ming-Cheng Chen, Yu-Jia Wei, Xing Ding, Qiang Zhang, Wang Yao, Xiaodong Xu, Chao-Yang Lu, and Jian-Wei Pan. Single quantum emitters in monolayer semiconductors. *Nature Nanotechnology*, 10(6):497–502, may 2015.

[171] Sonia Buckley, Kelley Rivoire, and Jelena Vučković. Engineered quantum dot single-photon sources. *Reports on Progress in Physics*, 75(12):126503, nov 2012.

[172] Raj B. Patel, Anthony J. Bennett, Ian Farrer, Christine A. Nicoll, David A. Ritchie, and Andrew J. Shields. Two-photon interference of the emission from electrically tunable remote quantum dots. *Nature Photonics*, 4(9):632–635, jul 2010.

[173] Luca Sapienza, Marcelo Davanço, Antonio Badolato, and Kartik Srinivasan. Nanoscale optical positioning of single quantum dots for bright and pure single-photon emission. *Nature Communications*, 6(1), jul 2015.

[174] X. Brokmann, E. Giacobino, M. Dahan, and J. P. Hermier. Highly efficient triggered emission of single photons by colloidal CdSe/ZnS nanocrystals. *Applied Physics Letters*, 85(5):712–714, aug 2004.

[175] X Brokmann, G Messin, P Desbiolles, E Giacobino, M Dahan, and J P Hermier. Colloidal CdSe/ZnS quantum dots as single-photon sources. *New Journal of Physics*, 6:99–99, jul 2004.

[176] Ferruccio Pisanello, Luigi Martiradonna, Godefroy Leménager, Piernicola Spinicelli, Angela Fiore, Liberato Manna, Jean-Pierre Hermier, Roberto Cingolani, Elisabeth Giacobino, Massimo De Vittorio, and Alberto Bramati. Room temperature-dipolelike single photon source with a colloidal dot-in-rod. *Applied Physics Letters*, 96(3):033101, jan 2010.

[177] Ferruccio Pisanello, Godefroy Leménager, Luigi Martiradonna, Luigi Carbone, Stefano Vezzoli, Pascal Desfonds, Pantaleo Davide Cozzoli, Jean-Pierre Hermier, Elisabeth Giacobino, Roberto Cingolani, Massimo De Vittorio, and Alberto Bramati. Non-blinking single-photon generation with anisotropic colloidal nanocrystals: Towards room-temperature, efficient, colloidal quantum sources. *Advanced Materials*, 25(14):1974–1980, jan 2013.

[178] Igor Aharonovich, Dirk Englund, and Milos Toth. Solid-state single-photon emitters. *Nature Photonics*, 10(10):631–641, sep 2016.

[179] P. Michler. A quantum dot single-photon turnstile device. *Science*, 290(5500):2282–2285, dec 2000.

[180] A. Badolato. Deterministic coupling of single quantum dots to single nanocavity modes. *Science*, 308(5725):1158–1161, may 2005.

[181] Z. Yuan. Electrically driven single-photon source. *Science*, 295(5552):102–105, dec 2001.

[182] Yu-Ming He, Yu He, Yu-Jia Wei, Dian Wu, Mete Atatüre, Christian Schneider, Sven Höfling, Martin Kamp, Chao-Yang Lu, and Jian-Wei Pan. On-demand semiconductor single-photon source with near-unity indistinguishability. *Nature Nanotechnology*, 8(3):213–217, feb 2013.

[183] Julien Claudon, Joël Bleuse, Nitin Singh Malik, Maela Bazin, Périne Jaffrennou, Niels Gregersen, Christophe Sauvan, Philippe Lalanne, and Jean-Michel Gérard. A highly efficient single-photon source based on a quantum dot in a photonic nanowire. *Nature Photonics*, 4(3):174–177, jan 2010.

[184] Michael E. Reimer, Gabriele Bulgarini, Nika Akopian, Moïra Hocevar, Maaike Bouwes Bavinck, Marcel A. Verheijen, Erik P.A.M. Bakkers, Leo P. Kouwenhoven, and Val Zwiller. Bright single-photon sources in bottom-up tailored nanowires. *Nature Communications*, 3(1), jan 2012.

[185] Mathieu Munsch, Nitin S. Malik, Emmanuel Dupuy, Adrien Delga, Joël Bleuse, Jean-Michel Gérard, Julien Claudon, Niels Gregersen, and Jesper Mørk. Dielectric gaas antenna ensuring an efficient broadband coupling between an inas quantum dot and a gaussian optical beam. *Physical Review Letters*, 110:177402, apr 2013.

[186] M. Gschrey, A. Thoma, P. Schnauber, M. Seifried, R. Schmidt, B. Wohlfeil, L. Krüger, J. H. Schulze, T. Heindel, S. Burger, F. Schmidt, A. Strittmatter, S. Rodt, and S. Reitzenstein. Highly indistinguishable photons from deterministic quantum-dot microlenses utilizing three-dimensional in situ electron-beam lithography. *Nature Communications*, 6(1), jul 2015.

[187] Je-Hyung Kim, Tao Cai, Christopher J. K. Richardson, Richard P. Leavitt, and Edo Waks. Two-photon interference from a bright single-photon source at telecom wavelengths. *Optica*, 3(6):577, jun 2016.

[188] Sebastian Zaske, Andreas Lenhard, Christian A. Keßler, Jan Kettler, Christian Hepp, Carsten Arend, Roland Albrecht, Wolfgang-Michael Schulz, Michael Jetter, Peter Michler, and Christoph Becher. Visible-to-telecom quantum frequency conversion of light from a single quantum emitter. *Physical Review Letters*, 109:147404, oct 2012.

[189] Serkan Ates, Imad Agha, Angelo Gulinatti, Ivan Rech, Matthew T. Rakher, Antonio Badolato, and Kartik Srinivasan. Two-photon interference using background-free quantum frequency conversion of single photons emitted by an inas quantum dot. *Physical Review Letters*, 109:147405, oct 2012.

[190] Mark J. Holmes, Kihyun Choi, Satoshi Kako, Munetaka Arita, and Yasuhiko Arakawa. Room-temperature triggered single photon emission from a III-nitride site-controlled nanowire quantum dot. *Nano Letters*, 14(2):982–986, jan 2014.

[191] Zhechao Wang, Amin Abbasi, Utsav Dave, Andreas De Groote, Sulakshna Kumari, Bernadette Kunert, Clement Merckling, Marianna Pantouvaki, Yuting Shi, Bin Tian, Kasper Van Gasse, Jochem Verbist, Ruijun Wang, Weiqiang Xie, Jing Zhang, Yunpeng Zhu, Johan Bauwelinck, Xin Yin, Zeger Hens, Joris Van Campenhout, Bart Kuyken, Roel Baets, Geert Morthier, Dries Van Thourhout, and Gunther Roelkens. Novel light source integration approaches for silicon photonics. *Laser & Photonics Reviews*, 11(4):1700063, jul 2017.

[192] Brahim Lounis and Michel Orrit. Single-photon sources. *Reports on Progress in Physics*, 68(5):1129–1179, apr 2005.

[193] P. Michler, A. Imamoğlu, M. D. Mason, P. J. Carson, G. F. Strouse, and S. K. Buratto. Quantum correlation among photons from a single quantum dot at room temperature. *Nature*, 406(6799):968–970, aug 2000.

[194] B. Lounis, H.A. Bechtel, D. Gerion, P. Alivisatos, and W.E. Moerner. Photon antibunching in single CdSe/ZnS quantum dot fluorescence. *Chemical Physics Letters*, 329(5-6):399–404, oct 2000.

[195] M. Nirmal, B. O. Dabbousi, M. G. Bawendi, J. J. Macklin, J. K. Trautman, T. D. Harris, and L. E. Brus. Fluorescence intermittency in single cadmium selenide nanocrystals. *Nature*, 383(6603):802–804, oct 1996.

[196] Yongfen Chen, Javier Vela, Han Htoon, Joanna L. Casson, Donald J. Werder, David A. Bussian, Victor I. Klimov, and Jennifer A. Hollingsworth. "giant" multishell CdSe nanocrystal quantum dots with suppressed blinking. *Journal of the American Chemical Society*, 130(15):5026–5027, apr 2008.

[197] Benoit Mahler, Piernicola Spinicelli, Stéphanie Buil, Xavier Quelin, Jean-Pierre Hermier, and Benoit Dubertret. Towards non-blinking colloidal quantum dots. *Nature Materials*, 7(8):659–664, jun 2008.

[198] Gautham Nair, Jing Zhao, and Moungi G. Bawendi. Biexciton quantum yield of single semiconductor nanocrystals from photon statistics. *Nano Letters*, 11(3):1136–1140, mar 2011.

[199] Young-Shin Park, Wan Ki Bae, Jeffrey M. Pietryga, and Victor I. Klimov. Auger recombination of biexcitons and negative and positive trions in individual quantum dots. *ACS Nano*, 8(7):7288–7296, jun 2014.

[200] C. T. Yuan, Pyng Yu, H. C. Ko, J. Huang, and Jau Tang. Antibunching single-photon emission and blinking suppression of CdSe/ZnS quantum dots. *ACS Nano*, 3(10):3051–3056, sep 2009.

[201] Hiroyuki Naiki, Sadahiro Masuo, Shinjiro Machida, and Akira Itaya. Single-photon emission behavior of isolated CdSe/ZnS quantum dots interacting with the localized surface plasmon resonance of silver nanoparticles. *The Journal of Physical Chemistry C*, 115(47):23299–23304, nov 2011.

[202] Loredana Protesescu, Sergii Yakunin, Maryna I. Bodnarchuk, Franziska Krieg, Riccarda Caputo, Christopher H. Hendon, Ruo Xi Yang, Aron Walsh, and Maksym V. Kovalenko. Nanocrystals of cesium lead halide perovskites (CsPbX3, x = cl, br, and i): Novel optoelectronic materials showing bright emission with wide color gamut. *Nano Letters*, 15(6):3692–3696, feb 2015.

[203] Young-Shin Park, Shaojun Guo, Nikolay S. Makarov, and Victor I. Klimov. Room temperature single-photon emission from individual perovskite quantum dots. *ACS Nano*, 9(10):10386–10393, oct 2015.

[204] Gabriele Raino, Georgian Nedelcu, Loredana Protesescu, Maryna I. Bodnarchuk, Maksym V. Kovalenko, Rainer F. Mahrt, and Thilo Stoeferle. Single cesium lead halide perovskite nanocrystals at low temperature: Fast single photon emission, reduced blinking, and exciton fine structure. *ACS Nano*, 10(2):2485–2490, feb 2016.

[205] Olga I. Micic, Calvin J. Curtis, Kim M. Jones, Julian R. Sprague, and Arthur J. Nozik. Synthesis and characterization of InP quantum dots. *The Journal of Physical Chemistry*, 98(19):4966–4969, may 1994.

[206] Xing Lin, Xingliang Dai, Chaodan Pu, Yunzhou Deng, Yuan Niu, Limin Tong, Wei Fang, Yizheng Jin, and Xiaogang Peng. Electrically-driven single-photon sources based on colloidal quantum dots with near-optimal antibunching at room temperature. *Nature Communications*, 8(1), oct 2017.

[207] Peter Reiss, Marie Carrière, Christophe Lincheneau, Louis Vaure, and Sudarsan Tamang. Synthesis of semiconductor nanocrystals, focusing on nontoxic and earth-abundant materials. *Chemical Reviews*, 116(18):10731–10819, jul 2016.

[208] Mickael D. Tessier, Dorian Dupont, Kim De Nolf, Jonathan De Roo, and Zeger Hens. Economic and size-tunable synthesis of InP/ZnE (e = s, se) colloidal quantum dots. *Chemistry of Materials*, 27(13):4893–4898, jun 2015.

[209] Virgilio Brunetti, Hicham Chibli, Roberto Fiammengo, Antonio Galeone, Maria Ada Malvindi, Giuseppe Vecchio, Roberto Cingolani, Jay L. Nadeau, and Pier Paolo Pompa. InP/ZnS as a safer alternative to CdSe/ZnS core/shell quantum dots: in vitro and in vivo toxicity assessment. *Nanoscale*, 5(1):307–317, 2013.

[210] Joel Q. Grim, Liberato Manna, and Iwan Moreels. A sustainable future for photonic colloidal nanocrystals. *Chemical Society Reviews*, 44(16):5897–5914, 2015.

[211] Sudarsan Tamang, Christophe Lincheneau, Yannick Hermans, Sohee Jeong, and Peter Reiss. Chemistry of InP nanocrystal syntheses. *Chemistry of Materials*, 28(8):2491–2506, apr 2016.

[212] Huaxiang Fu and Alex Zunger. Local-density-derived semiempirical nonlocal pseudopotentials for inp with applications to large quantum dots. *Physical Review B*, 55:1642–1653, jan 1997.

[213] Huaxiang Fu and Alex Zunger. Inp quantum dots: Electronic structure, surface effects, and the redshifted emission. *Physical Review B*, 56:1496–1508, jul 1997.

[214] D. Bertram, O. I. Mićić, and A. J. Nozik. Excited-state spectroscopy of inp quantum dots. *Physical Review B*, 57:R4265–R4268, feb 1998.

[215] Matthew D. Healy, Paul E. Laibinis, Paul D. Stupik, and Andrew R. Barron. The reaction of indium(III) chloride with tris(trimethylsilyl)phosphine: a novel route to indium phosphide. *Journal of the Chemical Society, Chemical Communications*, page 359, 1989.

[216] Richard L. Wells, Steven R. Aubuchon, Shreyas S. Kher, Michael S. Lube, and Peter S. White. Synthesis of nanocrystalline indium arsenide and indium phosphide from indium(III) halides and tris(trimethylsilyl)pnicogens. synthesis, characterization, and decomposition behavior of i3in.cntdot.p(SiMe3)3. *Chemistry of Materials*, 7(4):793–800, apr 1995.

[217] A. A. Guzelian, J. E. B. Katari, A. V. Kadavanich, U. Banin, K. Hamad, E. Juban, A. P. Alivisatos, R. H. Wolters, C. C. Arnold, and J. R. Heath. Synthesis of size-selected, surface-passivated InP nanocrystals. *The Journal of Physical Chemistry*, 100(17):7212–7219, jan 1996.

[218] David Battaglia and Xiaogang Peng. Formation of high quality InP and InAs nanocrystals in a noncoordinating solvent. *Nano Letters*, 2(9):1027–1030, sep 2002.

[219] Renguo Xie, David Battaglia, and Xiaogang Peng. Colloidal InP nanocrystals as efficient emitters covering blue to near-infrared. *Journal of the American Chemical Society*, 129(50):15432–15433, dec 2007.

[220] Liang Li, Myriam Protière, and Peter Reiss. Economic synthesis of high quality InP nanocrystals using calcium phosphide as the phosphorus precursor. *Chemistry of Materials*, 20(8):2621–2623, apr 2008.

[221] Taichi Matsumoto, Shinya Maenosono, and Yukio Yamaguchi. Organometallic synthesis of InP quantum dots using tris(dimethylamino)phosphine as a phosphorus source. *Chemistry Letters*, 33(11):1492–1493, nov 2004.

[222] Woo-Seuk Song, Hye-Seung Lee, Ju Chul Lee, Dong Seon Jang, Yoonyoung Choi, Moongoo Choi, and Heesun Yang. Amine-derived synthetic approach to color-tunable InP/ZnS quantum dots with high fluorescent qualities. *Journal of Nanoparticle Research*, 15(6), jun 2013.

[223] Alexander L. Efros and David J. Nesbitt. Origin and control of blinking in quantum dots. *Nature Nanotechnology*, 11(8):661–671, aug 2016.

[224] Mickael D. Tessier, Kim De Nolf, Dorian Dupont, Davy Sinnaeve, Jonathan De Roo, and Zeger Hens. Aminophosphines: A double role in the synthesis of colloidal indium phosphide quantum dots. *Journal of the American Chemical Society*, 138(18):5923–5929, may 2016.

Chapter 2.

Nearly blinking-free & high-purity single photon emission

Contents

Synopsis

This chapter discusses single-particle spectroscopy of InP/ZnSe QDs that reveals strong photon antibunching attributed to fast Auger recombination of multiple excitons. The antibunching is preserved when the QDs are excited above the saturation intensity of the fundamental-exciton transition. Single QDs exhibit good photostability under strong optical excitation with a nearly-blinking free emission. This result paves the way toward their usage as high-purity on-demand single-photon emitters at room temperature.

Based on the publication Nano Lett. 2017, 17, 10, 6104-6109
Synthesis of InP/ZnSe QDs by Dr. Dorian Dupont, Ghent University, Belgium
TEM images of InP/ZnSe QDs by Dr. Willem Walravens, Ghent University, Belgium
Ultrafast pump-probe spectroscopy of InP/ZnSe QDs by Prof. Pieter Geiregat, Ghent University, Belgium

2.1. Introduction

2.1.1. Quasi-two level system

Luminous intensity collected under continuous wave (CW) illumination on QDs can be used to find if the system under study is emitting in the single exciton regime. CW pumping of QDs at lower excitation intensity creates a single exciton at a time. The probability of creating a second exciton during the lifetime is very low at this lower intensity level and thus we can derive a model for a simple two-level system.

The rate equation for the population of the excited state is given by:

$$\frac{d}{dt}P_e(t) = WP_g(t) - \gamma P_e(t) \tag{2.1}$$

Since $P_g(t) + P_e(t) = 1$, the equation 2.1 becomes:

$$\frac{d}{dt}P_e(t) = W - (W + \gamma)P_e(t) \tag{2.2}$$

Assuming $P_e(0) = 0$ at t = 0, the equation 2.2 becomes:

$$P_e(t) = \frac{W}{W + \gamma}\left(1 - \exp^{-(W+\gamma)t}\right) \tag{2.3}$$

where W is the excitation pumping rate, e & g represent the excited and ground states, γ is the decay rate. Since $W = \sigma I/\hbar\omega$ and substituting $I_s = \gamma\hbar\omega/\sigma$, the probability to find one exciton in a QD or the average count rate is proportional to $I/(I + I_s)$ where I is the intensity, I_s is the saturation intensity, σ is the absorption cross section and ω is the emission frequency. This rate saturates upon increasing the excitation intensity in an effective two-level system which could be an indicator that the QD under study operates in a single exciton regime.

2.2. Ensemble properties

2.2.1. Photoluminescence

InP/ZnSe QDs for this study was synthesized according to the method described in section 1.5.2. As shown in Figure 2.1a, InP/ZnSe QDs studied had an equivalent diameter of about 10 nm with a core size of 3.2 nm (see inset) and their absorption spectrum exhibited the typical band-edge transition with a maximum at 594 nm. The crystallinity of the particles is evident from the HR-TEM image shown in the inset of Figure 2.1a. The photoluminescence (PL) in solution featured a concomitant single-peak spectrum around 629 nm, a full-width-at-half maximum (FWHM) of 47 nm, and had a PL quantum yield of 65% (see the synthesis protocol of this QD reported by Tessier *et al.*[1, 2] for further details). As shown before, this relatively large FWHM – Cd-based QDs, $CsPbBr_3$ or CdSe nanoplatelets can have an ensemble emission as narrow as 20, 12, and 10 nm, respectively – is not a characteristic of the emission of individual InP QDs, yet reflects inhomogeneous broadening related to size dispersion.[3–6]

The PL characterization of the InP/ZnSe QDs is done by analyzing thin films spincoated on a glass coverslip using the micro-PL setup shown in section C.1. Figure 2.1b represents the PL decay of an ensemble of QDs obtained after pulsed excitation at 445 nm with a repetition rate of 2.5 Mhz. The figure includes a best fit of the experimental data to a single exponential function, $I_{\mathrm{PL}}(t) \propto \exp(-\gamma\, t)$ with an offset, which yields a PL decay time $\gamma^{-1} = 25$ ns. Most interestingly, under CW excitation at 445 nm, the PL intensity I_{PL} first increases linearly with the excitation intensity I, then saturates according to $I_{\mathrm{PL}} \propto I/(I + I_{\mathrm{S}})$ as expected for an effective 2-level transition (see Figure 2.1c & description in section 2.1.1). The fitting of the PL intensity yields a saturation intensity $I_{\mathrm{S}} = 690 \pm 40\,\mathrm{W/cm^2}$.

Absorption cross section

The absorption cross-section σ of a QD is connected to its intrinsic absorption coefficient μ_{i} by the relation $\sigma = \mu_{\mathrm{i}}\, V_{\mathrm{QD}}$, where $V_{\mathrm{QD}} = 523.6\ \mathrm{nm}^3$ is the volume of a 10-nm spherical QD. For a core/shell QD suspended in an homogeneous solvent, the intrinsic absorption coefficient at a wavelength λ has been proposed by Neeves *et al.*:[7]

$$\mu_{\mathrm{i}} = \frac{2\pi}{\lambda\, n_{\mathrm{s}}}\, \mathrm{Im}(3\, \varepsilon_{\mathrm{s}}\, \beta), \tag{2.4}$$

where n_{s} is the refractive index of the solvent and ε_{s} its (relative) dielectric permittivity. The complex factor β is defined as

$$\beta = \frac{\varepsilon_{\mathrm{sh}}\, \varepsilon_a - \varepsilon_{\mathrm{s}}\, \varepsilon_b}{\varepsilon_{\mathrm{sh}}\, \varepsilon_a + 2\, \varepsilon_{\mathrm{s}}\, \varepsilon_b}, \tag{2.5}$$

where

$$\varepsilon_a = \varepsilon_{\mathrm{c}} \left(3 - 2\, \frac{V_{\mathrm{sh}}}{V_{\mathrm{QD}}}\right) + 2\, \varepsilon_{\mathrm{sh}}\, \frac{V_{\mathrm{sh}}}{V_{\mathrm{QD}}}, \tag{2.6}$$

$$\varepsilon_b = \varepsilon_{\mathrm{c}}\, \frac{V_{\mathrm{sh}}}{V_{\mathrm{QD}}} + \varepsilon_{\mathrm{sh}} \left(3 - \frac{V_{\mathrm{sh}}}{V_{\mathrm{QD}}}\right). \tag{2.7}$$

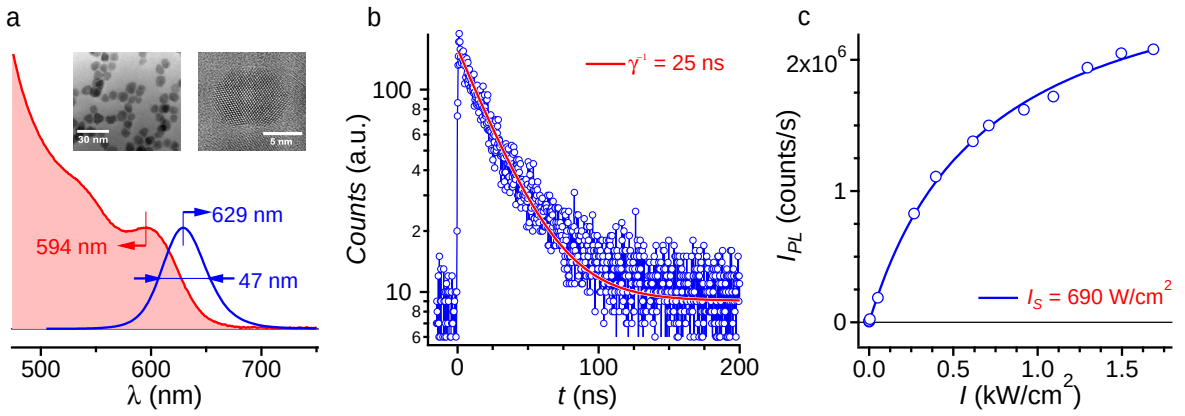

Figure 2.1. | Ensemble properties. (a) Absorption (red) and emission (blue) spectrum of InP/ZnSe quantum dots in solution at room temperature. Insets: TEM and HR-TEM image of the InP/ZnSe quantum dots. (b) Luminescence decay from InP/ZnSe quantum dots in a thin film for pulsed excitation at 445 nm & repetition rate of 2.5 Mhz. (c) Luminescence saturation of the thin film containing ensemble of QDs under high intensity CW excitation at 445 nm.

Here ε_c and ε_{sh} stand for the (relative) dielectric permittivities of the core and the shell, and V_{sh} for the shell volume (equal to $506.4\,\text{nm}^3$ for 3.2-nm cores). At an excitation wavelength of 445 nm, $\varepsilon_c = 16.4 + \text{i}\,6.5$ and $\varepsilon_{sh} = 7.9 + \text{i}\,1.7$. The computation shows that the absorption cross-section of InP/ZnSe QDs is $\sigma = 2.53 \times 10^{-14}$ cm^2 when they are suspended in toluene ($n_s = 1.47$) and $\sigma = 1.13 \times 10^{-14}$ cm^2 when they are suspended in air ($n_s = 1$).

From the experimental result explained in section 2.2.1 & subsequently shown in Figure 2.1 with the photon energy of the CW excitation laser ($\hbar\omega_p$) and the measured decay rate (γ), this translates into an average QD absorption cross section $\sigma = \hbar\omega_p\gamma/I_S$ of $(2.0 \pm 0.1) \times 10^{-14}\,\text{cm}^2$. The correspondence between the values for σ obtained experimentally and estimated theoretically for the QDs suspended in toluene indicates that the saturation of the PL reflects the emission saturation of the InP/ZnSe QDs and that they behave as effective 2-level systems (also see section 2.1.1).

2.2.2. Ultrafast pump-probe spectra

To investigate the charge carrier dynamics, ultrafast pump-probe spectroscopy is done on InP/ZnSe QDs (see Appendix C.2 for the setup layout). Samples were dispersed in toluene to achieve an optical density of 0.05 at the first exciton peak and were stirred during the measurements to avoid photocharging. Using the frequency doubled output of a 110 fs Ti:S laser (800 nm), the QDs are photo-excited at 400 nm and the decay of the band edge population is monitored using a broadband, time-delayed probe pulse (110 fs) generated in a CaF_2 crystal. At low pump fluence, only single excitons are created ($\langle N \rangle \ll 1$) which implies that the slow, about 600 ps, decay of the population observed at these pump levels is due to relaxation mechanisms of the single exciton. When increasing the pump fluence, a fast decay component with a lifetime of 70 $\pm$5 ps shows up (see Figure 2.2b). The weight of this additional component scales with $\langle N \rangle^2$ indicating it originates from biexcitons. In particular the 70 ps lifetime can be labeled as the biexciton Auger lifetime. A short-lived bleach near the P-states transition at 520 nm is also observed indicating carriers pass through these levels as they cool down. It is also

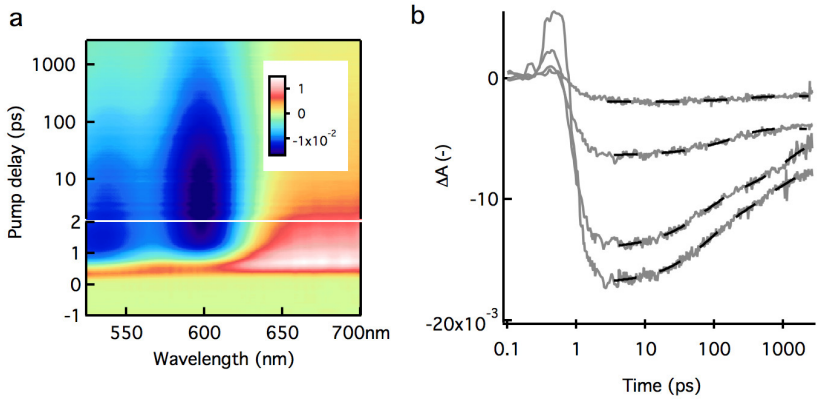

Figure 2.2. | Transient absorption spectra. (a) 2D time-wavelength map of the differential absorbance ΔA after excitation with a 400 nm pump & fluence of 0.5 mJ/cm^2. A clear bleach due to state-filling is observed around the band gap (600 nm). A strong photo-induced absorption at early times is attributed to spectral shifting and intraband absorption.[8] (b) Kinetics at 600 nm (band gap of InP/ZnSe) for increasing pump fluence (data from top to bottom: 0.1 mJ/cm^2, 0.25 mJ/cm^2, 0.75 mJ/cm^2 and 1.1 mJ/cm^2). The solid black lines are biexponential fits to the data showing a fast 70 $\pm$5 ps non-radiative decay decay of biexcitons and a slower single exciton dynamic of about 600 ps indicative of fine-structure relaxation.[9]

observed that state filling takes a total of 2.5 ps to build up, a relaxation comparable to other colloidal QD systems. When the surface is properly passivated, this time should be sufficiently short to avoid serious surface trapping as is evidenced by the high quantum yield of the samples. Multi-exciton emission is very efficiently quenched by non-radiative Auger recombination of charge carriers in this QD. While the fast Auger recombination of multiple exciton is not favorable for lasing application,[10, 11] this QD could be interesting for single photon emission (see section 2.4).

2.3. Single dot properties

2.3.1. Emission lifetime and linewidth

To address the PL of single InP/ZnSe QDs, a 1-nM solution of QDs in toluene was dropcast on a glass coverslip, producing a QD surface density of 0.25 μm^{-2} (See Appendix C.1 for the micro-PL setup). Note that the dropcast method normally do not produce homogeneous distribution of QDs and the indicated density reflects the well separated single QDs. Figure 2.3a shows that a single InP/ZnSe QD features a much more narrow emission line with a linewidth of 14 nm (46 meV) than those observed in QD ensembles with a linewidth of 47 nm (150 meV). Note that the single QD spectrum was integrated for 60 s. A systematic study of 72 single InP/ZnSe QDs showed similarly narrow lines falling within the ensemble emission spectrum (see Figure 2.3b), confirming that the ensemble emission is inhomogeneously broadened. The linewidths of single-QD emissions also show some variability (see Figure 2.3c). While the average FWHM amounts to 19.4 nm, the distribution shows a standard deviation of 2.5 nm and the measured values range from 13 to 24 nm. The PL decay of single InP/ZnSe QDs can be conveniently fitted with a single-exponential function (see Figure 2.3d), an observation suggesting that the contribution of single exciton is more significant without much involvement of either charged state or biexciton emission in which case the exponential fit would be typically a multi-exponential function. By investigating on 25 single QDs, it turned out that the distribution of the decay times γ^{-1} can be fitted to a normal law with an average value of 22.5 ns and a standard deviation of 5.4 ns (see

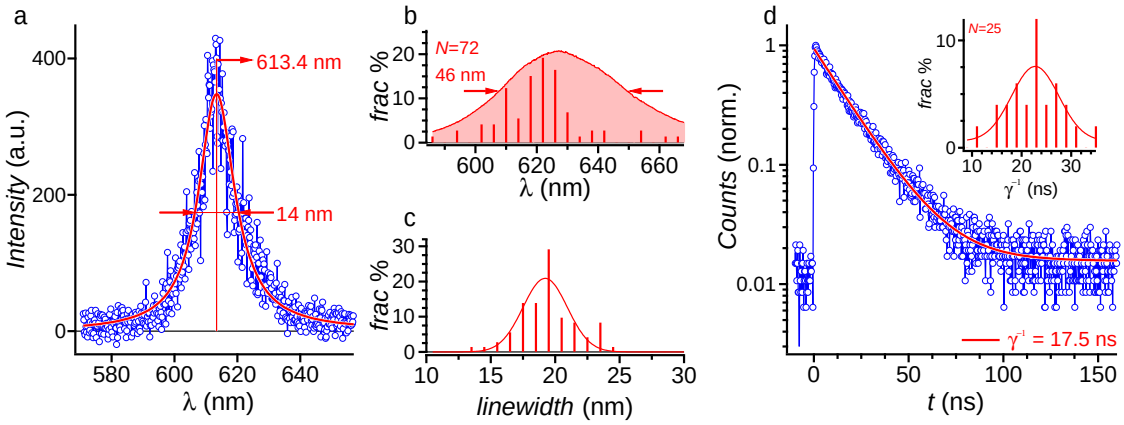

Figure 2.3. | Single dot properties. (a) Emission spectrum of a single QD fitted to a Lorentzian function. (b) Statistical distribution of the central emission wavelength in an ensemble of 72 single QDs. (c) Statistical distribution of emission linewidth for the same ensemble. Note: Histogram (bars) and Gaussian fit (line). (d) Luminescence decay trace of a single QD fitted to a single exponential function with a decay time of 17.5 ns. Inset: statistical distribution of the decay times based on an ensemble of 25 single QDs.

inset to Figure 2.3d). Similar variations in single QD lifetime have been reported before in the case of CdSe/ZnS QDs.[12] Note that the charged QDs were not observed possibly due to their much lower emission intensity compared to the selected single QDs.

Fluorescent decay rate of a QD has the contribution of both radiative and non-radiative part:

$$\Gamma_{QD} = \Gamma_{rad} + \Gamma_{non-rad} \tag{2.8}$$

The rate of a spontaneous emission from the lowest excited electron-hole pair $|e\rangle$ to the ground state $|g\rangle$ in a QD can be derived using 'Fermi's golden rule' given by:[13, 14]

$$\Gamma_{rad} = \frac{2e^4 n}{\pi\epsilon_0 m_0^3 c^3} |F_{loc}|^2 \left[\frac{2m_0 \omega \Theta P^2}{3e^2\hbar}\right] \tag{2.9}$$

where e is the electron charge, n is the refractive index, ϵ_0 is the permittivity of free space, m_0 is the electron rest mass, c is the speed of light, F_{loc} is the local field correction factor ($3\epsilon_m/\epsilon_1 + 2\epsilon_m$, where ϵ_m is the dielectric constant of the surrounding medium and ϵ_1 is the dielectric constant of the semiconductor), ω is the transition frequency, which is proportional to the transition energy E, Θ is the square of the overlap integral between the electron and the hole wave functions, and P is the Kane interband matrix element, $|\langle 1S_h|p|1S_e\rangle|$, which gives the transition electric dipole moment.

This implies that the radiative rate Γ_{rad} is proportional to the emission frequency ω and therefore the central emission energy of a QD. Since the emission energy of a QD is already dependent on its size (also F_{loc}), the spontaneous emission rate would also be then dependent on the size of the QD.

To find if there are correlations among emission wavelength, linewidth, and lifetime in InP/ZnSe QDs, the statistical distribution of the emission linewidths in an ensemble of 72 single QDs and the statistical distribution of the emission lifetimes in a subset of 25 QDs with respect to their central emission energy are shown in Figure 2.4. It is found that the emission lifetime of each QD fitted with single exponential is linearly correlated to the central emission energy. The plot of the decay rate γ versus the photon energy $E = h\,c/\lambda$ reveals a linear dependence with a slope of 300±33 μs^{-1}/eV (see Figure 2.4a). A

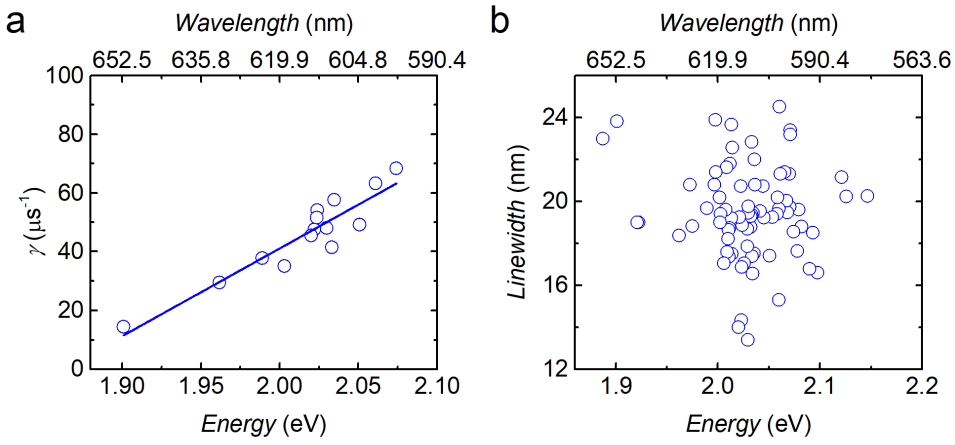

Figure 2.4. | Correlation between emission lifetime, linewidth, and central energy. (a) Correlation between the luminescence decay rate of single QDs and the energy of the photons they emit. The fit shows a linear dependence with a slope of 300±33 μs^{-1}/eV. (b) Correlation of linewidth with the emission energy.

similar correlation was previously reported for CdSe and CdTe QDs.[14, 15] Although the slope of the dependence ($\mathrm{d}\gamma/\mathrm{d}E$) is more than the one reported for CdSe and CdTe QDs for a similar spectral range, further investigation is needed to verify whether the theoretical explanation of this effect given for bare-core QDs[14] also applies to core/shell nanostructures such as InP/ZnSe QDs. No discernible correlation between the spectral linewidth and the photon energy was observed (see Figure 2.4b).

2.3.2. Origin of broad emission spectra in InP quantum dots

InP QDs have traditionally broader ensemble emission spectra and larger Stokes shifts than the counterpart CdSe QDs and the reason for this is still debatable which could be due to several factors such as a size-dependent exchange interaction induced fine structure states,[16, 17] polydispersity,[18] vibrational (Franck–Condon) contribution via excited states[19] & surface ligands,[20] defects and trap states.[21–23] InP has a larger exciton Bohr radius of ∼10 nm (1.35 eV bandgap) compared to ∼5 nm (1.7 eV bandgap) in CdSe and thus they could experience a stronger quantum confinement effect for a similar sized QD. This could explain the broadened ensemble emission spectra in InP compared to CdSe since a mere change in the size distribution could result in a shift in the peak emission energies. Though it is difficult to predict the size-dependent energies owing to their oxidation and poor contrast in TEM images, some studies observed a steeper relation between the bandgap and size in InP compared to CdSe.[23]

At room temperature, the homogeneous linewidth of a single QD is typically dominated by phonon-induced broadening in the order of several tens of meV which is much larger than the lifetime limited natural broadening in the μeV range.[24] The observation of narrow single QD spectra (14 nm / 46 meV) here compared to ensemble emission spectra (46 nm / 150 meV) at room temperature shown in Figure 2.3 emphasize that the single InP QDs are not inherently broadened and reflects the inhomogeneous distribution (size dispersion) of QDs in the ensemble. This observation was also supported by photon correlation Fourier spectroscopy on InP QDs.[5] As discussed before, the fluorescence lifetime is single exponential (average of ∼22.5 ns) and it will be shown next in the section 2.3.3 that the blinking or fluorescence intermittency is low in this QD. Taking into account a minor spectral diffusion due to charge fluctuations (see Figure 2.7), the single QD linewidth of 46 meV thus represents a value not too far from the homogeneous linewidth at room temperature. This linewidth and the lifetime value is also comparable to state of the art giant shell CdSe based QDs.[25]

The narrowest single QD linewidth reported at room temperature til now is the alloyed CdSe QDs with sub-thermal linewidth.[25] Even there and all the other reported linewidth values for single QDs are much narrower than the ensemble spectra indicating an inhomogeneous broadening due to size dispersion as the dominant factor in QDs.[4, 5, 26] On the contrary, it was recently reported by Janke *et al.* that both the broadness and the larger stokes shift in InP QDs are arising from the trap-associated emission pathway in core/shell heterostructures attributed to structural disorder induced hole traps. As explained in the section 1.2.4, a trap-assisted emission would be considerably redshifted from the absorption peak. To further support their attribution, Janke *et al.* claimed that the sizing curve for CdTe is similar to InP, yet the ensemble spectrum is narrower for former than the latter even without post-synthesis size fractionation.[23] However, the Supporting Information contained figures which showed the histogram of QD diameters from TEM images which appeared to have a standard deviation of ∼2 nm for InP while it is only ∼1.2 nm for CdTe. Even half a nm difference in the size, especially when the diameter of the QD is around 3-4 nm, could result in a drastic change in the emission energy. While this trapped state emission could still be a broadening mechanism for their InP QDs, the observation of narrow single QD spectra & mono-exponential lifetime with their size-dependence (see Figure 2.3

and Figure 2.4), efficient single photon emission (see section 2.4) and emission from band edge exciton states discussed in Chapter 3 indicates that the polydispersity explains the broadened spectra and larger Stokes shift for our ensemble of InP QDs, similar to other NCs (see section 1.2.4).

Single QDs are broadened by *natural radiative lifetime*, *exciton dephasing (including the effect of fine structure)*, *phonon assisted emission* and *spectral diffusion*. These factors also exhibit variations corresponding to the differences in size & shape. Since the ensemble of QDs is a convolution of several such single QDs, the ensemble linewidth is a cumulative of all the aforementioned factors varying for every single QDs. Hence the broadening of ensemble spectrum in InP QDs is attributed to *polydispersity*.

2.3.3. Nearly blinking-free emission

InP/ZnSe QDs show some fluorescence intermittency, a phenomenon commonly known as 'blinking'. At the ensemble level, blinking reduces the effective PLQY of the material. In quantum optics applications, however, blinking prohibits the use of single QDs as deterministic single-photon turnstile devices. The data in Figure 2.5a (red line) show the intensity of the light (photon counts per 10-ms time bin) collected from a single QD as a function of time at room temperature. The QD was excited with a CW 445-nm laser beam in the low-pumping regime ($I \ll I_S$) at 100 W/cm^2. The noise background of the measurement is shown in blue (measured in the region on the glass substrate where there is no QD emission). Although some dark periods (no emission, *off* state) can be seen, the histogram of counts displayed on the right of Figure 2.5a indicates that 99% of time the QD is bright (*on* state) and emits photons at a stable rate. The threshold between *on* and *off* states is indicated by the dashed gray line in Figure 2.5a. It was chosen 2-3 standard deviations above the background noise level as can be seen in Figure 2.5a. The blinking is very limited and follows a simple *on*/*off* pattern, without any intermediate or gray-state emission, as often reported in the case of CdSe/CdS QDs.[27] The blinking was studied

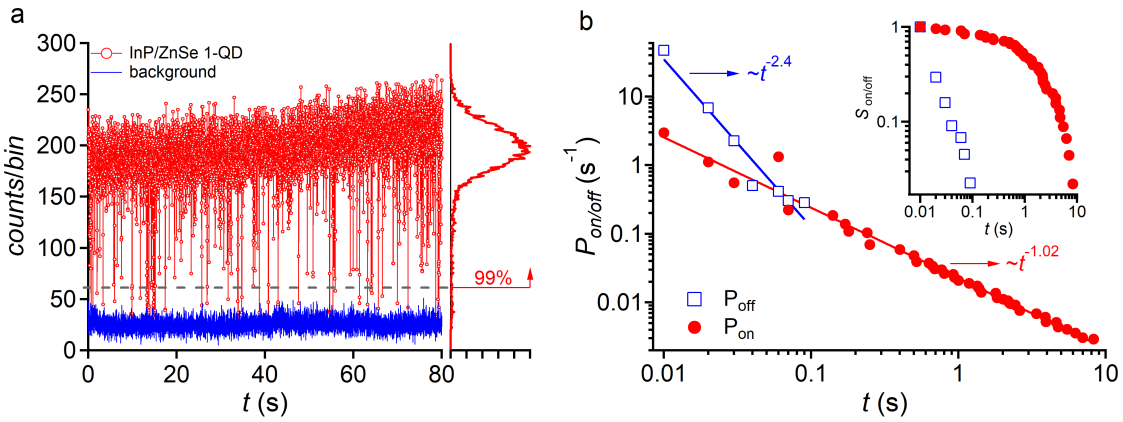

Figure 2.5. | Blinking properties. (a) Luminescence intensity of the QD in Figure 2.9 as a function of time (in counts per 10-ms time bin). The QD is excited with CW 445-nm laser light. (b) Probability density distributions of the *on* and *off* time periods. The data is fitted to power law distributions $P_{\text{on(off)}}(t) \propto t^{-k_{\text{on (off)}}}$ with $k_{\text{off}} = 2.44$ and $k_{\text{on}} = 1.02$. Inset: survival probabilities $S_{\text{on(off)}}(t) = \int_t^\infty P_{\text{on(off)}}(\tau)\,\tau$ constructed from the data in panel (b).

on 25 different QDs and it was observed with each time the same two-state (*on*/*off*) pattern, with a *on*-state fraction of 95.5% on average.

To benchmark the fluorescence intermittency in the InP/ZnSe QDs studied here against the extensively studied CdSe/CdS QDs, the probability density distributions $P_{\text{on}}(t)$ and $P_{\text{off}}(t)$ are defined for the QD to stay in an *on* or an *off* state during the time t. The shortest *on* or *off* duration is determined by the selected binning time, which is 10 ms, and the longest duration is limited by the emission characteristics of the QD and the time duration of the measurement. The two distributions are calculated from the data in Figure 2.5a in the following way:

$$P_{\text{on(off)}}(t_n) = \frac{\text{Number of "on" ("off") events of duration } t_n}{\text{Total number of "on" ("off") events}} \times \frac{1}{\Delta_{\text{avg}}(t_n)} \tag{2.10}$$

Here, $\Delta_{\text{avg}}(t_n) = (t_{n+1} - t_{n-1})/2$ is the average of the time intervals to the next shorter and next longer observed events.[28] The distributions $P_{\text{on}}(t)$ (red dots) and $P_{\text{off}}(t)$ (blue open squares) are plotted in Figure 2.5b in a log-log scale. The linear alignment of the data points in Figure 2.5b indicates that both $P_{\text{on}}(t)$ and $P_{\text{off}}(t)$ follow an inverse power law: $P_{\text{on(off)}}(t) \propto t^{-k_{\text{on(off)}}}$ and linear regression (plain lines in Figure 4.7b) shows that $k_{\text{off}} = 2.44$ and $k_{\text{on}} = 1.02$. The steeper slope of the *off* events makes *off* periods of 10 ms about 100 times more likely than 100-ms ones. A similar analysis was performed on 25 different QDs with an average value of 1.2 for k_{on} and 2.2 for k_{off}. A value of $k_{\text{off}} > 2$ is indicative of efficient blinking suppression and comparable to the values reported in nearly blinking-free CdSe/CdS QD.[4, 29] In the inset of Figure 2.5b, the survival probabilities $S_{\text{on(off)}}(t) = \int_t^{\infty} P_{\text{on(off)}}(\tau)\,\tau$ are shown, which represent the probability to find the QD in an *on* or an *off* state for a time longer than t. Given the power-law distribution of $P_{\text{on}}(t)$ and $P_{\text{off}}(t)$, the survival probabilities $S_{\text{on(off)}}(t)$ scale in principle as $t^{-(k_{\text{on(off)}}-1)}$. However, as $k_{\text{on}} \approx 1$, $S_{\text{on}}(t)$ departs from this power law. The survival probabilities show even more clearly that the *off* periods are remarkably short (10-100 ms) while the *on* periods often last a few seconds or more. As can be seen in the inset of Figure 2.5b, the probability that a QD turns on to remain bright during more than one second is about 50%. Such long *on* periods are comparable to those reported by Mahler *et al.* in their study on thick-shell non-blinking CdSe/CdS QDs.[30] Although the atomistic origin of blinking in QDs is still debated,[31] this observation puts the InP/ZnSe QDs studied here among today's state-of-the-art nearly blinking-free QDs.

Excitation-intensity dependence of blinking statistics

QDs were also excited at different excitation levels from the weak-pumping regime to saturation. Their luminescence was recorded with a same binning time of 10 ms, as shown in Figure 2.6 (a-d). The stability of the emission is preserved despite the excitation (and emission) intensities vary by about one order of magnitude. The blinking displays a standard *on-off* pattern. The histogram of intensity counts is plotted next to the blinking trace. It is observed that there is only a slight decrease in the *on*-time fraction (from 97% to 86%) when the QD is subjected to a higher excitation intensities. To quantify the blinking statistics, the probability-density distributions of the *on* and *off* states are plotted in Figure 2.6 (e-h). It is observed that they again follow an inverse-power law $P_{\text{off/on}}(t) \propto t^{-k_{\text{off/on}}}$. The fit yields the power-law factors k_{off} and k_{on} indicated in the figures with an increase of k_{on} from 1.1 to 1.6 and a decrease of k_{off} from 2.3 to ~2.0. At higher excitation power, the *on* periods become shorter and the *off* periods become longer, but still more than one order of magnitude shorter than the *on* ones. Even at excitation intensities close to saturation, the *off* states of the QD are still much shorter than the *on* states. Their survival probabilities shown in the insets confirm that the *on* periods remain significantly longer than the *off* periods. It is noted that while the density of low-emission photons

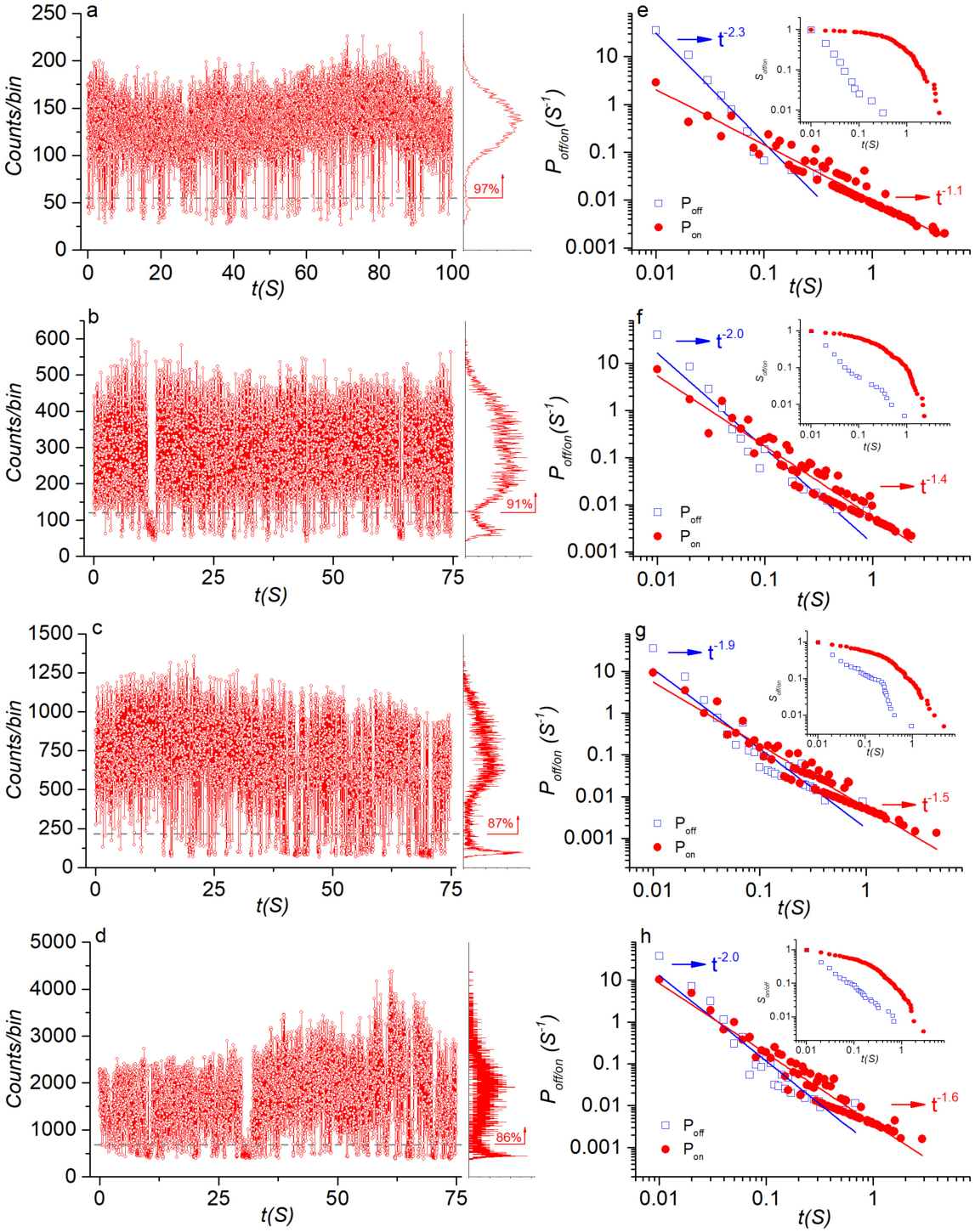

Figure 2.6. | Blinking at higher excitation intensity. (a-d) QD luminescence photon-counting traces (10-ms time bin) at different excitation intensities: 76 $\mathrm{W/cm^2}$, 420 $\mathrm{W/cm^2}$, 640 $\mathrm{W/cm^2}$, and 950 $\mathrm{W/cm^2}$ respectively. (e-h) Corresponding probability density distributions of the *on* and *off* time periods fitted to power law distributions $P_{\mathrm{off/on}}(t) \propto t^{-k_{\mathrm{off/on}}}$. Inset: survival probabilities $S_{\mathrm{off/on}}(t) = \int_t^{\infty} P_{\mathrm{off/on}}(\tau)\, d\tau$ constructed from the same data.

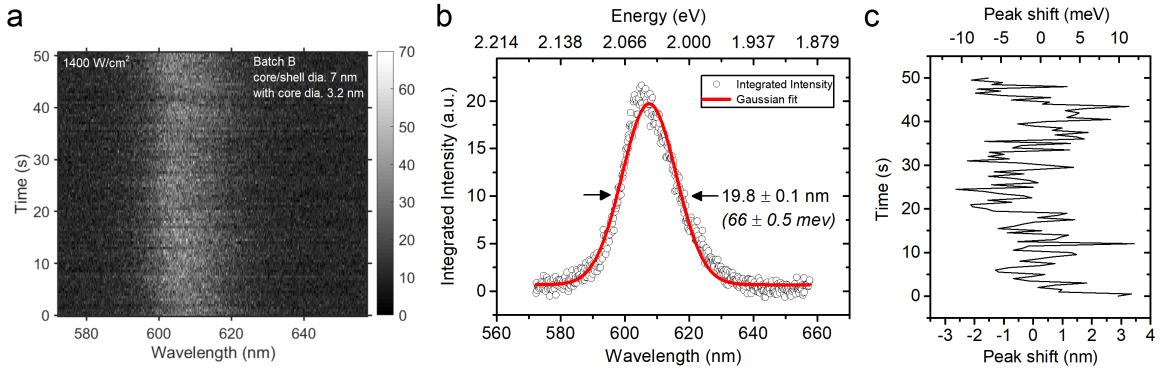

Figure 2.7. | Time dependent single QD spectrum at room temperature. (a) Time sequence of a single QD emission. Resolution of the CCD camera is 40 pm. (b) Integrated spectrum with a Gaussian fit that has a linewidth of 19.8 ± 0.1 nm. (c) A ±3 nm peak shift from central emission energy by fitting Gaussian function at each acquisition. [Integration time is 0.5 s]

is indeed very low, the histogram of the emission from the bright state show a quite large width. The larger width in the histogram is attributed to switching to extremely short *off* periods which creates an uncertainty in the emission counts when switching back to *on* periods. The stable emission in addition to the preserved antibunching at saturation intensities (see section 2.4.2) further consolidates that this type of InP/ZnSe QDs is suitable for applications in quantum optics.

Spectral diffusion at room temperature

To determine the effect of spectral diffusion of these QDs at room temperature, the time-dependent emission of single QDs (Batch-B InP/ZnSe QD having core/shell diameter of 7 nm with a core diameter of 3.2 nm) is measured by exciting them at 400 nm using a pulsed laser having a repetition rate of 8 MhZ with an integration time of 0.5 s. Figure 2.7a shows a time and spectral resolved image sequence of an emission from a single QD excited at 1400 W/cm^2. Note that the resolution of the CCD camera is 40 pm. Figure 2.7b shows a time-integrated spectrum with a Gaussian fit that has a linewidth of about 19.8 nm (66 meV). By fitting the Gaussian function at each acquisition, the central emission energy is extracted. Figure 2.7c shows the time-dependent spectral peak shift from the central emission energy with a range of ±3 nm (±10 meV). Note that this QD also exhibits nearly-blinking free emission with longer *on* periods. This measurement on a dropcasted single QD on glass substrate was done in an ambient condition which indicates that the photo-oxidation of the QDs is prevented by the protective shell, but subjected to a spectral jitter attributed to quantum confined stark effect. Note that the single QD linewidth of 14 nm (46 meV) shown in Figure 2.3 belonging to Batch-A was an integrated average spectrum for 60 s. See Chapter 5 for the detailed study on spectral diffusion and the structural conditions that determine the minimal SD for spherical QDs.

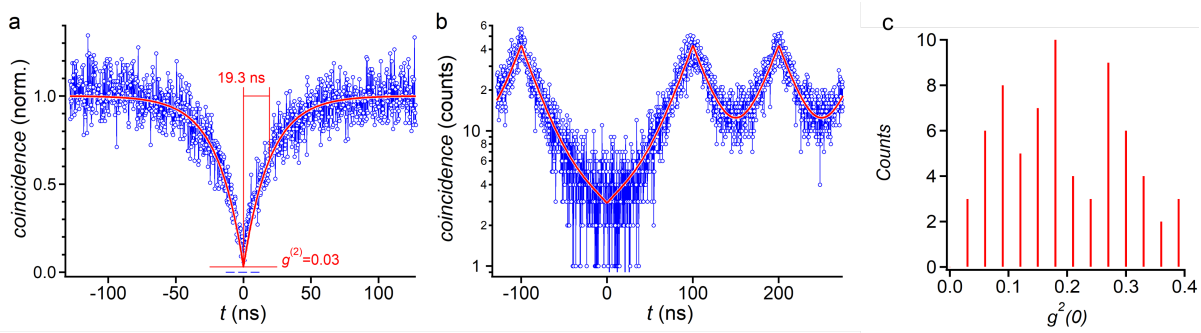

Figure 2.8. | Antibunching. (a) Second-order correlation function $g^{(2)}(t)$ of a QD under CW excitation at 445 nm. (b) Second-order correlation function of the same QD under 445-nm (picosecond) pulse excitation at a repetition rate of 10 MHz. The strong antibunching is raw data, without background subtraction nor compensation for intensity differences in start/stop channels. (c) Histogram of $g^{(2)}(0)$ values under CW excitation. The non-zero value of $g^{(2)}(0)$ is only attributed to the residual background noise and not the multi-exciton emission.

2.4. Efficient single photon emitter

2.4.1. Antibunching

Strong photon antibunching was observed from single InP/ZnSe QDs. Figure 2.8a shows the second-order correlation function $g^{(2)}(t)$ of a single QD measured under CW-laser pumping at 445 nm. The antibunching in Figure 2.8a is almost ideal with only a residual background-limited zero-delay value $g^{(2)}(0) = 0.03$. The data is fitted to the function $g^{(2)}(t) = 1 - [1 - g^{(2)}(0)] \exp(-(\gamma + w_p)\,|t|)$, where $w_p = \sigma I/(\hbar\omega_p)$ is the pumping rate of the QD and γ its luminescence decay rate.[32] The experiment was performed in a weak excitation regime ($w_p \ll \gamma$). The fit yields $(\gamma + w_p)^{-1} \approx \gamma^{-1} = 19.3$ ns in line with the luminescence decay time statistics measured by direct photon timing (see Figure 2.3). The same QD was also excited with 445-nm picosecond pulses at a repetition rate of 10 MHz. No zero-delay peak was seen in the second-order correlation function (see Figure 2.8b), even in logarithmic scale, confirming that multi-exciton emission is very efficiently quenched by non-radiative Auger recombination of charge carriers. The solid lines are single exponential fits to $\exp(-\gamma\,(|t - nT_{\text{rep}}|))$, where $n \neq 0$ is the order of the correlation peak and T_{rep} is the repetition rate of the pulse. The $g^{(2)}(0)$ value was measured for 70 single QDs in the CW-pumping regime and found a mean value of 0.19 with a standard deviation of 0.1 (see Figure 2.8c). In each case the antibunching was limited by the residual background noise, not by multi-exciton emission (see section 2.2.2 for faster biexciton Auger rate).

2.4.2. Purity at saturation excitation intensity

A high photoluminescence quantum yield (PLQY) and a strong antibunching are key for using InP/ZnSe QDs as integrated single-photon emitters in quantum technology applications. In this perspective, it is crucially important that antibunching be preserved in the saturation regime when $I \gg I_S$ (equivalently, $w_p \gg \gamma$), such that $I/(I + I_S) = w_p/(w_p + \gamma) \approx 1$. If this condition is fulfilled, the emitter can act as a *photon gun*, i.e, a short-pulse excitation with sufficient fluence can completely invert the population of the effective two-level system and trigger the spontaneous emission of a single

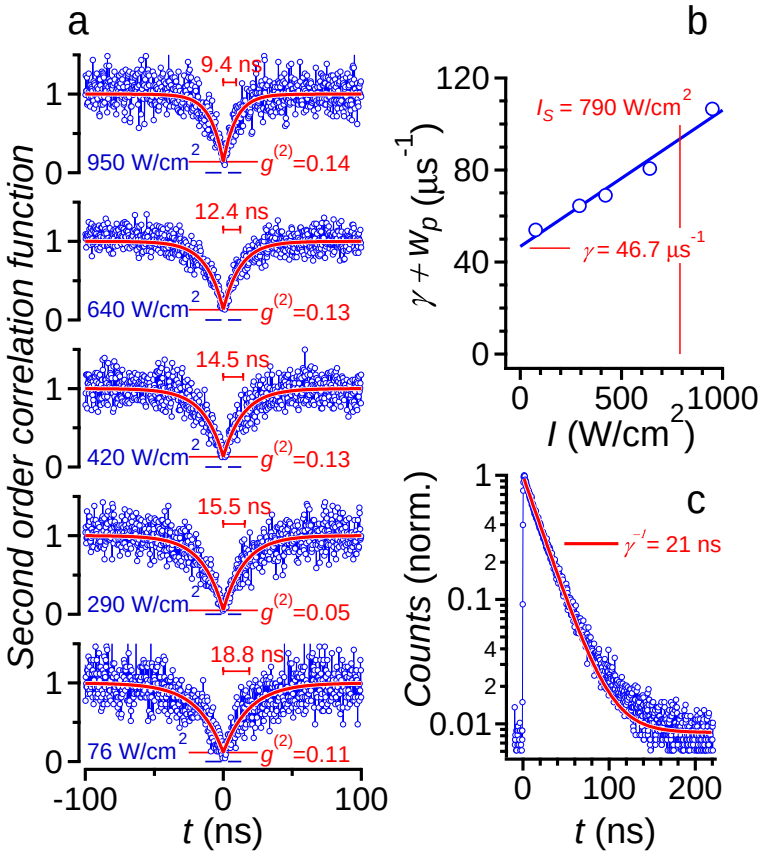

Figure 2.9. | Antibunching at higher excitation intensities. (a) Second-order correlation function of a single QD at different CW-pumping intensities at 445 nm. (b) Antibunching width-constant $\gamma + w_p$ as a function of the pump intensity. (c) Luminescence decay of the QD using a pulsed excitation with a repetition rate of 2.5 Mhz.

photon with a probability equal to the PLQY. In Figure 2.9a, the second-order correlation traces recorded on a single InP/ZnSe QD at pump intensities increasing from 76 $\mathrm{W/cm^2}$ to 950 $\mathrm{W/cm^2}$ is shown. Over the entire intensity range, the luminescence of the QD preserved a strong antibunching, with a narrowing of the zero-delay dip at higher pump intensity and a stable background-noise limited $g^{(2)}(0)$ between 0.05 and 0.14. By fitting the $g^{(2)}$-functions, the time constant $(\gamma + w_p)^{-1}$ could be determined as indicated in Figure 2.9a. It can be seen that this time constant is always smaller than the emission lifetime – determined at $\gamma^{-1} = 21$ ns for this particular QD (see Figure 2.9c), and drops from 18.8 ns to 9.4 ns with increasing pump intensity.

Figure 2.9b represents $\gamma + w_p$ as a function of the pump intensity I. In line with the linear dependence of w_p on the pump intensity, $\gamma + w_p$ changes linearly with I. A best fit yields a slope $\sigma/(\hbar\omega_p)$ of 5.9×10^4 $\mathrm{cm^2/J}$, from which the absorption cross-section of the QD obtained as $\sigma = 2.0 \times 10^{-14}$ $\mathrm{cm^2}$. This figure is equal to the ensemble value that was derived from the photoluminescence saturation as plotted in Figure 2.1c. By extrapolating the data in Figure 2.9b to the $I \to 0$ limit, the luminescence decay rate of the QD was found as $\gamma = 46.7$ μs^{-1} ($1/\gamma$= 21.4 ns), a figure that agrees well with the luminescence decay time $\gamma^{-1} = 21$ ns obtained in a direct photon-timing experiment (see Figure 2.9c). Combining σ and γ, the saturation intensity of this QD is determined as $I_S = \hbar\omega_p\gamma/\sigma = 790$ $\mathrm{W/cm^2}$. Hence, the data shown in Figure 2.9 demonstrate that strong antibunching is preserved for pumping

intensities up to $1.2 \times I_S$, with no sign of multi-exciton emission nor significant photo-degradation of the emitter, two essential properties enabling the use of InP/ZnSe QDs as triggered single-photon emitters in quantum optics applications.

In the case of CdSe/ZnS, the persistence of photon antibunching when pumping single QDs above the saturation intensity was attributed to the quenching of radiative recombination of multi-excitons by fast Auger recombination.[33] To quantify the rate of Auger recombination, and thus the yield of multi-exciton emission in the case of the InP/ZnSe QDs studied here, the transient absorbance of an InP/ZnSe dispersion was studied after femtosecond optical pumping. As discussed in the section 2.2.2, an additional decay component with a time constant of ~ 70 ps appeared in the transient absorption at high pump intensities. Such a fast component is a typical characteristic of Auger recombination of multi-excitons.[34] Therefore the corresponding decay rate $\gamma_{XX} = 14.3$ ns^{-1} is interpreted as the combined result of biexciton decay by radiative and non-radiative (Auger) recombination, *i.e.* $\gamma_{XX} = \gamma_{\mathrm{r},XX} + \gamma_{\mathrm{nr},XX}$. Writing the radiative recombination rate of biexcitons[35] $\gamma_{\mathrm{r},XX} = 4\gamma$ ($\gamma^{-1} = 36$ ns is the decay time of the fundamental exciton in solution), the radiative biexciton quantum yield is estimated in InP/ZnSe QDs as: $\mathrm{PLQY}_{XX} = \gamma_{\mathrm{r},XX}/\gamma_{XX} = 0.77\%$. This low value explains why single-photon emission is retained at high pumping power.

2.5. Conclusion

In conclusion, single InP/ZnSe colloidal QDs show a combination of narrow room-temperature emission spectrum, strong antibunching, mono-exponential luminescence decay, reduced blinking, and photostability. Single QD spectroscopy study demonstrates that single-photon emission is preserved at saturating intensities, which is attributed to fast non-radiative Auger recombination of multi-excitons. Although these fast multi-exciton recombination rates might limit their use for light amplification, these QDs are ideally suited for quantum optics applications as single-photon turnstile devices. Furthermore, reduced cytotoxicity compared to Cd-based QDs offers them a prospect in life-science applications.[36] Unconventionally, despite the strong Auger blockade mechanism, single QDs display very little luminescence intermittency (blinking), with good photostability, which places these QDs in the class of nearly blinking-free QDs, with emission stability comparable to state-of-the-art thick-shell and alloyed-interface CdSe/CdS.

Bibliography

[1] Mickael D. Tessier, Dorian Dupont, Kim De Nolf, Jonathan De Roo, and Zeger Hens. Economic and size-tunable synthesis of InP/ZnE (e = s, se) colloidal quantum dots. *Chemistry of Materials*, 27(13):4893–4898, jun 2015.

[2] Mickael D. Tessier, Kim De Nolf, Dorian Dupont, Davy Sinnaeve, Jonathan De Roo, and Zeger Hens. Aminophosphines: A double role in the synthesis of colloidal indium phosphide quantum dots. *Journal of the American Chemical Society*, 138(18):5923–5929, may 2016.

[3] S. Ithurria, M. D. Tessier, B. Mahler, R. P. S. M. Lobo, B. Dubertret, and Al. L. Efros. Colloidal nanoplatelets with two-dimensional electronic structure. *Nature Materials*, 10(12):936–941, oct 2011.

[4] Ou Chen, Jing Zhao, Vikash P. Chauhan, Jian Cui, Cliff Wong, Daniel K. Harris, He Wei, Hee-Sun Han, Dai Fukumura, Rakesh K. Jain, and Moungi G. Bawendi. Compact high-quality CdSe–CdS core–shell nanocrystals with narrow emission linewidths and suppressed blinking. *Nature Materials*, 12(5):445–451, feb 2013.

[5] Jian Cui, Andrew P. Beyler, Lisa F. Marshall, Ou Chen, Daniel K. Harris, Darcy D. Wanger, Xavier Brokmann, and Moungi G. Bawendi. Direct probe of spectral inhomogeneity reveals synthetic tunability of single-nanocrystal spectral linewidths. *Nature Chemistry*, 5(7):602–606, jun 2013.

[6] Loredana Protesescu, Sergii Yakunin, Maryna I. Bodnarchuk, Franziska Krieg, Riccarda Caputo, Christopher H. Hendon, Ruo Xi Yang, Aron Walsh, and Maksym V. Kovalenko. Nanocrystals of cesium lead halide perovskites (CsPbX3, x = cl, br, and i): Novel optoelectronic materials showing bright emission with wide color gamut. *Nano Letters*, 15(6):3692–3696, feb 2015.

[7] A. E. Neeves and M. H. Birnboim. Composite structures for the enhancement of nonlinear-optical susceptibility. *Journal of the Optical Society of America B*, 6(4):787, apr 1989.

[8] Bram De Geyter, Arjan J. Houtepen, Sergio Carrillo, Pieter Geiregat, Yunan Gao, Sybren ten Cate, Juleon M. Schins, Dries Van Thourhout, Christophe Delerue, Laurens D. A. Siebbeles, and Zeger Hens. Broadband and picosecond intraband absorption in lead-based colloidal quantum dots. *ACS Nano*, 6(7):6067–6074, jun 2012.

[9] Louis Biadala, Benjamin Siebers, Yasin Beyazit, Mickaël. D. Tessier, Dorian Dupont, Zeger Hens, Dmitri R. Yakovlev, and Manfred Bayer. Band-edge exciton fine structure and recombination dynamics in InP/ZnS colloidal nanocrystals. *ACS Nano*, 10(3):3356–3364, feb 2016.

[10] D.I. Chepic, Al.L. Efros, A.I. Ekimov, M.G. Ivanov, V.A. Kharchenko, I.A. Kudriavtsev, and T.V. Yazeva. Auger ionization of semiconductor quantum drops in a glass matrix. *Journal of Luminescence*, 47(3):113–127, oct 1990.

[11] George E. Cragg and Alexander L. Efros. Suppression of auger processes in confined structures. *Nano Letters*, 10(1):313–317, jan 2010.

[12] B. R. Fisher, H. J. Eisler, N. E. Stott, and M. G. Bawendi. Emission intensity dependence and single-exponential behavior in single colloidal quantum dot fluorescence lifetimes. *The Journal of Physical Chemistry B*, 108(1):143–148, jan 2004.

[13] Al. L. Efros and A. V. Rodina. Band-edge absorption and luminescence of nonspherical nanometer-size crystals. *Physical Review B*, 47:10005–10007, apr 1993.

[14] Celso de Mello Donegá and Rolf Koole. Size dependence of the spontaneous emission rate and absorption cross section of CdSe and CdTe quantum dots. *The Journal of Physical Chemistry C*, 113(16):6511–6520, mar 2009.

[15] A. F. van Driel, G. Allan, C. Delerue, P. Lodahl, W. L. Vos, and D. Vanmaekelbergh. Frequency-dependent spontaneous emission rate from CdSe and CdTe nanocrystals: Influence of dark states. *Physical Review Letters*, 95:236804, dec 2005.

[16] D. J. Norris, Al. L. Efros, M. Rosen, and M. G. Bawendi. Size dependence of exciton fine structure in CdSe quantum dots. *Physical Review B*, 53:16347–16354, jun 1996.

[17] Anjana Bagga, P. K. Chattopadhyay, and Subhasis Ghosh. Origin of stokes shift in inas and cdse quantum dots: Exchange splitting of excitonic states. *Physical Review B*, 74:035341, jul 2006.

[18] Oleksandr Voznyy, Larissa Levina, Fengjia Fan, Grant Walters, James Z. Fan, Amirreza Kiani, Alexander H. Ip, Susanna M. Thon, Andrew H. Proppe, Mengxia Liu, and Edward H. Sargent. Origins of stokes shift in PbS nanocrystals. *Nano Letters*, 17(12):7191–7195, nov 2017.

[19] A. Franceschetti and S. T. Pantelides. Excited-state relaxations and franck-condon shift in si quantum dots. *Physical Review B*, 68:033313, jul 2003.

[20] Timothy G. Mack, Lakshay Jethi, and Patanjali Kambhampati. Temperature dependence of emission line widths from semiconductor nanocrystals reveals vibronic contributions to line broadening processes. *The Journal of Physical Chemistry C*, 121(51):28537–28545, dec 2017.

[21] Justin R. Caram, Sophie N. Bertram, Hendrik Utzat, Whitney R. Hess, Jessica A. Carr, Thomas S. Bischof, Andrew P. Beyler, Mark W. B. Wilson, and Moungi G. Bawendi. PbS nanocrystal emission is governed by multiple emissive states. *Nano Letters*, 16(10):6070–6077, sep 2016.

[22] Yun Liu, Donghun Kim, Owen P. Morris, David Zhitomirsky, and Jeffrey C. Grossman. Origins of the stokes shift in PbS quantum dots: Impact of polydispersity, ligands, and defects. *ACS Nano*, 12(3):2838–2845, mar 2018.

[23] Eric M. Janke, Nicholas E. Williams, Chunxing She, Danylo Zherebetskyy, Margaret H. Hudson, Lili Wang, David J. Gosztola, Richard D. Schaller, Byeongdu Lee, Chengjun Sun, Gregory S. Engel, and Dmitri V. Talapin. Origin of broad emission spectra in InP quantum dots: Contributions from structural and electronic disorder. *Journal of the American Chemical Society*, 140(46):15791–15803, oct 2018.

[24] Mark J. Fernée, Philippe Tamarat, and Brahim Lounis. Spectroscopy of single nanocrystals. *Chemical Society Reviews*, 43(4):1311, 2014.

[25] Young-Shin Park, Jaehoon Lim, and Victor I. Klimov. Asymmetrically strained quantum dots with non-fluctuating single-dot emission spectra and subthermal room-temperature linewidths. *Nature Materials*, 18(3):249–255, jan 2019.

[26] Jian Cui, Andrew P. Beyler, Igor Coropceanu, Liam Cleary, Thomas R. Avila, Yue Chen, José M. Cordero, S. Leigh Heathcote, Daniel K. Harris, Ou Chen, Jianshu Cao, and Moungi G. Bawendi. Evolution of the single-nanocrystal photoluminescence linewidth with size and shell: Implications for exciton–phonon coupling and the optimization of spectral linewidths. *Nano Letters*, 16(1):289–296, dec 2015.

[27] P. Spinicelli, S. Buil, X. Quélin, B. Mahler, B. Dubertret, and J.-P. Hermier. Bright and grey states in CdSe-CdS nanocrystals exhibiting strongly reduced blinking. *Physical Review Letters*, 102(13), mar 2009.

[28] M. Kuno, D. P. Fromm, H. F. Hamann, A. Gallagher, and D. J. Nesbitt. "on"/"off" fluorescence intermittency of single semiconductor quantum dots. *The Journal of Chemical Physics*, 115(2):1028–1040, jul 2001.

[29] Sungchul Hohng and Taekjip Ha. Near-complete suppression of quantum dot blinking in ambient conditions. *Journal of the American Chemical Society*, 126(5):1324–1325, feb 2004.

[30] Benoit Mahler, Piernicola Spinicelli, Stéphanie Buil, Xavier Quelin, Jean-Pierre Hermier, and Benoit Dubertret. Towards non-blinking colloidal quantum dots. *Nature Materials*, 7(8):659–664, jun 2008.

[31] Alexander L. Efros and David J. Nesbitt. Origin and control of blinking in quantum dots. *Nature Nanotechnology*, 11(8):661–671, aug 2016.

[32] Peter Michler. *Nonclassical Light from Single Semiconductor Quantum Dots*, chapter 8, pages 315–347. Springer Berlin Heidelberg, Berlin, Heidelberg, nov 2003.

[33] B. Lounis, H.A. Bechtel, D. Gerion, P. Alivisatos, and W.E. Moerner. Photon antibunching in single CdSe/ZnS quantum dot fluorescence. *Chemical Physics Letters*, 329(5-6):399–404, oct 2000.

[34] V. I. Klimov, A. A. Mikhailovsky, D. W. McBranch, C. A. Leatherdale, and M. G. Bawendi. Quantization of multiparticle auger rates in semiconductor quantum dots. *Science*, 287(5455):1011–1013, feb 2000.

[35] Florencio García-Santamaría, Sergio Brovelli, Ranjani Viswanatha, Jennifer A. Hollingsworth, Han Htoon, Scott A. Crooker, and Victor I. Klimov. Breakdown of volume scaling in auger recombination in CdSe/CdS heteronanocrystals: The role of the core-shell interface. *Nano Letters*, 11(2):687–693, feb 2011.

[36] Peter Reiss, Marie Carrière, Christophe Lincheneau, Louis Vaure, and Sudarsan Tamang. Synthesis of semiconductor nanocrystals, focusing on nontoxic and earth-abundant materials. *Chemical Reviews*, 116(18):10731–10819, jul 2016.

Chapter 3.

Nearly isotropic bright exciton fine structure

Contents

Synopsis

Using polarization resolved single-QD PL, this chapter shows radiative recombination of bright exciton fine structure identifying emissions from exciton-doublet, trion-singlet & biexciton-doublet. Fluorescence line narrowing spectra of an ensemble of QDs in magnetic fields demonstrate that the bright exciton effectively consists of three states. The Zeeman splitting of these states is well described by an isotropic exciton model, where the fine structure is dominated by electron-hole exchange and shape anisotropy only leads to a minor splitting of the $F = 1$ triplet. It is postulated that excitons in InP-based QDs are nearly isotropic because of the particular ratio of light and heavy hole masses in InP.

Based on the publication J. Phys. Chem. Lett. 2019, 10, 18, 5468-5475
Synthesis of InP/ZnSe QDs by Dr. Dorian Dupont, Ghent University, Belgium
FLN measurements by Dr. Annalisa Brodu, Utrecht University, Netherlands

3.1. Introduction

3.1.1. Multi-band envelope function approximation

The electronic structure of semiconductors can be modelled using different theories: ab initio method, density functional method and semi-empirical methods like tight binding, pseudo-potential & envelope function. These methods differ in the choice of basis functions to represent the Schrödinger equation like atomic basis, plane wave basis and Bloch state basis in the aforementioned semi-empirical methods respectively. Colloidal quantum dots (QDs) are quasi-spherical semiconductor nanocrystals (NCs) in which an electron-hole pair is confined in a volume with dimensions smaller than the exciton Bohr radius of the corresponding bulk material. Under such strong confinement conditions, the conduction band (CB) and valence band (VB) edges are reduced to a set of quantized eigenstates that describe electron and hole motion. Periodic materials like NC can be easily modelled using envelope function method which form the basis for effective mass approximation (EMA) theory. For II-VI and III-V materials like CdSe, CdTe and InP having either wurtzite or zincblende lattice structures, the band edges are near the center of the Brillouin zone (Γ point). In these NCs, the CB has s-like symmetry with two-fold spin degenerate lowest level and VB has p-like symmetry with six-fold spin degenerate uppermost level. The VB has three sub-bands: heavy hole (HH), light hole (LH) and split-off (SO) bands, with HH & LH bands degenerate at the Γ-point and the SO band well separated from them due to spin-orbit interaction. For non-zero values of wavevector k, energy-dispersion curve shows that the HH component descends at a rate slower than LH corresponding to their effective masses and thus they get their names. The Hamiltonian for such a system was initially derived by Luttinger and Kohn.[1, 2]

A single band EMA described in section 1.2.2 do not include the complex nature of band edge structures. An improvement is a *multi-band EMA* or $k.p$ *perturbation method* which also includes the possibility of band-to-band tunneling due to the presence of a static field or a lattice defect producing free carriers. This model can be applied to QDs of arbitrary shape and material composition, including the effect of strain, piezoelectricity, spin-orbit interaction, crystal field splitting, VB mixing and CB-VB interaction.[3] Since the basis functions are described in terms of Hamiltonian matrices, the multi-band EMA gets its name from the number of bands that are included to evaluate the envelope wavefunctions. A simple model for VB is expressed in terms of a 4×4 Hamiltonian describing HH and LH. A 6×6 Hamiltonian adds the term Γ_7 SO band as well. The coupling of VB and CB is taken into account in a 8×8 Hamiltonian, also called as Kane Hamiltonian[4] or Pidgeon-Brown model,[5] by including Γ_6 CB to the above Luttinger Hamiltonian.

In wide bandgap NCs like InP, VB-CB coupling is weak and hence the VB can be expressed with a 6×6 Luttinger Hamiltonian while a single band EMA is sufficient to describe the CB. A mixing of VB levels occurs when applying the spherical boundary condition to the Hamiltonian. So the quantum numbers $J_h = L_h + S_h$ from the unit cell and L_h from the envelope function are not conserved. Here, L & S are total azimuthal & spin quantum numbers respectively. Only the total angular momentum of hole $F_h = J_h + L_h$ and the parity are the good quantum numbers. Further, the envelope function and the unit cell function also mix together, an effect called as S-D mixing.[6, 7] Due to the mixing of the L_h and $L_h + 2$ states in the hole wavefunction, the selection rule $\Delta_n = 0$ is relaxed causing multiple transitions at the band edge.[8] Here, n is the principal quantum number. Energy states are labeled as nL_F and this approach leads to a two-fold, spin degenerate lowest conduction-band state labeled $1\mathrm{S}_{1/2,e}$ and a fourfold degenerate upper valence band state labeled $1\mathrm{S}_{3/2,h}$. Note that a lack of inversion symmetry in zincblende structure slightly displaces the valence band maximum from $k = 0$,

though this effect is weak.[9] It is noted that some reports suggested $1S_{1/2,e}$ and $1P_{3/2,h}$ could form the lowest exciton state in InP QDs, especially for smaller sized QDs.[10, 11] While this requires a detailed theoretical analysis, our results seem to agree with the model of Efros *et al.* where the valence band mixing effect was discussed considering only the short-range exchange interaction.[12] However, this does not rule out the possibility of closely lying energy levels, but the correct ordering of levels for the specific size of the QDs requires further study.

The energy of the first quantum size level given by Efros *et al.*:[12]

For electrons:

$$E_{1S_{1/2,e}} = \frac{\hbar^2\pi^2}{2m_e a^2} \tag{3.1}$$

where where m_e is the electron effective mass and a is the radius of the crystal.

For holes:

$$E_{1S_{3/2,h}}(\beta) = \frac{\hbar^2\phi^2(\beta)}{2m_{hh}a^2} \tag{3.2}$$

where m_{hh} is the HH effective mass and $\phi(\beta)$ signifies the dependence of the hole ground state function on the light to heavy hole effective mass ratio $\beta = m_{lh}/m_{hh}$.[13]

The effect of interfaces in heterostructures affecting the Hamiltonian is beyond the scope of this dissertation and only the core material is taken into account describing the first quantum size levels and fine structures in InP material which agrees with the experimental results to be described later.

3.1.2. Fine structure

A multi-band EMA has the advantage of providing analytical expressions in which semiconductors are characterized by a limited set of parameters – which are often known for the corresponding bulk material – and the QD diameter is implemented as a continuously changing variable.[14] In the case of zinc blende or wurtzite semiconductors, which include II-VI and III-V materials such as CdSe, CdTe and InP, this approach leads to a two-fold degenerate lowest conduction-band state and a fourfold degenerate upper valence-band state.[14] As highlighted in Figure 3.1a-b, these degeneracies reflect the angular momentum of the Bloch states that make up the electron states at the edge of the conduction band ($s = 1/2$) and the valence band ($j = 3/2$), respectively.[14] The eigenstates of electron-hole pairs or excitons are then conveniently expressed using direct products of the two different conduction-band (electron) and four different valence-band (hole) states as a basis, see Figure 3.1c. The eightfold degeneracy of the spherical band edge exciton energy level in QDs is lifted by three significant factors such as: (1) electron-hole exchange interaction, (2) shape asymmetry Δ_{sh} and (3) intrinsic crystal field splitting Δ_{int} (only in case of hexagonal lattice structure). For cubic lattice structures like InP, only the first two terms need to be taken into account with $\Delta_{int} = 0$.

First, the exchange interaction splits the exciton levels in an optically dark low energy quintuplet and a high energy, bright triplet that are exciton eigenstates with total angular moment $F = j + s$ of 2 and 1, respectively (see Figure 3.1c). The exchange interaction has the following form given by the Hamiltonian:[12]

$$\hat{\boldsymbol{H}}_{exch} = -(2/3)\epsilon_{exch}(a_0)^3\delta(r_e - r_h)\sigma J \tag{3.3}$$

where a_0 is the lattice constant, ϵ_{exch} is the exchange strength constant, σ is the electron spin-1/2 matrix and J is the hole spin-3/2 matrix.

This exchange interaction induced splitting in terms of bulk exciton Bohr radius (a_B) can be written as:[12]

$$\hbar\omega_{ST} = (8/3)\pi(a_0/a_B)^3\epsilon_{exch} \tag{3.4}$$

Second, the shape asymmetry, by lifting the hole state degeneracies, split the exciton energy levels from a 3-fold degenerate bright and 5-fold degenerate dark state into further fine structures as shown in Figure 3.1c. The splitting due to this shape asymmetry can be written as:[12]

$$\Delta_{sh} = 2\mu u(\beta)E_{1S_{3/2,h}}(\beta) \tag{3.5}$$

where the deviation from the sphericity is characterized by the ratio c/b = 1 + μ of ellipsoid's major (c) to minor (b) axes. Here μ denotes the ellipticity of the crystal which is positive for prolate-like crystals and negative for oblate-like crystals. The dimensionless function $u(\beta)$ decreases from a positive value at β=0, becomes zero and then negative at β=0.14 and goes to zero again at β=1.[15] As discussed in section 3.3.4, this effective mass ratio of LH to HH is 0.149 for InP[16] making the energy level structure rather insensitive to shape anisotropy induced splitting.

The lowest exciton fine structure energy levels can be expressed by taking into account both the splitting parameters due to exchange interaction η and shape asymmetry $\Delta = \Delta_{sh} + \Delta_{int}$:[12]

$$\begin{aligned}
E_{\pm 2} &= -\frac{3}{2}\eta - \frac{1}{2}\Delta \\
E^L_{\pm 1} &= \frac{1}{2}\eta - \sqrt{\frac{(2\eta - \Delta)^2}{4} + 3\eta^2} \\
E^U_{\pm 1} &= \frac{1}{2}\eta + \sqrt{\frac{(2\eta - \Delta)^2}{4} + 3\eta^2} \\
E^L_0 &= -\frac{3}{2}\eta + \frac{1}{2}\Delta \\
E^U_0 &= \frac{5}{2}\eta + \frac{1}{2}\Delta
\end{aligned} \tag{3.6}$$

For CdSe-based colloidal QDs, multiple studies have shown that the multi-band effective mass description of exciton states agrees with the experimental characteristics of these states. First, the observation that CdSe QDs exhibit longer radiative lifetimes at cryogenic temperatures, was assigned to the presence of lowest energy dark exciton state.[17] Next, a more detailed study interpreted the different exciton features visible through fluorescence line narrowing (FLN) and photoluminescence excitation (PLE) spectroscopy using the combined contributions from electron-hole exchange, the crystal field and shape anisotropy to the exciton fine structure.[18] These reports were complemented by microphotoluminescence (μ-PL) on single CdSe-based QDs, which confirmed the presence of the lowest dark state and allowed for a direct measurement of the dark-bright splitting from the respective emission

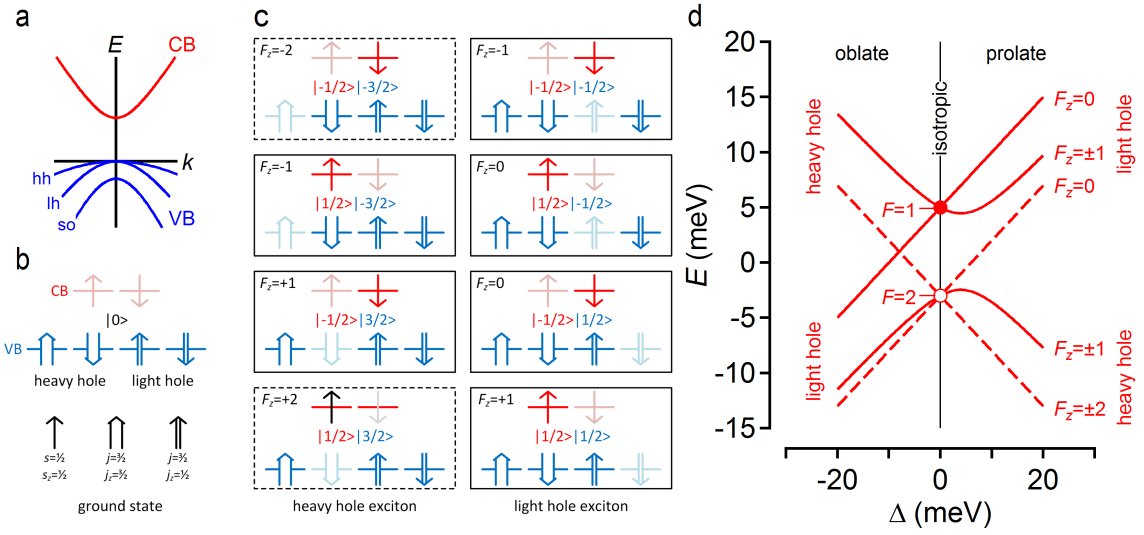

Figure 3.1. | Valence band mixing. (a) Outline of the edges of (blue, VB) the valence-band and (red, CB) the conduction of a zinc blende semiconductor around the center of the Brillouin zone, showing the (lh) light hole, (hh) heavy hole and (so) split off VB. (b) Representation of the CB and VB Bloch states at the Γ point, highlighting the degeneracy of both states in relation to their $s = 1/2$ and $j = 3/2$ angular momentum. Bright colors represent occupied states, semi-transparent colors empty states. (c) Overview of the 8 exciton states obtained as direct products of a CB electron and a VB hole state. The direct product states are labeled using the z-component of the total angular momentum F of the exciton. Transitions from the ground states to states boxed with a dashed line are spin forbidden. Again, bright colors represent occupied states and semi-transparent colors empty states. (d) Exciton eigenenergies calculated as a function of the anisotropy splitting energy Δ using an exchange splitting parameter $\eta = 2\,\mathrm{meV}$. States are labelled by means of the angular momentum projection quantum number F_z along the quantization axis. Full lines represent bright states, dashed lines dark states. Note that exchange couples the two $F_z = 0$ states to yield a bright (singlet) state and a dark (triplet) state. In the isotropic case, only the three $F = 1$ states are bright, whereas the five $F = 2$ states are dark as indicated by the filled and open circles.

lines.[19, 20] More recently, this body of work was extended by the analysis of the emission of wurtzite CdSe QDs in magnetic fields, both at the level of ensembles and single QDs. These investigations highlighted the additional contribution of lateral shape anisotropy,[21, 22] and resulted in estimates of the electron and hole g-factor.[23]

For InP QDs, however, the nature of the emissive state remains unclear. In line with the exciton model, time-resolved and FLN studies confirmed the presence of the lowest energy dark state and a higher energy bright state, with a 5-10 meV dark-bright splitting,[24, 25] Other reports, however, suggest that the PL may involve transitions between a conduction-band electron and a trapped hole.[26] In particular, a distribution of shallow hole traps may account for the persistently broad PL of InP QD ensembles and the remarkably high Stokes shift of the PL. On the other hand, studies using either photon-correlation Fourier spectroscopy in solution or μ-PL have shown that single InP/ZnSe QDs have an emission line at room temperature that is $\sim 50\,\mathrm{meV}$ wide, not unlike CdSe-based QDs.[27, 28] Such discrepancies call for a more in-depth study on the InP QD fine structure, such that experimental data can be compared to predictions of the multiband EMA model.

3.2. Bright exciton fine structure

3.2.1. Exciton, biexciton & trion

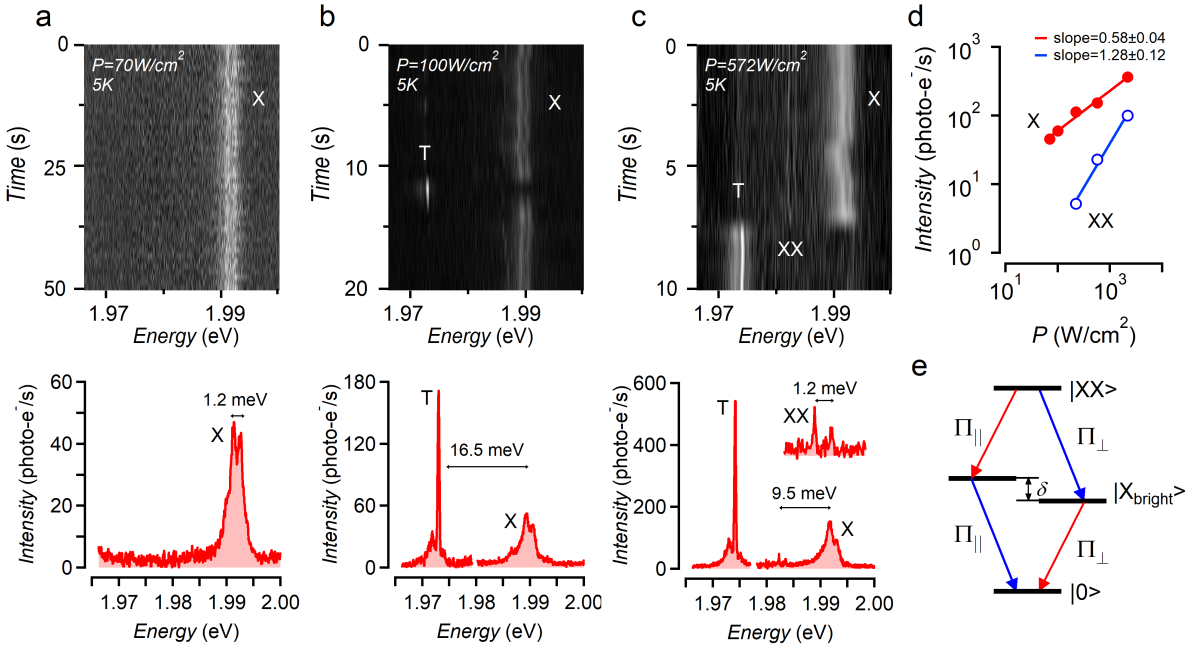

Figure 3.2. | Exciton, biexciton & trion. (a) (top) μ-PL time trace recorded on a single InP/ZnSe core/shell QD at cryogenic temperatures (5 K) showing emitted intensity as a function of the photon energy and measurement time under low power excitation. A doublet emission feature labeled X is clearly visible. (bottom) Time integrated spectrum highlighting the spectral doublet and the energy splitting δ of 1.2 meV. *Note:* The color scale in the time trace has the same scale the intensity axis in the time-integrated spectrum. (b) The same under higher excitation power, showing a temporal switch between the doublet X and a singlet emission line labeled T. Both features are retained in the integrated spectrum. (c) The same under even higher excitation power, showing a similar doublet-singlet switch as in (b) and the simultaneous occurrence of a second doublet labeled XX shifted by 9.5 meV to lower energy as compared to doublet X. The inset shows a close-up of the XX doublet. (d) Integrated intensity of the X and XX doublets as a function of excitation power. (e) Scheme showing that in a biexciton-exciton-ground state emission cascade, the biexciton line and the exciton line will exhibit the same splitting.

InP/ZnSe QDs for this study was prepared according to the method described in section 1.5.2. For single QD spectroscopy, we dropcast a nanomolar dispersion of InP/ZnSe QDs in a 1% solution of polystyrene-toluene on quartz coverslips, which was mounted in a PL microscope (see Appendix C.1). Using continuous wave excitation at 473 nm while keeping the temperature set at 5 K, we observed various characteristic features in the emission spectrum of a single InP/ZnSe QD. At relatively low excitation power, the image trace and the corresponding integrated spectrum feature a spectral doublet centered at 1.992 eV and split by an energy difference of $\delta = 1.2$ meV, see Figure 3.2a. Note that acoustic phonon sidebands (PSB) are visible on either side of the doublet line. Upon increasing the excitation power, the time trace represented in Figure 3.2b features an abrupt, temporal interruption of the doublet emission that leads to a single, narrow emission line 16.5 meV to the red of the doublet line. This singlet line exhibits clear phonon sidebands at either side of the central emission line. These sidebands account for 30% of the total emission and have a maximum intensity shifted by 1.1 meV with

respect to the main emission line, an energy shift that agrees with the vibrational modes of small InP nanocrystals.[29] A similar switching between emission spectra characterized by a doublet line and a single line was observed in a μ-PL study on CdSe/ZnS QDs by Fernee and coworkers.[30] Assigning the doublet to exciton emission and the singlet to trion emission, these authors interpreted the switching between the exciton and the trion emission to the random trapping of a band-edge carrier in a localized state.

Interestingly, at even higher power, the switching between the doublet at ~ 1.992 eV and the singlet line persists, yet the doublet line now concurs with a second, low-intensity doublet. This second doublet is shifted by 9.5 meV to lower energy and features the same splitting δ of 1.2 meV (see Figure 3.2c). Moreover, the intensity of the higher-energy doublet as recorded using continuous-wave excitation scales sub-linear with the excitation power, whereas the intensity of the additional, lower-energy doublet exhibits a supra-linear excitation power scaling. As indicated in see Figure 3.2d, fitting both power-dependent intensities to a power law yields two exponents with a ratio of 2.20 ± 0.25. Both observations support the assignment of the higher-energy doublet at ~ 1.992 eV to the bright exciton (X), and the lower energy doublet to the biexciton (XX). As outlined in Figure 3.2e, one indeed expects the transition from the biexciton to the exciton to yield an emission line that is the energetic mirror image of the bright exciton recombination. In that case, the singlet line can be assigned to a trion transition (T), not unlike previous studies on single CdSe/ZnS QDs.[30] The exciton doublet of single CdSe/ZnS QDs, on the other hand, was interpreted in terms of the exciton dark-bright splitting, where the high energy line of the doublet corresponds to the bright exciton and the low energy line to the dark exciton recombination. However, in the case of InP/ZnSe QDs emitting at a similar photon energy as the QDs studied here, the dark exciton was only observed through a broad, phonon-coupled emission feature shifted 5-15 meV to the red of the bright exciton.[25] Clearly, this observation supports the assignment of the high energy doublet in the case of InP/ZnSe QDs to a bright exciton doublet rather than a bright-dark combination. Possibly, the combination of strong broadening and long radiative lifetimes makes the dark exciton indiscernible in the emission spectrum of single InP/ZnSe QDs. In addition, the competition between radiative recombination of the bright exciton and cooling into the dark exciton state may account for the lower than expected power scaling of the exciton and biexciton emission with increasing pump power since the presence of a dark exciton will promote non-radiative Auger recombination.

3.2.2. Estimation of phonon temperature

Lineshape of the PL spectrum of the QD at cryogenic temperature is often a sharp ZPL superimposed by the broadband acoustic phonons.[31] The intensity of the broadband reflects the thermal distribution of phonons, described by the phonon population factor:

$$N_q = 1/(\exp\left(\frac{\hbar\omega}{k_B T}\right) - 1) \tag{3.7}$$

where k_B is the Boltzmann constant and ω is the emission frequency. At cryogenic temperatures, in the limit where multi-phonon processes are negligible, the phonon emission process proportional to $(N_q + 1)$ is dominant over phonon absorption process proportional to N_q, resulting in the asymmetric broadband visible in trion spectrum (see Figure 3.3) where the phonon emission is observed at lower energy to ZPL and phonon absorption at higher energy to ZPL. In PL experiments with the ZPL taken as the zero of frequency,[32]

$$\ln\left(\frac{I(-\hbar\omega)}{I(\hbar\omega)}\right) = \frac{\hbar\omega}{k_B T} \tag{3.8}$$

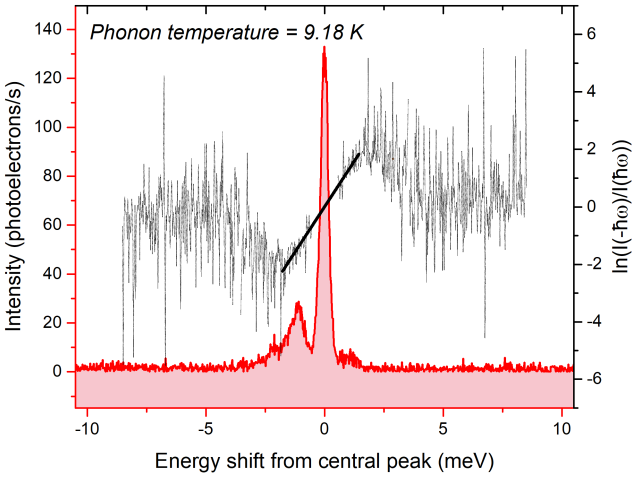

Figure 3.3. | Phonon temperature. Trion spectrum obtained at 5K is plotted with respect to the shift from the central emission energy (shown in red). The intensity ratio ln((I(-$\hbar\omega$))/(I($\hbar\omega$))) is also plotted (shown in black) and the solid line is the linear fit over the range of phonon processes from which a phonon temperature of about 9K is obtained.

This intensity ratio is also included in Figure 3.3 which is fitted with a linear function (with intercept fixed to zero), from which we determine a phonon temperature of ≈9K.

3.2.3. Trion tracking the polarization of exciton

To corroborate the assignment of the three emission features to the exciton, the trion and the biexciton, we further analyzed the polarization of the different emission lines. To do so, we successively passed the emitted light through a rotatable half-wave plate and a calcite beam displacer separating the linearly polarized components along and orthogonal to the displacement. Both parts were transmitted through the input slit of an imaging spectrometer at different positions along the slit and detected by the same CCD camera. Figure 3.4a shows the thus recorded spectra $I_{\parallel}$ and $I_{\perp}$ for a fixed orientation of the half-wave plate – characterized by an angle θ and thus a polarization rotation $\phi = 2\theta$ – under excitation conditions where the X, T and XX emission features are present. One sees that all the emission lines exhibit a pronounced polarization. Interestingly, the polarization of the lines constituting the X and XX doublets are each others mirror image. As outlined in Figure 3.2e, where the color coding agrees with the polarization analysis of 3.4a, this result is expected when both lines involve the same set of split bright exciton states. The trion polarization, on the other hand, appears to coincide with that of the high energy line of the X doublet. Focusing on the trion line, Figure 3.4b highlights that the intensities measured in both channels systematically change while rotating the half-wave plate. Starting at $\phi = 60°$, the trion emission intensity is highest in the parallel channel. Upon rotating the half-wave plate to $\phi = 110°$, one sees that the intensities in both channels become about equal, while the highest intensity is recorded in the perpendicular channel at an angle $\phi = 154°$.

Using the intensity $I_{\parallel}$ and $I_{\perp}$ recorded in both channels (compensated for the different grating efficiency of the two polarizations), we can define a degree of polarization (DOP) as:

$$\mathrm{DOP} = \frac{I_{\parallel} - I_{\perp}}{I_{\parallel} + I_{\perp}} \tag{3.9}$$

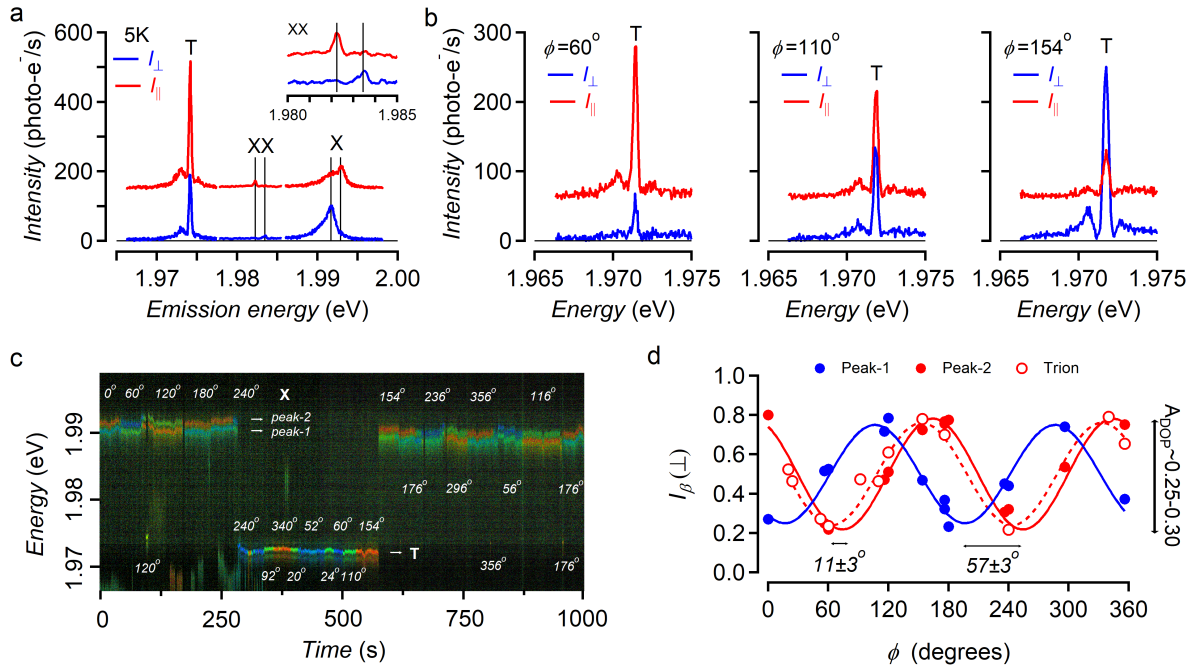

Figure 3.4. | Polarization resolved single dot spectra. (a) Time-integrated emission spectrum of a single InP/ZnSe QD under excitation conditions that lead to exciton, trion and biexciton emission as recorded in (blue) the perpendicular and (red) the parallel channel. The inset shows a zoom on the biexciton doublet. For clarity, an offset of 150 photo-electrons/s was added to the parallel trace. (b) Zooms on the trion emission for different orientations of the half-wave plate as recorded in the perpendicular and parallel channel. The polarization rotation introduced by the half-wave plate is given by the angle $\phi = 2\theta$, where θ gives the rotation of the half-wave plate relative to a reference. (c) Color value/hue representation of the emission spectrum of a single InP/ZnSe as a function of time. The hue represents the degree of polarization as indicated, whereas the brightness (value) is proportional to the logarithm of the signal intensity. For brightness, the same scale is used as in the trion spectra shown in b. The indicated angles ϕ represent the temporary orientation of the half-wave plate as outlined above. (d) Relative intensity measured in the perpendicular channel as a function of the orientation of the half-wave plate for (filled blue dots) the low energy peak of the exciton doublet, (filled red circles) the high energy peak of the exciton doublet, and (open red circles) the trion. Lines represent best fits to Eq 3.10.

Figure 3.4c shows an emission time trace recorded on the same InP/ZnSe QD as analyzed in Figure 3.2, but represented as a value/hue plot, where the color value and hue correspond to the total emission intensity and the DOP at each time point and emission energy. The figure highlights first of all the systematic difference in polarization of the two lines of the bright exciton doublet. Second, thanks to the switching between exciton and trion emission, it can be seen that the polarization of the trion indeed tracks the polarization of the high energy line of the exciton doublet. Both observations are confirmed in Figure 3.4d, which represents the relative intensity in the perpendicular channel for the two exciton lines and the trion as a function of the rotation induced by the half-wave plate. The full lines in Figure 3.4d represent fits of the different traces to the expression:

$$\frac{I_\perp}{I_\parallel + I_\perp} = \frac{1}{2} + A_{\mathrm{DOP}} \sin\left(2(\phi - \phi_0)\right) \tag{3.10}$$

As shown in Figure 3.4d, such fits yielded a DOP amplitude A_{DOP} in the range 0.25-0.3 for the different transitions. Moreover, the angular difference between the two lines of the exciton doublet amounted to $57 \pm 3°$, whereas the polarization angle of the triplet line and the high energy line of the exciton

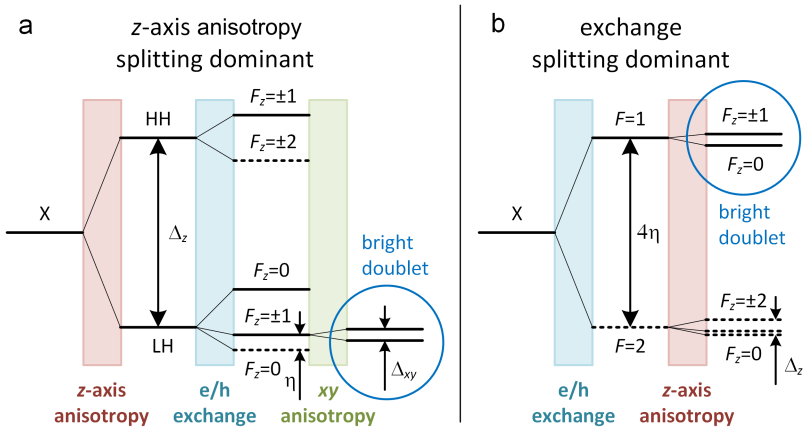

Figure 3.5. | Origin of random bright exciton splitting. (a) Sequence of splitting of the exciton states when z axis anisotropy dominates, for a case where the light hole exciton is lowered in energy. In that case, a bright exciton doublet can result from additional anisotropy in the $x-y$ plane. (b) Sequence of splitting of the exciton states when exchange dominates. In that case, a bright exciton doublet can result from a minor z-axis anisotropy (attributed to the exciton doublet splitting in InP/ZnSe QD shown in Figure 3.2). In both figures, η is the exchange parameter and Δ the anisotropy energy for the ground state exciton,[12] whereas full lines represent bright exciton states and dashed lines are dark exciton states.

doublet was only shifted by $11 \pm 3°$.

3.3. Origin of random bright exciton splitting

3.3.1. Fluorescence line narrowing spectra at higher magnetic fields

As argued above, the observation that the PL of a single InP/ZnSe QDs randomly switches at high illumination power between a spectrum showing two doublet lines, commensurate in terms of energy splitting and polarization, and a singlet line indicate that this PL results from recombination of band-edge charge carriers rather than trapped carriers. The multiband effective mass model of the band-edge exciton fine structure provides two possible interpretations of a bright doublet in QDs with a zinc blende crystal structure. First, as shown in Figure 3.1d, pronounced shape anisotropy brings either the light hole or heavy hole exciton states down in energy, which are both 4-fold degenerate states that are further split by exchange interaction to give exciton states with a fixed component of the angular moment F_z along the quantization axis z. This situation is detailed in Figure 3.5a for the case where the light hole is lowest in energy. This yields a fine structure in which a bright $F_z = \pm 1$ exciton doublet is separated from the $F_z = 0$ dark ground state by the exchange interaction and from the higher energy bright $F_z = 0$ exciton singlet by thrice the exchange interaction.[12] Additional anisotropy in the xy plane will split this isolated $F_z = \pm 1$ exciton in two components,[21, 22] emitting light linearly polarized along the x and y axis.[33] When the heavy hole states are lowest in energy, a similar situation arises where the lowest-energy bright state is an $F_z = \pm 1$ exciton that will be split by lateral anisotropy. Second, when the exchange interaction dominates, shape anisotropy will merely split the upper bright triplet in two components, a first with angular momentum $F_z = 0$ and a second with angular momentum $F_z = \pm 1$ (see Figure 3.5b). Such excitons will emit light linearly polarized along the z-axis and light circularly polarized within the xy plane, respectively. Finally, while shape anisotropy makes the low energy $F_z = \pm 1$ exciton bright through coupling with the high energy

$F_z = \pm 1$ exciton, this effect remains negligible for small deviations from the isotropic case. Hence the representation of the lower energy $F_z = \pm 1$ exciton by a dashed line in Figure 3.5b.

To determine the overall degeneracy of the bright exciton – 2-fold with a minor splitting due to anisotropy in the xy plane or 3-fold with a minor splitting due to anisotropy along the quantization axis z, see Figure 3.5 – the emission of an ensemble of InP/ZnSe QDs is analyzed by FLN spectroscopy in a magnetic field (see Appendix C.3 for the layout of the setup). For this study, a sample with a peak emission at 2.12 eV at 4 K was used (see Figure 3.6a), which was pumped resonantly at 2.06 eV using a monochromatic laser source. While not exactly identical, these experimental settings are in good correspondence with the single InP/ZnSe QDs discussed before. As shown in Figure 3.6b, FLN spectra were acquired in Faraday configuration with the excitation light parallel to the direction of the magnetic field. The excitation light had a σ^+ circular polarization, which dominantly excites the $F_z = +1$ state in the given configuration, while the emitted light was detected with σ^- polarization.

Figure 3.7a represents the FLN spectra acquired in the absence of a magnetic field using the excitation conditions described above. Note that the energy difference $\Delta E = \hbar\omega_{exc} - \hbar\omega_{em}$ between the excitation and emitted photons is used as the horizontal axis. The three broad features labelled C, D and E in the FLN spectrum were assigned previously to (C) the phonon activated dark exciton emission, and replicas of this transition involving the additional emission of (D) ZnSe or (E) InP LO phonons.[25] Using the latter two as a yardstick (taking into account the energy differences), the bright-dark splitting in these InP/ZnSe QDs was estimated at $\Delta E_{bd} = 6$ meV (see Figure 3.7a).

With increasing magnetic field, two additional features were observed that shift to lower energy relative to the $F_z = +1$ state. The central wavelength of the shifting emission features in the FLN spectrum is estimated by locally fitting the intensity $I(E)$ to a sum of a Gaussian and a quadratic background:

$$I(E) = A \exp\left(\frac{E - E_0}{w}\right)^2 + a_0 + a_1(E - E_0) + a_2(E - E_0)^2 \tag{3.11}$$

In Figure 3.7b, low energy part of various FLN spectra obtained on the same InP/ZnSe QD ensemble is shown, while increasing the magnetic field from 10 to 30 T. A first, labeled as A, can be discerned

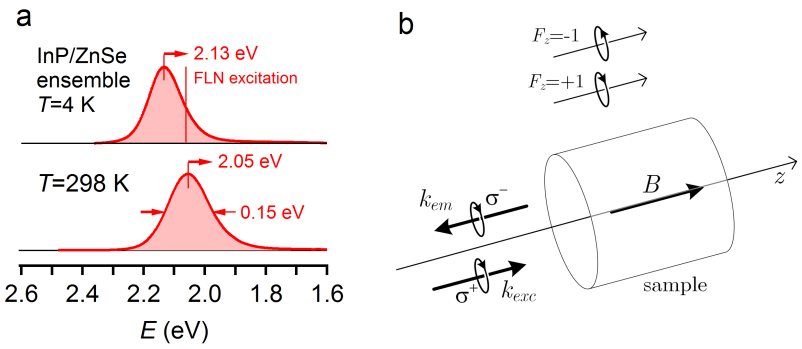

Figure 3.6. | FLN measurement. (a) Emission spectrum of the InP/ZnSe QD ensemble used for the FLN measurements as recorded at (bottom) 298 K and (top) 4 K. (b) Schematic outline of Faraday configuration used during the FLN measurements, where the direction of the magnetic field is used to determine the z axis and, accordingly, the $F_z = +1$ and $F_z = -1$ states as indicated. According to these conventions, σ^+ circularly polarized light will excite the $F_z = +1$ state, whereas recombination from the $F_z = -1$ will yield emitted light with a σ^- circular polarization.

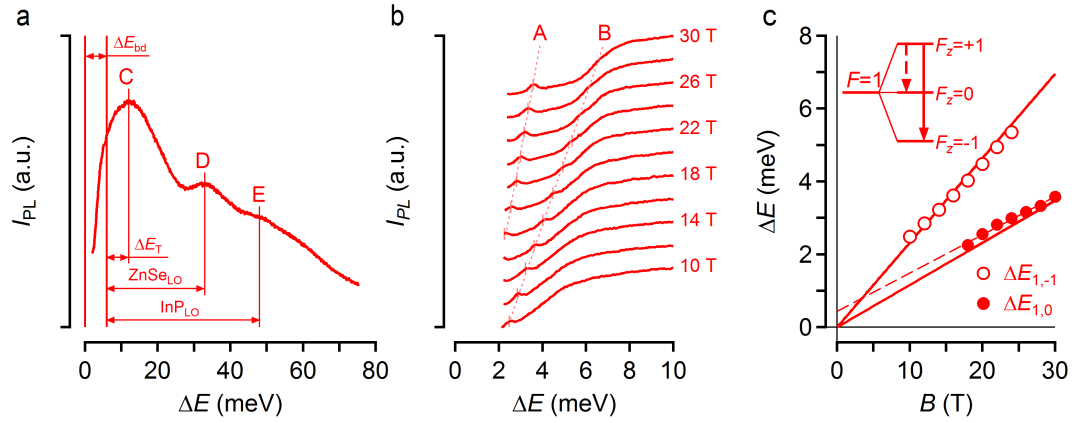

Figure 3.7. | FLN spectra. (a) Fluorescence line narrowing (FLN) spectrum of an ensemble of InP/ZnSe QDs excited using 2.06 eV, σ^+ polarized light. The energy difference ΔE measures the energy loss of the emitted phonons relative to 2.06 eV. Using the energy of the ZnSe and InP optical phonon as a yard stick, the indicated features are assigned to (C) acoustic phonon replica of dark state emission, (D) ZnSe LO phonon replica of dark state emission, and (E) InP LO phonon replica of dark state emission. From this analysis, we obtain a bright-dark splitting energy $\Delta E_{bd} = 6$ meV. (b) FLN spectra of the same InP/ZnSe QD ensemble in different magnetic fields as indicated. The dashed line highlights the two additional emission features, labeled A and B, that appear in the spectra, whereas the short vertical lines indicate the estimated shift of each feature relative to the excited level. (c) Energy shift of the features A and B with respect to the photo-excited $F_z = +1$ state. The full lines represent the result of a global fit to the expression of the isotropic exciton model, using g_h as the only adjustable parameter ($\Delta E_{bd} = 6$ meV, $g_e = 1.6$, $g_h = -1.925$). The thin dashed line is an extrapolation of the experimental data.

for fields of 18 T and higher and shifts from $\Delta E = 2.25$ meV to 3.58 meV at 30 T. A second, labeled B, appears first at fields of 10 T. This feature shifts more strongly with increasing field strength, from 2.48 meV at 10 T to 5.35 meV at 24 T. For the largest fields, the feature is reduced to a mere shoulder on top of the rising side of the phonon-assisted dark exciton emission, making unreliable any determination of the energy shift. For both features, Figure 3.7c summarizes the energy shift as a function of the magnetic field, where the features A and B are labelled as $\Delta E_{1,0}$ and $\Delta E_{1,-1}$, respectively. See section 3.3.3 for the estimation of g factor and the reason to choose $g_e = 1.6$ and $\Delta E_{bd} = 6$ meV to obtain $g_h = -1.925$.

The observation of two emission features, shifting to lower energy with respect to the excited $F_z = +1$ bright state shows that in the absence of a magnetic field, the excited bright exciton consists of 3 different, nearly degenerate states. This result strongly contrasts to similar measurements on wurtzite CdSe QDs, which showed a bright exciton doublet.[21] Thus the spectral doublet of the single InP/ZnSe QD analyzed in Figure 3.2 should be seen as a nearly isotropic exciton subject to minor splitting in a singlet and a doublet state due to anisotropy along the quantization axis z as shown in Figure 3.5b.

3.3.2. Isotropic exciton model

When the 8 direct product states of the conduction-band electron and the valence-band hole is taken as a basis (see Figure 3.1c), the exchange interaction couples states with the same angular momentum component F_z into different isotropic exciton states.[12] Taking the example of the $F_z = +1$ states, the two basis states can be defined as:

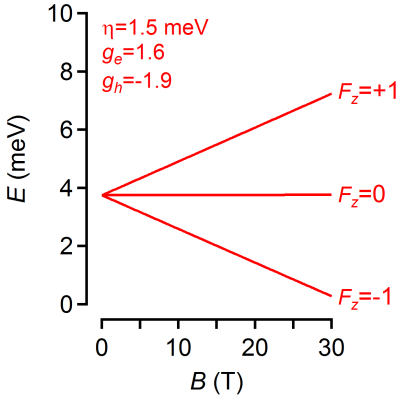

Figure 3.8. | Bright isotropic exciton. Representation of the energy of the bright isotropic exciton states $F_z = +1$, $F_z = 0$ and $F_z = -1$ state as a function of the applied magnetic fields, calculated using the parameters η, g_e and g_h as indicated.

$$|0\rangle = \left|\frac{1}{2}\right\rangle_e \left|\frac{1}{2}\right\rangle_h \tag{3.12}$$

$$|1\rangle = \left|-\frac{1}{2}\right\rangle_e \left|\frac{3}{2}\right\rangle_h \tag{3.13}$$

Using this convention, the Hamiltonian operator $\mathbf{H}$ reads:[12]

$$\mathbf{H} = \begin{pmatrix} -\frac{1}{2}\eta & -i\sqrt{3}\eta \\ i\sqrt{3}\eta & \frac{3}{2}\eta \end{pmatrix} \tag{3.14}$$

Here, η is a measure of the strength of the exchange interaction. The eigenenergies of $\mathbf{H}$ correspond to a bright high energy state $E_U = 5/2\eta$ and a dark low energy state $E_L = -3\eta/2$, as can be seen in Figure 3.1d for $\Delta = 0$. In the case of an isotropic exciton, the direction of the magnetic field B can be taken as the z-axis, which means that the Zeeman Hamiltonian is diagonal in the give basis.[12] For the $F_z = +1$ states,

$$\mathbf{H} = \begin{pmatrix} -\frac{1}{2}\eta + \mu_B B_z \frac{g_e - g_h}{2} & -i\sqrt{3}\eta \\ i\sqrt{3}\eta & \frac{3}{2}\eta - \mu_B B_z \frac{g_e + 3g_h}{2} \end{pmatrix} \tag{3.15}$$

where g_e and g_h are the gyromagnetic ratio of the electron and the hole, and μ_B is the Bohr magneton.

The upper eigenenergies $E_{1,U}$ of this Hamiltonian reads:

$$E_{1,U} = \frac{1}{2}\eta - g_h \mu_B B_z + \sqrt{3\eta^2 + \left(\eta^2 - \frac{g_e + g_h}{2}\mu_B B_z\right)^2} \tag{3.16}$$

Figure 3.8 represents the energy of the $E_{1,U}$ state for a given set of parameters η, g_e and g_h.

For the $F_z = 0$ states, the basis states can be similarly defined as:

$$|0\rangle = \left|\frac{1}{2}\right\rangle_e \left|-\frac{1}{2}\right\rangle_h \tag{3.17}$$

$$|1\rangle = \left|-\frac{1}{2}\right\rangle_e \left|\frac{3}{2}\right\rangle_h \tag{3.18}$$

In that case, the Hamiltonian operator in the presence of a magnetic field reads:[12]

$$\mathbf{H} = \begin{pmatrix} \frac{1}{2}\eta + \mu_B B_z \frac{g_e+g_h}{2} & -i2\eta \\ i2\eta & \frac{1}{2}\eta - \mu_B B_z \frac{g_e+g_h}{2} \end{pmatrix} \tag{3.19}$$

In this case, the upper eigenenergy is obtained as (see Figure 3.8):

$$E_{0,U} = \frac{1}{2}\eta + \sqrt{4\eta^2 + \left(\frac{g_e+g_h}{2}\mu_B B_z\right)^2} \tag{3.20}$$

Finally, for the $F_z = -1$ states, the basis states can be defined as:

$$|0\rangle = \left|\frac{1}{2}\right\rangle_e \left|-\frac{3}{2}\right\rangle_h \tag{3.21}$$

$$|1\rangle = \left|-\frac{1}{2}\right\rangle_e \left|-\frac{1}{2}\right\rangle_h \tag{3.22}$$

In that case, the Hamiltonian operator in the presence of a magnetic field reads:[12]

$$\mathbf{H} = \begin{pmatrix} \frac{3}{2}\eta + \mu_B B_z \frac{g_e+3g_h}{2} & -i\sqrt{3}\eta \\ i\sqrt{3}\eta & -\frac{1}{2}\eta - \mu_B B_z \frac{g_e-g_h}{2} \end{pmatrix} \tag{3.23}$$

In this case, the upper eigenenergy is obtained as (see Figure 3.8):

$$E_{-1,U} = \frac{1}{2}\eta + g_h\mu_B B_z + \sqrt{3\eta^2 + \left(\eta^2 + \frac{g_e+g_h}{2}\mu_B B_z\right)^2} \tag{3.24}$$

3.3.3. Estimation of the Hole g-Factor

Using the expressions derived in section 3.3.2 for $E_{1,U}$, $E_{0,U}$ and $E_{-1,U}$ (Eqs 3.16, 3.20, and 3.24, respectively), the magnetic field induced splitting between these exciton states can be written as (see Eqs 3.25 and 3.26):

$$\Delta E_{1,0} = -g_h\mu_B B + \sqrt{3\eta^2 + (\eta - \frac{g_e+g_h}{2}\mu_B B)^2} - \sqrt{4\eta^2 + (\frac{g_e+g_h}{2}\mu_B B)^2} \tag{3.25}$$

$$\Delta E_{1,-1} = -2g_h\mu_B B + \sqrt{3\eta^2 + (\eta - \frac{g_e+g_h}{2}\mu_B B)^2} - \sqrt{3\eta^2 + (\eta + \frac{g_e+g_h}{2}\mu_B B)^2} \tag{3.26}$$

Here, η is a quarter of the bright-dark splitting between the high energy $F = 1$ and the low energy $F = 2$ states, g_e and g_h are the gyromagnetic ratio of the electron and the hole, and μ_B is the Bohr magneton. From Eqs 3.25 and 3.26, when g_h is positive, the energy of hole states with the angular momentum parallel to the magnetic field is lowered, whereas for g_e positive, the energy of electron

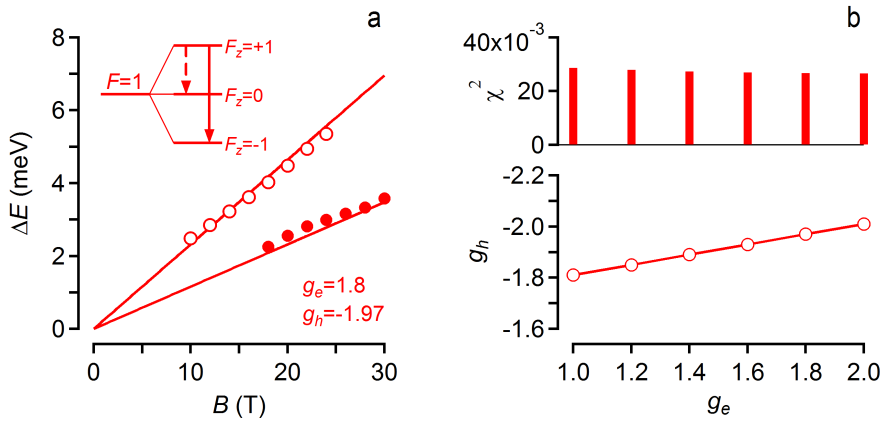

Figure 3.9. | Fitting of energy differences in FLN spectra. (a) Example of a global fit of the experimental data, where g_e was fixed at 1.8. (b) (bottom) Best fit values for g_h as obtained by a global fit of the experimental data as a function of the set value for g_e and (top) Mean square residuals for the best global fit as a function of the set value for g_e.

states with angular momentum anti-parallel to the field is lowered.[34] Unless $|g_h| \ll |g_e|$, the first term in Eqs 3.25 and 3.26 will be dominant, and a negative g_h is needed to make the $F_z = +1$ state the high energy state. Keeping η fixed at $1.5\,\mathrm{meV}$ yield satisfactory global fits of the experimental data to Eqs 3.25 and 3.26, yet such fits do not allow for an accurate determination of g_e and g_h separately. So one of the g factors has to be fixed to obtain a reasonable value for the other g factor that also agrees with the experimental and theoretically predicted values. Thus the g_e values were varied from 1.0 to 2.0 to estimate g_h and it is obtained that the mean square deviation between the experimental and fitted data hardly changes as shown in Figure 3.9b. Further, this variation of g_e has little effect on the best fit value of g_h, which decreases from -1.8 to -2.0 across this g_e range. Thus g_h can be estimated reasonably with an average value of -1.9 ± 0.1 (see Figure 3.9b). Since $g_e = 1.6$ was reported for self-assembled InP-based QDs,[35] a global fit was done by fixing g_e to this value and η fixed at $1.5\,\mathrm{meV}$. This yielded a best fit for $g_h = -1.93 \pm 0.03$ which is shown in Figure 3.7c.

To compare this value of g_h with the theoretically predicted value, the g-factor of a hole localized in a spherically symmetric potential can be calculated as:[12]

$$g_h = \frac{4}{5}\gamma_1 I_2 + \frac{8}{5}\gamma(I_1 - I_2) + 2(\frac{5}{3}\gamma - \frac{1}{3}\gamma_1 - \frac{2}{3})(1 - \frac{4}{5}I_2) \tag{3.27}$$

Here, I_1 and I_2 are integrals that can be calculated from the hole envelope wavefunction, whereas γ_1 and γ are Luttinger parameters. In the case that $\beta = 0.149$ for InP, the integrals I_1 and I_2 are approximately equal to -0.95 and 0.3, respectively.[12] With the Luttinger parameters $\gamma_1 = 5.1$ and $\gamma = 1.65$ for InP,[36] it is calculated that $g_h \approx -1.49$ which reasonably agrees with the estimated value of $g_h = -1.49$ shown above. Similarly negative values have been predicted for multiple spherical II-VI QDs,[34] and a value of $g_h = -0.73$ was derived from Faraday rotation measurements in the case of wurtzite CdSe QDs.[37]

3.3.4. Impact of light hole to heavy hole effective mass ratio

Looking at Figure 3.7c in detail, it appears that the isotropic exciton model slightly underestimates the energy splitting $\Delta E_{1,0}$ between the $F_z = +1$ and the $F_z = 0$ state. At least, a linear fit to the

experimental data yields a line lying systematically higher than the global fit. This could reflect a minor splitting of the three $F = 1$ exciton states at zero field, in line with the bright exciton doublet measured on a single InP/ZnSe QD. Given the slightly larger than expected $\Delta E_{1,0}$ splitting, the low energy line of the doublet would then correspond to the $F_z = 0$ state and the high energy line to the $F_z = \pm 1$ states. Such an assignment can explain the different polarization of both lines since the $F_z = 0$ state emits linearly polarized light with an electric field along the quantization axis, whereas the $F_z = \pm 1$ states emit circularly polarized with the electric field in the xy plane. Note that the particular viewing angle on a given QD can make that circularly polarized emission appears as partially linearly polarized in the detection system used, and that the phase difference between both emission lines differs from $90°$. Interestingly, in the case of isotropic QDs, theoretical work indicates that the negative trion ground state emits circularly polarized light since the hole occupies either the $j_z = 3/2$ or $j_z = -3/2$ heavy hole level.[38] The positive trion, on the other hand, has a mixed ground state that leads to set of recombination pathways emitting either circular or linear polarized light.[38] Hence, the correspondence between the polarization of the high energy exciton doublet line and the trion singlet line might point towards emission from the negative trion. Such a conclusion need, however, the confirmation from a more in-depth study of these emission lines, for example to account for artefacts induced by the viewing angle on a given QD.

Both through single QD PL and FLN spectroscopy discussed above, it appears that radiative exciton recombination contributes to the PL of InP/ZnSe QDs. While this finding does not rule out trap-related emission pathways,[26] it does highlight that trap-related emission does not have to be dominant recombination process in these QDs. More in general, the observation that excitons in InP/ZnSe QDs are nearly isotropic is far from trivial. In the case of CdSe QDs, for example, little difference was observed between the exciton fine structure of nanocrystals with a wurtzite or a zinc blende crystal structure.[39] Whereas wz-CdSe is intrinsically anisotropic, it was argued that relatively small deviations from a spherical shape can account for the similar anisotropy of the exciton in zb-CdSe QDs. Similary, an exciton model including exchange and shape anisotropy was used to describe the emission features of single zinc blende CdTe QDs.[40] Both examples suggest that deviations from an isotropic, spherical shape are to be expected in the case of colloidal QDs, and it is not clear why InP QDs should be an exception here. According to the exciton description developed by Efros, however, the impact of deviations from a spherical shape on the exciton fine structure depends on the light hole to heavy hole mass ratio $\beta = m_{lh}/m_{hh}$. Interestingly, the model predicts that the fine structure of the exciton will be insensitive to shape anisotropy when $\beta = 0.14$, which means that under such conditions also prolate or oblate ellipsoids will host isotropic excitons since Δ_{sh} = 0 in equation 3.5.[12] In the case of InP, β depends on the direction in reciprocal space, yet an average of β over the (100), (110) and (111) directions yields $\beta = 0.149$.[16] In contrast, for wz-CdSe, the hole mass ratio amounts to 0.28,[18] a value at which the impact of shape anisotropy on the fine structure is about maximal.[12] Possibly, having an average hole mass ratio close to the critical value of 0.14 is what makes that InP-based QDs host nearly isotropic excitons.

3.4. Conclusion

In summary, the emission of InP/ZnSe QDs is investigated using a combination of cryogenic micro-PL spectroscopy of single InP/ZnSe QDs and FLN spectroscopy on an ensemble of InP/ZnSe QDs. It is showed that the emission is related to exciton recombination, where the spectrum of a single InP/ZnSe QD features a bright exciton doublet, a trion singlet and a biexciton doublet. FLN spectra recorded versus magnetic field demonstrate that this bright exciton doublet reflects a minor deviation from the

3-fold degenerate, isotropic bright exciton expected in spherical QDs with a zinc-blende structure. The observation of isotropic excitons in InP/ZnSe QDs is assigned to the average hole mass ratio β of InP being 0.149. In contrast with CdSe ($\beta = 0.28$), this number is close to the value of 0.14 at which the exciton fine structure is insensitive to shape anisotropy.[12] From a fundamental perspective, isotropic excitons are highly interesting model systems for experimental studies and theory development. Different from anisotropic excitons, isotropic excitons have a fine structure solely determined by the exchange splitting. This makes the bright-dark splitting of isotropic excitons ideally suited to compare the predicted size-dependence of the exchange interaction with experimental data. In addition, the interaction between an isotropic exciton and an external field is independent of the QD orientation. As exemplified by the FLN study shown here, this makes that ensemble measurements in external fields are not compounded by orientation averaging, such that material characteristics can be determined in a direct manner from the analysis of ensembles. It is believed that the observation of nearly isotropic excitons in InP-based QDs opens a new direction to investigate the exciton fine structure in other nanoscale semiconductors.

Bibliography

[1] J. M. Luttinger and W. Kohn. Motion of electrons and holes in perturbed periodic fields. *Physical Review*, 97:869–883, 1955.

[2] J. M. Luttinger. Quantum theory of cyclotron resonance in semiconductors: General theory. *Physical Review*, 102:1030–1041, 1956.

[3] Matthias Ehrhardt and Thomas Koprucki, editors. *Multi-Band Effective Mass Approximations*. Springer International Publishing, 2014.

[4] Evan O. Kane. Band structure of indium antimonide. *Journal of Physics and Chemistry of Solids*, 1(4):249 – 261, 1957.

[5] C. R. Pidgeon and R. N. Brown. Interband magneto-absorption and faraday rotation in insb. *Physical Review*, 146:575–583, 1966.

[6] A. Baldereschi and Nunzio C. Lipari. Energy levels of direct excitons in semiconductors with degenerate bands. *Physical Review B*, 3(2):439–451, 1971.

[7] N. Chestnoy, R. Hull, and L. E. Brus. Higher excited electronic states in clusters of ZnSe, CdSe, and ZnS: Spin-orbit, vibronic, and relaxation phenomena. *The Journal of Chemical Physics*, 85(4):2237–2242, 1986.

[8] Jian-Bai Xia. Electronic structures of zero-dimensional quantum wells. *Physical Review B*, 40(12):8500–8507, 1989.

[9] M. L. A. Robinson. Evidence from cyclotron-resonance measurements for spin-degeneracy splitting of the valence band of InSb near k→=0. *Physical Review Letters*, 17(18):963–965, 1966.

[10] U. Banin, G. Cerullo, A. A. Guzelian, C. J. Bardeen, A. P. Alivisatos, and C. V. Shank. Quantum confinement and ultrafast dephasing dynamics in inp nanocrystals. *Physical Review B*, 55:7059–7067, mar 1997.

[11] Peter C. Sercel and Alexander L. Efros. Band-edge exciton in CdSe and other II–VI and III–v compound semiconductor nanocrystals - revisited. *Nano Letters*, 18(7):4061–4068, jun 2018.

[12] Al. L. Efros, M. Rosen, M. Kuno, M. Nirmal, D. J. Norris, and M. Bawendi. Band-edge exciton in quantum dots of semiconductors with a degenerate valence band: Dark and bright exciton states. *Physical Review B*, 54:4843–4856, 1996.

[13] A. I. Ekimov, A. A. Onushchenko, A. G. Plyukhin, and Efros Al. L. Size quantization of excitons and determination of the parameters of their energy spectrum in cucl. *Zh. Eksp. Teor. Fiz.*, 88:1490–1501, Apr 1985.

[14] Al. L. Efros and M. Rosen. The electronic structure of semiconductor nanocrystals. *Annual Review of Materials Science*, 30(1):475–521, aug 2000.

[15] Al. L. Efros and A. V. Rodina. Band-edge absorption and luminescence of nonspherical nanometer-size crystals. *Physical Review B*, 47(15):10005–10007, apr 1993.

[16] Yoon-Suk Kim, Kerstin Hummer, and Georg Kresse. Accurate band structures and effective masses for inp, inas, and insb using hybrid functionals. *Physical Review B*, 80:035203, jul 2009.

[17] M. Nirmal, D. J. Norris, M. Kuno, M. G. Bawendi, Al. L. Efros, and M. Rosen. Observation of the "dark exciton" in cdse quantum dots. *Physical Review Letters*, 75:3728–3731, Nov 1995.

[18] D. J. Norris, Al. L. Efros, M. Rosen, and M. G. Bawendi. Size dependence of exciton fine structure in cdse quantum dots. *Physical Review B*, 53:16347–16354, Jun 1996.

[19] Olivier Labeau, Philippe Tamarat, and Brahim Lounis. Temperature dependence of the luminescence lifetime of single $\mathrm{CdSe/ZnS}$ quantum dots. *Physical Review Letters*, 90:257404, Jun 2003.

[20] L. Biadala, Y. Louyer, Ph. Tamarat, and B. Lounis. Direct observation of the two lowest exciton zero-phonon lines in single $\mathrm{CdSe/ZnS}$ nanocrystals. *Physical Review Letters*, 103:037404, Jul 2009.

[21] M. Furis, H. Htoon, M. A. Petruska, V. I. Klimov, T. Barrick, and S. A. Crooker. Bright-exciton fine structure and anisotropic exchange in CdSe nanocrystal quantum dots. *Physical Review B*, 73:241313, Jun 2006.

[22] H. Htoon, M. Furis, S. A. Crooker, S. Jeong, and V. I. Klimov. Linearly polarized 'fine structure' of the bright exciton state in individual cdse nanocrystal quantum dots. *Physical Review B*, 77:035328, Jan 2008.

[23] A. Granados del Águila, G. Pettinari, E. Groeneveld, C. de Mello Donegá, D. Vanmaekelbergh, J. C. Maan, and P. C. M. Christianen. Optical spectroscopy of dark and bright excitons in CdSe nanocrystals in high magnetic fields. *The Journal of Physical Chemistry C*, 121(42):23693–23704, oct 2017.

[24] Louis Biadala, Benjamin Siebers, Yasin Beyazit, Mickaël. D. Tessier, Dorian Dupont, Zeger Hens, Dmitri R. Yakovlev, and Manfred Bayer. Band-edge exciton fine structure and recombination dynamics in inp/zns colloidal nanocrystals. *ACS Nano*, 10(3):3356–3364, 2016. PMID: 26889780.

[25] Annalisa Brodu, Mariana V. Ballottin, Jonathan Buhot, Elleke J. van Harten, Dorian Dupont, Andrea La Porta, P. Tim Prins, Mickael D. Tessier, Marijn A. M. Versteegh, Val Zwiller, Sara Bals, Zeger Hens, Freddy T. Rabouw, Peter C. M. Christianen, Celso de Mello Donega, and Daniel Vanmaekelbergh. Exciton fine structure and lattice dynamics in inp/znse core/shell quantum dots. *ACS Photonics*, 5(8):3353–3362, 2018.

[26] Eric M. Janke, Nicholas E. Williams, Chunxing She, Danylo Zherebetskyy, Margaret H. Hudson, Lili Wang, David J. Gosztola, Richard D. Schaller, Byeongdu Lee, Chengjun Sun, Gregory S. Engel, and Dmitri V. Talapin. Origin of broad emission spectra in inp quantum dots: Contributions from structural and electronic disorder. *Journal of the American Chemical Society*, 140(46):15791–15803, 2018.

[27] Jian Cui, Andrew P. Beyler, Lisa F. Marshall, Ou Chen, Daniel K. Harris, Darcy D. Wanger, Xavier Brokmann, and Moungi G. Bawendi. Direct probe of spectral inhomogeneity reveals synthetic tunability of single-nanocrystal spectral linewidths. *Nature Chemistry*, 5(7):602–606, jun 2013.

[28] Vigneshwaran Chandrasekaran, Mickaël D. Tessier, Dorian Dupont, Pieter Geiregat, Zeger Hens, and Edouard Brainis. Nearly blinking-free, high-purity single-photon emission by colloidal inp/znse quantum dots. *Nano Letters*, 17(10):6104–6109, 2017. PMID: 28895398.

[29] Mina Talati and Prafulla K. Jha. Acoustic phonons in semiconductor nanocrystals. *Computational Materials Science*, 37(1-2):58–63, aug 2006.

[30] Mark J. Fernée, Bradley N. Littleton, and Halina Rubinsztein-Dunlop. Detection of bright trion states using the fine structure emission of single cdse/zns colloidal quantum dots. *ACS Nano*, 3(11):3762–3768, 2009.

[31] L. Besombes, K. Kheng, L. Marsal, and H. Mariette. Acoustic phonon broadening mechanism in single quantum dot emission. *Physical Review B*, 63:155307, mar 2001.

[32] Roland Zimmermann and Egor Muljarov. Dephasing of optical transitions in quantum dots — Where exact solutions meet sophisticated experiments. In *Nanostructures: Physics and Technology*, page 3, 2004.

[33] Yahel Barak, Itay Meir, Arthur Shapiro, Youngjin Jang, and Efrat Lifshitz. Fundamental properties in colloidal quantum dots. *Advanced Materials*, 30(41):1801442, 2018.

[34] Elena V. Shornikova, Louis Biadala, Dmitri R. Yakovlev, Donghai Feng, Victor F. Sapega, Nathan Flipo, Aleksandr A. Golovatenko, Marina A. Semina, Anna V. Rodina, Anatolie A. Mitioglu, Mariana V. Ballottin, Peter C. M. Christianen, Yuri G. Kusrayev, Michel Nasilowski, Benoit Dubertret, and Manfred Bayer. Electron and hole g-factors and spin dynamics of negatively charged excitons in cdse/cds colloidal nanoplatelets with thick shells. *Nano Letters*, 18(1):373–380, 2018.

[35] M. Syperek, D. R. Yakovlev, I. A. Yugova, J. Misiewicz, M. Jetter, M. Schulz, P. Michler, and M. Bayer. Electron and hole spins in inp/(ga,in)p self-assembled quantum dots. *Physical Review B*, 86:125320, sep 2012.

[36] W. Hackenberg, R. T. Phillips, and H. P. Hughes. Investigation of the luttinger parameters for inp using hot-electron luminescence. *Physical Review B*, 50:10598–10607, Oct 1994.

[37] J. A. Gupta, D. D. Awschalom, Al. L. Efros, and A. V. Rodina. Spin dynamics in semiconductor nanocrystals. *Physical Review B*, 66:125307, sep 2002.

[38] A. Shabaev, A. V. Rodina, and Al. L. Efros. Fine structure of the band-edge excitons and trions in cdse/cds core/shell nanocrystals. *Physical Review B*, 86:205311, nov 2012.

[39] Iwan Moreels, Gabriele Rainò, Raquel Gomes, Zeger Hens, Thilo Stöferle, and Rainer F. Mahrt. Band-edge exciton fine structure of small, nearly spherical colloidal CdSe/ZnS quantum dots. *ACS Nano*, 5(10):8033–8039, sep 2011.

[40] Jenya Tilchin, Freddy T. Rabouw, Maya Isarov, Roman Vaxenburg, Relinde J. A. Van Dijk-Moes, Efrat Lifshitz, and Daniel Vanmaekelbergh. Quantum confinement regimes in CdTe nanocrystals probed by single dot spectroscopy: From strong confinement to the bulk limit. *ACS Nano*, 9(8):7840–7845, jul 2015.

Chapter 4.

Dephasing dominated by phonon-scattering within bright exciton triplet

Contents

Synopsis

In this chapter, a transient resonant four wave mixing spectroscopy (FWM) on ensemble of QDs is performed to study both the photon echo (temperature range: 5 K - 31 K) and population density dynamics (temperature range: 5 K - 107 K). Contrary to a rapid spin-flip mediated dephasing from bright-to-dark exciton in CdSe QDs, it is found that the ZPL dephasing is dominated by phonon-scattering within closely spaced bright exciton triplet with a 0 K dephasing rate of 0.0346 $\pm$ 0.0004 ps^{-1} and an activation energy of 0.95 $\pm$ 0.01 meV. Further, there is a correspondence between the narrowest ZPL of single QDs (50 $\pm$ 1 μeV) and the homogeneous linewidth obtained using FWM (56.8 $\pm$ 2.1 μeV) at 5 K.

Manuscript in preparation
Synthesis of InP/ZnSe QDs by Dr. Dorian Dupont, Ghent University, Belgium
TEM images of InP/ZnSe QDs by Dr. Ali Khan, Ghent University, Belgium
FWM optical setup & measurements by Dr. Francesco Masia & Dr. Lorenzo Scarpelli, Cardiff University, United Kingdom

4.1. Introduction

Non-classical light sources, such as single photon sources, are essential for realizing quantum technologies like quantum communication, quantum computation, quantum simulation and quantum sensing.[1] An ideal single photon source interacts only with the electromagnetic environment producing single photons with higher purity, higher on-demand emission rate and identical photon wave packets.[2] Indistinguishable single photons can be expected if both the spatial and temporal overlaps of their wavepackets are identical in terms of emission frequency, pulse-width, spectral bandwidth, polarization, transverse mode profile and arrival time at the beam splitter.[3] The emission spectral linewidth of such an ideal single photon source would have a Fourier-transform-limited spectral bandwidth. However, the spectrum of the single photon source is broadened arising from fluctuations of the optical resonance frequency, described in terms of *dephasing* (loss of coherence of the emitter to the environment) and *spectral diffusion* (fluctuations in the emission energy, see Chapter 5). Note: A two-photon interference effect is commonly used to determine the indistinguishability since two identical single photons entering a 50:50 beam-splitter would leave from the same end because of the 'coalescing' behavior of photons. The degree of indistinguishability is measured using a Hong-Ou-Mandel setup where a delay is applied to the arrival times of the two single photons and the coincidence counts are monitored on the two output detectors.[4] In ideal case, the coincidence counts would fall to zero at exactly the zeroth delay which is commonly known as Hong-Ou-Mandel (HOM) dip.

Scalability and on-demand emission make the solid state quantum emitters as favorable two-level system,[5] where the single photon is emitted upon relaxation of the excited electron-hole pair to the ground state. This electron-hole pair known as exciton is a quasi-particle state bounded by the Coulomb interaction energy. Overall, the exciton coherence (conversely, the dephasing) in these materials is influenced by coupling of the optical transition to the environment predominantly due to radiative processes, carrier-phonon scattering and carrier-carrier scattering processes.[6] In strongly quantum confined systems like colloidal quantum dots (QDs), exchange interaction & shape anisotropy tweaks the ideal two-level system to exciton-manifolds near the band edge.[7] The presence of such fine structure split states explains the physical origin of intrinsic zero phonon line (ZPL) dephasing in widely studied CdSe QDs. This is attributed to the rapid spin-flip from the lowermost optically-allowed bright exciton to optically-forbidden dark exciton.[8, 9]

As InP QDs are considered an alternative to heavy metal ion based QDs for opto-electronic applications, an understanding of their fundamental optical properties is required. As discussed in Chapter 2, InP/ZnSe core/shell QDs exhibited high pure single photon emission at room temperature with the emission stability comparable to state-of-the-art CdSe/CdS QDs.[10] As discussed in Chapter 3, exchange interaction and negligible contribution of shape-anisotropy in InP/ZnSe QDs split the band-edge exciton level to have a threefold nearly-degenerate bright and fivefold degenerate dark exciton.[11] On one study, a study of temperature dependent photoluminescence decay rates reported a slower bright-to-dark spin flip rate in the order of 0.001 ps^{-1} for 3 nm core-diameter sized InP/ZnS QDs.[12] On another study, the presence of such band-edge exciton was questioned by attributing a domination of trap-assisted recombination in InP-based QDs.[13] These contradicting reports could benefit from a fundamental knowledge on the mechanism responsible for the exciton dephasing in InP-based QDs. The physical origin of exciton ZPL dephasing in these QDs, currently unknown, also needs to be understood to know the limiting factor for their homogeneous linewidth.

4.2. Decoherence mechanism

4.2.1. Primary source of exciton dephasing in quantum dots

The coherence of the single photon emitted describes the phase stability of the light and the photon linewidth can be expressed as:[14]

$$\gamma = \frac{1}{T_2} = \frac{1}{2T_1} + \frac{1}{T_2^*} \tag{4.1}$$

where T_2 is the coherence (conversely, the dephasing) time, T_1 is the radiative lifetime, and T_2^* is the pure dephasing time where the coherence is lost without any recombination. An ideal photon wavepacket having no pure dephasing would be naturally broadened by the radiative lifetime such that the Fourier transform limited linewidth is achieved under the condition: $T_2 = 2\ T_1$. If the pure dephasing is happening much faster than the radiative lifetime, the coherence of the optical transition is already lost to the environment and the photon linewidth is expressed as shown in equation 4.1.

The dephasing of the optical transition in any type of QDs can happen due to both intrinsic and extrinsic factors.[15] The intrinsic dephasing can be of both non-Markovian (broad acoustic phonon pedastal surrounding the ZPL)[16] and Markovian (acoustic phonon assisted virtual transitions involving a higher energy level).[17] The extrinsic dephasing factors include: spectral diffusion or charge noise (fluctuating electric field) and spin noise (fluctuating magnetic field).[18]

In QDs, spontaneous & stimulated phonon emission and stimulated phonon absorption processes broaden the exciton linewidth. The stimulated processes require a phonon occupation and therefore are absent at zero temperature but increase with temperature. Two types of processes can be distinguished. On the one hand, transitions between excitonic states, such as phonon-assisted scattering within the fine structure manifold. These processes are broadening the ZPL. Here transitions to a lower energy state occur also via spontaneous phonon emission and thus remain at zero temperature. For instance, the spontaneous spin-flip from the bright to the lower lying dark exciton state in colloidal CdSe QDs dominates the zero-temperature exciton ZPL dephasing.[8] On the other hand there are phonon assisted radiative transitions, resulting in sidebands to the ZPL, which reflect the phonon density of states and their coupling strength to the exciton. Typically there is an acoustic phonon band close to the ZPL having a width of a few meV, given by the transit time of acoustic phonon propagation through the QD, and separate optical phonon bands at a few tens of meV separation to the ZPL, given by the specific optical phonon energies in the QD.

In quasi-spherical colloidal CdSe QDs, the exciton ZPL dephasing (in the order of ps) is faster than the radiative lifetime (in the order of ns) and thus the homogeneous linewidth is far from the natural lifetime broadened linewidth.[8] Since the presence of exciton-manifolds near the band edge due to the exchange interaction & shape anisotropy in QDs (fine structure) influence the exciton ZPL dephasing, further attempts were made to reduce the splitting energies. Accordingly, the exciton dephasing time was altered by simply tuning the size & shape of CdSe QDs.[9] For example, a larger core size and a thicker shell CdSe/CdS QD have a longer dephasing time than a smaller core QD. This is attributed to the reduced exchange interaction as the smaller band-offsets allow a delocalization of electron wavefunction onto the shell. To date, the dephasing time in NCs limited only by radiative lifetime (1 ps) was observed in 2D nanoplatelets that have larger in-plane coherence area compared to spherical NCs.[19]

It is noted that perovskite NCs have a dephasing time close to the radiative lifetime limit.[20] In self assembled QDs, the dephasing time is closer to the radiative lifetime limit.[16] ZPL weight reported in self assembled QDs amount to 90% which was improved by reducing the phonon induced decoherence in cavity structures and resonant excitation.[15]

4.2.2. Experimental methods to determine dephasing time

The dephasing time T_2 of an optical transition can be measured experimentally in different ways. The homogeneous width of the spectral absorption is inversely proportional to the dephasing time, thus experiments can be performed either in the time domain to directly address the transient decay of the polarization induced by a pulsed coherent light field or in the spectral domain by measuring the steady-state optical absorption lineshape. Generally, the response of the medium to the incident field depends on the field intensity. For example, only in the linear response limit (i.e. in the first order of the incident field amplitude) the absorption lineshape is Lorentzian energy full width at half maximum (FWHM) given by $\gamma = 2\hbar/T_2$. At higher orders, effects such as power broadening, quadratic Stark shift, and the optical Stark splitting which is the signature of Rabi oscillations in the spectral domain become too evident.[6]

Linear spectroscopy has the limitation of measuring the homogeneous lineshape in an ensemble of QDs which are inhomogeneously broadened by size dispersion. In the time domain, this translates into an additional decay rate of the macroscopic first-order polarization.[21] The dephasing rate in QDs which is much below the inhomogeneous linewidth cannot be measured accurately in linear spectroscopy. To circumvent the inhomogeneous broadening, one can spatially isolate a single QD and perform a resonant linear spectroscopy. However, this is limited by the poor signal-to-noise ratio, directional selectivity from an emitter and the single QDs have extrinsic dephasing (spectral diffusion) in the time scales faster than the experimental acquisition time. Moreover, the optical properties vary from one QD to another depending on their size. For instance, the varying factors are oscillator strength, fine structure splitting and phonon energy. Experiments based on third-order signals, such as four wave mixing in the transient coherent domain after pulsed excitation[22] or spectral hole-burning in the frequency domain with continuous wave excitation[23] allow one to overcome the presence of an inhomogeneous distribution and can be detected free of backgrounds with appropriate selection in

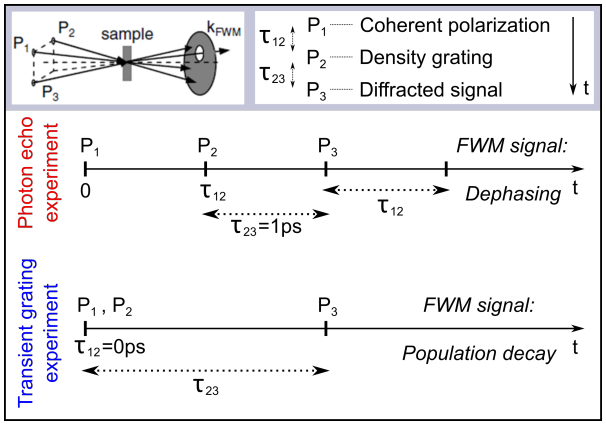

Figure 4.1. | Four wave mixing experiment. Sketch of the three-beam FWM directional geometry and scheme of FWM experiments.

the direction and/or frequency domain. In particular, using transient four wave mixing (FWM) spectroscopy in heterodyne detection, the diffracted third order non-linearity have been used to determine the dephasing mechanism with a timing resolution given by the fs-pulses and their respective delay between them.[24]

Transient four wave mixing spectroscopy

To measure the exciton-decoherence dynamics, a three-beam transient resonant four-wave mixing technique in heterodyne detection is used to determine the dephasing time of InP/ZnSe QDs. The experimental setup for FWM spectroscopy shown in Appendix C.4 is same as described in previous works.[8, 9, 19] Each beam entering the sample in a three-beam degenerate transient FWM spectroscopy is a train of 150 fs pulses with 76 MHz repetition rate. The first pulse P_1 induces a coherent polarization in the sample, which is then converted to a density grating by the second pulse P_2 after a time delay τ_{12}. The third pulse P_3 arriving after a delay of τ_{23} from P_2 is diffracted by the already formed density grating. Thus the three input pulses with different wavevectors (k_1, k_2, k_3) arriving at certain time delay between them (τ_{ij}) produces the total diffracted field (FWM signal) along the phase-matched direction ($k_T = k_3 + k_2 - k_1$). In heterodyne technique, the excitation pulses are radio-frequency upshifted by acousto–optic modulators and the resulting frequency shifted FWM signal is detected by its interference with a reference pulse using lock-in amplifier.

For in-homogeneously broadened systems like QDs, two experiments can be performed using the three pulse photon echo method.[24] One, the exciton dephasing time can be extracted in a photon echo (PE) experiment by plotting the time-integrated FWM signal (Ti-FWM) versus τ_{12} which decays exponentially at longer delay times with a time constant proportional to exciton dephasing time of the ZPL. Here, τ_{23} is usually fixed to a specific value to suppress addditional nonlinearities. Two, the exciton population density dynamics can be extracted in transient grating (TG) experiment by plotting the Ti-FWM signal versus τ_{23} by keeping τ_{12} = 0 which often decays in a multiple-exponential manner depending on the carrier dynamics of the samples. Note that the FWM signal in such a broad system is a photon echo indicating a rephasing of the transitions from different frequency components and thus

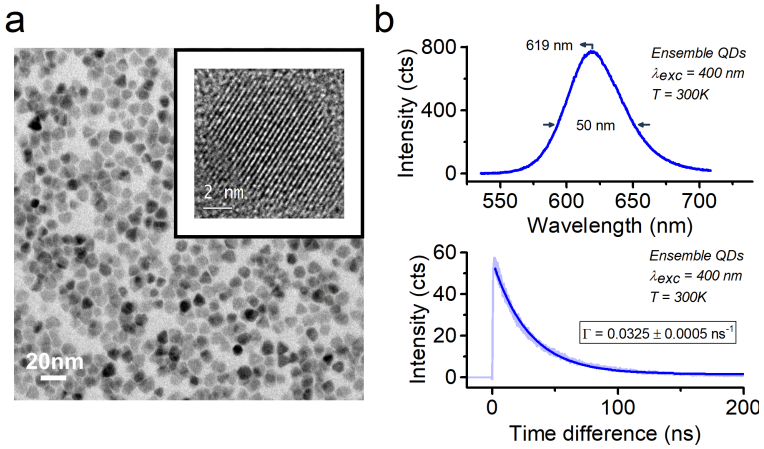

Figure 4.2. | Sample details. (a) TEM and HR–TEM images of InP/ZnSe QDs under study. Mean diameter is 7.6 ± 1.1 nm for a core size of 3.2 nm. (b) Room temperature emission spectrum and PL decay fitted with a single exponential rate of 0.0325 ± 0.0005 ns^{-1}.

unaffected by in-homogeneity. The dephasing is faster than the typical timescale of spectral diffusion and thus remains unaffected by such slow diffusion.

4.3. Exciton dephasing & population density

4.3.1. Photon echo experiment

InP/ZnSe QDs for this study was prepared according to the method described in section 1.5.2. Figure 4.2a shows the TEM and HR-TEM images of the QD that has a mean diameter of 7.6 $\pm$ 1.1 nm for a core size of 3.2 nm. Figure 4.2b shows the room temperature photoluminescence (PL) spectrum that has an emission peak at 619 nm (2.002 eV) with a linewidth of about 50 nm (160 meV). PL decay at room temperature is also shown in Figure 4.2b which is fitted with a single exponential rate of 0.0325 $\pm$ 0.0005 ns^{-1}. The sample for FWM study is prepared by dropcasting the QDs suspended in toluene mixed with plasticizer (a transparent nail varnish of make Seche Vite) and sandwiched between two c-cut quartz windows. A temperature dependent absorption spectroscopy on the sample from room temperature to 8 K is done to find the fundamental exciton peak at cryogenic temperatures (see Figure 4.3a), where a blueshift of about 20 nm (74 meV) is observed probably due to the combination of both thermal contraction and phonon coupling. For temperatures below 50 K, the lowest exciton state is at around 570 $\pm$ 1 nm. Hence, two excitation wavelengths are chosen for FWM study, one resonantly at 570 nm and the other in the absorption tail at 580 nm to reduce the excitation into excited state levels. Excitation pulses are also shown in Figure 4.3a that have a $\Delta\lambda$ = 6 nm ($\sim$22 meV). A power-dependent FWM measurement was done which showed little effect of the excitation power on the results. Therefore, an excitation power of 400 μW was used which was well within the third-order nonlinear regime and resulting in negligible local heating.

In PE experiment, the photon echo amplitude decays with an initial sub-picosecond term followed by a slower term at longer delay times. The ultrafast initial term gets even faster with increasing temperature which is attributed to the contribution from acoustic phonon sidebands and excited states.

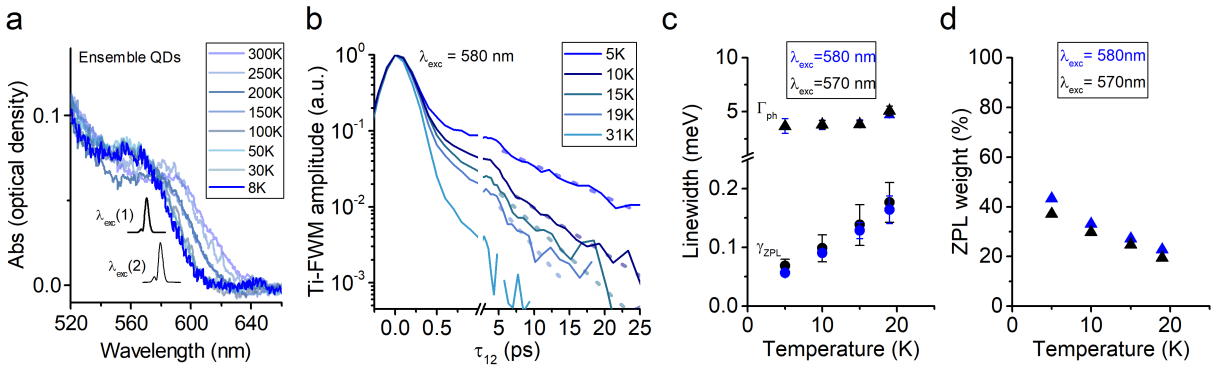

Figure 4.3. | Photon echo experiment. (a) Temperature dependent absorption spectra. At 8 K, the lowest exciton state is at 570 nm and thus the chosen excitation wavelength for FWM study are 570 nm and 580 nm (shown in inset) (b) Ti-FWM amplitude versus τ_{12} for λ_{exc} = 580 nm at different temperatures has an initial sub-ps term followed by a longer mono-exponential term which is a representation of acoustic phonon sidebands & Lorentzian exciton ZPL respectively. The dotted lines are exponential fits at longer delay times.(c) Corresponding ZPL linewidth $2\hbar/T_2$ and estimated cumulative phonon linewidth Γ_{ph} by fitting an exponential to the initial sub-ps component. (d) ZPL weight.

a

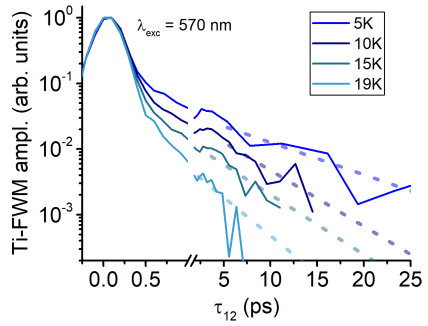

b

Dephasing rate		
Temperature	λ_{exc} = 570 nm	λ_{exc} = 580 nm
K	ps^{-1}	ps^{-1}
5	0.0521 ± 0.008	0.0431 ± 0.001
10	0.0751 ± 0.017	0.0685 ± 0.003
15	0.1052 ± 0.026	0.0978 ± 0.010
19	0.1341 ± 0.025	0.1247 ± 0.017

Figure 4.4. | Photon echo experiment. (a) Ti-FWM amplitude versus τ_{12} for λ_{exc} = 570 nm at different temperatures has an initial sub-ps term followed by a longer term which is a representation of acoustic phonon sidebands & exciton ZPL respectively. The dotted lines are exponential fits at longer delay times.(b) Dephasing rate for λ_{exc} = 570 nm and λ_{exc} = 580 nm.

The slower term has a mono-exponential character and thus represent the exciton ZPL. This also agrees with a model of Lorentzian ZPL coupling to acoustic PSB in different types of QDs.[8, 16, 25] Figure 4.3a shows the Ti-FWM amplitude versus τ_{12} at cryogenic temperatures with λ_{exc} of 580 nm (see Figure 4.4a for results with λ_{exc} of 570 nm). The dotted lines are exponential fits at longer delay times and the obtained time constant is $T_2/2$ for an in-homogeneously broadened system.[24] It is noted that an ultrafast dephasing on InP QDs was investigated two decades ago where the attributed dephasing of the band-edge exciton actually belongs to the pure dephasing via acoustic phonons due to the limited dynamic range studied.[26] Here, we observe this ultrafast component (cumulative of excited states and acoustic phonon sidebands) and the mono-exponential component at longer delay times which is the representation of the exciton ZPL.

The dephasing rate (T_2^{-1}) expectedly increases with temperature (see Figure 4.4b), especially at 31 K where the FWM amplitude is closer to the noise level indicating the lesser contribution of ZPL compared to the acoustic phonon sidebands. Figure 4.3b shows the corresponding ZPL homogeneous linewidth ($2\hbar/T_2$) and estimated cumulative phonon linewidth Γ_{ph} by fitting an exponential to the initial sub-ps component. Note that the PSB are non-exponential in nature and thus the values are an approximation. ZPL weight calculated using the procedure described by Borri *et al.*[27] at different temperatures are shown in Figure 4.3d for both the excitation wavelengths. It is found that the ZPL weight at λ_{exc} = 570 nm is lower than at λ_{exc} = 580 nm which is attributed to the more contribution of excited state levels at 570 nm. In earlier theoretical studies on the electronic structure of InP QDs, a multi band effective mass approximation method predicted the excited state levels are closely spaced near the band edge.[26, 28]

4.3.2. Transient grating experiment

Next the result of TG experiment is shown in Figure 4.5a for λ_{exc} = 580 nm at 5K where Ti-FWM amplitude is plotted against τ_{23}. The solid lines represent a fit to complex three-exponential response function (also described by Scarpelli *et al.*[29]):

$$R(\tau) = A_{nr}\, e^{i\phi_{nr}}\, \delta(\tau) \;+\; \sum_n A_n\, \theta(\tau)\, \exp\!\left(i\phi_n - \frac{\tau}{\tau_n}\right) \tag{4.2}$$

where A_n, ϕ_n and τ_n are amplitude, phase and decay time of the nth decay process and A_{nr} is a non-resonant instantaneous component such as Kerr effect or two-photon absorption.

The response function shown in equation 4.2 is convoluted with a periodic Gaussian to reflect the excitation pulses of FWHM $2\sqrt{ln(2)}\tau_0$ in amplitude, and repetition period T_r, resulting in the fit function:

$$F(t,\tau) = \exp(i(\phi_0 + \phi_0' t)) \left[A_{nr} \exp\left(i\phi_{nr} - \frac{\tau^2}{\tau_0^2}\right) + \sum_n A_n \left(\frac{1}{e^{\frac{T_r}{\tau_n}} - 1} + \frac{1}{2}\left[1 + \mathrm{erf}\left(\frac{\tau}{\tau_0} - \frac{\tau_0}{2\tau_n}\right)\right] \right) \times \exp\left(i\phi_n + \frac{\tau_0^2}{4\tau_n^2} - \frac{\tau}{\tau_n}\right) \right] \tag{4.3}$$

This complex fit takes into account different phases of the components, given by the relative effect on absorption and refractive index. The fit equation also considers the possibility of slow drift of phase, included as $\exp(i(\phi_0 + \phi_0' t))$, caused by temperature drift of the setup changing the relative phase of reference and probe pulses over the time of the measurement of a few minutes. Since the radiative lifetime of QD (usually in the order of several ns) is longer than the maximum pulse delay τ_{23} (up to 1.6 ns), there is a possibility for the presence of leftover signal, i.e. proportional to the population, before the arrival of the next excitation pulse. This pile-up signal is also included in the equation as $1/(e^{\frac{T_r}{\tau_n}} - 1)$ after taking the sum of the geometric progression of events of all pulse sequences. The signal amplitude is fitted to $\sqrt{(\mathrm{Re}[F])^2 + (\mathrm{Im}[F])^2}$ and the phase to $\psi_0 + (180/\pi)\,\mathrm{atan2}(\mathrm{Im}[F], \mathrm{Re}[F])$ where ψ_0 is an arbitrary phase offset.

The obtained time constants from the fit at different temperatures from 5 K to 107 K are shown in Figure 4.5b. The first time constant Γ_1 is an ultrafast decay which we attribute to the relaxation rate of the excited states. The second time constant Γ_2 has a temperature independent response which we attribute to the Auger rate of the charged state. The third time constant Γ_3 is attributed to the recombination rate of the exciton. Relative amplitudes of these three time constants are shown in Figure 4.5c. At 5K, relative weights of 67.4 ± 6.3 % for A_1 and 10.3 ± 1.3 % for A_3 suggest a significant contribution of the excited states to the FWM amplitude. An increase in A_3 with temperature is understandable

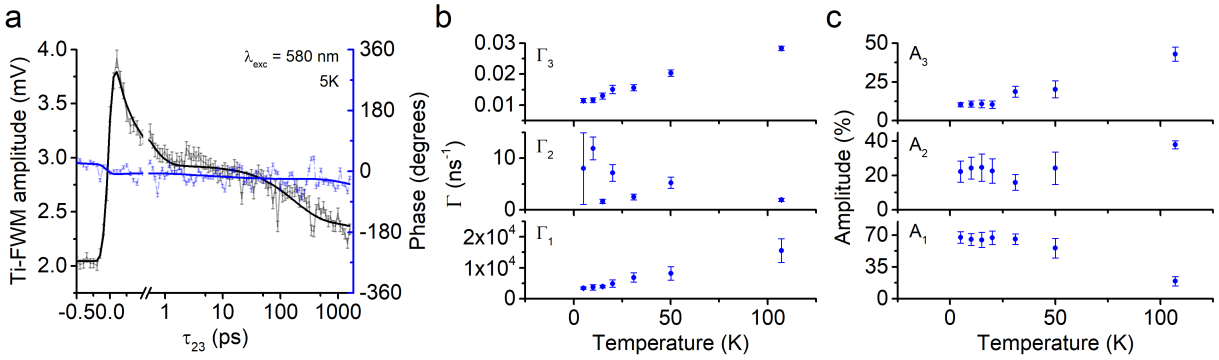

Figure 4.5. | Transient grating experiment. (a) Ti-FWM amplitude versus τ_{23} at 5 K for λ_{exc} = 580 nm with the solid lines representing the fit to a complex three-exponential response function shown in the equation 4.3.2. (b) The obtained time constants from the fit at different temperatures. Γ_1 - relaxation rate of excited states, Γ_2 – Auger rate of the charged state, Γ_3 - recombination rate of the exciton.

since the thermal expansion would induce a redshift in absorption peak bringing closer to a resonance at λ_{exc} = 580 nm. Note that the fluctuating A_2 also determines the relative proportions.

4.4. Origin of exciton dephasing in InP/ZnSe quantum dots

4.4.1. Influence of exciton fine structure

In order to understand the temperature dependent changes in the exciton ZPL dephasing and population density in our QD, the γ_{ZPL} from PE experiment and Γ_3 from TG experiment are fitted according to the model sketched in Figure 4.6a for λ_{exc} = 580 nm. First, we explain the electronic structure of our QD for choosing the fit model. As explained in section 3.3.4, there is a negligible contribution of shape anisotropy in the band-edge exciton fine structure of InP/ZnSe QDs and thus it only has exchange-interaction induced splitting between a threefold nearly-degenerate bright exciton and a fivefold degenerate dark exciton.[11] Accordingly, Γ_3 is fitted to the equation:

$$\Gamma_3 = [3\gamma_B + 5\gamma_D \exp(\Delta_{BD}/K_B T)] \,/\, [3 + 5\exp(\Delta_{BD}/K_B T)] \tag{4.4}$$

where γ_B & γ_D are the radiatively limited dephasing of the bright & dark exciton state and Δ_{BD} is the energetic splitting between them. K_B is the Boltzmann constant. The obtained fit parameters for Γ_3 from TG experiment are: γ_B = 0.0802 ± 0.005 ns^{-1}, γ_D = 0.0118 ± 0.0004 ns^{-1} and Δ_{BD} = 5.92 ± 0.71 meV. Note that the population density dynamics from TG experiment has the contribution of dark state since a smaller fraction of photons could still relax to the lower-lying dark state. The observation of increase in exciton recombination rate Γ_3 with temperature further agrees with the presence of dark exciton below the bright exciton and the obtained energetic splitting value of Δ is comparable to the expected bright-dark splitting energy of around 6 meV for similar sized InP/ZnSe QDs.[11] It should be noted that generally dark exciton recombination in QDs is activated by admixing with bright exciton through various physical mechanisms such as acoustic phonon, optical phonon & dangling bond[30] and hyperfine interaction between electron and nuclear spin.[31] The energy difference between the optically active and passive states determined using the temperature dependence of longer component in PL-decay in QDs has been attributed to confined acoustic phonons.[32] A similar observation was found in the long component of PL decay rate of InP/ZnSe QDs as well.[33]

Next, γ_{ZPL} is fitted to the equation:

$$\gamma_{ZPL} = \gamma_0(1 + 2\,N_B) \tag{4.5}$$

where γ_0 is the relaxation within the closely spaced bright exciton triplets via spontaneous phonon emission from one of the upper state. The latter part of the equation is the stimulated phonon emission process which is a thermally activated process with $N_B = 1/[\exp(\Delta/k_B T) - 1]$ representing the phonon occupation number. Here, the factor 2 is chosen considering the average between the two cases (final state below the initial state & vice versa) with Δ representing the activation energy of the bright exciton split states. The obtained fit parameters for γ_{ZPL} from PE experiment are: γ_0 = 0.034 ± 0.0004 ps^{-1}and Δ = 0.95 ± 0.01 meV.

Certainly, there are additional dephasing pathways: a spin-flip mediated relaxation into the dark state via spontaneous phonon emission (γ_{BD}) and natural radiative lifetime (γ_B). Since these are much

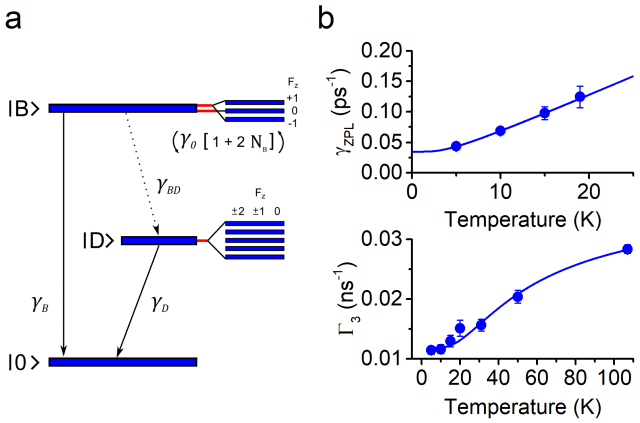

Figure 4.6. | Exciton dephasing & population dynamics. (a) Sketch of the model. (b) The solid lines represent the fits to Γ_3 and γ_{ZPL} values according to the equation 4.4 & 4.5 respectively.

lower than γ_0 , they are not included in the fit of γ_{ZPL} . For instance, the measured exciton dephasing time from PE experiment at 5 K (∼23 ps) is faster than γ_B (∼12.5 ns) from TG experiment. So, the exciton dephasing is far from the natural radiative limit in InP QDs similar to CdSe QDs. Contrary to a rapid spin-flip mediated dephasing from bright-to-dark exciton in CdSe QDs,[8] it is found here that the ZPL dephasing in InP QDs is dominated by phonon-scattering within closely spaced bright exciton states. Note that the inclusion of bright-to-dark state spin-flip parameter in the equation 4.5 did not influence the result as the dominant dephasing factor is the phonon-scattering within the bright exciton triplet indicating a slower bright-to-dark spin-flip in this QD. The zero-Kelvin exciton dephasing rate of 0.0346 ± 0.0004 ps^{-1} from the fit suggests that the spontaneous phonon-scattering process broadens the natural linewidth of the exciton ZPL. The obtained activation energy of 0.95 ± 0.01 meV is comparable to the bright exciton doublet splitting observed in the single QD spectrum shown in Figure 3.2. The ordering of F_z for bright exciton triplet shown in Figure 4.6a is based on the FLN measurement on a similar InP/ZnSe QD (see Figure 3.7). As already explained in section 3.3, the fivefold dark exciton remains degenerate for a minor anisotropy in this QD.

The temperature dependent dephasing rate γ_{ZPL} shown in Figure 4.6b is more steeper than observed in CdSe QDs,[8] which agrees with a similar finding in an ultrafast dephasing study of InP QDs where it was attributed to deformation potential coupling to acoustic phonon modes.[26] In the PE experiment studied here, τ_{23} was chosen as 1 ps to suppress additional non-linearities, taking into account the optical phonon energies of both InP (39∼47 meV) and ZnSe (24∼32 meV).[33] The contribution of oscillating LO and TO phonons are suppressed by this way, which can also be validated by the virtual absence of quantum beats in the TG experiment (see Figure 4.5a). Thus the phonon being discussed in this article are the low frequency vibrational modes which explains our such attribution to the initial femtosecond component in PE experiment. This kind of initial ultrafast decoherence, has been attributed to pure dephasing induced by acoustic phonons.[34] Note that the more covalent nature of InP compared to CdSe leads to a decreased polar optical phonon coupling in InP QDs.[26]

In the PE shown in Fig 4.3b, there is a small bump (at around τ_{12} =3.5 ps) between the ultrafast initial component and the monoexponential ZPL component at longer delay times. Since the PSB shown in the single QD (see Figure 3.2) is located at 1.1 meV from the ZPL, this small bump at similar range is attributed to a coherent phonon oscillation from the confined acoustic phonon modes on the ensemble of QDs. This value also agrees with vibrational modes of similar sized spherical InP QDs.[35] Acoustic phonon energies can be approximately determined using Lamb theory by assuming the QD as an

isotropic elastic sphere under stress free boundary condition.[36] This class of vibrational modes can be either spheroidal or torsional but the former is predicted to be dominant in QDs mediated through deformation potential coupling increasing linearly with temperature.[37, 38] The spheroidal phonon mode itself can be of longitudinal (LA) and transverse (TA) in nature. Spherical symmetry allows the frequency of these phonon modes to be determined based on the angular momentum quantum number for every $l \geq 0$, but the dominant contributions arise from l=0 and l=2 modes, which is also supported by such visibility in Raman transitions.[39] Further, the addition of shell around the spherical QD may modify the frequency of acoustic phonon by introducing a damping factor, and thus a continuum of phonon bands can also be expected.[40] It was reported that l=0 mode has the characteristic of LA while the l=2 mode has the mix of both with more TA nature.[41] In any case, l=2 mode is energetically lower than the higher frequency l=0 mode and contributes to the enhanced phonon coupling at elevated temperatures obtained from the PL decay rates in QDs.[32] So, it can be inferred that there are both discrete and continuum of acoustic phonon modes in QDs which reduce the overall contribution to the ZPL weight.

4.4.2. Narrow single quantum dot spectra

To compare the homogeneous linewidth and ZPL weight obtained from the FWM study on ensemble of QDs, emission from single QDs using micro-photoluminescence setup (see Appendix C.1) were measured with a quasi-resonant 532 nm CW excitation. Three such single QD spectra are shown in Figure 4.7. QD1 is a nearly-isotropic singlet having a linewidth of 50 μeV, without resolvable splitting between two polarization components. The inset shows that the ZPL weight is 72.3% with respect to PSB. QD2 is a doublet having a linewidth of 85 μeV, with a splitting of 0.42 meV between doublet. Both polarization components have equal intensities suggesting a circularly polarized emission. The inset shows that the ZPL weight is 75.8% with respect to PSB. QD3 is a nearly-isotropic singlet having a linewidth of 460 μeV, without resolvable splitting ($\sim$ 20 µeV) between two polarization components. A broad phonon feature, named B, is visible next to the PSB. The inset shows that the ZPL weight is 64.5% with respect to PSB and 49.6% with respect to both PSB and B. Note that the linewidth value of 50 $\pm$ 1 μeV at 5 K obtained with an acquisition time of 500 ms is among the narrowest reported linewidth for colloidal QDs using linear spectroscopy. A resolution limited 80 μeV linewidth was reported for CdSe/CdZnS QDs at 3.2 K.[42] A linewidth of 10 μeV was reported over an integration time of 100 ms using resonant photoluminescence excitation spectroscopy at 2 K.[43] Spectral-hole burning experiment on a 9 nm core diameter CdSe/ZnS QDs revealed a ZPL homogeneous linewidth of 6 μeV.[44] An upper limit of 6.5 μeV linewidth was reported for CdSe/ZnS QDs using photon-correlation Fourier spectroscopy.[45]

The observation of singlet ZPL line could be a trion emission as a charged state or it could be the exciton emission without noticeable fine structure splitting as expected for isotropic bright excitons. Nevertheless, the linewidth value of 50 $\pm$ 1 μeV for QD1-singlet and 85 $\pm$ 1 μeV for QD2-doublet at 5 K gives an upper limit to the exciton dephasing time of this QD which agrees with the direct measurement of the homogeneous linewidth of 56.8 $\pm$ 2.1 μeV using PE experiment at 5 K (see section 4.3.1). Further, the ZPL weight of 43.4% obtained using PE experiment at 5 K (see section 4.3.1) is comparable to the ZPL weight of 49.6% obtained for QD3 with respect to the immediate PSB on either side of ZPL in addition to the broad acoustic phonon feature observed in the lower energy (emission) side of the ZPL. This broad acoustic phonon feature is not visible in QD1 and QD2 since they are ultrafast component which are broader in the spectral domain with lower intensity, obtained using linear spectroscopy. The signal-to-noise ratio is better in QD3 that allowed the broad phonon feature

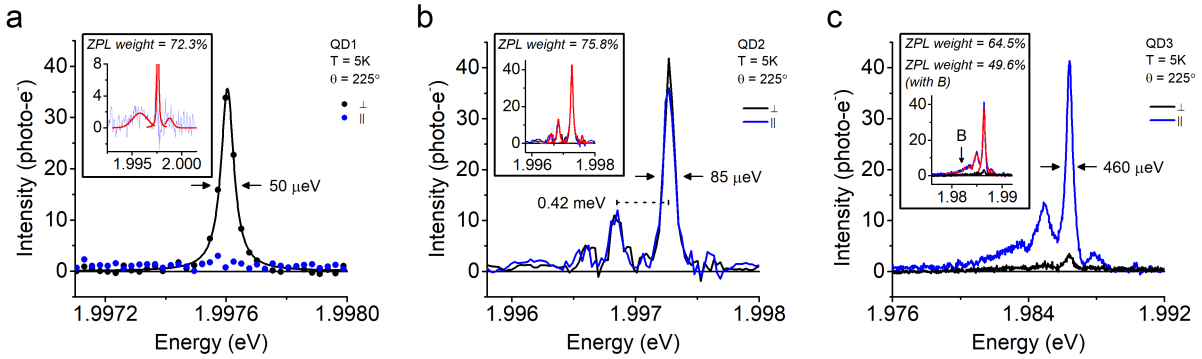

Figure 4.7. | Single QD spectra. (a) QD1 is a nearly-isotropic singlet having a linewidth of 50 μeV, without resolvable splitting between two polarization components. Inset: ZPL weight is 72.3% with respect to PSB. (b) QD2 is a doublet having a linewidth of 85 μeV, with a splitting of 0.42 meV between doublet. Both polarization components have equal intensities suggesting a circularly polarized emission. Inset: ZPL weight is 75.8% with respect to PSB. (c) QD3 is a nearly-isotropic singlet having a linewidth of 460 μeV, without resolvable splitting ($\sim$ 20 μeV) between two polarization components. A broad phonon feature, named B, is visible next to the PSB. Inset: ZPL weight is 64.5% with respect to PSB and 49.6% with respect to both PSB and B. Integration time is 500 ms. λ_{exc} = 532 nm.

to appear in the spectral domain. Such presence of both the confined discrete and continuum of acoustic phonons in QDs has been recently reported.[46]

4.5. Conclusion

In conclusion, a transient four wave mixing spectroscopy (FWM) on ensemble of InP/ZnSe QDs is performed to study both the photon echo (temperature range: 5 K - 31 K) and population density dynamics (temperature range: 5 K - 107 K). Contrary to a rapid spin-flip mediated dephasing from bright-to-dark exciton in CdSe QDs, it is found the ZPL dephasing is dominated by phonon-scattering within the closely spaced bright exciton triplet with a 0 K dephasing rate of 0.0346 $\pm$ 0.0004 ps^{-1} and an activation energy of 0.95 $\pm$ 0.01 meV. This indicates a slower spin-flip from bright-to-dark exciton state in this QD compared to CdSe QDs. The recombination rate of the exciton determined from the population density is fitted to an isotropic exciton model and subsequently the values of γ_B = 0.0802 $\pm$ 0.005 ns^{-1}, γ_D = 0.0118 $\pm$ 0.0004 ns^{-1} and Δ_{BD} = 5.92 $\pm$ 0.71 meV are determined. Further, the correspondence between the narrowest ZPL of single QDs (50 $\pm$ 1 μeV at 5 K) and the homogeneous linewidth obtained using FWM (56.8 $\pm$ 2.1 μeV at 5 K) indicates the presence of band edge exciton rather than a trap assisted recombination hitherto believed to be prevalent in InP core/shell QDs.

Bibliography

[1] Antonio Acín, Immanuel Bloch, Harry Buhrman, Tommaso Calarco, Christopher Eichler, Jens Eisert, Daniel Esteve, Nicolas Gisin, Steffen J Glaser, Fedor Jelezko, Stefan Kuhr, Maciej Lewenstein, Max F Riedel, Piet O Schmidt, Rob Thew, Andreas Wallraff, Ian Walmsley, and Frank K Wilhelm. The quantum technologies roadmap: a european community view. *New Journal of Physics*, 20(8):080201, aug 2018.

[2] Pascale Senellart, Glenn Solomon, and Andrew White. High-performance semiconductor quantum-dot single-photon sources. *Nature Nanotechnology*, 12(11):1026–1039, nov 2017.

[3] Peter Michler. Quantum dot single-photon sources. In *Single Semiconductor Quantum Dots*, pages 185–225. Springer Berlin Heidelberg, 2009.

[4] C. K. Hong, Z. Y. Ou, and L. Mandel. Measurement of subpicosecond time intervals between two photons by interference. *Physical Review Letters*, 59:2044–2046, nov 1987.

[5] Igor Aharonovich, Dirk Englund, and Milos Toth. Solid-state single-photon emitters. *Nature Photonics*, 10(10):631–641, sep 2016.

[6] Paola Borri and Wolfgang Langbein. Transient four-wave mixing of excitons in quantum dots from ensembles and individuals. In Fritz Henneberger and Oliver Benson, editors, *Semiconductor Quantum Bits*. Pan Stanford, 2008.

[7] Al. L. Efros, M. Rosen, M. Kuno, M. Nirmal, D. J. Norris, and M. Bawendi. Band-edge exciton in quantum dots of semiconductors with a degenerate valence band: Dark and bright exciton states. *Physical Review B*, 54:4843–4856, aug 1996.

[8] Francesco Masia, Nicolò Accanto, Wolfgang Langbein, and Paola Borri. Spin-flip limited exciton dephasing in $\mathrm{CdSe/ZnS}$ colloidal quantum dots. *Physical Review Letters*, 108(8):087401, feb 2012.

[9] Nicolò Accanto, Francesco Masia, Iwan Moreels, Zeger Hens, Wolfgang Langbein, and Paola Borri. Engineering the spin–flip limited exciton dephasing in colloidal CdSe/CdS quantum dots. *ACS Nano*, 6(6):5227–5233, may 2012.

[10] Vigneshwaran Chandrasekaran, Mickaël D. Tessier, Dorian Dupont, Pieter Geiregat, Zeger Hens, and Edouard Brainis. Nearly blinking-free, high-purity single-photon emission by colloidal InP/ZnSe quantum dots. *Nano Letters*, 17(10):6104–6109, sep 2017.

[11] Annalisa Brodu, Vigneshwaran Chandrasekaran, Lorenzo Scarpelli, Jonathan Buhot, Francesco Masia, Mariana V. Ballottin, Marion Severijnen, Mickaël D. Tessier, Dorian Dupont, Freddy T. Rabouw, Peter C. M. Christianen, Celso de Mello Donega, Daniël Vanmaekelbergh, Wolfgang Langbein, and Zeger Hens. Fine structure of nearly isotropic bright excitons in InP/ZnSe colloidal quantum dots. *The Journal of Physical Chemistry Letters*, 10(18):5468–5475, aug 2019.

[12] Louis Biadala, Benjamin Siebers, Yasin Beyazit, Mickaël. D. Tessier, Dorian Dupont, Zeger Hens, Dmitri R. Yakovlev, and Manfred Bayer. Band-edge exciton fine structure and recombination dynamics in InP/ZnS colloidal nanocrystals. *ACS Nano*, 10(3):3356–3364, feb 2016.

[13] Eric M. Janke, Nicholas E. Williams, Chunxing She, Danylo Zherebetskyy, Margaret H. Hudson, Lili Wang, David J. Gosztola, Richard D. Schaller, Byeongdu Lee, Chengjun Sun, Gregory S. Engel, and Dmitri V. Talapin. Origin of broad emission spectra in InP quantum dots: Contributions from structural and electronic disorder. *Journal of the American Chemical Society*, 140(46):15791–15803, oct 2018.

[14] Peter Michler, editor. *Quantum Dots for Quantum Information Technologies*. Springer International Publishing, 2017.

[15] T. Grange, N. Somaschi, C. Antón, L. De Santis, G. Coppola, V. Giesz, A. Lemaître, I. Sagnes, A. Auffèves, and P. Senellart. Reducing phonon-induced decoherence in solid-state single-photon sources with cavity quantum electrodynamics. *Physical Review Letters*, 118:253602, jun 2017.

[16] P. Borri, W. Langbein, S. Schneider, U. Woggon, R. Sellin, D. Ouyang, and D. Bimberg. Ultralong dephasing time in InGaAs quantum dots. *Physical Review Letters*, 87(15):157401, sep 2001.

[17] E. A. Muljarov and R. Zimmermann. Dephasing in quantum dots: Quadratic coupling to acoustic phonons. *Physical Review Letters*, 93:237401, nov 2004.

[18] Andreas V. Kuhlmann, Julien Houel, Arne Ludwig, Lukas Greuter, Dirk Reuter, Andreas D. Wieck, Martino Poggio, and Richard J. Warburton. Charge noise and spin noise in a semiconductor quantum device. *Nature Physics*, 9(9):570–575, jul 2013.

[19] Ali Naeem, Francesco Masia, Sotirios Christodoulou, Iwan Moreels, Paola Borri, and Wolfgang Langbein. Giant exciton oscillator strength and radiatively limited dephasing in two-dimensional platelets. *Physical Review B*, 91(12):121302, mar 2015.

[20] Michael A. Becker, Lorenzo Scarpelli, Georgian Nedelcu, Gabriele Rainò, Francesco Masia, Paola Borri, Thilo Stöferle, Maksym V. Kovalenko, Wolfgang Langbein, and Rainer F. Mahrt. Long exciton dephasing time and coherent phonon coupling in CsPbBr2cl perovskite nanocrystals. *Nano Letters*, 18(12):7546–7551, nov 2018.

[21] Von L. Allen and J. H. Eberly. Optical resonance and two level atoms. *Physik in unserer Zeit*, 7(1):31–32, 1976.

[22] R. W. Schoenlein, D. M. Mittleman, J. J. Shiang, A. P. Alivisatos, and C. V. Shank. Investigation of femtosecond electronic dephasing in cdse nanocrystals using quantum-beat-suppressed photon echoes. *Physical Review Letters*, 70:1014–1017, feb 1993.

[23] D. J. Norris, A. Sacra, C. B. Murray, and M. G. Bawendi. Measurement of the size dependent hole spectrum in cdse quantum dots. *Physical Review Letters*, 72:2612–2615, apr 1994.

[24] Jagdeep Shah. *Ultrafast Spectroscopy of Semiconductors and Semiconductor Nanostructures*. Springer Berlin Heidelberg, 1999.

[25] L. Besombes, K. Kheng, L. Marsal, and H. Mariette. Acoustic phonon broadening mechanism in single quantum dot emission. *Physical Review B*, 63:155307, Mar 2001.

[26] U. Banin, G. Cerullo, A. A. Guzelian, C. J. Bardeen, A. P. Alivisatos, and C. V. Shank. Quantum confinement and ultrafast dephasing dynamics in inp nanocrystals. *Physical Review B*, 55:7059–7067, mar 1997.

[27] P. Borri, W. Langbein, U. Woggon, V. Stavarache, D. Reuter, and A. D. Wieck. Exciton dephasing via phonon interactions in inas quantum dots: Dependence on quantum confinement. *Physical Review B*, 71:115328, Mar 2005.

[28] Al. L. Efros and M. Rosen. The electronic structure of semiconductor nanocrystals. *Annual Review of Materials Science*, 30(1):475–521, aug 2000.

[29] L. Scarpelli, F. Masia, E. M. Alexeev, F. Withers, A. I. Tartakovskii, K. S. Novoselov, and W. Langbein. Resonantly excited exciton dynamics in two-dimensional mose_2 monolayers. *Physical Review B*, 96(4):045407, jul 2017.

[30] Anna V. Rodina and Alexander L. Efros. Radiative recombination from dark excitons in nanocrystals: Activation mechanisms and polarization properties. *Physical Review B*, 93:155427, apr 2016.

[31] Annalisa Brodu, Mickael D. Tessier, Damien Canneson, Dorian Dupont, Mariana V. Ballottin, Peter C. M. Christianen, Celso de Mello Donega, Zeger Hens, Dmitri R. Yakovlev, Manfred Bayer, Daniel Vanmaekelbergh, and Louis Biadala. Hyperfine interactions and slow spin dynamics in quasi-isotropic InP-based core/shell colloidal nanocrystals. *ACS Nano*, 13(9):10201–10209, aug 2019.

[32] Dan Oron, Assaf Aharoni, Celso de Mello Donega, Jos van Rijssel, Andries Meijerink, and Uri Banin. Universal role of discrete acoustic phonons in the low-temperature optical emission of colloidal quantum dots. *Physical Review Letters*, 102:177402, apr 2009.

[33] Annalisa Brodu, Mariana V. Ballottin, Jonathan Buhot, Elleke J. van Harten, Dorian Dupont, Andrea La Porta, P. Tim Prins, Mickael D. Tessier, Marijn A. M. Versteegh, Val Zwiller, Sara Bals, Zeger Hens, Freddy T. Rabouw, Peter C. M. Christianen, Celso de Mello Donega, and Daniel Vanmaekelbergh. Exciton fine structure and lattice dynamics in InP/ZnSe core/shell quantum dots. *ACS Photonics*, 5(8):3353–3362, jul 2018.

[34] A. Vagov, V. M. Axt, T. Kuhn, W. Langbein, P. Borri, and U. Woggon. Nonmonotonous temperature dependence of the initial decoherence in quantum dots. *Physical Review B*, 70:201305, nov 2004.

[35] Mina Talati and Prafulla K. Jha. Acoustic phonons in semiconductor nanocrystals. *Computational Materials Science*, 37(1-2):58–63, aug 2006.

[36] Horace Lamb. On the vibrations of an elastic sphere. *Proceedings of the London Mathematical Society*, s1-13(1):189–212, 1881.

[37] T. Takagahara. Electron-phonon interactions and excitonic dephasing in semiconductor nanocrystals. *Physical Review Letters*, 71:3577–3580, nov 1993.

[38] T. Takagahara. Electron—phonon interactions in semiconductor nanocrystals. *Journal of Luminescence*, 70(1-6):129–143, oct 1996.

[39] Eugeʿne Duval. Far-infrared and raman vibrational transitions of a solid sphere: Selection rules. *Physical Review B*, 46:5795–5797, sep 1992.

[40] Mayrose R. Salvador, Matthew W. Graham, and Gregory D. Scholes. Exciton-phonon coupling and disorder in the excited states of CdSe colloidal quantum dots. *The Journal of Chemical Physics*, 125(18):184709, nov 2006.

[41] Lucien Saviot and Daniel B. Murray. Longitudinal versus transverse spheroidal vibrational modes of an elastic sphere. *Physical Review B*, 72:205433, nov 2005.

[42] Mark J. Fernée, Brad N. Littleton, Steven Cooper, Halina Rubinsztein-Dunlop, Daniel E. Gómez, and Paul Mulvaney. Acoustic phonon contributions to the emission spectrum of single CdSe nanocrystals. *The Journal of Physical Chemistry C*, 112(6):1878–1884, feb 2008.

[43] L. Biadala, Y. Louyer, Ph. Tamarat, and B. Lounis. Direct observation of the two lowest exciton zero-phonon lines in Single CdSe/ZnS Nanocrystals. *Physical Review Letters*, 103:037404, jul 2009.

[44] Phedon Palinginis, Sasha Tavenner, Mark Lonergan, and Hailin Wang. Spectral hole burning and zero phonon linewidth in semiconductor nanocrystals. *Physical Review B*, 67:201307, may 2003.

[45] L. Coolen, X. Brokmann, P. Spinicelli, and J.-P. Hermier. Emission characterization of a single cdsezns nanocrystal with high temporal and spectral resolution by photon-correlation fourier spectroscopy. *Physical Review Letters*, 100:027403, jan 2008.

[46] Albert Liu, Diogo B. Almeida, Wan-Ki Bae, Lazaro A. Padilha, and Steven T. Cundiff. Simultaneous existence of confined and delocalized vibrational modes in colloidal quantum dots. *The Journal of Physical Chemistry Letters*, 10(20):6144–6150, sep 2019.

Chapter 5.

Reduced spectral diffusion in multi-excitonic species compared to neutral-exciton

Contents

Synopsis

Spectral diffusion (SD) due to quantum confined stark effect (QCSE) is well observed for exciton, but it is rarely explored in multiple exciton species in colloidal QDs. Using single-QD PL, this chapter correlates the level of SD in exciton, biexciton and trion emissions. It is observed that the QCSE is minimized in trion-to-carrier and biexciton-to-exciton transitions compared to neutral exciton. Using InP/ZnSe QDs as an optimized system to minimize SD, this chapter provides theoretical understanding of the structural conditions that determine the magnitude of QCSE in core-shell QDs. This allows to show that minimal SD can be expected for strongly confined cores (large band-offset, moderately small core) and multi-excitonic species.

Manuscript in preparation
Synthesis of InP/ZnSe QDs by Dr. Dorian Dupont, Ghent University, Belgium
Spectral jitter correction algorithm by Dr. Francesco Masia, Cardiff University, United Kingdom
Theoretical model by Prof. Juan Ignacio Climente Plasencia, Universitat Jaume I, Spain

5.1. Introduction

5.1.1. Quantum confined stark effect

Nanocrystals, or colloidal quantum dots, (QDs) can be seen as artificial atoms considering the discrete electronic energies arising due to quantum confinement.[1] While an ideal quantum emitter, interacting only with the electromagnetic environment, is emitting indistinguishable photons having a lifetime-limited spectral distribution intended for quantum photonic applications, the additional interaction with vibrational degrees of freedom and the environment results in more complex spectral features in QDs.[2] At room temperature, the homogeneous lineshape is typically dominated by phonon-induced broadening in the order of 10-100 meV, orders of magnitude larger than the lifetime limited broadening in the μeV range.[3] Reducing the temperature, the lattice vibrations are frozen out and the zero phonon lines in the emission spectra can be observed.[4] Furthermore, the spatial ground state of the exciton shows a fine structure splitting between the different spin configurations of electron and hole, which is sensitive to the size and shape of the QDs.[5] To access this information, one first has to remove the inhomogeneous broadening of an ensemble of QDs due to their structural inhomogeneity, which can be done by spatial dilution and micro-spectroscopy observing the emission of single QDs.[6–9] Even when observing single QDs, slow time-evolutions compared to the emission lifetime (in the order of nanoseconds) influence the emission spectra observed in typical experimental settings (in the order of seconds). These slow time-evolutions, which are mostly due to charge trapping in the QDs and their surroundings, lead to an effective inhomogeneous broadening known under the terms spectral diffusion[10] (SD) and blinking.[11] Reciprocally, the SD via the quantum confined Stark effect (QCSE) contains information about the polarizability of the band-edge excitonic species. As such, the Coulomb interactions and the spatial separation of electron-hole wavefunctions can be experimentally estimated by observing the magnitude of shift in transition energies.

Charge fluctuations in the vicinity of quantum dots

Since the early report of SD in single colloidal particles,[10] much research has gone into identifying its origin, and an accepted model are local field fluctuations due to fluctuating number and position of charges in the vicinity of the nanocrystal causing a QCSE.[12–17] Nanocrystals have a large surface to volume ratio and and they play a significant part in their optical properties from a simple observation of enhanced fluorescence in a surface-trap passivated core/shell heterostructure compared to a simple core-only nanocrystals.[18] QDs have a size-dependent intrinsic dipole moment arising from the surface localized charges among other possible contributions like shape asymmetry & surface strain.[19] This indicates that the influence of surface charges is evident in creating a local electric field fluctuation in QDs. QCSE causing a redshift & broadening of spectra was observed for both spherical & rod-like QD.[13, 14, 16] It was also observed that the QCSE changes the optical phonon coupling.[14] Signal-to-noise ratio of single QD spectra collected using micro-photoluminescence setup is generally lower for a single acquisition time (usually in the order of ms to s) and thus an integration over longer acquisition times is necessary to build the spectra. But the presence of SD broadens the time-integrated spectra,[20] hiding the significant characteristics behind the lineshape of a QD, for instance a Lorentzian zero-phonon line on a broadband acoustic phonon pedastal.[21] Studies have been done to identify a continuous or discrete charge motion based on the statistics of spectral jumps.[14, 22] It was also observed that the spectral shifts are not entirely random but also the positions are repeated showing a memory of the previous shifts.[23] Thus a detailed study of SD on exciton emission has been done by means of

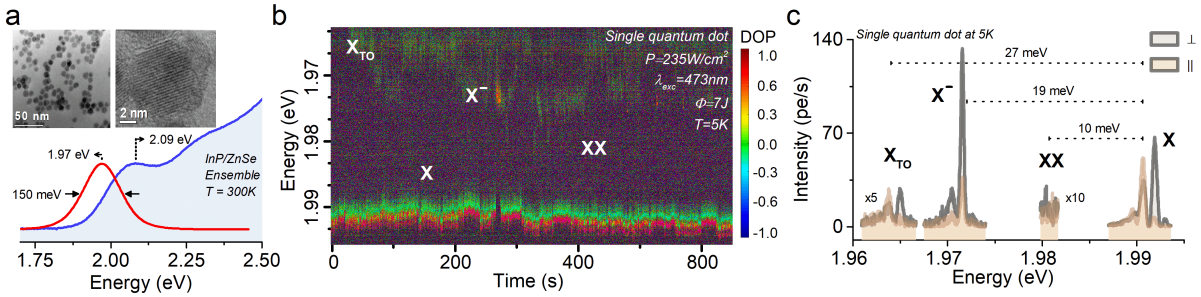

Figure 5.1. | Spectra of InP/ZnSe QDs. (a) Ensemble emission and absorption spectra at room temperature. Inset shows the TEM and HR-TEM images of the QD. (b) Polarization resolved emission spectral sequence of a single QD at 5K exhibiting emissions from exciton (X), biexciton (XX), negative trion (X^-) and ZnSe TO-phonon replica of exciton emission (X_{TO}). Acquisition time is 1s. Half-wave plate angle is 82°. (c) Corresponding spectral jitter corrected spectra.

single QD spectroscopy. However, SD of biexciton & trion which have faster radiative lifetime than exciton have been rarely explored at cryogenic temperature, to our knowledge. Though there is a report of QCSE observed on both exciton and trion at room temperature in a blinking study, the trion was considered as an intermediate state with lower intensity than exciton.[24, 25]

5.2. Spectral diffusion of band edge excitonic species

5.2.1. Redshift, broadening & enhanced phonon coupling in neutral-exciton

InP/ZnSe QDs under study were synthesized according to the method described in section 1.5.2. Figure 5.1a shows the ensemble emission and absorption spectra of the QD at room temperature and the inset shows the TEM & HR-TEM images of the QD that has an overall diameter of 10 nm with a core diameter of 3.2 nm. The sample for single QD spectroscopy was prepared by diluting InP/ZnSe QDs to a nanomolar concentration which is then mixed with 1% solution of polystyrene-toluene in the ratio of 1:9 and dropcasted on a quartz coverslip. QDs were excited either at 473 nm or 532 nm keeping the temperature at 5K and the polarization resolved spectra were collected using the micro-photoluminescence setup described in Appendix C.1. As shown in section 3.2, the single QD spectra of InP/ZnSe QDs at 5 K under 473 nm excitation had distinct features such as: doublet feature as exciton (X) due to minor anisotropy in z-axis, a doublet feature with inverted polarization to Xas biexciton (XX) and a singlet as a negatively charged trion (X^-).[26] Figure 5.1b,c shows an overview of these spectral features for a single QD at 5K consisting of X, XX (10 meV binding energy), X^- (19 meV binding energy from lower energy feature of exciton doublet) and also a spectral doublet replica of X with similar polarization directions observed 27 meV below X, which is attributed to ZnSe TO phonon (X_{TO}). Note that the spectral image sequence is shown as a value/hue plot, where the color value and hue correspond to the total emission intensity and the degree of polarization (DOP) at each time point and emission energy. Only X emission was observed at lower excitation power and increasing the excitation intensity induces the switching transition from the X to a charged state (or trion X^-). The trion forms a spin singlet state of the two equal charge carriers, so that the opposite charge carrier does not encounter exchange interaction. Hence the trion emission has no fine structure splitting at B=0.[27] Emission from XX is confirmed by the inverted polarization to X and a supra-linear dependence to input excitation intensity (see Figure 3.2d). The XX state with two electron-hole pairs

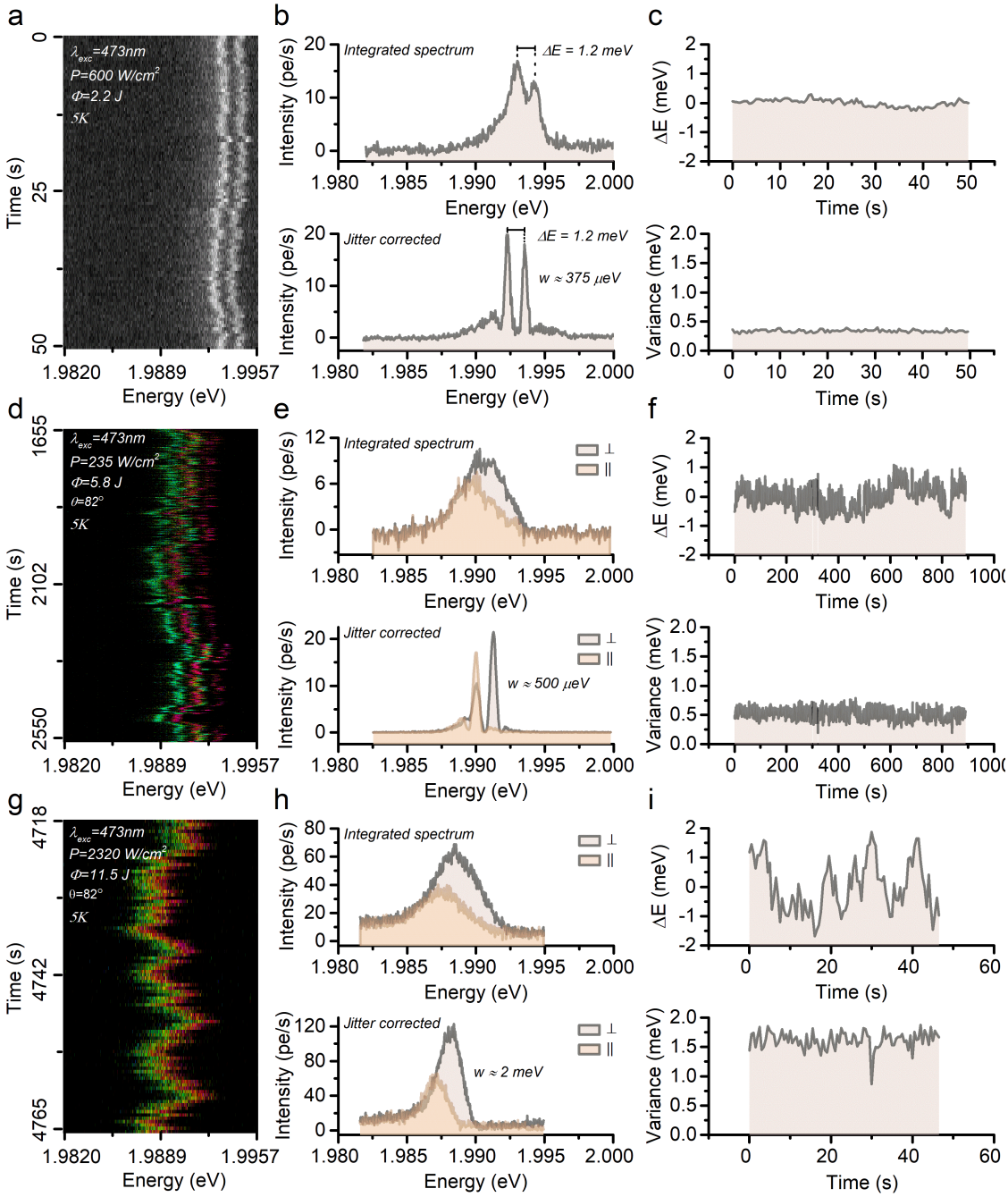

Figure 5.2. | Effect of QCSE on exciton. (a) At low flux, exciton emission is at higher energy (1.994 eV) with little SD. (b) above: Integrated spectra resolve the doublet splitting of 1.2 meV, below: Jitter-corrected spectra showing a linewidth of 375 μeV also clearly resolves the PSB on either side of the ZPL. (c) above: relative spectral shift from central emission energy in the order of 0.15 meV, (below): variance of the emission which is proportional to the linewidth of the QD. (d, e, f) At increased flux, exciton emission shifts to lower energy, (1.991 eV), with SD in the order of 1 meV. (g, h, i) At larger flux, exciton emission at (1.988 eV) showing high SD in the order of 2 meV. The linewidth values are indicated. Acquisition time of each pixel is 0.5s in (a, g) and 1s in (d).

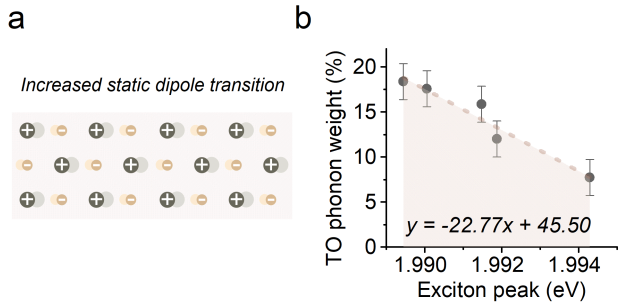

Figure 5.3. | Effect of QCSE on optical phonon coupling to exciton. (a) Increase in QCSE separates the charge carriers and causes redshift in exciton emission energy, a reduction in oscillator strength, and an increase of the static dipole of the exciton, increasing the coupling to optical phonons. (b) TO phonon replica weight to ZPL versus exciton emission peak energy. The redshift due to QCSE results in more phonon coupling.

is a spin singlet, and the recombination of the XX leaves a bright exciton.[28] Hence the doublet splitting of 1.2 meV from X is also observed in the XX emission, but with opposite polarization order.

The emission energy and the SD observed for the investigated QD depended on excitation intensity and integrated excitation flux over a continuous illumination. Generally, increasing of either of the two quantities increased redshift and SD, and switching between emission from the X and X^-, indicating QD charging by unbalanced escape of charge carriers. The movement of the charge carriers created by the optical excitation on the surface or the environment of the QD causes a change of the local field which shifts the QD emission. The QCSE causes a redshift in the excitonic emission with increasing field, and the induced static dipole moment in turn increases the sensitivity to the local electric field and thus the SD. The spectra shown in Figure 5.1c for the corresponding sequence displayed in Figure 5.1b is a result of a spectral jitter correction which factorizes the spectra into an underlying jitter-corrected spectrum and time dependent probabilities of a set of shifts of the spectra. This jitter-correction algorithm takes into account the level of spectral shifts on consecutive acquisitions by aligning their peaks and gives a time-dependent probability for such transitions. This is done by a non-negative matrix factorization technique that disentangles spectral diffusion from intrinsic lineshape, since the QCSE induces a spectral shift but maintains the same spectral shape. Thus the spectral diffusion data is factorized as a linear combination of components identified by non-negative spectra and corresponding probability. After applying this jitter-correction algorithm to the data, the phonon sidebands (PSB) are then clearly resolved on both X & X^- spectra at either side of the central ZPL emission line, which account for 30% of the total emission.

First the effect of SD on X is discussed, showing in Figure 5.2 polarization resolved spectral sequences, time integrated spectra, spectral jitter corrected spectra and their respective level of spectral shifts, for different excitation powers and total fluxes. In Figure 5.2a, at low flux and power, when the QCSE was less with negligible SD, the corresponding time integrated spectra shown in Figure 5.2b (above) still resolved the doublet splitting and were centered around 1.994 eV. Figure 5.2b (below) shows the jitter-corrected spectrum, clearly resolving the PSB on either side of ZPL, and a linewidth of 375 μeV gives an upper limit for the homogeneous broadening at 473 nm excitation, but is dominated by SD during the acquisition time of 0.5 s. Figure 5.2c (above) shows the spectral shift from the central emission energy in the order of 0.15 meV and Figure 5.2c (below) shows the respective variance of the emission in the order of $\sim$0.4 meV which is proportional to the linewidth. For higher accumulated flux but lower intensity shown in Figure 5.2(d, e, f), we find SD revealing discrete energy steps around 1 meV, likely due to a carrier trap close to the QD surface. The average emission energy has now shifted about 3

meV to the red (peak energy of 1.991 eV with a linewidth of 500 μeV), indicative of the higher average local field. At higher excitation intensity and even more accumulated flux shown in Figure 5.2(g, h, i), the emission has redshifted about 6 meV (peak energy of 1.988 eV with a linewidth of 2 meV) and the SD is fast and strong with the spectral shift in the order of 1.5 meV.

QCSE also influences the optical phonon coupling to the exciton emission. An increase in the QCSE separates the charge carrier reducing the overlap of electron-hole wavefunction and thus a reduction in the oscillator strength. This increases the static dipole of the transition as shown in Figure 5.3a and thus increases the coupling to optical phonons. We observe that the weight of the X_{TO} phonon line is increasing from 8% to 18% with a redshift in the exciton emission energy from 1.994 eV to 1.989 eV respectively, as shown in Figure 5.3b.

5.2.2. Reduced spectral diffusion in biexciton and trion

Though the SD of X emission in QDs is studied extensively in literature,[12–17] a correlative SD study of multiple exciton species to X is rarely explored at cryogenic temperature for QDs. In Figure 5.4a, polarization resolved spectral sequences showing the XX and X emission simultaneously and the X^- emission during intermittent charging are shown. Interestingly, the linewidth of XX and X^- is

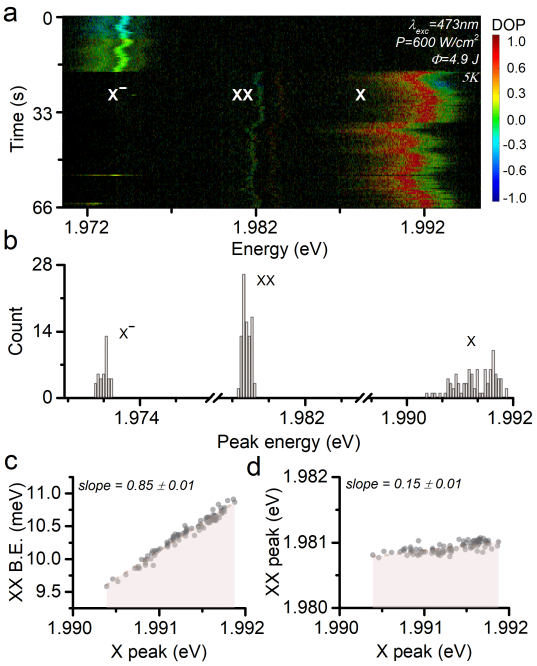

Figure 5.4. | QCSE in exciton & multiple exciton species. (a) Polarization resolved spectral sequence of the same QD showing the SD of X, XX and X^-. Integration time is 0.5 s. Half-wave plate angle is varied initially and later set to 82°. Note that the XX has an inverted DOP for the doublets compared to X. (b) Histogram of their respective peak energies which confirms that linewidth of XX & X^- is much narrower than X. (Lower energy peak value is shown for X & XX doublets). (c) Dependence of XX binding energy on X peak energy. The redshift of exciton decreases the binding energy of XX and thus confirming a change in band offset & electron delocalization due to QCSE. (d) Dependence of XX transition energy with respect to X peak energy, showing a much weaker QCSE on the XX to X transition.

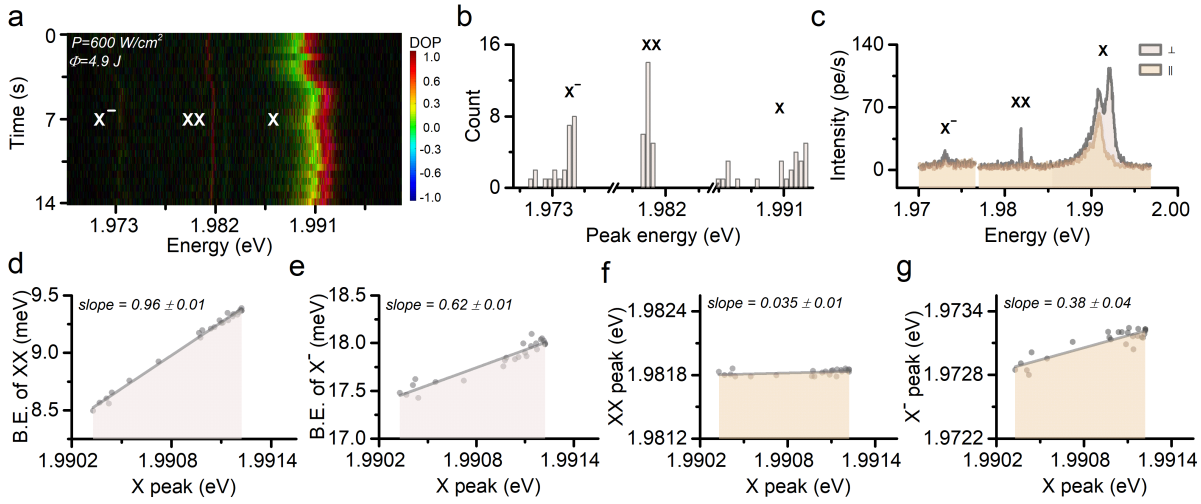

Figure 5.5. | QCSE in exciton & multiple exciton species. (a) Polarization resolved spectral sequence of the QD with the simultaneous observation of X, XX & X^-. Integration time is 0.5s. (b) Histogram of their respective peak energies (lower energy peak values shown for X & XX doublets) (c) Corresponding spectral jitter corrected spectra (d-e) The redshift of exciton decreases the binding energy of XX and X^-, thus confirming a change in band offsets and charge delocalization due to QCSE. (f-g) Dependence of XX & X^- transition energy with respect to exciton peak energy, showing the much weaker QCSE on the XX to X transition & X^- to X transition.

much narrower than X as analyzed in the peak energy histogram in Figure 5.4b. Since the XX emission is simultaneously observed as the X emission with jittering transitions in a similar direction in the energy scale, their emission peak energies can be correlated. Thus a linear dependence of the XX binding energy on the X energy is obtained with a slope of 0.85±0.01 as shown in Figure 5.4c. The peak energy of XX emission accordingly shows linear dependence on X energy with a slope of only 0.15 ± 0.01, as shown in Figure 5.4d. These two are correlated by the sum of slopes adding to 1.

Further in an another acquisition, both the XX and X^- emission are observed together with the X emission (see Figure 5.5), which is attributed to a fast charging dynamics within a single integration time of 0.5 s. The redshift of X decreases the binding energy of both XX & X^-, suggesting a reduced electron-hole wavefunction overlap due to QCSE.[29, 30] Again, a minimal SD of XX & X^- emission compared to X emission is observed. Notably, a slope of 0.035 ± 0.01 for the XX emission and 0.38 ± 0.04 for the X^- emission was found. While the stark shift is smaller for XX than X^-, the change in binding energy has an opposite effect with a slope of 0.96 ± 0.01 and 0.62 ± 0.01 respectively. Again, note that these two are correlated by the sum of slopes adding to 1.

5.3. Influence of QD environment

5.3.1. Polarizability as a tool to distinguish band edge emissions

The light induced SD has been attributed to the random field fluctuations induced by trapping & release of free carriers at defects in the environment of self-assembled QD.[31, 32] In case of our QD, presence of trap sites, for instance, resulting from an un-passivated surface may cause a rapid charging with fluctuating transition energies. The simultaneous observation of X, XX & X^- emission shown in Figure

5.5 indicates a rapid charging dynamics happening much faster than a single experimental acquisition time. As shown in Figure 5.2, the stronger local field arising from the larger charge fluctuation happens especially for accumulated flux after longer excitation of the QD with CW pumping. This implies that the prolonged excitation creates a non-equilibrium charge distribution in the QD environment, for example via Auger escape of carriers from the QD and subsequent carrier hopping via further photon absorption by the carriers in the dielectric environment. Monitoring the SD of a QD could give an indication of the kind of environment it experiences.

Figure 5.6 shows two examples for fluctuating positions of a charge carrier. Figure 5.6a shows the spectral sequence of a single QD and a selected spectrum shown in Figure 5.6b has a linewidth as narrow as 50 μeV with the experimental acquisition time of 500 ms. The inset shows the spectral shift from the central emission energy, where a 55 distinct number of spectral components emitting at different energies is identified. Figure 5.6c shows the spectral sequence of another QD whose spectrum is shown in Figure 5.6d. Here, the spectral shift shown in inset has only a 5 distinct number of spectral components emitting at different energies is identified. Hence it can be inferred that the fluctuations in the emission energy may arise via trapping of just one charge carrier fluctuating in the surrounding trap sites depending on the particular QD environment.

Note that the QDs shown here are quasi-resonantly excited onto the InP core using 532 nm CW laser where an increase in the quantum yield of the emission is observed (more observation of single QD emissions ∼40) compared to the non-resonant 473 nm excitation shown before (∼10). At 473 nm excitation, the corresponding excess energy of 290 meV could be sufficient to activate a hole over the ZnSe barrier. It is therefore speculated that the resulting electron charging creates Auger recombination and broad emission lineshapes, which are not visible. Using 532 nm excitation instead, the excess energy is below this activation energy and a narrow linewidth is expected with more quantum yield. The observation of singlet emission here could be either a trion or an isotropic exciton without notice-

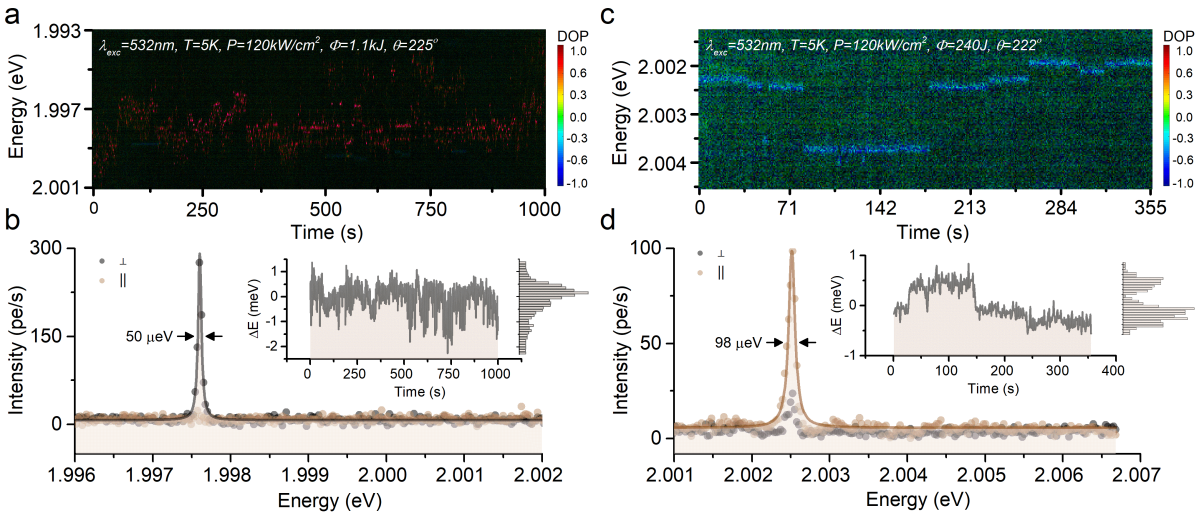

Figure 5.6. | Influence of QD environment. (a) Spectral sequence of a single QD. Integration time is 0.5s. (b) Selected spectrum showing a linewidth of 50 μeV. Inset: relative spectral shift from central emission energy where a 55 distinct number of spectral components emitting at different energies are identified. (c) Spectral sequence of a single QD. Integration time is 1 s. (d) Spectrum has a linewidth of 98 μeV. Inset: relative spectral shift from central emission energy where a 5 distinct number of spectral components emitting at different energies are identified.

able fine structure splitting. They are tentatively assigned to an isotropic exciton expected for these QDs,[26] which is also supported by the magnitude of spectral shift in the order of meV comparable to the values shown in Figure 5.2 for exciton.

Cryogenic spectroscopy of single QDs have been used to identify the band edge exciton emission features.[4] The spectral feature can be a singlet or multiplet depending on the fine structure of the QDs. However, a care must be taken in assigning the reasoning for the multiplet emission spectra since the multiplet could also be the result of the SD of a single line jumping in the energy scale, due to charge fluctuations within the experimental acquisition time. Also the lineshape of the spectra has to be considered since an acoustic phonon with a non-Lorentzian shape could also be wrongly considered as a multiplet. Using polarization resolved spectroscopy would confirm multiplet emission, for instance a bright exciton fine structure arising due to xy-anisotropy would be polarized perpendicular to each other and thus have different DOP.[33, 34] Further the polarization of the acoustic phonon would be similar to the polarization of ZPL emission, as can be seen in Figure 5.1c. As described in this chapter, the combination of polarization resolved spectroscopy of single QDs and spectral jitter correction to extract the cleaner spectra reveals the correct identity of band edge emissions. Further, from the observation of minimal effect of QCSE on XX & X^- emission compared to X, it is proposed that the polarizability could be used as a tool to distinguish the band edge emissions. To confirm this, a valid theoretical model is needed to find the energy shifts in the presence of a point charge on the QD surface for excitonic species such as X, XX, X^- & X^+.

5.4. Theoretical model

5.4.1. Configuration interaction

The influence of stark effect in quantum dots has been studied theoretically where a clear difference in the emission energies was observed at higher field intensity.[35, 36] In electrically injected self assembled QDs, the field dependence of the transition energies obtained experimentally has been adequately modeled with $E = E_0 + \rho F + \beta F^2$ where E_0 is the energy at zero electric field $F = 0$, ρ depends on the built-in dipole moment and β describes the polarizability of electron and hole wavefunction.[37, 38] While some studies observed a reduction of dipole moment and polarizability in multiple exciton species compared to a neutral exciton,[39–43] other studies reported contradicting results.[44–47] In case of colloidal QDs, the exciton polarizability for ensemble of QD under applied electric field was determined both experimentally[48, 49] and theoretically.[50, 51] A blinking study on single QD at room temperature revealed a smaller polarizability for intermediate states (trions) than neutral excitons.[24, 25]

Our observation of reduced SD in multiple excitons due to QCSE in single InP/ZnSe QD at cryogenic temperature, as shown in Figure 5.4 & Figure 5.5, implies a reduced polarizability for them compared to a neutral exciton. To validate this hypothesis, a theoretical model is developed by *Prof. Juan Ignacio Climente Plasencia (Universitat Jaume I, Spain)* to monitor the effect of a point charge on the QD surface on the ground state energy of excitonic species. See Figure 5.7 for the model of QD system under study. Here, there are three concentric circles with core in the middle surrounded by shell and this is followed by the outer matrix where the point charge is located 0.5 nm away from the QD surface. The electron and hole single-particle states are described with three-dimensional effective mass Hamiltonians:

$$H_j = \frac{\mathbf{p}_\perp^2}{2m_{j,\perp}} + \frac{\mathbf{p}_\parallel^2}{2m_{j,\parallel}} + V_{offset}^j + V_{strain}^j \pm \frac{e^2}{\epsilon(\mathbf{r})|r - r_{charge}|} \tag{5.1}$$

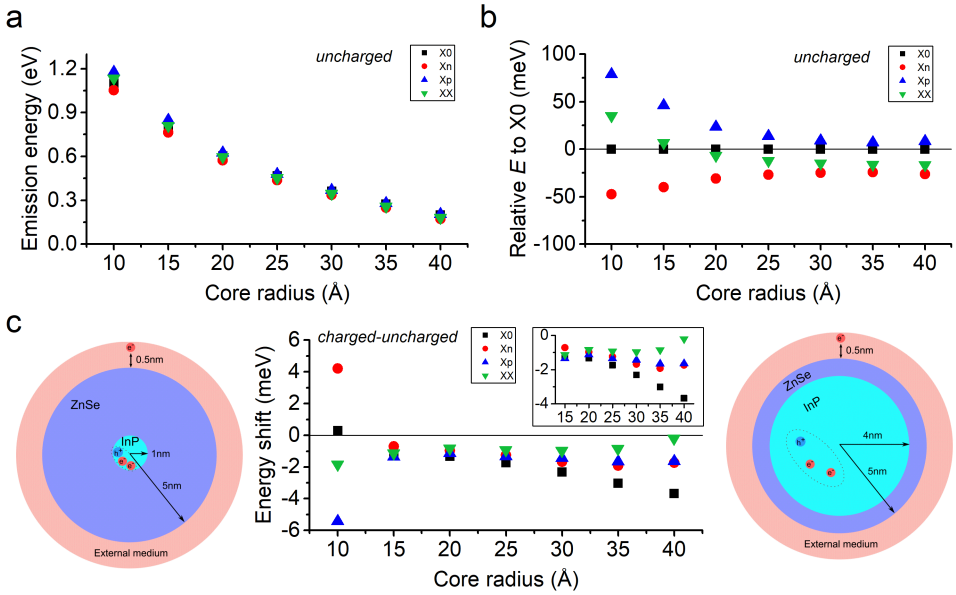

Figure 5.7. | CI calculations. (a) Emission peak energies of excitonic species for different core sizes of QDs with same shell radius of 5 nm. Notation: X0 is X, Xn is X^-, Xp is X^+ and XX is XX. (b) Relative emission peak energies of excitonic species XX, X^- & X^+ with X taken as reference. (c) Surface point charge induced shift of emission peaks of excitonic species for different core sizes by keeping the shell size constant at 5 nm. Examples of a point charge on surface of the QD for two extreme core sizes is shown.

where the subscript $j = e, h$ represent the electron and hole. The chosen band offset values are: V^e_{offset} in (eV): InP (0) and ZnSe (0.77), V^h_{offset} in (eV): InP (0) and ZnSe (-0.57) and the chosen lattice parameter in (Ang): InP (5.87) and ZnSe (5.67).[52] In InP/ZnSe QD studied, the large band offset indicates a type-I structure, but a compressive strain could unstabilize the core states which may induce a leakage into the shell. The presence of external charge gives a very deep but short-ranged potential inside the core with a potential along y (impurity) axis being ∼10 meV/nm for the dimension of our QD. The last term in the equation 5.1 is the Coulomb interaction term with e representing the electron charge and ϵ denoting the relative dielectric constant (10 for core, 6 for shell and 2 for outer matrix).

The Hamiltonian for excitonic species such as X, XX, X^-, X^+ can be calculated using a Configuration interaction method and a general Hamiltonian for such states including the interactions among electron & hole (e-h, e-e and h-h interactions) can be written as:

$$H = \sum_i H^i_e + \sum_j H^j_h + \sum_{ij} V^{ij}_{eh} + \sum_{i>i'} V^{ii'}_{ee} + \sum_{j>j'} V^{jj'}_{hh} \tag{5.2}$$

Using the single-particle terms from equation (5.1), Coulomb integrals in equation (5.2) are calculated through integration of Poisson equation accounting for dielectric mismatch.

The Hamiltonian is expanded in a basis formed by all possible combinations of the 8 lowest single-particle electron and 8 highest hole spin-orbitals. The eigenfunctions are then of the form:

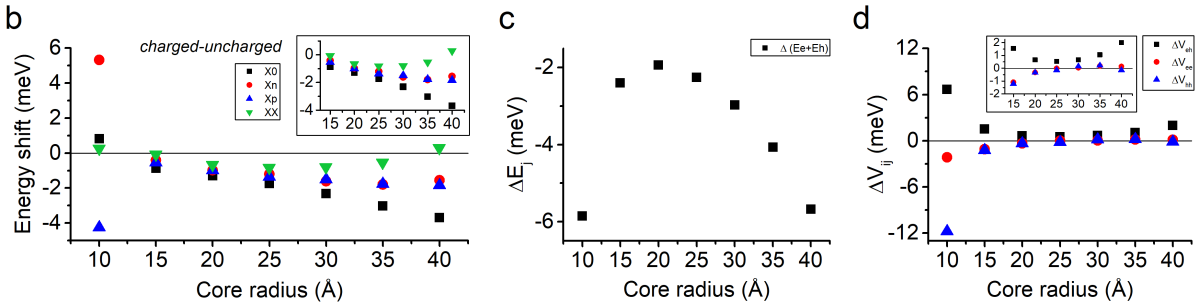

Figure 5.8. | Perturbational calculations. (a) Surface point charge induced shift of emission peaks of excitonic species for different core sizes with same shell radius of 5 nm. Notation: X0 is X, Xn is X^-, Xp is X^+ and XX is XX. (b,c) ΔE_j, ΔV_{ee}, ΔV_{hh} & ΔV_{eh} for different core sizes.

$$\begin{aligned}\Psi_X &= \sum_{ij} c_{ij}\ \phi_e^i\ \phi_h^j \\ \Psi_{X^-} &= \sum_{ijk} c_{ijk}\ \det(\phi_e^i\phi_e^j)\ \phi_h^k \\ \Psi_{XX} &= \sum_{ijkl} c_{ijkl}\ \det(\phi_e^i\phi_e^j)\ \det(\phi_h^k\phi_h^l)\end{aligned} \tag{5.3}$$

where ϕ denotes a single-particle spin-orbital and $\det(\phi^i\phi^j)$ represents the corresponding Slater determinant. Ψ_{X^+} is relative to Ψ_{X^-}.

Using configuration interaction (CI) method where the Basis set are taken from s and p shells of electrons and holes with 8 spin-orbitals per band, the emission energies of uncharged system is calculated which is shown in Figure 5.7a. The relative emission energies of multiple excitonic species from the neutral-exciton is shown in Figure 5.7b where one can deduce the expected binding energies of different excitonic species like XX, X^-, X^+ from X. It can be inferred that the binding energies of multiple excitons are reduced for larger core sized QDs due to weaker confinement where the electrons and holes have larger space to accommodate their wave functions (Coulomb interaction scaling as 1/r is smaller). Note that the X^- has a redshift while the X^+ has a blueshift with respect to X, which agrees our assignment of a redshifted singlet emission as X^- in Figure 5.1c. Figure 5.7c shows the examples of model where a point charge is present on the surface of the QD with two extreme core dimensions for the same shell size. As shown in Figure 5.7c, the electric field induced by a point charge redshifts all excitonic species, except in very small cores of Rc = 1 nm where Coulomb terms are very large (1/r is small) which competes with ΔE_e+ΔE_h. The redshift is more pronounced for X than for multiple excitons with XX being the lesser affected species. The binding energy of multiple excitons from X becomes larger for larger core sized QDs which indicates a more polarizable nature of wavefunctions.

5.4.2. First order perturbations

To infer the results obtained using CI mathematically, a 1st order perturbation on the basis of non-interacting electron and hole orbitals is used. The different response of X, XX, X^-, X^+ can be understood by simply comparing the effect of surface point charge on e-h, e-e and h-h interactions.

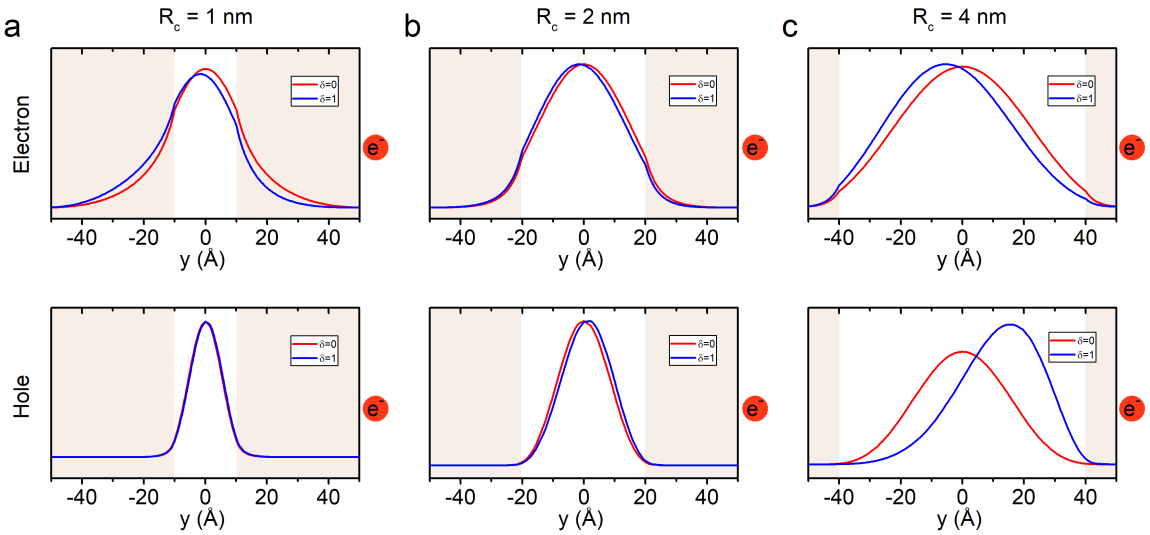

Figure 5.9. | Polarizability of wavefunctions. (a-c) Wavefunctions for smaller (Rc = 1 nm), medium (Rc = 2 nm) and larger (Rc = 4 nm) sizes of InP core having same shell size (Rs = 5 nm) in the absence (δ = 0) and presence (δ = 1) of a surface point charge. For smaller cores the electron tunnels into ZnSe and becomes more polarizable. For larger cores, electron and hole are both more polarizable.

Moreover, the polarizability of the wavefunctions by introducing a surface point charge could be inferred for different sizes of QDs using the perturbational analysis.

The emission energies of excitonic species are calculated as:

$$\begin{aligned} E_X^{PL} &= E_X - 0 = E_e + E_h + V_{eh} \\ E_{X^-}^{PL} &= E_{X^-} - E_e = E_e + E_h + 2V_{eh} + V_{ee} \\ E_{X^+}^{PL} &= E_{X^+} - E_h = E_e + E_h + 2V_{eh} + V_{hh} \\ E_{XX}^{PL} &= E_{XX} - E_X = E_e + E_h + 3V_{eh} + V_{ee} + V_{hh} \end{aligned} \tag{5.4}$$

where $E_e = \langle\Psi|H_e|\Psi\rangle$, $E_h = \langle\Psi|H_h|\Psi\rangle$, $V_{eh} = \langle\Psi|V_{eh}|\Psi\rangle$, $V_{ee} = \langle\Psi|V_{ee}|\Psi\rangle$, $V_{hh} = \langle\Psi|V_{hh}|\Psi\rangle$. Note that Ψ refers to the wave function of the excitonic species.

The stark shift $E_{charged} - E_{uncharged}$ for excitonic species are calculated as:

$$\begin{aligned} \Delta E_X &= \Delta(E_e + E_h) + \Delta V_{eh} \\ \Delta E_{X^-} &= \Delta(E_e + E_h) + 2\Delta V_{eh} + \Delta V_{ee} \\ \Delta E_{X^+} &= \Delta(E_e + E_h) + 2\Delta V_{eh} + \Delta V_{hh} \\ \Delta E_{XX} &= \Delta(E_e + E_h) + 3\Delta V_{eh} + \Delta V_{ee} + \Delta V_{hh} \end{aligned} \tag{5.5}$$

The change in binding energy upon charging (stark shift differences as compared to that of exciton) can be defined as $\Delta\Delta E_i^j = \Delta E_j - \Delta E_i$ such that:

$$\begin{aligned} \Delta\Delta E_X^{X^-} &= \Delta V_{eh} + \Delta V_{ee} \\ \Delta\Delta E_X^{X^+} &= \Delta V_{eh} + \Delta V_{hh} \\ \Delta\Delta E_X^{XX} &= 2\Delta V_{eh} + \Delta V_{ee} + \Delta V_{hh} \end{aligned} \tag{5.6}$$

Figure 5.8a shows the energy shift of X, XX, X^- & X^+ for different core sizes calculated by perturbational simulations. X has the strongest redshift because the surface point charge weakens e-h interaction more than e-e or h-h interactions. The heavier holes introduce stronger Coulomb correlations and thus there is a small deviations for XX & X^+, otherwise the perturbational data reasonably agrees well with the CI calculations. Figure 5.8b,c shows the ΔE_j, ΔV_{ee}, ΔV_{hh} & ΔV_{eh} for different core sizes. ΔV_{ee} & ΔV_{hh} get gradually stronger with core sizes because the charge succeeds in concentrating charge in a region (away/close) to the charge (for electron/hole). Changes in ΔV_{eh} are more conspicuous because the surface charge is more efficient in separating electron and hole than concentrating charges in a narrow region (due to competition with quantum confinement).

Figure 5.9a-c shows the polarizability of wavefunctions for smaller (Rc = 1 nm), medium (Rc = 2 nm) and larger (Rc = 4 nm) sizes of InP core having same shell size (Rs = 5 nm) in the absence (δ = 0) and presence (δ = 1) of a surface point charge. The wavefunctions are more polarized by surface point charge when core is too small (Rc = 1 nm) where electron leaks out in a strong confinement regime, or core is large (Rc = 4 nm) where both the electron and hole move in response to the point charge in a weak confinement regime. The medium sized core has only minor effect on the symmetry of wavefunctions remaining in a comparatively stronger confinement regime.

5.4.3. Field strength dependence

The redshift of exciton is larger for accumulated flux shown in Figure 5.2 which means the local field induced by the surface charge is more compared to earlier measurements when the local field would have been comparatively lower. To understand this phenomenon, we multiply the full point charge intensity by a certain Δ=0-1 for the core size of 1.5 nm with 5 nm shell. Note that the surface charge is likely to be less than full charge in QDs.[53] The corresponding energy shifts of the excitonic species are shown in Figure 5.10a,b calculated by CI and perturbational simulations respectively. This again exhibits a larger redshift for X than muliple excitons. A 3% configuration mixing makes a difference in the energy scale in the order of 1 meV with larger redshifts for XX & X^+. Since this result overestimates the shift of XX, it is speculated that the actual shell size of our QDs could be less than 5 nm. It should also be noted that the simulations are done by taking into account the heavy hole mass which could also alter the theoretical result. Figure 5.10c,d shows the perturbational calculations of ΔV_{ee}, ΔV_{hh} & ΔV_{eh} and $\Delta 1_e$ & $\Delta 1_h$ respectively. In this dissertation, the influence of one surface charge to the different exciton species is studied that agrees with the experimental result. Note that the result could be extrapolated for a presence of more number of charges by simply multiplying the factors. However, the mutual attraction/repulsion and the location of charges could complicate the situation and influence the results from the theoretical model. It is speculated that the relative effect of more number of charges on different exciton species could be similar to the case of one surface charge studied here, which evidently requires a more detailed study that is beyond the scope of this dissertation.

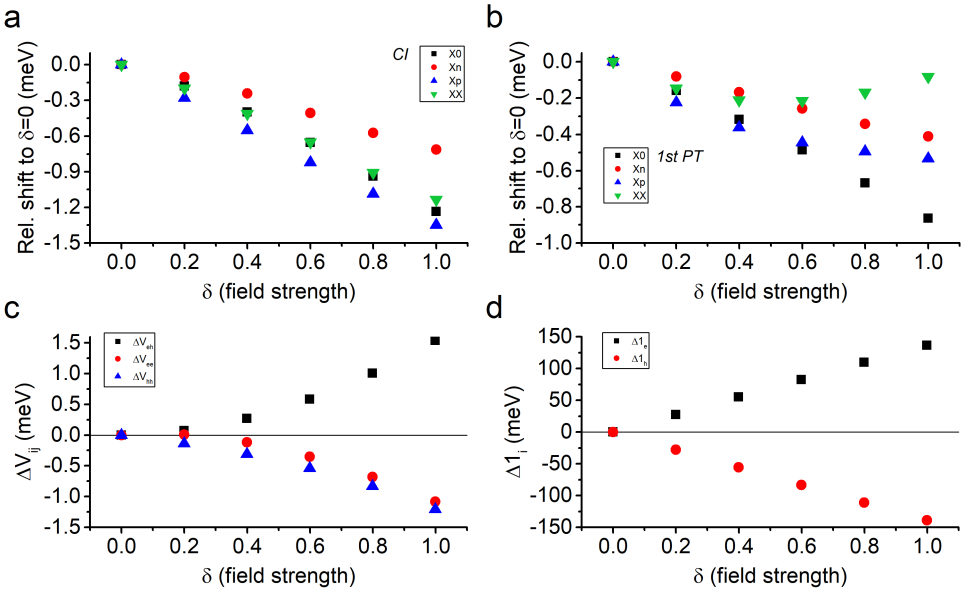

Figure 5.10. | Field strength dependence. (a,b) Field dependent energy shifts of excitonic species in a QD having a core radius of 1.5 nm and a shell radius of 5 nm, calculated from CI and perturbational simulations respectively. Notation: X0 is X, Xn is X^-, Xp is X^+ and XX is XX. (c,d) Perturbational calculations of ΔV_{ee}, ΔV_{hh} & ΔV_{eh} and $\Delta 1_e$ & $\Delta 1_h$ respectively. In all the plots, δ=0-1 represent the factor of surface point charge intensity.

5.4.4. Structural conditions for minimizing spectral diffusion

Generally, theoretically predicted values may not quantitatively agree with the experimental results for smaller dimensional systems like QDs due to several factors like band non-parabolicity, valence band mixing and possibly missing a part of Coulomb correlations. In our case here, the most important factor is the uncertainty about the precise nature of the surface charge (its position, nature - point-like or delocalized, strength, number). Nevertheless, it can be concluded from the obtained results that the external charge splits electron and hole weakening their mutual interaction (V_{eh}) which has a stronger effect than electron-electron (V_{ee}) or hole-hole (V_{hh}) interaction. This makes all exciton complexes redshift with external charge. X is usually the most redshifted complex, because the decrease of V_{eh} under the influence of a point surface charge is not balanced by V_{ee} or V_{hh} which tend to compensate. InP cores of 1.5 nm to 2.5 nm are in the strong confinement regime and the electrostatic shifts are minimal (∼1 meV). For smaller cores the electron tunnels into ZnSe and becomes more polarizable. For larger cores, electron and hole are both more polarizable with energy shifts more than 1 meV.

Blinking in colloidal QDs are believed to be suppressed by either having anti-blinking agents on surface or having ultra-thick shell.[54] While thick-shell could distance the point charge away from the central core, more shell means larger surface area and thus there is a possibility of larger number of trap states leading to more surface charges. In the limit of a homogeneous surface charge (instead of a point charge), the electrostatic potential is constant all over the dot which would not give much spectral shifts. However, a more number of point charges with an in-homogeneous charge distribution around the QD environment may cause a significant spectral shift, depending on whether the effect of field is compensated by some random charge localization. Also, the band offset of the QD and the core size has a major contribution as evident from our theoretical results. Recently, giant shell CdSe/CdS QDs were shown to be having more spectral diffusion than homogeneously alloyed CdSe QDs with a

spectral shift of 10 meV & 1 meV respectively at room temperature.[55] As opposed to CdSe/CdS QD, our InP/ZnSe QD has a larger band-offset and a thick shell here would certainly separate surface charges from volumetric (exciton) charges. This explains the observed SD in the order of around 1 meV for our QD which is smaller in size than giant-shell CdSe/CdS QDs. Room temperature spectral shifts in our QD vary from one to another with negligible to around 10 meV (see section 2.3.3). Our results on the polarizability of wavefunctions for different sizes of QD, band-offsets and excitonic species could be utilized to aim engineering the QD structure for required applications.

5.5. Conclusion

In conclusion, the polarizability of different band-edge excitonic species such as X, XX and X^- is addressed by the observation of their respective SD at cryogenic temperature using micro-PL spectroscopy on single InP/ZnSe QDs. A redshift in X emission is accompanied with more SD, broaden linewidth and increased phonon coupling, explained by the QCSE for accumulated flux. This redshift in X emission reduces the binding energy of both XX and X^-, attributed to the reduced wavefunction overlap due to QCSE. By correlating their level of SD, it is found that the QCSE reduces in trion-to-carrier and biexciton-to-exciton transitions compared to neutral-exciton. Further, by monitoring SD of QDs having linewidth as narrow as 50 μeV, we find the environmental influence in creating charge fluctuations. These results are supported by theoretically predicting the energy shifts of excitonic species in the presence of a point charge on the QD surface, using configuration interaction and perturbational simulations. Using InP/ZnSe QDs as an optimized system to minimize SD, a theoretical understanding of the structural conditions that determine the magnitude of QCSE in core-shell QDs is provided. This allows to show that minimal SD can be expected for strongly confined cores (large band-offset, moderately small core) and multi-excitonic species. Concomitantly, it is proposed that the polarizability could be used as a tool to distinguish the band-edge emissions, especially for smaller sized QDs. From these results, future synthetic protocols could aim engineering the QD structure for required applications such as quantum photonics.

Bibliography

[1] A. P. Alivisatos. Semiconductor clusters, nanocrystals, and quantum dots. *Science*, 271(5251):933–937, feb 1996.

[2] Mark J. Fernée, Philippe Tamarat, and Brahim Lounis. Spectroscopy of single nanocrystals. *Chemical Society Reviews*, 43(4):1311, 2014.

[3] Francesco Masia, Nicolò Accanto, Wolfgang Langbein, and Paola Borri. Spin-flip limited exciton dephasing in $\mathrm{CdSe/ZnS}$ colloidal quantum dots. *Physical Review Letters*, 108:087401, feb 2012.

[4] Mark J. Fernée, Philippe Tamarat, and Brahim Lounis. Cryogenic single-nanocrystal spectroscopy: Reading the spectral fingerprint of individual CdSe quantum dots. *The Journal of Physical Chemistry Letters*, 4(4):609–618, feb 2013.

[5] Al. L. Efros and M. Rosen. The electronic structure of semiconductor nanocrystals. *Annual Review of Materials Science*, 30(1):475–521, aug 2000.

[6] J. Y. Marzin, J. M. Gérard, A. Izraël, D. Barrier, and G. Bastard. Photoluminescence of single InAs quantum dots obtained by self-organized growth on GaAs. *Physical Review Letters*, 73(5):716–719, aug 1994.

[7] S. A. Empedocles, D. J. Norris, and M. G. Bawendi. Photoluminescence spectroscopy of single CdSe nanocrystallite quantum dots. *Physical Review Letters*, 77(18):3873–3876, oct 1996.

[8] D. Gammon, E. S. Snow, B. V. Shanabrook, D. S. Katzer, and D. Park. Fine structure splitting in the optical spectra of single GaAs quantum dots. *Physical Review Letters*, 76(16):3005–3008, apr 1996.

[9] W. Langbein, H. Kalt, and J. M. Hvam. Luminescence dynamics in type-II GaAs/AlAs superlattices near the type-i to type-II crossover. *Physical Review B*, 54(20):14589–14594, nov 1996.

[10] Sean A. Blanton, Margaret A. Hines, and Philippe Guyot-Sionnest. Photoluminescence wandering in single CdSe nanocrystals. *Applied Physics Letters*, 69(25):3905–3907, dec 1996.

[11] M. Nirmal, B. O. Dabbousi, M. G. Bawendi, J. J. Macklin, J. K. Trautman, T. D. Harris, and L. E. Brus. Fluorescence intermittency in single cadmium selenide nanocrystals. *Nature*, 383(6603):802–804, oct 1996.

[12] S. A. Empedocles. Quantum-confined stark effect in single CdSe nanocrystallite quantum dots. *Science*, 278(5346):2114–2117, dec 1997.

[13] J. Müller, J. M. Lupton, A. L. Rogach, J. Feldmann, D. V. Talapin, and H. Weller. Monitoring surface charge movement in single elongated semiconductor nanocrystals. *Physical Review Letters*, 93(16):167402, oct 2004.

[14] J. Müller, J. M. Lupton, A. L. Rogach, J. Feldmann, D. V. Talapin, and H. Weller. Monitoring surface charge migration in the spectral dynamics of single CdSe/CdS nanodot/nanorod heterostructures. *Physical Review B*, 72(20):205339, nov 2005.

[15] Eli Rothenberg, Miri Kazes, Ehud Shaviv, and Uri Banin. Electric field induced switching of the fluorescence of single semiconductor quantum rods. *Nano Letters*, 5(8):1581–1586, aug 2005.

[16] Daniel E. Gómez, Joel van Embden, and Paul Mulvaney. Spectral diffusion of single semiconductor nanocrystals: The influence of the dielectric environment. *Applied Physics Letters*, 88(15):154106, apr 2006.

[17] Daniel Braam, Andreas Mölleken, Günther M. Prinz, Christian Notthoff, Martin Geller, and Axel Lorke. Role of the ligand layer for photoluminescence spectral diffusion of CdSe/ZnS nanoparticles. *Physical Review B*, 88(12):125302, sep 2013.

[18] Margaret A. Hines and Philippe Guyot-Sionnest. Synthesis and characterization of strongly luminescing ZnS-capped CdSe nanocrystals. *The Journal of Physical Chemistry*, 100(2):468–471, jan 1996.

[19] Moonsub Shim and Philippe Guyot-Sionnest. Permanent dipole moment and charges in colloidal semiconductor quantum dots. *The Journal of Chemical Physics*, 111(15):6955–6964, oct 1999.

[20] S. A. Empedocles and M. G. Bawendi. Influence of spectral diffusion on the line shapes of single CdSe nanocrystallite quantum dots. *The Journal of Physical Chemistry B*, 103(11):1826–1830, mar 1999.

[21] Mark J. Fernée, Brad N. Littleton, Steven Cooper, Halina Rubinsztein-Dunlop, Daniel E. Gómez, and Paul Mulvaney. Acoustic phonon contributions to the emission spectrum of single CdSe nanocrystals. *The Journal of Physical Chemistry C*, 112(6):1878–1884, feb 2008.

[22] Mark J. Fernée, Brad Littleton, Taras Plakhotnik, Halina Rubinsztein-Dunlop, Daniel E. Gómez, and Paul Mulvaney. Charge hopping revealed by jitter correlations in the photoluminescence spectra of single CdSe nanocrystals. *Physical Review B*, 81(15):155307, apr 2010.

[23] Mark J. Fernée, Taras Plakhotnik, Yann Louyer, Bradley N. Littleton, Christian Potzner, Philippe Tamarat, Paul Mulvaney, and Brahim Lounis. Spontaneous spectral diffusion in CdSe quantum dots. *The Journal of Physical Chemistry Letters*, 3(12):1716–1720, jun 2012.

[24] Toshiyuki Ihara and Yoshihiko Kanemitsu. Spectral diffusion of neutral and charged exciton transitions in single CdSe/ZnS nanocrystals due to quantum-confined stark effect. *Physical Review B*, 90(19):195302, nov 2014.

[25] Hiroto Ibuki, Toshiyuki Ihara, and Yoshihiko Kanemitsu. Spectral diffusion of emissions of excitons and trions in single CdSe/ZnS nanocrystals: Charge fluctuations in and around nanocrystals. *The Journal of Physical Chemistry C*, 120(41):23772–23779, oct 2016.

[26] Annalisa Brodu, Vigneshwaran Chandrasekaran, Lorenzo Scarpelli, Jonathan Buhot, Francesco Masia, Mariana V. Ballottin, Marion Severijnen, Mickaël D. Tessier, Dorian Dupont, Freddy T. Rabouw, Peter C. M. Christianen, Celso de Mello Donega, Daniël Vanmaekelbergh, Wolfgang Langbein, and Zeger Hens. Fine structure of nearly isotropic bright excitons in InP/ZnSe colloidal quantum dots. *The Journal of Physical Chemistry Letters*, ASAP:5468–5475, sep 2019.

[27] M. Bayer, G. Ortner, O. Stern, A. Kuther, A. A. Gorbunov, A. Forchel, P. Hawrylak, S. Fafard, K. Hinzer, T. L. Reinecke, S. N. Walck, J. P. Reithmaier, F. Klopf, and F. Schäfer. Fine structure of neutral and charged excitons in self-assembled in(ga)as/(al)GaAs quantum dots. *Physical Review B*, 65(19):195315, may 2002.

[28] V. D. Kulakovskii, G. Bacher, R. Weigand, T. Kümmell, A. Forchel, E. Borovitskaya, K. Leonardi, and D. Hommel. Fine structure of biexciton emission in symmetric and asymmetric CdSe/ZnSe single quantum dots. *Physical Review Letters*, 82(8):1780–1783, feb 1999.

[29] A. J. Shields, F. M. Bolton, M. Y. Simmons, M. Pepper, and D. A. Ritchie. Electric-field-induced ionization of negatively charged excitons in quantum wells. *Physical Review B*, 55:R1970–R1972, jan 1997.

[30] L. Besombes, K. Kheng, L. Marsal, and H. Mariette. Few-particle effects in single cdte quantum dots. *Physical Review B*, 65:121314, mar 2002.

[31] H. D. Robinson and B. B. Goldberg. Light-induced spectral diffusion in single self-assembled quantum dots. *Physical Review B*, 61:R5086–R5089, feb 2000.

[32] V. Türck, S. Rodt, O. Stier, R. Heitz, R. Engelhardt, U. W. Pohl, D. Bimberg, and R. Steingrüber. Effect of random field fluctuations on excitonic transitions of individual cdse quantum dots. *Physical Review B*, 61:9944–9947, apr 2000.

[33] M. Furis, H. Htoon, M. A. Petruska, V. I. Klimov, T. Barrick, and S. A. Crooker. Bright-exciton fine structure and anisotropic exchange in CdSe nanocrystal quantum dots. *Physical Review B*, 73:241313, jun 2006.

[34] H. Htoon, M. Furis, S. A. Crooker, S. Jeong, and V. I. Klimov. Linearly polarized 'fine structure' of the bright exciton state in individual CdSe nanocrystal quantum dots. *Physical Review B*, 77:035328, jan 2008.

[35] Sandra Ritter, Paul Gartner, Norman Baer, and Frank Jahnke. Anomalous stark effect in semiconductor quantum dots. *Physical Review B*, 76:165302, oct 2007.

[36] Thomas Garm Pedersen. Stark effect in spherical quantum dots. *Physical Review A*, 99:063410, jun 2019.

[37] P. W. Fry, I. E. Itskevich, D. J. Mowbray, M. S. Skolnick, J. J. Finley, J. A. Barker, E. P. O'Reilly, L. R. Wilson, I. A. Larkin, P. A. Maksym, M. Hopkinson, M. Al-Khafaji, J. P. R. David, A. G. Cullis, G. Hill, and J. C. Clark. Inverted electron-hole alignment in inas-gaas self-assembled quantum dots. *Physical Review Letters*, 84:733–736, jan 2000.

[38] J. Seufert, M. Obert, M. Scheibner, N. A. Gippius, G. Bacher, A. Forchel, T. Passow, K. Leonardi, and D. Hommel. Stark effect and polarizability in a single CdSe/ZnSe quantum dot. *Applied Physics Letters*, 79(7):1033–1035, aug 2001.

[39] J. J. Finley, M. Sabathil, P. Vogl, G. Abstreiter, R. Oulton, A. I. Tartakovskii, D. J. Mowbray, M. S. Skolnick, S. L. Liew, A. G. Cullis, and M. Hopkinson. Quantum-confined stark shifts of charged exciton complexes in quantum dots. *Physical Review B*, 70:201308, nov 2004.

[40] Anthony J. Bennett, Raj B. Patel, Joanna Skiba-Szymanska, Christine A. Nicoll, Ian Farrer, David A. Ritchie, and Andrew J. Shields. Giant stark effect in the emission of single semiconductor quantum dots. *Applied Physics Letters*, 97(3):031104, jul 2010.

[41] Ł. Kłopotowski, V. Voliotis, A. Kudelski, A. I. Tartakovskii, P. Wojnar, K. Fronc, R. Grousson, O. Krebs, M. S. Skolnick, G. Karczewski, and T. Wojtowicz. Stark spectroscopy and radiative lifetimes in single self-assembled cdte quantum dots. *Physical Review B*, 83:155319, apr 2011.

[42] Ł. Kłopotowski, K. Fronc, P. Wojnar, M. Wiater, T. Wojtowicz, and G. Karczewski. Stark spectroscopy of CdTe and CdMnTe quantum dots embedded in n-i-p diodes. *Journal of Applied Physics*, 115(20):203512, may 2014.

[43] J. D. Mar, J. J. Baumberg, X. L. Xu, A. C. Irvine, and D. A. Williams. Precise measurements of the dipole moment and polarizability of the neutral exciton and positive trion in a single quantum dot. *Physical Review B*, 95:201304, may 2017.

[44] W. Heller, U. Bockelmann, and G. Abstreiter. Electric-field effects on excitons in quantum dots. *Physical Review B*, 57:6270–6273, mar 1998.

[45] T. M. Hsu, W.-H. Chang, C. C. Huang, N. T. Yeh, and J.-I. Chyi. Quantum-confined stark shift in electroreflectance of InAs/InxGa1-xAs self-assembled quantum dots. *Applied Physics Letters*, 78(12):1760–1762, mar 2001.

[46] Mitsuru Sugisaki, Hong-Wen Ren, Selvakumar V. Nair, Kenichi Nishi, and Yasuaki Masumoto. External-field effects on the optical spectra of self-assembled inp quantum dots. *Physical Review B*, 66:235309, dec 2002.

[47] S. M. Ulrich, R. Hafenbrak, M. M. Vogel, L. Wang, A. Rastelli, O. G. Schmidt, and P. Michler. Control of single quantum dot emission characteristics and fine structure by lateral electric fields. *physica status solidi (b)*, 246(2):302–306, feb 2009.

[48] Feng Wang, Jie Shan, Mohammad A. Islam, Irving P. Herman, Mischa Bonn, and Tony F. Heinz. Exciton polarizability in semiconductor nanocrystals. *Nature Materials*, 5(11):861–864, oct 2006.

[49] Lei Zhang, Bihu Lv, Hongyu Yang, Ruilin Xu, Xiaoyong Wang, Min Xiao, Yiping Cui, and Jiayu Zhang. Quantum-confined stark effect in the ensemble of phase-pure CdSe/CdS quantum dots. *Nanoscale*, 11(26):12619–12625, 2019.

[50] Shudong Wu and Weiwei Xia. Exciton polarizability and absorption spectra in CdSe/ZnS nanocrystal quantum dots in electric fields. *Journal of Applied Physics*, 114(4):043709, jul 2013.

[51] Worasak Sukkabot. Atomistic tight-binding computations of the electronic properties of ZnSe/ZnS core/shell nanocrystals under applied electric field. *Materials Science in Semiconductor Processing*, 41:252–256, jan 2016.

[52] Reyhaneh Toufanian, Andrei Piryatinski, Andrew H. Mahler, Radhika Iyer, Jennifer A. Hollingsworth, and Allison M. Dennis. Bandgap engineering of indium phosphide-based core/shell heterostructures through shell composition and thickness. *Frontiers in Chemistry*, 6, nov 2018.

[53] Marco Califano, Alberto Franceschetti, and Alex Zunger. Temperature dependence of excitonic radiative decay in CdSe quantum dots: the role of surface hole traps. *Nano Letters*, 5(12):2360–2364, dec 2005.

[54] Ou Chen, Jing Zhao, Vikash P. Chauhan, Jian Cui, Cliff Wong, Daniel K. Harris, He Wei, Hee-Sun Han, Dai Fukumura, Rakesh K. Jain, and Moungi G. Bawendi. Compact high-quality CdSe–CdS core–shell nanocrystals with narrow emission linewidths and suppressed blinking. *Nature Materials*, 12(5):445–451, feb 2013.

[55] Young-Shin Park, Jaehoon Lim, and Victor I. Klimov. Asymmetrically strained quantum dots with non-fluctuating single-dot emission spectra and subthermal room-temperature linewidths. *Nature Materials*, 18(3):249–255, jan 2019.

Chapter 6.

Single quantum dots on chip - an initial exploration

Contents

Synopsis

Though clearly promising, isolated QDs as single photon sources are only usable when they can be deterministically positioned on a silicon chip, both for scalability and to couple the QDs to nanophotonic devices. The latter will be required to further boost the brightness and directionality of single photon emission. In this chapter, deterministic positioning of single InP/ZnSe QDs using electron-beam lithography is attempted with a result of 'probabilistic' 30% accuracy. Further, single QDs are embedded in a silicon nitride host matrix that not only protects the QDs from environment but also acts as a waveguide. While the collection efficiency currently limits the demonstration of single photon emission with high purity, there are greater prospects to further improve the design which are also discussed in this chapter.

6.1. Introduction

6.1.1. Need for integration

The ultimate aim of a functional quantum photonic chip is to have a material that acts as a good single photon emitter, a material that modulates & guides the emitted single photon and a material that detects the single photon, with all of them integrated in the same chip.[1] Such a photonic integrated circuit (PIC) requires both active & passive components to perform complex optical functionality on a chip at low cost. While colloidal QDs have been demonstrated to be a good single photon emitter under both optical[2] and electrical[3] excitation, isolated QDs by means of either dropcasting or spincoating a diluted solution on a substrate of choice is a random process.

First, single QDs needs to be placed in a pre-determined position on a silicon chip which requires a successful transformation of the chemically synthesized QDs from a solution phase. The level of accuracy of placing single QDs in a precise location needs to be determined. Then, a pure single photon emission from a such a single QD needs to be demonstrated. Even before the on-chip detection of single photon, an intermediary step could be employed by using a confocal microscope to check whether the optical properties of single QD on a silicon chip are as same as for an isolated QD on a glass substrate. However, this requires an efficient method of guiding the emitted fluorescence from the single photon source to the objective microscope. A better out-coupling of the mode of the emitted light could be achieved by using a combination of waveguide (for guiding the emitted light with minimal loss), cavity (for enhancing the spontaneous emission), & antenna (for better directionality of the emission). To give a basic understanding of the need for having a cavity or antenna structure, see Figure 6.1 for the

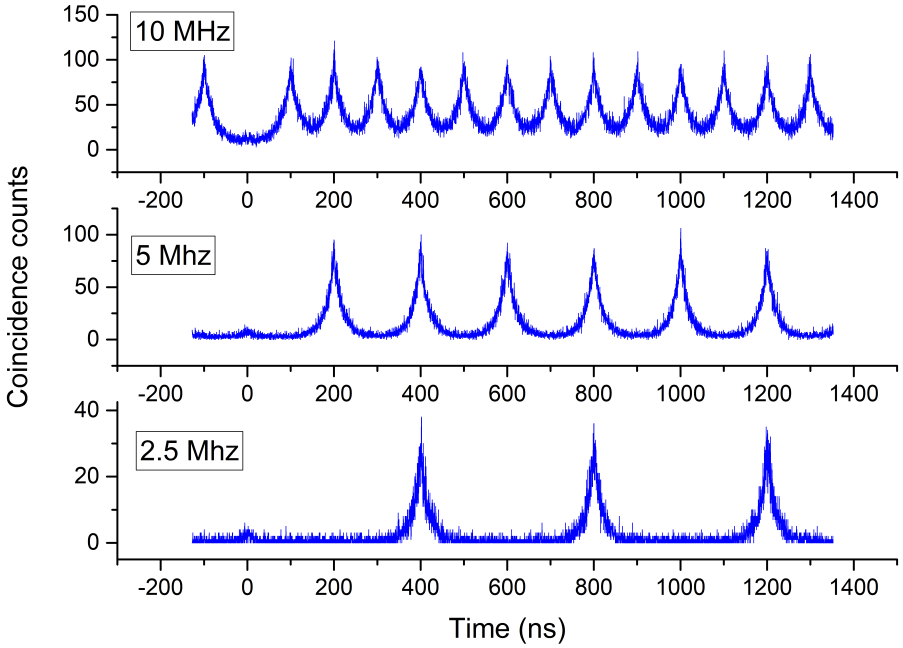

Figure 6.1. | Single photon emission rate. Single photon emission from a single InP/ZnSe QD (dropcasted on a glass coverslip) under pulsed excitation with repetition rates of 2.5 MhZ, 5 Mhz and 10 Mhz. Colloidal QDs have a typical lifetime in ns range, which means that the maximum repetition rate of pulsed excitation that can be used is around 10 MhZ. So an integration of QDs to a cavity structure to enhance the spontaneous emission rate is critical for higher rate operation.

single photon emission from a dropcasted single InP/ZnSe QD under pulsed excitation with repetition rates of 2.5 MhZ, 5 Mhz and 10 Mhz. As discussed in section 2.3, the typicial lifetime of InP/ZnSe QDs at room temperature is ∼22.5 ns and hence a mechanism to enhance the spontaneous emission rate is critical for higher rate operation.

As a pre-requisite for achieving a practical single photon source, this chapter discusses the initial investigations of placing the single InP/ZnSe QDs in a pre-determined position in combination with silicon nitride (Si_3N_4) photonics for low loss waveguide. Regarding the cavity and antenna structures, references to the similar in-house work on ensemble of QDs using silicon nitride photonics are provided. For instance, plasmonic antennas on top of Si_3N_4 waveguides were shown to be exhibiting Purcell enhancement with an increase of the count rate (spontaneous emission), speeding up the microsecond radiative lifetime of ensemble of infrared-emitting colloidal PbS/CdS QDs.[4] Also, a Purcell enhancement up to a factor of 7 was reported for the SiN_x/Au nanopatch cavity containing the ensemble of CdSe/CdS QDs.[5] Information on integrating colloidal QDs with cavity structures can be found in the other references,[6–9] for more details.

6.1.2. Integration technology

Silicon photonics is the technology platform in which PICs are fabricated using the technology and processes available in a standard complementary metal oxide semiconductor (CMOS) fab. Here, the optical components are designed & constructed on silicon-on-insulator (SOI) wafers. These wafers contain a crystalline silicon layer on top of a silicon oxide buffer layer. Silicon photonics are mainly utilized in telecommunication applications integrating high speed transmitters and receivers where there is also a possibility of implementing several passive optical components like wavelength division multiplexers, resonators, filters, splitters, coupling to optical fibers, etc.[10]

Alternative platform is silicon nitride Si_3N_4 which has an optical index of ∼2.0 that provides a lower index contrast compared with the SOI platform (∼3.5). Since the waveguide propagation loss is proportional the square of the refractive index $\Delta n^2 = n^2_{\text{core}} - n^2_{\text{cladding}}$,[11] Si_3N_4 waveguide has a lower propogation loss with a reported value of 0.003 dB/cm.[12] Contrary to silicon, Si_3N_4 has a weaker Kerr nonlinearity with nearly-zero TPA and thereby the extra waveguide loss at high power is comparatively reduced. Additionally, Si_3N_4 exhibits transparency from the visible to the mid-infrared wavelength making it suitable for various photonic applications including integrated photonic circuits, nonlinear optics, high quality optical cavities, and on-chip biosensing. Note that Si_3N_4 platform is also compatible with CMOS technology. Si_3N_4 can be deposited with plasma enhanced chemical vapour deposition (PECVD) at low temperature (270 °C) or low pressure chemical vapour deposition (LPCVD) at high temperature (700 °C). This provides a flexibility in choosing the substrates. For instance, LPCVD provides a homogeneous layer of Si_3N_4 that are commonly used in telecom wavelength of around 1550 nm since the high temperature operation also removes the hydrogen content. On the other hand, PECVD provides flexibility with a different composition of Si_3N_4 layer with required refractive indexes.[10]

Colloidal QDs being an efficient light emitting material (both lasing & single photon emission) in the visible wavelength range can act as an integrated light source utilizing the Si_3N_4 platform as a waveguide. It was recently reported that Si_3N_4 platform is favorable for colloidal QDs by demonstrating successful integration onto silicon chip.[13] Further, low-loss waveguiding was demonstrated in a monolayer of CdSe/CdS colloidal QDs in a Si_3N_4 waveguide.[14] CdSe/CdS core/shell QDs, embedded as a sandwiched layer between Si_3N_4 layers, did not lose photostability by checking their fluorescence

before and after depositing the Si_3N_4 layer using PECVD. Furthermore, several optical functionalities were demonstrated in CdSe/CdS QDs using Si_3N_4 photonics, such as a microdisk laser,[15] distributed feedback laser (DFB) laser[16] and microcavity on ensemble of QDs.[5] Using electron-beam lithography, both the SiN_x/Au nanopatch cavity and the ensemble of CdSe/CdS QDs within the cavity with an accuracy of 10 nm was demonstrated.[5]

6.2. On-chip emission

6.2.1. Placing single quantum dots on a pre-determined position

Several methods have been proposed and demonstrated for patterning NCs into defined arrays such as: electron-beam lithography,[9, 17–21] photolithography,[22] plasma lithography,[23] scanning probe lithography & chemical functionalization,[6, 24] dip-pen nanolithography,[25] photoresist contact patterning,[26] DNA-mediated assembly,[27–29] electrostatic self-assembly,[30–32] template-assisted self-assembly,[33, 34] and laser direct writing.[35] Among them, electron-beam lithography provides an excellent control over the pattern structure down to the single QD level.

Knowing that InP/ZnSe are suitable single-photon emitters, an established electron beam lithographical patterning technique[17] was used to place the single InP/ZnSe QDs on a pre-determined position on a silicon chip. It consists of three major steps: (i) the deposition area where the QDs needed to be placed is patterned on a resist using electron-beam lithography, (ii) the formation of a uniform QD-monolayer using Langmuir-Blodgett (LB) deposition on top of resist, and (iii) a lift-off process to remove the QDs in non-patterned area.

The first step is the spincoating of the resist (ZEP 520A positive resist) on top of the silicon substrate. This is followed by baking for 4 minutes ramped from 100 °C to 150 °C and 2 min at 200 °C to obtain a thickness of 30 nm. A 50 kV electron beam lithography (Raith Voyager) is used to define the hole pattern for placing single QDs. Electron beam is focused on the resist film to create the spot for single QDs and this is achieved by exposing dot by dot in a pattern. Dot exposure is varied by linearly multiplying the amount of exposure dose factor to increase the diameter of the spot size. There is no one universal value of this dose factor for single QD pattern as this depends on the thickness of the resist and the size of the QD as well. For this study, a multiplying factor of 1 to 5 was used for a 0.25 fC/dot with dose area of 100 $\mu C/cm^2$. Finally, a 0.5 fC/dot was chosen to be good for single InP/ZnSe QD deposition. Afterwards, the patterned resist was developed for 30s in n-amyl acetate, 30s stopper in isopropyl alcohol (IPA), and 5-10s O2 Reactive-ion etching (RIE) plasma. Note that the diameter of the QD studied is around 10 nm.

The second step is the deposition of a monolayer of QDs on top of the pattern. This is achieved using a widely known LB (Nima 312D) technique where a suitable dilution of QDs is dropcasted on the trough containing DI-water.[36] The hydrophobic QDs with their organic ligands float on the water which is then compressed until a certain pressure is reached (20 mN/m for this QD), that is optimum for the QDs to form a monolayer. Once this pressure is reached, the substrate is slowly lifted upwards so that a monolayer of QDs is deposited on them. See Figure 6.2a for a perfect monolayer of QDs imaged using a high resolution scanning electron microscope SEM (FEI Nova 600). Figure 6.2b-d shows some examples of voids in the monolayer of QDs. To minimize cluster formation, QDs can be purified before LB deposition. This is done by adding ethanol/methanol/acetone to QD solution to remove the ligands, followed by a centrifuge that precipitates the QDs. This can be mixed with a solvent of choice like

toluene/hexane to the needed concentration. An optimization and repetition of the steps mentioned above is necessary until a proper monolayer can be formed.

The third step is the lift-off process which removes the layer of QDs and the resist leaving behind the QDs in the pattern designed. This is achieved by ultrasonication of the substrate on a mix of toluene and acetone in the ratio of 1:4. The thickness of the resist is an important parameter as it can influence the outcome. For instance, thicker resist results in a good lift-off process without re-deposition of QDs in non-defined area. However, a QD layer around the pattern having sharp edges might bend and

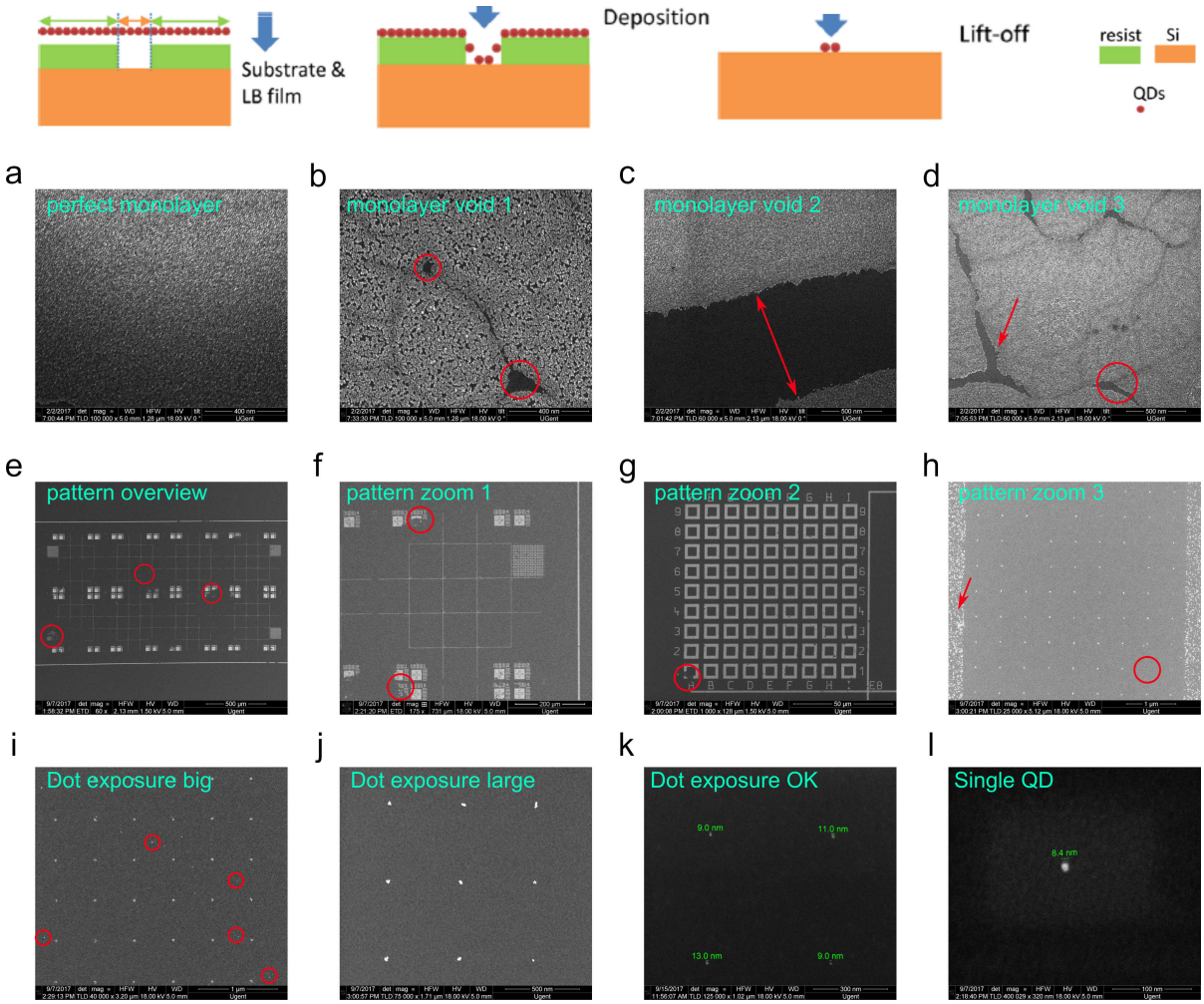

Figure 6.2. | Positioning of single QDs on silicon chip. Top: According to the method proposed by Xie *et al.*,[17] an electron-beam lithography is used to draw a pattern on the positive resist. This is followed by depositing a monolayer of QDs using Langmuir-Blodgett technique on the patterned substrate. Then a lift-off process is carried out to remove the resist leaving the QDs inside the pattern. SEM images: (a) A perfect monolayer (b-d) Some voids in monolayer indicated in red. (e-h) Pattern after the lift-off process with QDs in the pre-determined positions. Red highlights the void due to non-perfect monolayer and lift-process. (i-k) Dot exposure can be varied to create different sized holes in the photo-resist during electron-beam lithography and accordingly a group of QDs to single QDs can be deposited. Red highlights the re-deposition of QDs in the area not defined in the patter due to non-perfect lift-off process leaving QDs residue. (l) A perfect monolayer and lift-off process would result in a deterministic placement of single QD. Finally, a dot exposure of 0.5 fC/dot with a dose area of 100 μC/cm^2 was chosen for single QD deposition.

break up for a thicker resist. Hence there is a trade-off between reducing the thickness of the resist and establishing a good lift-off process.[17]

See Figure 6.2e-h for the QD patterns from an overview to zoom-in of regions where single or cluster of QDs can be clearly seen. Red color arrows and circle indicates voids in the monolayer where the regions are defined in the pattern. A multiplying dot exposure is used as indicated before (see Figure 6.2i-j) and accordingly a pattern of different sizes was formed which 'captures' the QDs in those pre-defined positions. Red color circles indicate redeposition of QDs residue in the non-defined area.

Examples for a good combination of LB monolayer film and the lift-process are shown in Figure 6.2k-l where single QDs are seen in the pre-determined area. In this case, the chosen dot exposure was the above mentioned 0.5 fC/dot with a dose area of 100 μC/cm^2. However, the overall accuracy of placing the single QDs by imaging using SEM in the entire patterned area only amounts to 30%. While a deterministic deposition of single QDs is attempted using electron-beam lithography, only a 'probabilistic' 30% positioning accuracy of single QDs was achieved. This lower value is attributed to the combination of both monolayer voids and the residue of QDs after lift-off process. In addition, the differences in the sizes of single QDs from one another further cause either void (too big) or multiple QDs (too small) in the pre-defined positions. A proper study on the surface chemistry of the QD under study is also necessary to find the role of ligands during the LB deposition.

6.2.2. Single quantum dots embedded in Si_3N_4 waveguide

After attempting a deterministic deposition of single QD onto a silicon chip, the key objective is to demonstrate on-chip single photon emission. QDs on silicon substrate is useful for SEM imaging, however, the collection efficiency of emission from such a design is poor owing to the ~3.4 refractive index of silicon. Hence the QDs were embedded in a silicon nitride Si_3N_4 host matrix, which not only protects them from the oxidative environment but also acts as a waveguide.

First, the emission characteristics of ensemble of InP/ZnSe QDs in such an embedded structure was studied before integrating single QDs. Si_3N_4 was deposited using plasma-enhanced chemical vapor

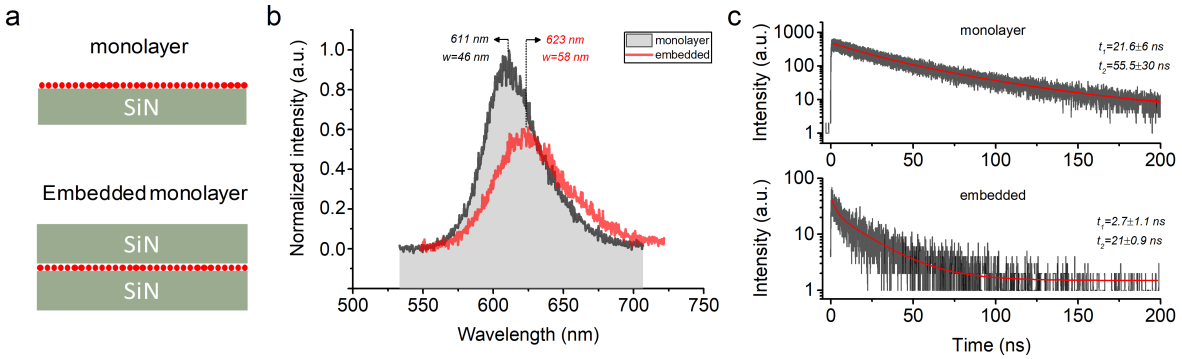

Figure 6.3. | Monolayer of QDs embedded in Si_3N_4 waveguide. (a) Collection of emission from a monolayer of QDs with and without top Si_3N_4 . (b) Spectrum showing a redshift and broadening for the embedded layer attributed to the background fluorescence from Si_3N_4 . Emission intensity reduces to 60% after the top Si_3N_4 layer deposition using PE-CVD at room temperature. (c) PL decay trace shows a bi-exponential fit with t_1 = 21.6 ns & t_2 = 55.5 ns for QDs without top Si_3N_4 layer and t_1 = 2.7 ns & t_2 = 21 ns for embedded QD layer with a relative amplitude weight of 48% & 52% respectively.

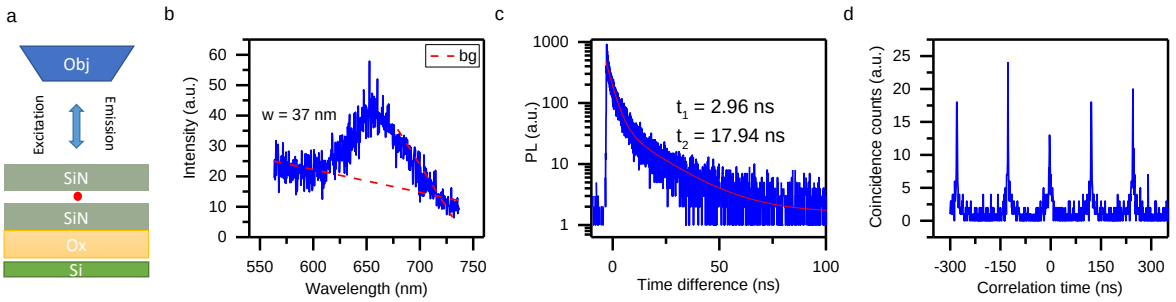

Figure 6.4. | Single QD embedded in Si_3N_4 waveguide. (a) Collection of emission from a single QD embedded in Si_3N_4 waveguide (b) Spectrum of a single QD has the background emission from the substrate when collecting using objective on top. (c) PL decay trace shows a bi-exponential fit with t_1 = 2.96 ns and t_2 = 17.94 ns. (d) Second order correlation function has a non-zero peak at t=0 which is attributed to the background fluorescence from Si_3N_4 layer.

deposition (PECVD). PECVD forms a uniform Si_3N_4 layer at 270 °C (HT), but it can be tuned to deposit a layer at room temperature (RT) as well with a minor deviation in the homogeneity. The base Si_3N_4 was deposited at HT to form a homogeneous layer on a buried oxide substrate. This was followed by a deposition of monolayer of QDs using LB technique. Finally, the top Si_3N_4 layer was deposited at RT so that the damage is minimized on the QDs underneath during the processing. By measuring the relative emission intensity of a monolayer of QDs with and without top Si_3N_4 , it was found that around 60% QDs withstand the top Si_3N_4 deposition as shown in Figure 6.3b. Further, the spectrum of the embedded QDs (peak at 623 nm with a linewidth of 58 nm) showed a redshift and broadening of about 12 nm each compared to just a monolayer of QDs on top of Si_3N_4 (peak at 611 nm with a linewidth of 46 nm). This is attributed to the background fluorescence from the Si_3N_4 layer. Figure 6.3c shows the PL decay trace of monolayer of QDs with and without top Si_3N_4 fitted to a double exponential function. The fit yielded t_1 = 21.6 ns and t_2 = 55.5 ns for the monolayer of QDs without top Si_3N_4 , whereas it was t_1 = 2.7 ns and t_2 = 21 ns for the embedded QDs with a relative amplitude weight of 48% & 52% respectively. As explained in Chapter 2, the average lifetime at room temperature for single InP/ZnSe QDs is around ∼22.5 ns. Thus the extracted value of ∼21 ns for the monolayer of QDs with/without top Si_3N_4 corresponds to the average lifetime of QDs. An energy transfer can happen on the monolayer of QDs in a closely packed state which could explain the 55.5 ns obtained for QDs without top Si_3N_4 . The absence of this value in the embedded QDs indicate that the closely packed form is no longer present possibly due to the damage of layer after PECVD deposition of top Si_3N_4 layer. The 2.7 ns in the embedded layer could be the background fluorescence from Si_3N_4 . Note that the thicknesses of the top & bottom Si_3N_4 layers are 100 nm each.

Next the single QDs were embedded in a Si_3N_4 waveguide following the similar method as above. The base Si_3N_4 was deposited at HT which was followed by the electron beam lithography method described in section 6.2.1 for placing the single QDs on pre-determined positions. Finally, the top Si_3N_4 was deposited at RT. Importantly, different grades of Si_3N_4 was investigated on monolayer of QDs to find the host that gives the lowest background fluorescence so that emission from single QDs can be easily distinguished. As such, a low frequency Si_3N_4 was chosen to be the top Si_3N_4 layer. But, even the best grade Si_3N_4 tested on a monolayer of QDs still had the background fluorescence when collecting the emission from a single QD. The emission was collected from top using an objective microscope (see Figure 6.4a) having a diffraction limited resolution spot size of 300 nm. This excitation spot size is much larger than the spatial region of single QD and hence the collected fluorescence could

have a mix of both the exciton emission and the background fluorescence from Si_3N_4 layer. Figure 6.4b shows a single QD spectrum that has a well pronounced background emission. The linewidth of 37 nm (peak at 660 nm) is still narrower than the ensemble linewidth of 58 nm for the embedded QDs (peak at 623 nm) shown in Figure 6.3b. While there is a possibility that there could be more than one QD in this region, subtracting the 12 nm Si_3N_4 background fluorescence calculated from the analysis of embedded QDs discussed above yields a linewidth of 25 nm at a peak emission wavelength of 648 nm for this QD. Since this value agrees with the linewidth of single QDs discussed in section 2.3, we attribute that the emission in this region is stemming from a single QD. Moreover, Figure 6.4c shows the PL decay trace of this QD with a bi-exponential fit yielding time constants of t_1 = 2.96 ns and t_2 = 17.94 ns, which agrees well with the value shown in Figure 6.3c for an embedded monolayer of QDs that had the contribution from both the background fluorescence and the QDs. Again, the PL lifetime of 17.94 ns for this QD is comparable to the 22.5 ns average PL lifetime of single QDs discussed in section 2.3. While the magnitudes of spectral linewidth and PL decay lifetime collected for this QD suggests an emission from a single QD, only a pure single photon emission could confirm this attribution. To check for the single photon emission from this QD, the fluorescence collected via objective microscope was directed to a Hanbury Brown Twiss setup to calculate the second order correlation function. Figure 6.4d shows the second order correlation function for this single QD with a non-zero peak at time t=0, which is attributed to the background emission from the Si_3N_4 layer. A contribution of background is also evident from an uneven second order correlation peaks under pulsed excitation as visible in Figure 6.4d.

6.2.3. Design improvements

By studying QDs closer to the dielectric interface, it was reported that the collection efficiency of photons emitted by a single QD depends strongly on the optical environment and the numerical aperture of the objective used to collect the light emission.[37] Further, finite-difference time-domain (FDTD) simulations predicted that a suspended Si_3N_4 waveguide structure provides a better light confinement of the guided modes and improves the coupling to the emitter.[38] Therefore, it is proposed to integrate single InP/ZnSe QDs in such a suspended waveguide structure rather than a stacked structure decribed before. The light out-coupling also needs to be improved. Currently the emitted photons are collected vertically by using a microscope with high numerical aperture. However, a grating coupler can improve the coupling between a suspended Si_3N_4 waveguide and a microscopy system.[39] In addition to the grating coupler, a distributed Bragg layer on top of the substrate rather than a mirror as reflector to direct the emission to the guided mode can be effective. Next to the out-coupling, the effect of the Si_3N_4 thickness on the waveguiding properties needs to be understood. Probing the differences in the collected emission intensity from an embedded single QD with progressively increased Si_3N_4 thickness can be studied to find the optimum condition. An on-chip detection of the single photon emission would mitigate such complex requirements which could be attempted by integrating single QDs and superconducting nanowire single photon detectors coupled by the waveguide on the same silicon chip.

6.3. Conclusion

The integration of quantum emitters in silicon chip is necessary for both scalability and to further improve their optical properties by means of coupling to nanophotonic devices. As such, this chapter explored the possibility of positioning single InP/ZnSe QDs on pre-determined positions using electron

beam lithography. While the method attempted was deterministic by defining the hole pattern, the net result achieved was a 'probabilistic' 30% accuracy. This lower value is attributed to the combination of both monolayer voids and the residue of QDs after liftoff process. In addition, the differences in the sizes of single QDs from one another further cause either void (too big) or multiple QDs (too small) in the pre-defined positions. Further, single QDs are embedded in a silicon nitride host matrix that not only protects the QDs from environment but also acts as a waveguide. While the collection efficiency currently limits the demonstration of single photon emission with high purity in such a device structure, there are greater prospects to further improve the design which are also discussed in this chapter.

Bibliography

[1] Jeremy L. O'Brien, Akira Furusawa, and Jelena Vučković. Photonic quantum technologies. *Nature Photonics*, 3(12):687–695, 2009.

[2] Vigneshwaran Chandrasekaran, Mickaël D. Tessier, Dorian Dupont, Pieter Geiregat, Zeger Hens, and Edouard Brainis. Nearly blinking-free, high-purity single-photon emission by colloidal InP/ZnSe quantum dots. *Nano Letters*, 17(10):6104–6109, sep 2017.

[3] Xing Lin, Xingliang Dai, Chaodan Pu, Yunzhou Deng, Yuan Niu, Limin Tong, Wei Fang, Yizheng Jin, and Xiaogang Peng. Electrically-driven single-photon sources based on colloidal quantum dots with near-optimal antibunching at room temperature. *Nature Communications*, 8(1), oct 2017.

[4] Lukas Elsinger, Ronan Gourgues, Iman E. Zadeh, Jorick Maes, Antonio Guardiani, Gabriele Bulgarini, Silvania F. Pereira, Sander N. Dorenbos, Val Zwiller, Zeger Hens, and Dries Van Thourhout. Integration of colloidal PbS/CdS quantum dots with plasmonic antennas and superconducting detectors on a silicon nitride photonic platform. *Nano Letters*, 19(8):5452–5458, jul 2019.

[5] Suzanne Bisschop, Pieter Geiregat, Lukas Elsinger, Emile Drijvers, Dries Van Thourhout, Zeger Hens, and Edouard Brainis. Fabrication and characterization of SiNx/au cavities with colloidal nanocrystals. *Optics Express*, 26(5):6046, feb 2018.

[6] A. G. Curto, G. Volpe, T. H. Taminiau, M. P. Kreuzer, R. Quidant, and N. F. van Hulst. Unidirectional emission of a quantum dot coupled to a nanoantenna. *Science*, 329(5994):930–933, aug 2010.

[7] Pavel Kolchin, Nitipat Pholchai, Maiken H. Mikkelsen, Jinyong Oh, Sadao Ota, M. Saif Islam, Xiaobo Yin, and Xiang Zhang. High purcell factor due to coupling of a single emitter to a dielectric slot waveguide. *Nano Letters*, 15(1):464–468, dec 2014.

[8] Thang B. Hoang, Gleb M. Akselrod, and Maiken H. Mikkelsen. Ultrafast room-temperature single photon emission from quantum dots coupled to plasmonic nanocavities. *Nano Letters*, 16(1):270–275, dec 2015.

[9] Yueyang Chen, Albert Ryou, Max R. Friedfeld, Taylor Fryett, James Whitehead, Brandi M. Cossairt, and Arka Majumdar. Deterministic positioning of colloidal quantum dots on silicon nitride nanobeam cavities. *Nano Letters*, 18(10):6404–6410, sep 2018.

[10] Roel Baets, Ananth Z. Subramanian, Stéphane Clemmen, Bart Kuyken, Peter Bienstman, Nicolas Le Thomas, Günther Roelkens, Dries Van Thourhout, Philippe Helin, and Simone Severi. Silicon photonics: silicon nitride versus silicon-on-insulator. In *Optical Fiber Communication Conference*. OSA, 2016.

[11] P. K. Tien. Light waves in thin films and integrated optics. *Applied Optics*, 10(11):2395, nov 1971.

[12] Jared F. Bauters, Martijn J. R. Heck, Demis John, Daoxin Dai, Ming-Chun Tien, Jonathon S. Barton, Arne Leinse, René G. Heideman, Daniel J. Blumenthal, and John E. Bowers. Ultra-low-loss high-aspect-ratio si_3n_4 waveguides. *Optics Express*, 19(4):3163, feb 2011.

[13] Zhechao Wang, Amin Abbasi, Utsav Dave, Andreas De Groote, Sulakshna Kumari, Bernadette Kunert, Clement Merckling, Marianna Pantouvaki, Yuting Shi, Bin Tian, Kasper Van Gasse, Jochem Verbist, Ruijun Wang, Weiqiang Xie, Jing Zhang, Yunpeng Zhu, Johan Bauwelinck, Xin Yin, Zeger Hens, Joris Van Campenhout, Bart Kuyken, Roel Baets, Geert Morthier, Dries Van Thourhout, and Gunther Roelkens. Novel light source integration approaches for silicon photonics. *Laser & Photonics Reviews*, 11(4):1700063, jul 2017.

[14] Weiqiang Xie, Yunpeng Zhu, Tangi Aubert, Steven Verstuyft, Zeger Hens, and Dries Van Thourhout. Low-loss silicon nitride waveguide hybridly integrated with colloidal quantum dots. *Optics Express*, 23(9):12152, apr 2015.

[15] Weiqiang Xie, Thilo Stöferle, Gabriele Rainò, Tangi Aubert, Suzanne Bisschop, Yunpeng Zhu, Rainer F. Mahrt, Pieter Geiregat, Edouard Brainis, Zeger Hens, and Dries Van Thourhout. On-chip integrated quantum-dot-silicon-nitride microdisk lasers. *Advanced Materials*, 29(16):1604866, feb 2017.

[16] Yunpeng Zhu, Weiqiang Xie, Suzanne Bisschop, Tangi Aubert, Edouard Brainis, Pieter Geiregat, Zeger Hens, and Dries Van Thourhout. On-chip single-mode distributed feedback colloidal quantum dot laser under nanosecond pumping. *ACS Photonics*, 4(10):2446–2452, sep 2017.

[17] Weiqiang Xie, Raquel Gomes, Tangi Aubert, Suzanne Bisschop, Yunpeng Zhu, Zeger Hens, Edouard Brainis, and Dries Van Thourhout. Nanoscale and single-dot patterning of colloidal quantum dots. *Nano Letters*, 15(11):7481–7487, oct 2015.

[18] J. Abramson, M. Palma, S. J. Wind, and J. Hone. Quantum dot nanoarrays: Self-assembly with single-particle control and resolution. *Advanced Materials*, 24(16):2207–2211, mar 2012.

[19] Tamar S. Mentzel, Darcy D. Wanger, Nirat Ray, Brian J. Walker, David Strasfeld, Moungi G. Bawendi, and Marc A. Kastner. Nanopatterned electrically conductive films of semiconductor nanocrystals. *Nano Letters*, 12(8):4404–4408, jul 2012.

[20] Vitor R Manfrinato, Darcy D Wanger, David B Strasfeld, Hee-Sun Han, Francesco Marsili, Jose P Arrieta, Tamar S Mentzel, Moungi G Bawendi, and Karl K Berggren. Controlled placement of colloidal quantum dots in sub-15 nm clusters. *Nanotechnology*, 24(12):125302, mar 2013.

[21] Dana B. Dement, Matthew K. Quan, and Vivian E. Ferry. Nanoscale patterning of colloidal nanocrystal films for nanophotonic applications using direct write electron beam lithography. *ACS Applied Materials & Interfaces*, 11(16):14970–14979, apr 2019.

[22] Joon-Suh Park, Jihoon Kyhm, Hong Hee Kim, Shinyoung Jeong, JoonHyun Kang, Song ee Lee, Kyu-Tae Lee, Kisun Park, Nilesh Barange, JiYeong Han, Jin Dong Song, Won Kook Choi, and Il Ki Han. Alternative patterning process for realization of large-area, full-color, active quantum dot display. *Nano Letters*, 16(11):6946–6953, oct 2016.

[23] Michael Junkin, Jennifer Watson, Jonathan P. Vande Geest, and Pak Kin Wong. Template-guided self-assembly of colloidal quantum dots using plasma lithography. *Advanced Materials*, 21(12):1247–1251, mar 2009.

[24] Andras G. Pattantyus-Abraham, Haijun Qiao, Jingning Shan, Keith A. Abel, Tian-Si Wang, Frank C. J. M. van Veggel, and Jeff F. Young. Site-selective optical coupling of PbSe nanocrystals to si-based photonic crystal microcavities. *Nano Letters*, 9(8):2849–2854, aug 2009.

[25] Ying Wang, Yi Zhang, Bin Li, Junhong Lü, and Jun Hu. Capturing and depositing one nanoobject at a time: Single particle dip-pen nanolithography. *Applied Physics Letters*, 90(13):133102, mar 2007.

[26] Hohyun Keum, Yiran Jiang, Jun Kyu Park, Joseph C. Flanagan, Moonsub Shim, and Seok Kim. Photoresist contact patterning of quantum dot films. *ACS Nano*, 12(10):10024–10031, sep 2018.

[27] A. Paul Alivisatos, Kai P. Johnsson, Xiaogang Peng, Troy E. Wilson, Colin J. Loweth, Marcel P. Bruchez, and Peter G. Schultz. Organization of 'nanocrystal molecules' using DNA. *Nature*, 382(6592):609–611, aug 1996.

[28] R K Kramer, N Pholchai, V J Sorger, T J Yim, R Oulton, and X Zhang. Positioning of quantum dots on metallic nanostructures. *Nanotechnology*, 21(14):145307, mar 2010.

[29] Da Huang, Mark Freeley, and Matteo Palma. DNA-mediated patterning of single quantum dot nanoarrays: A reusable platform for single-molecule control. *Scientific Reports*, 7(1), mar 2017.

[30] Qiang Zhang, Cuong Dang, Hayato Urabe, Jing Wang, Shouheng Sun, and Arto Nurmikko. Large ordered arrays of single photon sources based on II–VI semiconductor colloidal quantum dot. *Optics Express*, 16(24):19592, nov 2008.

[31] Yue Zhao, Kari Thorkelsson, Alexander J. Mastroianni, Thomas Schilling, Joseph M. Luther, Benjamin J. Rancatore, Kazuyuki Matsunaga, Hiroshi Jinnai, Yue Wu, Daniel Poulsen, Jean M. J. Fréchet, A. Paul Alivisatos, and Ting Xu. Small-molecule-directed nanoparticle assembly towards stimuli-responsive nanocomposites. *Nature Materials*, 8(12):979–985, oct 2009.

[32] Mingming Jiang, Jonathan A. Kurvits, Yao Lu, Arto V. Nurmikko, and Rashid Zia. Reusable inorganic templates for electrostatic self-assembly of individual quantum dots, nanodiamonds, and lanthanide-doped nanoparticles. *Nano Letters*, 15(8):5010–5016, jul 2015.

[33] Yadong Yin, Yu Lu, Byron Gates, and Younan Xia. Template-assisted self-assembly: a practical route to complex aggregates of monodispersed colloids with well-defined sizes, shapes, and structures. *Journal of the American Chemical Society*, 123(36):8718–8729, sep 2001.

[34] Yi Cui, Mikael T. Björk, J. Alexander Liddle, Carsten Sönnichsen, Benjamin Boussert, and A. Paul Alivisatos. Integration of colloidal nanocrystals into lithographically patterned devices. *Nano Letters*, 4(6):1093–1098, jun 2004.

[35] Jun Chen, Ye Wu, Xiaoming Li, Fei Cao, Yu Gu, Kai Liu, Xuhai Liu, Yuhang Dong, Jianping Ji, and Haibo Zeng. Simple and fast patterning process by laser direct writing for perovskite quantum dots. *Advanced Materials Technologies*, 2(10):1700132, jul 2017.

[36] Yolanda Justo, Iwan Moreels, Karel Lambert, and Zeger Hens. Langmuir–blodgett monolayers of colloidal lead chalcogenide quantum dots: morphology and photoluminescence. *Nanotechnology*, 21(29):295606, jul 2010.

[37] Xavier Brokmann, Laurent Coolen, Jean-Pierre Hermier, and Maxime Dahan. Emission properties of single CdSe/ZnS quantum dots close to a dielectric interface. *Chemical Physics*, 318(1-2):91–98, nov 2005.

[38] Suzanne Bisschop, Antoine Guille, Dries Van Thourhout, Zeger Hens, and Edouard Brainis. Broadband enhancement of single photon emission and polarization dependent coupling in silicon nitride waveguides. *Optics Express*, 23(11):13713, may 2015.

[39] Yunpeng Zhu, Jie Wang, Weiqiang Xie, Bin Tian, Yanlu Li, Edouard Brainis, Yuqing Jiao, and Dries Van Thourhout. Ultra-compact silicon nitride grating coupler for microscopy systems. *Optics Express*, 25(26):33297, dec 2017.

Chapter 7.

Conclusion

Contents

Synopsis

This chapter answers the title question of this dissertation by providing a summary of main results from each chapters. These summaries address the key inhibiting factors in using colloidal QDs for quantum photonics introduced in section 1.4.2. A factual comparison with other solid state single photon sources and the differences in exciton properties of colloidal QDs to that of epitaxial QDs are provided. An outlook for using colloidal QDs as single photon sources and their exciton properties are also discussed.

7.1. Recap

7.1.1. Summary

To answer the title of this dissertation *"Are the excitons in colloidal InP quantum dots suitable for quantum photonics?"*, a brief description of motivation of this dissertation & available technologies for a single photon source are recapped. This is followed by a summary of main results from each chapters addressing the key inhibiting factors in using colloidal QDs for quantum photonics, introduced in section 1.4.2.

Motivation: With wave-particle duality and the quantization of light, the first quantum revolution enabled the advent of modern devices from transistors to lasers. Now we are on the verge of a second quantum revolution with devices that are able to generate, manipulate and measure the quantum states of light.[1] Quantized electromagnetic field consists of discrete particles known as photons and a single photon is one such quantum state of light. Single photon sources form an integral part in realizing quantum technological applications such as quantum computing,[2] quantum cryptography,[3–5] quantum simulation[6–8] and quantum metrology.[9, 10]

Technology: Single photon sources are either based on nonlinear frequency conversion or on the spontaneous emission of single quantum emitters.[11] Spontaneous parametric down-conversion sources belonging to the former set the benchmark for single-photon technology but they are probablistic in nature, not scalable and have lower brightness.[12] Solid state sources belonging to the latter have an on-demand emission and takes advantage of their host matrix system for scalability. These include color centers or defects in crystalline hosts,[13–15] carbon nanotubes,[16] transition metal dichalcogenides,[17] epitaxial QDs[18–20] and colloidal QDs.[21–24]

Colloidal QDs: Main advantages are economical synthesis, versatile synthesis protocols allow to easily prepare complex heterostructures and room temperature operation. The fundamental optical properties of excitons in colloidal InP QDs addressing the key inhibiting factors for quantum photonics are described below:

- *Bleaching & Blinking*: As discussed in Chapter 2 under optical excitation at room temperature, thiol-capped single InP/ZnSe QDs show a combination of narrow room-temperature emission spectrum (average of 19.4 nm), pure single photon emission ($g^{(2)}(0) \approx 0$) under both CW and pulsed excitation, mono-exponential luminescence decay (average of 22.5 ns), reduced blinking (99% on-time), and photostability. Furthermore, strong antibunching is preserved even at saturating intensities which is attributed to fast non-radiative Auger recombination of multi-excitons. While the single QDs are efficient single photon emitters, the longer lifetime limits the rate of single photon operation to around 10 MhZ. A resonant excitation of QD coupled to a cavity structure could enhance the spontaneous emission rate and reduce the timing jitter.[25]
- *Fine structure*: As discussed in Chapter 3, electronic structure of InP/ZnSe QDs exhibit quasi-isotropic band-edge exciton fine structure with the main contribution from electron-hole exchange interaction and negligible contribution of shape anisotropy. The presence of exciton-manifold with the dark exciton below the bright exciton is not favorable for quantum photonics as this causes additional prolongation of the lifetime.
- *Dephasing*: Chapter 4 describes the effect of this deviation from an ideal two-level system to exciton-manifolds influencing the dephasing of the optical transition which is dominated by phonon-scattering within the bright exciton fine structure with a 0 K dephasing rate of 0.0346 $\pm$

$0.0004ps^{-1}$. $T_2/2T_1 \approx 0.001$ at 5K for this QD is not favorable for indistinguishability that ideally requires a unity relation with a naturally broadened Fourier transform limited linewidth. While a slower spin-flip from bright-to-dark exciton state is predicted for this QD, a further detailed study using a magnetic field dependence would be required for validation. In addition, future synthetic protocols could be attempted to engineer the structures with an aim of prolonging the dephasing time.

- *Spectral diffusion or jitter or wandering*: Chapter 5 discussed the polarizability of exciton, biexciton and trion by correlating their level of spectral shifts due to quantum confined stark effect (QCSE). It is observed that the QCSE is minimized in trion-to-carrier and biexciton-to-exciton transitions compared to neutral exciton. Using InP/ZnSe QDs as an optimized system to minimize SD, a theoretical understanding of the structural conditions that determine the magnitude of QCSE in core-shell QDs was provided. As such, it was reported that minimal spectral diffusion can be expected for strongly confined cores (large band-offset, moderately small core) and multi-excitonic species. A trion emission from a single QD would be a good single photon emitter considering the minimal spectral diffusion and absence of fine structure. However, a stable trion emission is needed rather than a random switching transition which could be achieved by versatile synthesis procedures similar to alloyed CdSe QDs.[26]

- *Non-deterministic integrated source*: Chapter 6 discussed the initial investigations of integrating single QDs on a silicon nitride photonic platform, with the aim of making a practical single-photon source. A deterministic positioning of single InP/ZnSe QDs from solution phase to silicon chip is attempted using eletcron-beam lithography, but only with a result of a 'probabilistic' 30% accuracy. This lower value is attributed to the combination of both monolayer voids and the residue of QDs after liftoff process. In addition, the differences in the sizes of single QDs from one another further cause either void (too big) or multiple QDs (too small) in the pre-defined positions. A proper study on the surface chemistry of the QD under study is also necessary to find the role of ligands during the LB deposition. While the collection efficiency currently limits the demonstration of single photon emission with high purity from a single QD embedded in Si_3N_4 waveguide, there are greater prospects to further improve the design which were also discussed in this chapter. The suitability of this QD for electrical excitation is beyond the scope of this dissertation as it only addresses the fundamental exciton properties under optical excitation.

7.1.2. Comparison with other single photon sources

A recent review article on solid state single photon emitters omitted colloidal QD to be included as a promising material citing the reason of "unstable optical emission".[27] Though the reasoning behind this statement was not explained in detail, it can be inferred that colloidal QDs bleach, blink and charge trapping at interfaces and in the local environment typically occurs closer to the exciton in QDs (due to their small size and often amorphous environment such as organic polymers) increasing the corresponding spectral shifts. Nevertheless, this dissertation discussed the fundamental exciton properties in colloidal InP QDs to be used as single photon sources. Figure 7.1 shows the table from the same review article[27] summarizing the important photophysical properties in solid state single photon emitters. The results from this dissertation are also added in the bottom of the table for factual comparison to the state-of-the-art solid state single photon emitters.

Table 1 | Summary of photophysical properties of solid-state SPEs.

	Maximum count rate (without a cavity, continuous wave) (counts s^{-1})	Lifetime (ns)	Homogeneous linewidth at 4 K	Indistinguishable photons (IP) and entanglement (E)	Spatial targeted fabrication of single emitters	Operation temperature	Integration of SPEs with dielectric cavities or plasmonic resonators
Colour centres in diamond	SiV: ~3×10^6 (ref. 138)* NV: ~1×10^6 (ref. 139)† For other sources see ref. 28	SiV: ~1 NV: ~12–22	NV, SiV lifetime-limited[29,30] Cr-related: 4 GHz (ref. 140)	NV: IP, E SiV: IP	Only for NV and SiV (ref. 28)	RT	Dielectric: NV, SiV only Plasmonics: NV only
Defects in SiC, ZnO and BN Rare earths in YAG/YOS	YAG: ~60×10^3 (ref. 141) ZnO: ~1×10^5 (ref. 44) SiC: ~2×10^6 (ref. 35) BN: ~3×10^6 (ref. 56)	19 (ref. 49)§ 1–4 (ref. 44) 1–4 (ref. 35) ~3 (ref. 56)	N/A	No	No	RT	No
Arsenide QDs	~1×10^7 (ref. 84)‡	~1 (refs 6,84)	Lifetime-limited	Yes	Yes	4 K	Yes
Nitride QDs	N/A	~0.3 (ref. 85)	~1.5 meV (ref. 85)	No	Yes	RT	Dielectric: yes Plasmonics: no
CNTs	~3×10^3 (ref. 68)	~0.4 (ref. 68)	N/A	No	No	RT	Dielectric: yes Plasmonics: no
2D TMDCs	~3.7×10^5 (ref. 57)	~1–3 (ref. 57)	N/A	No	No	4 K	No
Colloidal QDs	2×10^5 (Chapter 2)	~22 ns (Chapter 2)	~50 μeV, not lifetime-limited (Chapter 4)	No	No 30% accuracy (Chapter 6)	RT	Yes (ref: 28-30)

Figure 7.1. | Comparison of photophysical properties of solid state single photon emitters. This figure is adapted from the reference,[27] a review article on the solid state single photon emitters. The data for colloidal QDs from this dissertation are added in the bottom of the table. Literature for integrating single and ensemble of colloidal QDs with cavity structures can be found in the references:[28–33]

Differences with epitaxial QDs

The first single photon emission for both colloidal & epitaxial QDs was demonstrated in the same year 2000.[34, 35] While epitaxial QDs have progressed well in technology,[11] the progress of colloidal QDs remains stalled.[27] See section 1.3.3 for a list of key progresses achieved in case of epitaxial QDs as single photon sources.

The differences in the excitonic behavior in epitaxial QDs and colloidal QDs are due to the smaller dimensionality and a stronger quantum confinement in the latter. Hence the bright-dark splitting is larger (several meV) in colloidal QDs compared to few tens-hundreds of μeV in epitaxial QDs. This leads to a larger stokes shift in colloidal QDs. These larger bright-dark splitting energies are more than the thermal energies at cryogenic temperatures under measurement. One way of understanding this phenomenon is that the input excitation is absorbed by the bright exciton, but the resulting PL decay is through dark exciton which usually is longer in terms of several hundred nanoseconds.[36]

It is possible to synthesize colloidal NCs with targeted dimensions like nanoplatelets and 2D-materials. The dephasing time in nanoplatelets is limited only by the natural radiative lifetime (1 ps) since they have larger in-plane coherence area compared to spherical QDs.[37] However, single photon emission has not been reported in these NCs as they are not quasi-two level emitter. These NCs are efficient multiple exciton emitter and thus a spectral post selection may be attempted to isolate the biexciton emission, for instance, to be used as entangled photon sources.

Epitaxially grown QDs have a continuation of the crystal structure that minimizes charge carrier trapping at the QD interface/surface compared to colloidal QDs.[38] Importantly, the epitaxial QDs suitable for quantum photonic applications are devised for operations at cryogenic temperatures where the ZPL contribution is higher than at room temperature. They are already integrated to cavity structures

such that their spontaneous emission rate is higher and, further, it was reported that the phonon induced decoherence can be controlled in QDs embedded in cavity structures.[39] A resonant excitation of QD coupled to a cavity structure was shown to be having an enhanced spontaneous emission rate, a reduction in timing jitter and a higher degree of photon indistinguishability.[25, 40, 41]

Indistinguishability on epitaxial QDs have been reported by checking the emission of the same QD with a delay to check any differences in the subsequent emissions.[27] In order to use these inhomogeneously broadened materials for quantum information processing, it is required to have multiple QDs emitting identical single photon wavepackets. The stream of single photon pulses are ideally required to be Fourier transform limited. This means both the spatial and temporal overlaps of their wavepackets should be identical in terms of emission frequency, pulse-width, spectral bandwidth, polarization, transverse mode profile and arrival time at the beam splitter.[42] In epitaxial QDs, external factors are used to tune the optical properties such as: emission frequency tuning,[43–47] electronic structure tuning (for instance, making the light hole come higher than the heavy hole which is promising for quantum technological applications,[48]) and to achieve zero splitting of bright exciton or to have splitting less than their radiative linewidth for entangled photon sources.[49–53] While spherical NCs experience a uniform stress on them by growing a shell around it, this can be checked in other dimensional NCs if the stress and strain induced on the surface of the core can indeed be utilized to tune their optical properties.

Other NCs of interest are colloidal lead halide perovskite quantum dots that are shown to be exhibiting minimal spectral diffusion and longer exciton coherence with $T_2/2T_1 \approx 0.2$.[54] Of course, as described in Chapter 6, the integration of NCs to nanophotonic devices in silicon chip is necessary for both scalability and to improve their optical properties.

7.2. Outlook

7.2.1. Criteria for colloidal QDs to be used as single photon sources

From the literature overview of performances of colloidal QDs and the spectroscopy of single InP/ZnSe QDs studied here, criteria for colloidal QDs to be used as single photon sources can be devised:

- For artificial atoms like QD to be a good single photon source, it needs to be operating as a two-level system for a spontaneous emission of single photon from a single exciton state. A type I structure in QDs has a stronger confinement and thus produces discrete exciton levels similar to atomic or molecular levels acting as a quasi-two level system. But a large number of optically active electrons could give rise to complex features as multi-exciton states. However, the charge carriers relax back to the first excited state rapidly such that no emission from these higher excited states can be detected and also Auger process in QDs quenches the radiative recombination of the multiple excitons.
- This Auger process was also considered to be one of the causes of blinking phenomenon in QDs.[55] While this Auger process was shown to be suppressed by the versatile synthesis of CdSe QDs in an attempt to reduce the blinking, this also enhanced the multiple exciton recombination especially at higher excitation intensities. So blinking needs to be controlled with better photostability, but importantly not compromising the single photon purity at higher excitation intensities. At higher fluence, the effective two level system is sufficiently populated which can trigger the spontaneous emission of a single photon with a probability equal to the PLQY.

- Single photon operation needs to be demonstrated under pulsed laser excitation so that it can be used as single photon turnstile devices. Since the colloidal QDs have a typical lifetime in ns range, the maximum repetition rate of pulsed excitation that can be used is around 10 MhZ. An enhancement in the spontaneous emission rate is critical for higher rate operation and this could be achieved by integrating QDs in a nanophotonic structure (with a resonant excitation).
- A mechanism to efficiently extract the emission from deterministically positioned integrated source would be required to calculate the brightness factor to compare with state-of-the-art single photon emitters. Devices can be designed to improve the out-coupling of emission via waveguide/nanofibers/grating couplers to the objective microscope. An on-chip detection of the single photon emission would mitigate such complex requirements which could be attempted by integrating single QDs and superconducting nanowire single photon detectors coupled by the waveguide on the same silicon chip. Even if the on-chip single photon emission is achieved successfully in such a structure, then the following step would be to tune the emission of multiple QDs to align emission peak energies for indistinguishability.

While indistinguishable photons are obligatory for a quantum information processing applications such as qubits, it is not necessary for quantum cryptography like random number generator which only requires a high pure single photon emission at room temperature. Colloidal QDs could be suitable for this application except that the emission needs to be stable and free from blinking.

7.2.2. Exciton properties for quantum photonics

Exciton fine structure & dephasing

As discussed in Chapter 3, the lowest exciton state is not an ideal two level but a manifold of exciton levels attributed to exchange interaction and minor anisotropy. As discussed in Chapter 4, the presence of these exciton-manifolds in colloidal QDs influence the exciton dephasing rate to be much faster than the natural radiative rate, which is undesirable for producing indistinguishable photons. Since it was observed that the phonon induced decoherence is reduced in cavity structures,[39] it is imperative to integrate colloidal QDs with nanophotonic devices to improve their optical properties. Further, a modification in the synthesis to tune the fine structure would be required to prolong the dephasing time.[56]

Spectral diffusion

Chapter 5 discussed the energy shifts of different excitonic species due to QCSE and structural conditions to minimize SD. From these results, future synthetic protocols could aim engineering the QD structure for required applications. The reduced SD due to QCSE in multiple exciton species makes them interesting for quantum photonic applications. In addition to the reduced SD, a trion emission has no exchange interaction induced fine structure splitting with emission only from the bright state and thus could be used as single photon sources having higher emissive rate and also for spintronics. However, a stable trion emission is needed rather than a random switching transition which could be achieved by versatile synthesis procedures similar to alloyed CdSe QDs.[26] XX-X radiative cascade

with a narrow linewidth, shorter lifetime and reduced SD (see section 5.2.2) could be useful for entangled photon sources if the fine structure splitting is reduced to zero and the emission is linearly polarized.[57] While InP/ZnSe QDs have nearly isotropic bright exciton fine structure as described in Chapter 3, this QD has a lower biexciton quantum yield,[58] the minor anisotropy resulting from z-axis anisotropy emits a circularly polarized light[59] and there is a presence of dark exciton separated by 5-10 meV from bright exciton.[60] So a modification in the synthesis to have improved biexciton quantum yield with elongated structures would be necessary for such applications, though an external stimulus might be additionally required to tune the fine structure splitting to zero in such a case.

The influence of electric field in changing the emission wavelength of QDs could be utilized as a frequency tuning mechanism to align the peak emission of multiple QDs to have the same value. For indistinguishability, currently the latest trend from the established materials like epitaxial QDs is to tune the emission frequency of QDs by means of electric field, piezoelectric, stress and strain.[47] Also, the stark tuning mechanism can also be used to control QD emissions in cavity structures.[38]

While SD affects the usage of colloidal QDs as indistinguishable photons at cryogenic temperatures as described in Chapter 5, the sensitivity of the excitonic emission to the charge fluctuations of the NCs can well be utilized for other applications. For instance, as a charge sensor, electro-optical modulators, cell tracking and laser absorption spectroscopy. Other than quantum photonics requiring minimal SD, it is shown that larger QCSE and SD enhances the phonon coupling (see section 5.2.1). For example, one could attempt charge doping or introduce polar shell to have more phonon coupling for applications like charge transport devices and superconductivity.

Polydispersity

NCs with different sizes and shapes in both cores and/or shells may have variations in the biexciton lifetime & therefore the single photon emission purity could be depended on the wavefunction overlap.[61] Also, NCs of different shapes like dot-in-rods with small core and thick shells was shown to be having a reduced fine structure splitting.[62] As discussed in section 5.4, QDs having smaller band-offset increases the polarizability of the wavefunctions. This indicates a variation in the optical properties of QDs owing to their size/shape differences.

As discussed in section 6.2.1, electron-beam lithography is used to devise a uniform pattern to place the single QDs. A proper monolayer of colloidal QDs is required for higher probability of placing single QDs on the predetermined position. If there is a larger degree of polydispersity in a sample, then the probability of placing the QDs would be low. This can be checked by using QDs made of SILAR method where shell layers are added successively thus having better control over their shell growth. A size-selective precipitation could also be quite effective, and, if necessary, density-gradient ultracentrifugation could be used as well.[63] Larger sized particles could have an increased accuracy of placing single QDs in the predetermined position using electron-beam lithography. For instance, growing a silica shell around the QD to increase their overall size could be attempted for single QD patterning.

7.2.3. Perspectives on integrated single photon sources

The exciton properties in QDs need to be well understood before going for integration of single QDs in silicon chip where one expects a different environment a single QD might encounter during the transition from a solution phase surrounded by ligands. In this dissertation, single InP/ZnSe QDs are

shown to be an efficient single photon emitter by studying their optical properties at room temperature. Deterministic deposition of single QDs from solution-phase onto a silicon chip is attempted in Chapter 6 with a net result of only 30% accuracy. Currently, the emission collection efficiency from a single QD embedded in a Si_3N_4 waveguide is limited by both the design of the structure and the background fluorescence. Finite-difference time-domain (FDTD) simulations predicted that a suspended Si_3N_4 waveguide structure provides a better light confinement of the guided modes and improves the coupling to the emitter.[64] Therefore, it is proposed to integrate single InP/ZnSe QDs in such a suspended waveguide structure. The light out-coupling also needs to be improved. Currently the emitted photons are collected vertically by using an objective microscope with high numerical aperture. A grating coupler can improve the coupling between a suspended Si_3N_4 waveguide and a microscopy system.[65] In addition to the grating coupler, a distributed Bragg layer on top of the substrate rather than a mirror as reflector to direct the emission to the guided mode can be effective. Next to the out-coupling, the effect of the Si_3N_4 thickness on the waveguiding properties needs to be understood. Probing the differences in the collected emission intensity from a waveguide embedded single QD with progressively increased thickness could be used to find the optimum condition.

To achieve the elusive integrated quantum photonic chip, a solution is proposed where the single photon source based on InP colloidal QDs form the light emitting material, Si_3N_4 form the light guiding material and a superconducting nanowire single photon detectors (SNSPDs) form the light detecting material. A light modulating functionality could be an another active material depending on the required functionality. From the available library of materials in UGent, suitable visible and near-infrared QDs are selected by studying their optical properties before and after the integration in the chip. After integration, it was found that CdSe/CdS/ZnS QDs preserve their fluorescence intensity better than CdSe/CdS QDs, possibly due to an improved protection from the ambient atmosphere by using multiple layered shell. However, this QD is not a good single photon emitter due to enhanced multiple exciton recombination rate. While CdSe-based QDs were used to study the optimum conditions for integration of both QDs and SNSPD in the same silicon chip, the final implementation could be done using InP/ZnSe QDs for the demonstration of on-chip single photon emission.

Though the InP/ZnSe core/shell QDs studied in this dissertation are in visible emitting wavelength ranges, the results could be extended to near-infrared by the versatility of synthesis in III-V materials. For quantum cryptography, an infrared operation at room temperature would be required for practical purposes to match the telecommunication wavelengths. Also, the detector efficiency in SNSPD is higher in infrared wavelength ranges.

While the quantum territory is gargantuan to be covered in its entirety and the photophysical mechanism behind the exciton properties differ from one material to another, this dissertation limits itself in explaining the mechanisms behind the 'behavior' of colloidal InP QDs that could be used as a model system to emulate for other types of colloidal QDs as well to be ultimately used for quantum photonics.

Bibliography

[1] Jonathan P. Dowling and Gerard J. Milburn. Quantum technology: the second quantum revolution. *Philosophical Transactions of the Royal Society of London. Series A: Mathematical, Physical and Engineering Sciences*, 361(1809):1655–1674, 2003.

[2] E. Knill, R. Laflamme, and G. J. Milburn. A scheme for efficient quantum computation with linear optics. *Nature*, 409(6816):46–52, 2001.

[3] Nicolas Gisin, Grégoire Ribordy, Wolfgang Tittel, and Hugo Zbinden. Quantum cryptography. *Reviews of Modern Physics*, 74:145–195, 2002.

[4] Alexios Beveratos, Rosa Brouri, Thierry Gacoin, André Villing, Jean-Philippe Poizat, and Philippe Grangier. Single photon quantum cryptography. *Physical Review Letters*, 89:187901, oct 2002.

[5] Tobias Heindel, Christian A Kessler, Markus Rau, Christian Schneider, Martin Fürst, Fabian Hargart, Wolfgang-Michael Schulz, Marcus Eichfelder, Robert Roßbach, Sebastian Nauerth, Matthias Lermer, Henning Weier, Michael Jetter, Martin Kamp, Stephan Reitzenstein, Sven Höfling, Peter Michler, Harald Weinfurter, and Alfred Forchel. Quantum key distribution using quantum dot single-photon emitting diodes in the red and near infrared spectral range. *New Journal of Physics*, 14(8):083001, aug 2012.

[6] S. Lloyd. Universal quantum simulators. *Science*, 273(5278):1073–1078, aug 1996.

[7] M. A. Broome, A. Fedrizzi, B. P. Lanyon, I. Kassal, A. Aspuru-Guzik, and A. G. White. Discrete single-photon quantum walks with tunable decoherence. *Physical Review Letters*, 104:153602, apr 2010.

[8] Max Tillmann, Borivoje Dakić, René Heilmann, Stefan Nolte, Alexander Szameit, and Philip Walther. Experimental boson sampling. *Nature Photonics*, 7(7):540–544, 2013.

[9] Vittorio Giovannetti, Seth Lloyd, and Lorenzo Maccone. Quantum metrology. *Physical Review Letters*, 96:010401, jan 2006.

[10] Keith R. Motes, Jonathan P. Olson, Evan J. Rabeaux, Jonathan P. Dowling, S. Jay Olson, and Peter P. Rohde. Linear optical quantum metrology with single photons: Exploiting spontaneously generated entanglement to beat the shot-noise limit. *Physical Review Letters*, 114:170802, Apr 2015.

[11] Pascale Senellart, Glenn Solomon, and Andrew White. High-performance semiconductor quantum-dot single-photon sources. *Nature Nanotechnology*, 12(11):1026–1039, nov 2017.

[12] N. Somaschi, V. Giesz, L. De Santis, J. C. Loredo, M. P. Almeida, G. Hornecker, S. L. Portalupi, T. Grange, C. Antón, J. Demory, C. Gómez, I. Sagnes, N. D. Lanzillotti-Kimura, A. Lemaítre, A. Auffeves, A. G. White, L. Lanco, and P. Senellart. Near-optimal single-photon sources in the solid state. *Nature Photonics*, 10(5):340–345, 2016.

[13] Igor Aharonovich and Elke Neu. Diamond nanophotonics. *Advanced Optical Materials*, 2(10):911–928, jul 2014.

[14] Anthony J. Morfa, Brant C. Gibson, Matthias Karg, Timothy J. Karle, Andrew D. Greentree, Paul Mulvaney, and Snjezana Tomljenovic-Hanic. Single-photon emission and quantum characterization of zinc oxide defects. *Nano Letters*, 12(2):949–954, 2012.

[15] Tobias Utikal, Emanuel Eichhammer, Lutz Petersen, Alois Renn, Stephan Götzinger, and Vahid Sandoghdar. Spectroscopic detection and state preparation of a single praseodymium ion in a crystal. *Nature Communications*, 5:3627, 2014.

[16] Xuedan Ma, Nicolai F Hartmann, Jon KS Baldwin, Stephen K Doorn, and Han Htoon. Room-temperature single-photon generation from solitary dopants of carbon nanotubes. *Nature nanotechnology*, 10(8):671–675, 2015.

[17] Yu-Ming He, Genevieve Clark, John R. Schaibley, Yu He, Ming-Cheng Chen, Yu-Jia Wei, Xing Ding, Qiang Zhang, Wang Yao, Xiaodong Xu, Chao-Yang Lu, and Jian-Wei Pan. Single quantum emitters in monolayer semiconductors. *Nature Nanotechnology*, 10(6):497–502, may 2015.

[18] Sonia Buckley, Kelley Rivoire, and Jelena Vučković. Engineered quantum dot single-photon sources. *Reports on Progress in Physics*, 75(12):126503, nov 2012.

[19] Raj B. Patel, Anthony J. Bennett, Ian Farrer, Christine A. Nicoll, David A. Ritchie, and Andrew J. Shields. Two-photon interference of the emission from electrically tunable remote quantum dots. *Nat. Photonics*, 4(9):632–635, 2010.

[20] Luca Sapienza, Marcelo Davanço, Antonio Badolato, and Kartik Srinivasan. Nanoscale optical positioning of single quantum dots for bright and pure single-photon emission. *Nat. Commun.*, 6:7833, 2015.

[21] X. Brokmann, E. Giacobino, M. Dahan, and J. P. Hermier. Highly efficient triggered emission of single photons by colloidal CdSe/ZnS nanocrystals. *Applied Physics Letters*, 85(5):712–714, aug 2004.

[22] X Brokmann, G Messin, P Desbiolles, E Giacobino, M Dahan, and J P Hermier. Colloidal CdSe/ZnS quantum dots as single-photon sources. *New Journal of Physics*, 6:99–99, jul 2004.

[23] Ferruccio Pisanello, Luigi Martiradonna, Godefroy Leménager, Piernicola Spinicelli, Angela Fiore, Liberato Manna, Jean-Pierre Hermier, Roberto Cingolani, Elisabeth Giacobino, Massimo De Vittorio, and Alberto Bramati. Room temperature-dipolelike single photon source with a colloidal dot-in-rod. *Appl. Phys. Lett.*, 96(3):033101, 2010.

[24] Ferruccio Pisanello, Godefroy Leménager, Luigi Martiradonna, Luigi Carbone, Stefano Vezzoli, Pascal Desfonds, Pantaleo Davide Cozzoli, Jean-Pierre Hermier, Elisabeth Giacobino, Roberto Cingolani, Massimo De Vittorio, and Alberto Bramati. Non-blinking single-photon generation with anisotropic colloidal nanocrystals: towards room-temperature, efficient, colloidal quantum sources. *Adv. Mater.*, 25(14):1974–1980, 2013.

[25] Dirk Englund, Arka Majumdar, Andrei Faraon, Mitsuru Toishi, Nick Stoltz, Pierre Petroff, and Jelena Vučković. Resonant excitation of a quantum dot strongly coupled to a photonic crystal nanocavity. *Physical Review Letters*, 104:073904, feb 2010.

[26] Mark J. Fernée, Chiara Sinito, Yann Louyer, Christian Potzner, Tich-Lam Nguyen, Paul Mulvaney, Philippe Tamarat, and Brahim Lounis. Magneto-optical properties of trions in non-blinking charged nanocrystals reveal an acoustic phonon bottleneck. *Nature Communications*, 3(1):1287, jan 2012.

[27] Igor Aharonovich, Dirk Englund, and Milos Toth. Solid-state single-photon emitters. *Nature Photonics*, 10(10):631–641, sep 2016.

[28] A. G. Curto, G. Volpe, T. H. Taminiau, M. P. Kreuzer, R. Quidant, and N. F. van Hulst. Unidirectional emission of a quantum dot coupled to a nanoantenna. *Science*, 329(5994):930–933, aug 2010.

[29] Pavel Kolchin, Nitipat Pholchai, Maiken H. Mikkelsen, Jinyong Oh, Sadao Ota, M. Saif Islam, Xiaobo Yin, and Xiang Zhang. High purcell factor due to coupling of a single emitter to a dielectric slot waveguide. *Nano Letters*, 15(1):464–468, dec 2014.

[30] Thang B. Hoang, Gleb M. Akselrod, and Maiken H. Mikkelsen. Ultrafast room-temperature single photon emission from quantum dots coupled to plasmonic nanocavities. *Nano Letters*, 16(1):270–275, dec 2015.

[31] Suzanne Bisschop, Pieter Geiregat, Lukas Elsinger, Emile Drijvers, Dries Van Thourhout, Zeger Hens, and Edouard Brainis. Fabrication and characterization of SiNx/au cavities with colloidal nanocrystals. *Optics Express*, 26(5):6046, feb 2018.

[32] Yueyang Chen, Albert Ryou, Max R. Friedfeld, Taylor Fryett, James Whitehead, Brandi M. Cossairt, and Arka Majumdar. Deterministic positioning of colloidal quantum dots on silicon nitride nanobeam cavities. *Nano Letters*, 18(10):6404–6410, sep 2018.

[33] Lukas Elsinger, Ronan Gourgues, Iman E. Zadeh, Jorick Maes, Antonio Guardiani, Gabriele Bulgarini, Silvania F. Pereira, Sander N. Dorenbos, Val Zwiller, Zeger Hens, and Dries Van Thourhout. Integration of colloidal PbS/CdS quantum dots with plasmonic antennas and superconducting detectors on a silicon nitride photonic platform. *Nano Letters*, 19(8):5452–5458, jul 2019.

[34] P. Michler, A. Imamoğlu, M. D. Mason, P. J. Carson, G. F. Strouse, and S. K. Buratto. Quantum correlation among photons from a single quantum dot at room temperature. *Nature*, 406(6799):968–970, aug 2000.

[35] P. Michler. A quantum dot single-photon turnstile device. *Science*, 290(5500):2282–2285, dec 2000.

[36] Manfred Bayer. Bridging two worlds: Colloidal versus epitaxial quantum dots. *Annalen der Physik*, page 1900039, may 2019.

[37] Ali Naeem, Francesco Masia, Sotirios Christodoulou, Iwan Moreels, Paola Borri, and Wolfgang Langbein. Giant exciton oscillator strength and radiatively limited dephasing in two-dimensional platelets. *Physical Review B*, 91(12):121302, mar 2015.

[38] Mark J. Fernée and Halina Rubinsztein-Dunlop. Quantum gate based on stark tunable nanocrystal interactions with ultrahigh-qv field modes in fused silica microcavities. *Physical Review B*, 74:115321, sep 2006.

[39] T. Grange, N. Somaschi, C. Antón, L. De Santis, G. Coppola, V. Giesz, A. Lemaître, I. Sagnes, A. Auffèves, and P. Senellart. Reducing phonon-induced decoherence in solid-state single-photon sources with cavity quantum electrodynamics. *Physical Review Letters*, 118:253602, jun 2017.

[40] A. Kiraz, M. Atatüre, and A. Imamoğlu. Quantum-dot single-photon sources: Prospects for applications in linear optics quantum-information processing. *Physical Review A*, 69:032305, mar 2004.

[41] Alexia Auffèves, Jean-Michel Gérard, and Jean-Philippe Poizat. Pure emitter dephasing: A resource for advanced solid-state single-photon sources. *Physical Review A*, 79:053838, may 2009.

[42] Peter Michler. Quantum dot single-photon sources. In *Single Semiconductor Quantum Dots*, pages 185–225. Springer Berlin Heidelberg, 2009.

[43] Prem Kumar. Quantum frequency conversion. *Optics Letters*, 15(24):1476, dec 1990.

[44] Sebastian Zaske, Andreas Lenhard, Christian A. Keßler, Jan Kettler, Christian Hepp, Carsten Arend, Roland Albrecht, Wolfgang-Michael Schulz, Michael Jetter, Peter Michler, and Christoph Becher. Visible-to-telecom quantum frequency conversion of light from a single quantum emitter. *Physical Review Letters*, 109:147404, oct 2012.

[45] Michael G. Raymer and Kartik Srinivasan. Manipulating the color and shape of single photons. *Physics Today*, 65(11):32–37, nov 2012.

[46] Jonas H. Weber, Benjamin Kambs, Jan Kettler, Simon Kern, Julian Maisch, Hüseyin Vural, Michael Jetter, Simone L. Portalupi, Christoph Becher, and Peter Michler. Two-photon interference in the telecom c-band after frequency conversion of photons from remote quantum emitters. *Nature Nanotechnology*, 14(1):23–26, oct 2018.

[47] Anshuman Singh, Qing Li, Shunfa Liu, Ying Yu, Xiyuan Lu, Christian Schneider, Sven Höfling, John Lawall, Varun Verma, Richard Mirin, Sae Woo Nam, Jin Liu, and Kartik Srinivasan. Quantum frequency conversion of a quantum dot single-photon source on a nanophotonic chip. *Optica*, 6(5):563, apr 2019.

[48] Y. H. Huo, B. J. Witek, S. Kumar, J. R. Cardenas, J. X. Zhang, N. Akopian, R. Singh, E. Zallo, R. Grifone, D. Kriegner, R. Trotta, F. Ding, J. Stangl, V. Zwiller, G. Bester, A. Rastelli, and O. G. Schmidt. A light-hole exciton in a quantum dot. *Nature Physics*, 10(1):46–51, nov 2013.

[49] A. I. Tartakovskii, M. N. Makhonin, I. R. Sellers, J. Cahill, A. D. Andreev, D. M. Whittaker, J-P. R. Wells, A. M. Fox, D. J. Mowbray, M. S. Skolnick, K. M. Groom, M. J. Steer, H. Y. Liu, and M. Hopkinson. Effect of thermal annealing and strain engineering on the fine structure of quantum dot excitons. *Physical Review B*, 70:193303, nov 2004.

[50] Stefan Seidl, Martin Kroner, Alexander Högele, Khaled Karrai, Richard J. Warburton, Antonio Badolato, and Pierre M. Petroff. Effect of uniaxial stress on excitons in a self-assembled quantum dot. *Applied Physics Letters*, 88(20):203113, may 2006.

[51] B. D. Gerardot, S. Seidl, P. A. Dalgarno, R. J. Warburton, D. Granados, J. M. Garcia, K. Kowalik, O. Krebs, K. Karrai, A. Badolato, and P. M. Petroff. Manipulating exciton fine structure in quantum dots with a lateral electric field. *Applied Physics Letters*, 90(4):041101, jan 2007.

[52] Andreas Muller, Wei Fang, John Lawall, and Glenn S. Solomon. Creating polarization-entangled photon pairs from a semiconductor quantum dot using the optical stark effect. *Physical Review Letters*, 103:217402, nov 2009.

[53] Ranber Singh and Gabriel Bester. Lower bound for the excitonic fine structure splitting in self-assembled quantum dots. *Physical Review Letters*, 104:196803, may 2010.

[54] Hendrik Utzat, Weiwei Sun, Alexander E. K. Kaplan, Franziska Krieg, Matthias Ginterseder, Boris Spokoyny, Nathan D. Klein, Katherine E. Shulenberger, Collin F. Perkinson, Maksym V. Kovalenko, and Moungi G. Bawendi. Coherent single-photon emission from colloidal lead halide perovskite quantum dots. *Science*, 363(6431):1068–1072, feb 2019.

[55] Alexander L. Efros and David J. Nesbitt. Origin and control of blinking in quantum dots. *Nature Nanotechnology*, 11(8):661–671, aug 2016.

[56] Nicolò Accanto, Francesco Masia, Iwan Moreels, Zeger Hens, Wolfgang Langbein, and Paola Borri. Engineering the spin–flip limited exciton dephasing in colloidal CdSe/CdS quantum dots. *ACS Nano*, 6(6):5227–5233, may 2012.

[57] N. Akopian, N. H. Lindner, E. Poem, Y. Berlatzky, J. Avron, D. Gershoni, B. D. Gerardot, and P. M. Petroff. Entangled photon pairs from semiconductor quantum dots. *Physical Review Letters*, 96:130501, apr 2006.

[58] Vigneshwaran Chandrasekaran, Mickaël D. Tessier, Dorian Dupont, Pieter Geiregat, Zeger Hens, and Edouard Brainis. Nearly blinking-free, high-purity single-photon emission by colloidal InP/ZnSe quantum dots. *Nano Letters*, 17(10):6104–6109, sep 2017.

[59] Annalisa Brodu, Vigneshwaran Chandrasekaran, Lorenzo Scarpelli, Jonathan Buhot, Francesco Masia, Mariana V. Ballottin, Marion Severijnen, Mickaël D. Tessier, Dorian Dupont, Freddy T. Rabouw, Peter C. M. Christianen, Celso de Mello Donega, Daniël Vanmaekelbergh, Wolfgang Langbein, and Zeger Hens. Fine structure of nearly isotropic bright excitons in InP/ZnSe colloidal quantum dots. *The Journal of Physical Chemistry Letters*, 10(18):5468–5475, aug 2019.

[60] Annalisa Brodu, Mariana V. Ballottin, Jonathan Buhot, Elleke J. van Harten, Dorian Dupont, Andrea La Porta, P. Tim Prins, Mickael D. Tessier, Marijn A. M. Versteegh, Val Zwiller, Sara Bals, Zeger Hens, Freddy T. Rabouw, Peter C. M. Christianen, Celso de Mello Donega, and Daniel Vanmaekelbergh. Exciton fine structure and lattice dynamics in InP/ZnSe core/shell quantum dots. *ACS Photonics*, 5(8):3353–3362, jul 2018.

[61] Y.-S. Park, A. V. Malko, J. Vela, Y. Chen, Y. Ghosh, F. García-Santamaría, J. A. Hollingsworth, V. I. Klimov, and H. Htoon. Near-unity quantum yields of biexciton emission from $\mathrm{CdSe/CdS}$ nanocrystals measured using single-particle spectroscopy. *Physical Review Letters*, 106:187401, may 2011.

[62] Gabriele Rainò, Thilo Stöferle, Iwan Moreels, Raquel Gomes, Zeger Hens, and Rainer F. Mahrt. Controlling the exciton fine structure splitting in CdSe/CdS dot-in-rod nanojunctions. *ACS Nano*, 6(3):1979–1987, mar 2012.

[63] David Zhitomirsky, Illan J. Kramer, André J. Labelle, Armin Fischer, Ratan Debnath, Jun Pan, Osman M. Bakr, and Edward H. Sargent. Colloidal quantum dot photovoltaics: The effect of polydispersity. *Nano Letters*, 12(2):1007–1012, jan 2012.

[64] Suzanne Bisschop, Antoine Guille, Dries Van Thourhout, Zeger Hens, and Edouard Brainis. Broadband enhancement of single photon emission and polarization dependent coupling in silicon nitride waveguides. *Optics Express*, 23(11):13713, may 2015.

[65] Yunpeng Zhu, Jie Wang, Weiqiang Xie, Bin Tian, Yanlu Li, Edouard Brainis, Yuqing Jiao, and Dries Van Thourhout. Ultra-compact silicon nitride grating coupler for microscopy systems. *Optics Express*, 25(26):33297, dec 2017.

Appendices

A. Publications

Journal articles

- Chandrasekaran, V.; Tessier, M. D.; Dupont, D.; Geiregat, P.; Hens, Z.; Brainis, E. Nearly Blinking-Free, High-Purity Single-Photon Emission by Colloidal InP/ZnSe Quantum Dots. *Nano Letters* **17**, 6104 (2017).
- *Brodu, A.; *Chandrasekaran, V.; Scarpelli, L.; Buhot, J.; Masia, F.; Ballottin, M. V.; Severijnen, M.; Tessier, M. D.; Dupont, D.; Rabouw, F. T.; Christianen, P. C. M.; de Mello Donegá, C.; Vanmaekelbergh, D.; Langbein, W.; Hens, Z. Fine Structure of Nearly Isotropic Bright Excitons in InP/ZnSe Colloidal Quantum Dots. *The Journal of Physical Chemistry Letters* **10**, 5468 (2019)
  * - contributed equally to this work
- Chandrasekaran, V.; Climente, J. I.; Scarpelli, L.; Masia, F.; Dupont, D.; Tessier, M. D.; Planelles, J.; Moreels I.; Langbein, W.; Hens, Z. Polarizability of band-edge excitonic species in single InP/ZnSe colloidal quantum dots. *in preparation*
- Chandrasekaran, V.; Scarpelli, L.; Dupont, D.; Tessier, M. D.; Borri, P.; Masia, F.; Hens, Z.; Langbein, W. Dephasing dominated by phonon-scattering within bright exciton triplet in InP/ZnSe colloidal quantum dots. *in preparation*

Conference papers & presentations

- Chandrasekaran, V.; Dupont, D.; Tessier, M. D.; Drijvers, E.; Aubert, T.; Hens, Z.; Brainis, E. New materials for single photon emission from colloidal quantum dots. *21st Annual symposium of the IEEE Photonics Benelux Chapter : symposium proceedings*, Ghent, 97-100, 2016. *talk*
- Chandrasekaran, V.; Tessier, M. D.; Dupont, D.; Geiregat, P.; Brainis, E; Hens, Z. Single photon sources from InP based colloidal quantum dots. *Lasers and Electro-Optics Europe & European Quantum Electronics conference (CLEO/Europe-EQEC)*, Munich, 2017. *poster*
- Chandrasekaran, V.; Dupont, D.; Tessier, M. D.; Geiregat, P.; Elsinger L.; Yunpeng Z.; Scarpelli, L.; Masia, F.; Langbein, W.; Thourhout, D. V.; Hens, Z. On-chip single-photon emission from deterministically positioned and embedded InP-based colloidal quantum dots. *Quantum Dots, 10th Biannual Conference*, Toronto, 2018 *talk*
- Chandrasekaran, V.; Scarpelli, L.; Masia, F.; Dupont, D.; Tessier, M. D.; Geiregat, P.; Moreels I.; Langbein, W.; Hens, Z. Spectral dynamics of linearly polarized bright exciton in InP/ZnSe colloidal quantum dots. *nanoGe Fall meeting*, Torremolinos, 2018 *talk*
- Chandrasekaran, V.; Dupont, D.; Tessier, M. D.; Geiregat, P.; Scarpelli, L.; Masia, F.; Langbein, W.; Hens, Z. Spectroscopy of single colloidal quantum dots. *Optical Spectroscopy Workshop, NB Photonics*, Ghent, 2018 *poster*

B. Acronyms

CB . . . . . Conduction Band
CdS . . . . . Cadmium Sulphide
CdSe . . . . . Cadmium Selenide
CMOS . . . . . Complementary Metal Oxide Semiconductor
CW . . . . . Continuous Wave
DFB . . . . . Distributed Feedback Laser
EMA . . . . . Effective Mass Approximation
FDTD . . . . . Finite-Difference Time-Domain
FLN . . . . . Fluorescence Line Narrowing
FWM . . . . . Four Wave Mixing
HH . . . . . Heavy Hole
InP . . . . . Indium Phosphide
IPA . . . . . Isopropyl Alcohol
LB . . . . . Langmuir-Blodgett technique
LH . . . . . Light Hole
LPCVD . . . . . Low Pressure Chemical Vapour Deposition
NC . . . . . Nanocrystal
NP . . . . . Nanoparticle
PE . . . . . Photon Echo
PECVD . . . . . Plasma Enhanced Chemical Vapour Deposition
PIC . . . . . Photonic Integrated Circuit
PL . . . . . Photoluminescence
PSB . . . . . Phonon-Sideband
QD . . . . . Quantum Dot
RIE . . . . . Reactive-Ion Etching
RT . . . . . Room Temperature
SD . . . . . Spectral Diffusion
SEM . . . . . Scanning Electron Microscope
Si_3N_4 . . . . . Silicon Nitride
SNSPD . . . . . Superconducting Nanowire Single Photon Detector
SO . . . . . Split-Off
SOI . . . . . Silicon-On-Insulator
TEM . . . . . Transmission Electron Micrograph
TG . . . . . Transient Grating
VB . . . . . Valence Band
ZnS . . . . . Zinc Sulphide
ZnSe . . . . . Zinc Selenide
ZPL . . . . . Zero Phonon Line

C. Optical spectroscopy set-up layout

C.1. Micro-photoluminescence

Setup 1 for room temperature spectroscopy

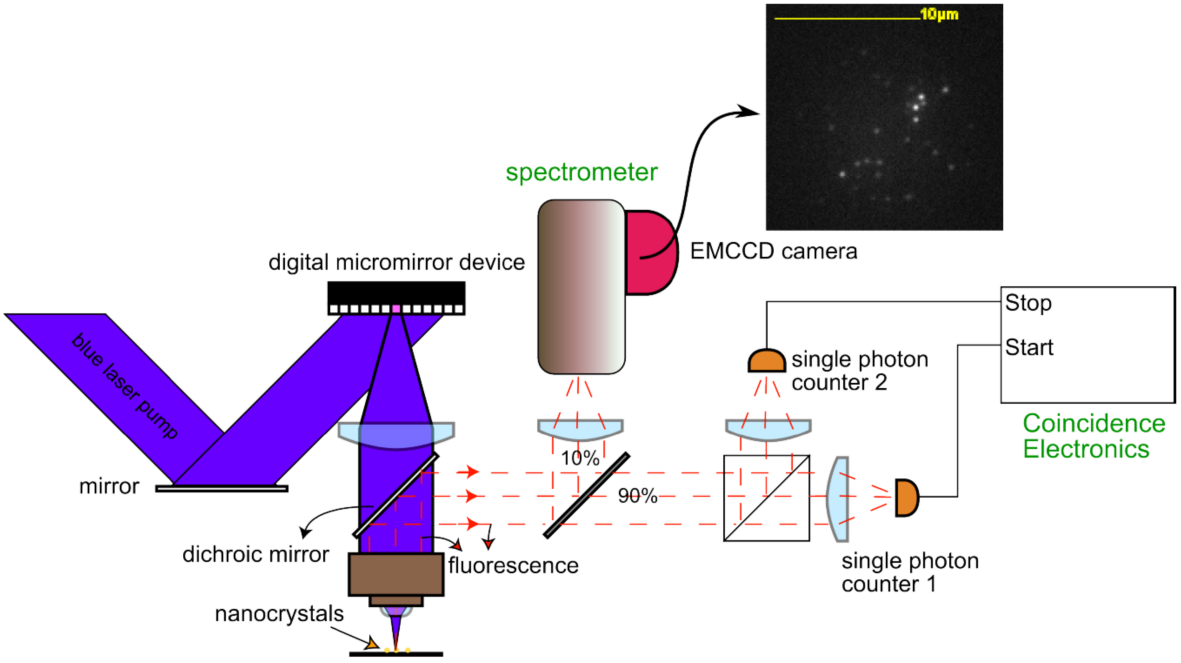

Figure 1. | Layout of the micro-PL set-up.

Thin films and single QDs were studied using a micro-photoluminescence setup. The excitation beam at 445 nm was produced by a PicoQuant LDH-D-C-440M laser diode. The laser diode operates in either cw or pulsed mode (in which case it produces short pulses of less than 100 ps). The excitation beam was focused on the sample using an Olympus oil-immersion objective lens (100x, 1.40 NA) and shaped using a digital micro-mirror device (Texas Instrument, 0.55" XGA 2x LVDS DMD) to allow custom excitation patterns (e.g. exciting a single diffraction-limited spot or the entire field of view). The luminescence was collected through the same objective lens and directed either to an imaging spectrometer (Andor Shamrock 330i) equipped with an EMCCD camera (Andor iXon DU897) or to an Hanbury-Brown Twiss setup. The imaging spectrometer was used to image the surface of the sample and record the emission spectra of single QDs. The Hanbury-Brown Twiss setup consisted of a 50/50 beam-splitter, two silicon photon-counting modules (Perkin Elmer SPCM-AQRH-14) with a time resolution of about 500 ps, and start-stop time correlator (PicoQuant, PicoHarp 300). The Hanbury-Brown Twiss setup was used to measure the luminescence decay, the $g^{(2)}$-function and the blinking statistics of single QDs.

Setup 2 for cryogenic spectroscopy

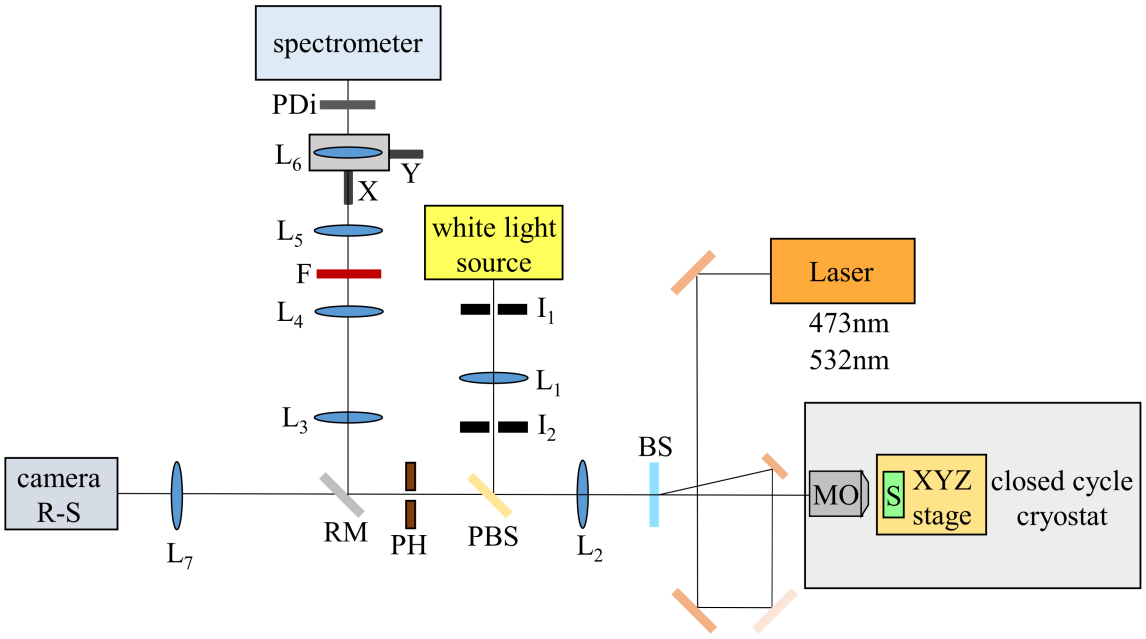

Figure 2. | Layout of the micro-PL optical set-up. MO: microscope objective; BS: 96:4 beam splitter; PBS: pellicle beam splitter; L: lens; I:iris; PH: pinhole; RM: removable mirror; PDi: polarisation displacer; R-S: real-space.

The sample was mounted on to a brass sample holder inside a low vibration closed cycle optical cryostat (Montana Instruments Cryostation C2). An 0.85NA objective is mounted on the cold-shield inside the cryostat at a temperature of 20 – 40 K allowing for a stable focal position and negligible radiation heating. The position of the sample was adjusted by a piezo-electric positioner (Attocube) inside the cryostat with 0.1 μm resolution and 5 mm of travel in three dimensions. QDs were excited at either 473nm or 532nm with a continuous wave (CW) laser. QD emission is passed through a half-waveplate ($\lambda/2$) which is rotated by an angle θ to adjust the direction of the two detected orthogonal linear polarization components. An intermediate pinhole is used to select the region of emission, which is imaged into the input slit of an imaging spectrometer with 1.9 m focal length and a 1200 l/mm holographic grating. A polarization displacer splits the emission along the input slit into components polarized along and across the input slit, which is subsequently detected by a CCD camera with a spectral window of 34meV at a resolution of 25 μeV per pixel. All measurements are done at 5K.

C.2. Transient absorption

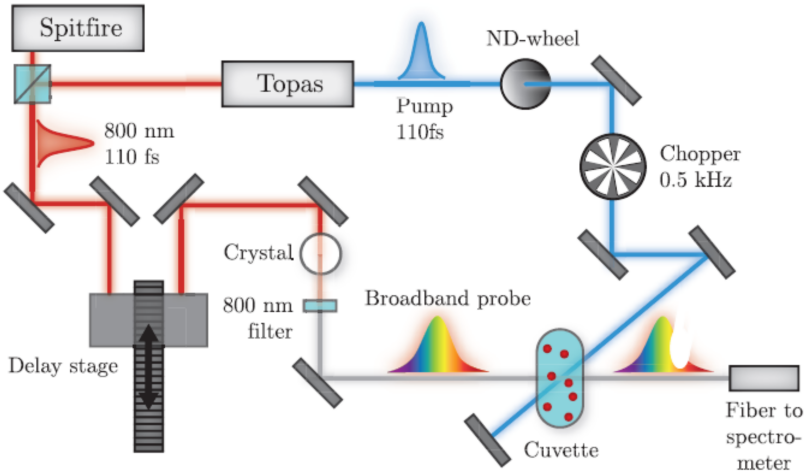

Figure 3. | Layout of the TAS set-up.

To investigate the quantum yield for biexcitons, an ultrafast pump-probe experiment on InP/ZnSe QD was performed. Samples were dispersed in toluene to achieve an optical density of 0.05 at the first exciton peak and were stirred during the measurements to avoid photocharging. QDs were photo-excited at 400 nm using the frequency double output of a 110 fs Ti:S laser created from the 800 nm fundamental source (Spitfire Ace, Spectra Physics) through non-linear conversion in an optical parametric amplifier (OPA) (Light Conversion TOPAS). Then the decay of the band edge population was monitored using a broadband, time-delayed probe pulse (110 fs) generated in a CaF_2 crystal. In this set-up, the pulses can be delayed relative to the pump using a delay stage with a maximum delay of 6 ns and the probe spectrum can cover the UV-VIS window from 350 nm up to 750 nm.

C.3. Fluorescence line narrowing

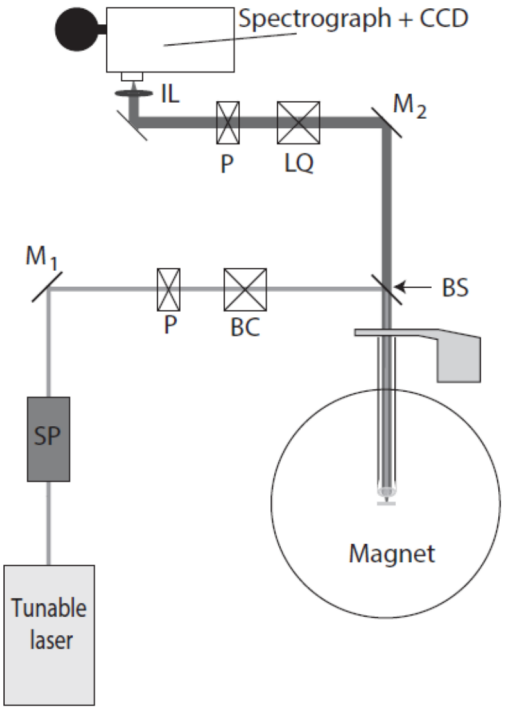

Figure 4. | Layout of the FLN set-up. SP: Small spectrograph to clean the laser line; P: Linear polarizer; BC: Babinet-Soleil compensators; BS:beam splitter; LQ: Lambda-quarter wave plate; IL: Imaging lens;

FLN experiments at low temperatures were performed at the High Field Magnet Laboratory (Radboud University, Nijmegen, The Netherlands). For these experiments, QD films dropcast on crystalline silicon substrate were used, which were mounted in a titanium sample holder on top of a three-axis piezo-positioner. The FLN measurements were performed in a Faraday configuration (see Figure **??**b) using a spectrally narrow excitation source, achieved by using a tunable jet-stream dye (Rhodamine 6G) laser. This monochromatic laser beam was circularly polarized by means of a linear polarizer and a Babinet-Soleil compensator. The laser beam was focused on the sample by a singlet lens (10 mm focal length). The same lens was used to collect the PL emission and direct it to the detection setup (backscattering geometry). The samples and optical probe were mounted inside a liquid-helium bath cryostat. The high-resolution FLN emission was detected in crossed polarization mode relative to the laser polarization by using a linear polarizer and a lambda-quarter wave plate. The resonant-PL emission was analyzed by a 0.5 m long triple-grating spectrometer (3×1800 grooves/mm holographic gratings) in subtractive mode, equipped with a liquid nitrogen cooled CCD camera (Symphony-Horiba).

C.4. Four wave mixing

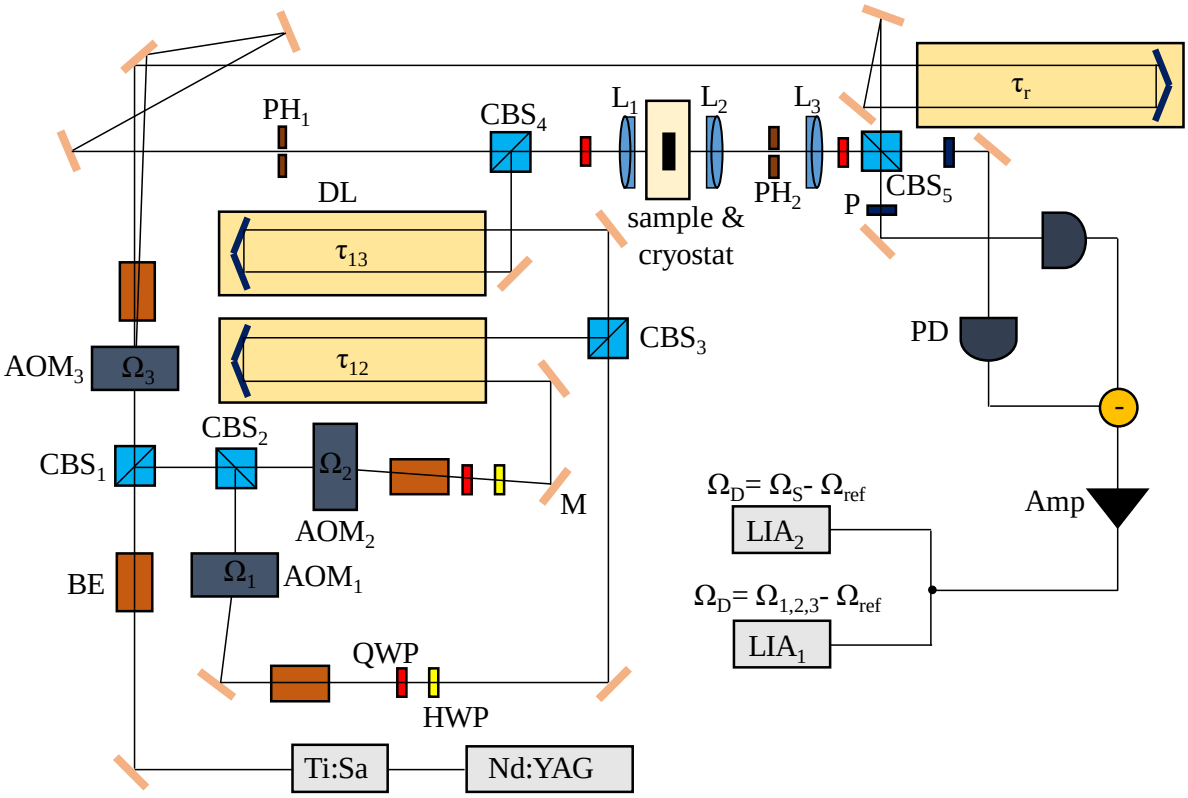

Figure 5. | Layout of the transient FWM optical set-up. BE: beam expander; CBS: cube beam splitter; AOM: acousto-optic modulator; QWP: quarter waveplate; HWP: half waveplate; DL: delay line; M:mirror; PD: photodiode; AMp: amplifier; PH: pinhole; L: lens; P: polariser; LIA: lock-in amplifier.

The train of pulses is generated by a titanium-sapphire (Ti:Sa) laser pumped by an intracavity frequency doubled neodymium-doped yttrium aluminum garnet (Nd:YAG) laser pumped by a semiconductor diode laser. The pulses have an intensity FWHM of 150 fs, and a repetition rate of 76 MHz, corresponding to a time separation between consecutive pulses of about 13 ns. Two cube beam splitters (CBS_1) and (CBS_2) are used to generate three trains of pulses, two pumps and probe beams, which are passed through the corresponding acousto-optic modulators (AOMs). The beam expander (BE) is used to reduce the size of the input beam to match the AOM aperture. The effect of the AOM is to deflect a fraction of the input beam by Bragg diffraction, with frequency shift Ω_i and an amplitude given by the carrier frequency and the amplitude of the electrical drive respectively. The deflected beams are passed through BEs which are used to adjust the beams divergence and size, and they are called P_1, P_2 and P_3 in the following, which are pump one, pump two and the probe respectively, with the corresponding optical frequencies upshifted by Ω_1, Ω_2 and Ω_3, respectively. The polarisation of P_1 and P_2 is adjusted with combinations of quarter waveplate (QWP) and half waveplate (HWP). P_3 is horizontally linearly polarised after the CBS_4, and can be converted to circular polarisation by rotating the QWP in front of L_1. P_2 is delayed by τ_{12} with respect to P_1 using a delay line (DL) made of a linear stage and a retro-reflector. After recombining at the CBS_3, both P_1 and P_2 are delayed by τ_{13} with respect to P_3 using a second delay line. Pumps and probe finally recombine at CBS_4 and are then focused by the lens L_1 on the sample plane. The sample is mounted into a cold finger helium flow

cryostat, which allows cooling down to 4 K. The transmitted field is imaged by L_2 onto the pinhole PH_2, which is used to block spurious reflections. L_3 collimates the beam, and another QWP converts the circular polarisation back to linear. The undeflected part of P_3 is used as a reference field for the employed heterodyne detection scheme. This is delayed by τ_r with respect to the FWM signal using the corresponding delay line. The FWM and reference fields recombine and interfere at the CBS_5. The two output beams are then projected onto horizontal polarisation by polarisers (P), and detected by photodiodes (PD).

D. Acknowledgements

Thank you **Zeger** for your guidance & support during my entire PhD duration, without which this dissertation would not have been possible. I have learned a lot of skills from you, which comprises not only the science & research part, but also on how to present the results. Your questioning & feedbacks on making presentations or developing figures or writing articles have made me realize that there is a lot to learn when it comes to scientific dissemination. The ornate & baroque ways of my expressions come from writing poetry which is very far from the clear, concise, logical & simple way of scientific writing. As an ambitious person, I would think myself that I should leave no stone unturned and get muddled in the process. Thank you **Zeger** for keeping me on the track and aiding me in completing my PhD. I am amazed at how you are managing so many different projects. I was thrilled when you thought of light hole to heavy hole ratio to explain the isotropic exciton and your fitting of dephasing rate has culminated in getting the conclusion. Your decisions allowed me to be involved in different projects, made collaborations with researchers around the world and provided funding which all have motivated me and I believe they have now created new opportunities for me.

Thank you **Wolfgang** for allowing me to do experiments in Cardiff where more than half of the results in this dissertation were made possible. I would like to thank you for sharing your knowledge, supervision and the world-class facilities which are a pedagogical dream for any fledgling student like myself. It was ingenious to think of using nail varnish during the sample preparation for four wave mixing spectroscopy. I have admired your expertise in various subjects and the interactions with you have enlightened me about an importance of having knowledge on theory and software for an experimental scientist. Your questioning and attention to minute details whether it is a phrase (my personal favorite is 'due to' became 'attributed to') or a graph (unit of intensity is photoelectrons and not a.u.) or even a quote (you dissected one of the quotes by Schrödinger I used in the first version of this dissertation) have improved my observation skills. Thank you for all the Skype sessions. There is no doubt that my career has benefited immensely by associating with your research group.

The journey of my PhD to Belgium would not have commenced if it was not for my former co-promotor **Edouard**, who recruited me for this project along with **Zeger** and **Bart**. Initially, I came second in ranking for this Marie Curie ITN scholarship. **Edouard** told me to patiently wait for some more time as the person who ranked first needed to accept this position formally. I thought it was a wild-goose chase since no-one would deny this kind of scholarship. While I was anxiously contemplating whether to accept an alternative offer for another PhD, an email arrived from **Edouard** congratulating me for obtaining this position. I wondered if it was 'written', as my parents fondly said. Thank you **Edouard** for allowing me to work in Brussels lab, pushing me to characterize InP QDs, my first article and I have learned optics & constructing microscope from you. Similar to **Zeger** who said that I complicate things by bringing in unrelated stuffs in my first version of the dissertation, **Edouard** also mentioned like this in my earlier PhD days, well, in French. The translation goes like this: *"killing a fly with a bazooka!"*.

Thank you to the jury members in the examination board for their availability and patiently reading my dissertation among their busy schedules: **Christophe**, **Dirk**, **Iwan**, **Dries**, and **David**. I believe that your questioning, comments and suggestions have improved my dissertation.

Thank you **Dorian** for synthesizing & providing me the best QDs in the world (when I asked for a part number of a QD, you wrote down 'World's best' on the vial). I must say that the analysis of fundamental optical properties of excitons in InP QDs took precedence in my PhD because of the availability of your QDs at the right time and fortunately (for me!) it was rarely explored in the literature. You also helped

me in dropcasting the single QDs for single photon emission and I got the best result from this sample. Thank you **Mickaël** for also providing the samples, your support and advice. I still remember your teaching of inhomogeneous broadening & single QD spectra on the white board in the lab, your idea of the layout for my first article and sharing a Matlab code for blinking analysis during my initial days. I would like to thank **Emile** for providing me CdSe QDs and being nice with asking me how is it going whenever we see each other. Thank you **Tangi** for providing me CdSe QDs and I remember you were shocked when I asked for a QD that has faster Auger rate!

Thank you **Francesco** and **Lorenzo** for making my stay in Cardiff very productive at both times! I cannot forget looking at the blank screen for the emission from single QDs unsuccessfully for more than a week. **Lorenzo** and I were ready to leave in a late evening when suddenly a QD emission popped up. Then we recorded a video registering our state of mind at that time and I still have that video in my archive! The second visit for four wave mixing spectroscopy was even more daunting. Thank you **Lorenzo** for visiting a beauty shop and buying a near-obsolete nail varnish from a surprised-looking lady who was handed over a paper with a specific name & specifications written on it! Thank you **Francesco** for measuring the data with me till 3-4 am in the morning and coming to work on the next day as well! I am very much thankful to both of you for your time, sharing knowledge and availability for Skype discussions till the end of my PhD.

Thank you **Pieter G.** for your anytime availability for a scientific discussion and your encouragement. I would like to thank you for sharing books & articles during my initial days and conversations in the laser lab. Also, thank you for doing ultrafast pump-probe spectroscopy which helped me in getting the estimate of Auger rate for the QD. Thank you **Iwan** for coming up with an idea of modeling spectral diffusion and introducing **Juan** from Universitat Jaume I, Spain who did a phenomenal theoretical work to understand the polarizability of excitonic species in QDs. I have learned a lot from your questioning during the meetings and sharing your vast knowledge on QDs. Sorry that I could not make it to the presentation in a conference for which you were the chair!

Thank you to the colleagues in PCN for a great time both on- and off-work.

Cool office: **Leila** for your warm hello in the morning. Are you still talking to your laptop? **Valeriia** for the travel, movies & food during initial days and the Christmas gift. I wish you the best in whatever you do! **Kim** for touring of the department & introducing me to everyone on my first day and for the tips about Belgium like where to buy stuffs; **Willem** for showing how to manage work-life balance with a 9-to-5 schedule and providing me TEM images, sorry that you were not a co-author; **Jorick** for discussion on QDs, AFM tip-replacement training, chemical orders and being professional; **Suzanne** for showing me all the way from Ghent station to Brussels lab and thanks for the invite for concerts, tips about Belgium, and being nice & helpful; **Igor** for being a teetotaler with a sane mind, especially when others drink and act like imbeciles. Also, thanks for sending your cute baby picture! **Chandu**, **Ali** and **Abhi** for many fun conversations including about politics, cricket, dartboard games, and India! **Chandu** for storing the wine for a long time without drinking it! **Ali** for TEM images and I wish you get the position that you desire; **Abhi** for Tamil conversations and all the best for your PhD; Best wishes to the past staffs **Jonathan**, **Jakob**, **Sofie** and **Anatolii**. **Jakob** for the AFM images as well.

Sick office: **Hannes** for being a jovial person and thanks for estimating Cd-content in alloyed QDs, sorry that it did not make into this dissertation; **Pieter S.** for the Christmas gift and being nice. Thanks for the silica & gold encapsulated QDs; **Arnau** for pizza on a snowy day in your place; **Filipe** for the relaxed chats and good luck with the TA & I wish you get lasing in InP QDs! **Ivo** for being friendly and good luck with the frequency comb project; Best wishes to the past staffs: **Kishu** for the fun chats, movies, food and drinks; **Chen** for the Christmas gift and being a kind person.

Fun office: **Jari** for being a friendly & sensible person. Thank you very much for translating the preface part in Dutch. I understand that it is quite difficult to do technical translation and you agreed & provided me the translated copy without any hesitation. I wish you have a bright future! **Shalini** for inviting for Indian dinner & being a cheerful person; **Renu** for being nice and all the help during my initial days from lending money to inviting me for a Diwali dinner in Harish & Kanmani's place. Sorry I put a lot of hot spices in the food! **Carmelita** for being friendly with a hi always. Good luck with the micro-PL setup and your PhD; **Pengshang** for your waving-hand hi and smile all the time; **Kim CD** for the Christmas gift and managing lab in a fun way; **Gabriele** for suggesting where to spend sodexo coupon; **Alessio** for inquiring how my PhD is going; **Natalia** for being Natalia with fun & energy; **Min** for listening to what my PhD is about. Good luck to the new recruits: **Alina**, **Ben**, **Delphine**, **Fadi** and **Wouter**.

Thanks to **Himanshu** & **Chidharth** for discussions about India and conversations in Hindi, English and Tamil! **Sara** & **Parviz** for being nice from the moment we joined this department around the same time; **Dimitrije**, **Jing**, **Flavia**, **Kaili** and **Anna** for helping with the spectrometer; **Kevin** for the movie, **Norini** and all the other people in S3 for saying hi when walking down the corridor and in the coffee room. My sincere thanks to **Pierre** and **Kathleen** for the administration work and being available for any query at any time. My time in Belgium would not have been smooth if it was not for the help from you; I also would like to thank **Pat** for fixing the computer; **Bart** for making a sample holder; **Chokri** for keeping the workplace hygiene.

I would like to thank the Photonics Research Group: **Dries**, **Lukas**, **Yunpeng**, **Weiqiang**, **Muhammad**, **Steven**, **Liesbet** for helping me in the cleanroom. I would like to thank **Ronan** and **Gabriele** for accomodating me in Single Quantum, Netherlands for a collaboration. Thanks to **Juan** from Universitat Jaume I, Spain for the theoretical model on spectral diffusion. Many thanks to **Annalisa** and **Daniël** from Utrecht University for their collaboration and the article on the exciton fine structure.

I would like to thank my funding Marie Curie ITN - Phonsi for all the travel, seminar, workshop and allowing me to meet & interact with scientists all around the world. Thanks to **Richard** & **Kamal** for managing Phonsi and also organizing nb-photonics seminars. Thanks to the unforgettable memories with diverse cuisine, party, wandering around, all thanks to the wonderful people who were also part of the funding network: **Adam**, **Annalisa**, **Bogdan**, **Darius**, **Federico**, **Joanna**, **Lukas**, **Maryam**, **Michael**, **Nayyera**, **Niall**, **Renu**, **Ronan** and **Ye**. My personal favorite is the trip to Israel visiting historic places! And singing *'Sweet Caroline'* as a sing-along on a roadtrip!

I would like to recognize the *'shoulders of giants'* whose work has set the pace for my PhD. Thanks to all the scientists who have inspired me right from the time of my childhood. I would like to quote Dr. A.P.J Abdul Kalam who said *"Dream is not that which you see while sleeping, it is something that does not let you sleep"*. I did not think it would happen literally with a lot of sleepless nights during my PhD ;) Thanks to the modern technology that allowed me to access information in my fingertip. When I asked the Google assistant consecutive questions, a response came which I will never forget *"If I knew everything, it would be easier. But I am pretty good at some things!"*.

Finally, I would like to thank my beloved **Amma**, **Appa**, **Murali** and **Sweta** for your unconditional care and motivation. This PhD has started, progressed and ended well, all because of your support & blessings and I would like to dedicate this PhD dissertation to you.

Vignesh